

IDENTIFICATION OF LOCALIZED NONLINEARITY FOR DYNAMIC ANALYSIS OF  
STRUCTURES

A THESIS SUBMITTED TO  
THE GRADUATE SCHOOL OF NATURAL AND APPLIED SCIENCES  
OF  
MIDDLE EAST TECHNICAL UNIVERSITY

BY

MURAT AYKAN

IN PARTIAL FULFILLMENT OF THE REQUIREMENTS  
FOR  
THE DEGREE OF DOCTOR OF PHILOSOPHY  
IN  
MECHANICAL ENGINEERING

JANUARY 2013



**IDENTIFICATION OF LOCALIZED NONLINEARITY FOR DYNAMIC ANALYSIS  
OF STRUCTURES**

submitted by **MURAT AYKAN** in partial fulfillment of the requirements for the degree of  
**Doctor of Philosophy in Mechanical Engineering Department, Middle East Technical  
University** by,

Prof. Dr. Canan Özgen  
Dean, Graduate School of **Natural and Applied Sciences** \_\_\_\_\_

Prof. Dr. Suha Oral  
Head of Department, **Mechanical Engineering** \_\_\_\_\_

Prof. Dr. H. Nevzat Özgüven  
Supervisor, **Mechanical Engineering Dept., METU** \_\_\_\_\_

**Examining Committee Members:**

Assist. Prof. Dr. Gökhan O. ÖZGEN  
Mechanical Engineering Dept., METU \_\_\_\_\_

Prof. Dr. H. Nevzat Özgüven  
Mechanical Engineering Dept., METU \_\_\_\_\_

Prof. Dr. Yavuz Yaman  
Aerospace Engineering Dept., METU \_\_\_\_\_

Assist. Prof. Dr. Ender CİĞEROĞLU  
Mechanical Engineering Dept., METU \_\_\_\_\_

Assist. Prof. Dr. M. Bülent ÖZER  
Mechanical Engineering Dept., TOBB ETU \_\_\_\_\_

**Date:** 25.01.2013

**I hereby declare that all information in this document has been obtained and presented in accordance with academic rules and ethical conduct. I also declare that, as required by these rules and conduct, I have fully cited and referenced all material and results that are not original to this work.**

Name, Last name : Murat AYKAN

Signature :

## ABSTRACT

### IDENTIFICATION OF LOCALIZED NONLINEARITY FOR DYNAMIC ANALYSIS OF STRUCTURES

AYKAN, Murat

Ph.D., Department of Mechanical Engineering

Supervisor: Prof. Dr. H. Nevzat ÖZGÜVEN

January 2013, 172 pages

Most engineering structures include nonlinearity to some degree. Depending on the dynamic conditions and level of external forcing, sometimes a linear structure assumption may be justified. However, design requirements of sophisticated structures such as satellites, stabilized weapon systems and radars may require nonlinear behavior to be considered for better performance. Therefore, it is very important to successfully detect, localize and parametrically identify nonlinearity in such cases. In engineering applications, the location of nonlinearity and its type may not be always known in advance. Furthermore, as the structure will be excited from only a few coordinates, the frequency response function matrices will not be complete. In order to parametrically identify more than one type of nonlinearity which may co-exist at the same location with the above mentioned limitations, a method is proposed where restoring force surface plots are used which are evaluated by describing function inversion. Then, by reformulating this method, a second method is proposed which can directly evaluate the total describing function of more than one type of nonlinearity which may co-exist at the same location without using any linear frequency response function matrix. It is also aimed in this study to use the nonlinearity localization formulations for damage localization purposes. The validation of the methods developed in this study is demonstrated with case studies based on simulated experiments, as well as real experiments with nonlinear structures and it is concluded that the methods are very promising to be used in engineering structures.

Keywords: Nonlinear Structural Dynamics, Parametric Nonlinearity Identification, Nonlinear Restoring Force, Experimental Verification, Damage Detection, Damage Localization

## ÖZ

### MEKANİK YAPILARIN DİNAMİK ANALİZLERİ İÇİN YEREL VE DOĞRUSAL OLMAYAN ÖZELLİKLERİN BELİRLENMESİ

AYKAN, Murat  
Doktora, Makina Mühendisliği Bölümü  
Tez Yöneticisi: Prof. Dr. H. Nevzat ÖZGÜVEN

Ocak 2013, 172 sayfa

Mekanik yapıların birçoğunda belirli seviyelerde doğrusal olmayan özellikler bulunmaktadır. Dinamik koşullar ve yükleme seviyeleri bazen yapının doğrusal olarak varsayılmasını mümkün kılarsa da uydu, stabilize silah sistemleri ve radar gibi karmaşık tasarımların gerekleri, daha iyi performans elde edilebilmesi için doğrusal olmayan özelliklerin düşünülmesini gerektirebilir. Dolayısıyla, doğrusal olmayan elemanların doğru bir şekilde belirlenmesi, bulunması ve parametrik olarak tanımlanması büyük önem taşımaktadır. Mühendislik uygulamalarında doğrusal olmayan elemanların yeri ve çeşidinin önceden bilinmesi bazı durumlarda mümkün olmamaktadır. Ayrıca, çoğu yapısal dinamik uygulamalarında deneysel ölçümlerde yapı sadece birkaç koordinatından tahrik edileceği için doğrusal Frekans Tepki Fonksiyonu (FTF) matrisleri eksiksiz olmayacaktır. Aynı bölgede bulunabilecek birden fazla doğrusal olmayan elemanın parametrik olarak belirlenebilmesi için doğrusal olmayan eleman tanımlama fonksiyonlarının tersi alınarak doğrusal olmayan kuvvet grafiklerinin elde edilebileceği bir yöntem önerilmektedir. Ayrıca bu yöntemin yeniden formüle edilmesiyle doğrusal FTF bilgisine ihtiyaç duymayan ve aynı bölgede bulunabilecek birden fazla doğrusal olmayan elemanın doğrusal olmayan eleman tanımlama fonksiyonlarını doğrudan elde edebilen bir yöntem geliştirilmiştir. Çalışmanın diğer bir amacı ise, doğrusal eleman konumu belirleme denklemlerinin hasar konumu belirleme amacı için kullanımınıdır. Yöntemlerin doğrulamaları sayısal ve deneysel çalışmalarla yapılmış ve yöntemlerin mühendislik uygulamalarında kullanımlarının başarıyla kullanılabilecekleri gösterilmiştir.

Anahtar Kelimeler: Doğrusal Olmayan Yapı Dinamiği, Parametrik Doğrusal Olmayan Eleman Tanımlama, Doğrusal Olmayan Kuvvet, Deneysel Doğrulama, Hasar Tespiti, Hasar Konum Tespiti

To My Family

## ACKNOWLEDGMENTS

The author wishes to express his deepest gratitude to his supervisor Prof. Dr. H. Nevzat Özgüven for his guidance, advice, criticism, encouragements and insight throughout the research.

The author would also like to thank Özge Mencek, Fatih Altunel, Taner Karagöz, Yiğit Özpak, Anıl Koyuncu, Tolga Köktürk and Serkan Kayılı for their suggestions and comments.

Finally, the author wishes to express his deepest gratitude to his wife and son, Fatma Serap and Ahmet Aykan for their love and understanding. Without their full support and encouragement, this thesis would not have been completed.

## LIST OF SYMBOLS

$[M]$	Mass matrix
$m$	Mass
$[C]$	Damping matrix
$c$	Damping
$[K]$	Stiffness matrix
$k$	Stiffness
$[H]$	Structural damping
$[Z]$	Dynamic stiffness matrix of the linear part
$\{N\}$	Nonlinear internal force vector
$n$	Degrees of freedom, nonlinear force element
$x$	Response
$X$	Complex amplitude of the response
$p$	Number of harmonic terms
$\{f\}$	Harmonic forcing vector
$\{F\}$	Amplitude vector of the forcing
$t$	Time
$A$	Scaled modal constants
$N$	Number of modes
$\omega$	Frequency
$\omega_n$	Undamped natural frequency
$\omega_d$	Damped natural frequency
$v$	Describing function representation of the nonlinearity
$[\Delta]$	Response dependent nonlinearity matrix
$a$	Receptance
$\theta$	Phase angle
$\zeta$	Damping ratio
$\emptyset$	Modal constant

### Subscripts

$m, l$	Harmonic number
$r, i, j, k, p$	Coordinate
$lin$	Linear part

### Superscripts

*	Complex conjugate
~	Approximate
$k$	Mode number
$NL$	Nonlinear

### Abbreviations

FRF	Frequency Response Function
DF	Describing Function
DFF	Describing Function Footprint
SDOF	Single Degrees of Freedom
MDOF	Multi Degrees of Freedom
DF method	Nonlinearity Identification by Describing Functions
DFI method	Nonlinearity Identification by DF Inversion
DDF method	Direct Nonlinearity Identification by DFs
$NLI$	Nonlinearity Index

## TABLE OF CONTENTS

ABSTRACT .....	v
ÖZ .....	vi
ACKNOWLEDGMENTS .....	viii
LIST OF SYMBOLS .....	ix
TABLE OF CONTENTS .....	x
CHAPTERS	
1. INTRODUCTION .....	1
1.1. Structural System Identification .....	1
1.2. Motivation .....	2
1.3. Scope of Thesis .....	6
1.4. Outline of Thesis .....	7
2. LITERATURE REVIEW AND SUMMARY OF THE THESIS .....	9
2.1. Nonlinear System Identification .....	9
2.2. Damage Detection and Localization .....	11
3. IDENTIFICATION OF NONLINEARITY AND NONLINEAR RESPONSE CALCULATION BY USING DESCRIBING FUNCTIONS .....	13
3.1. DF Representation of Nonlinearity .....	13
3.2. Harmonic Balance Method .....	14
3.3. Calculation of Harmonic Response of Nonlinear Systems by Using DFs .....	16
3.4. Identification of Nonlinearity Using DFs .....	17
3.5. Calculation of Multi-harmonic Response of Nonlinear Systems by Using DFs .....	20
3.5.1. Multi-harmonic System Modeling Theory .....	20
3.5.2. Multi-harmonic Nonlinear Response Calculation .....	22
3.5.3. Adaptive Multi-harmonic Solution Method .....	23
3.6. Case Study: Nonlinearity Identification and Multi-harmonic Response Calculation .....	23
3.7. Spatial Incompleteness and FRF Synthesis with an Application .....	27
3.8. Nonlinearity Localization from Spatially Incomplete FRF Data .....	32
3.8.1. Case Study 1: Nonlinearity Localization from Spatially Incomplete Noise Free FRFs .....	34
3.8.2. Case Study 2: Nonlinearity Localization from Spatially Incomplete FRF Data with Noise #1 .....	36
3.8.3. Case Study 3: Nonlinearity Localization from Spatially Incomplete FRF Data with Noise #2 .....	38
3.8.4. Case Study 4: Nonlinearity Localization from Spatially Incomplete FRF Data with Missing Coordinates .....	39
4. NONLINEARITY IDENTIFICATION BY RESTORING FORCE APPROACH .....	41
4.1. Introduction to Nonlinearity Identification Process Using DFs .....	41
4.2. Nonlinearity Identification by DF Inversion (DFI Method) .....	43
4.2.1. Nonlinearity Characterization .....	43
4.2.2. Nonlinearity Coefficient Identification .....	50
4.3. Accuracy of Approximate DF Inversion .....	50
4.3.1. Cubic Stiffness .....	50
4.3.2. Coulomb Friction .....	50
4.3.3. Piecewise Stiffness .....	50
4.3.4. Backlash .....	52
4.4. Case Studies .....	52
4.4.1. Case Study 1: Nonlinear Elements at Different Locations .....	52
4.4.2. Case Study 2: Two Different Nonlinear Elements at the Same Location .....	56
4.4.3. Case Study 3: Two Different Nonlinear Elements at the Same Location-Finite Element Model .....	60
4.4.4. Case Study 4: Stiffness and Friction Nonlinear Elements at Different Locations ..	64
5. IDENTIFICATION OF RESTORING FORCE SURFACES IN NONLINEAR MDOF SYSTEMS FROM FRF DATA USING NONLINEARITY MATRIX .....	69

5.1. Nonlinearity Matrix Evaluation.....	69
5.2. Application of the DDF Method .....	70
5.3. Case Studies .....	71
5.3.1. Case Study 1: Backlash and Coulomb Friction Nonlinear Elements at the Same Location .....	71
5.3.2. Case Study 2: Cubic Stiffness and Coulomb Friction Nonlinear Elements at the Same Location .....	74
5.3.3. Case Study3: Cubic Stiffness and Backlash Nonlinear Elements at the Same Location .....	76
6. EXPERIMENTAL WORK AND VERIFICATION OF THE NONLINEAR IDENTIFICATION METHODS .....	81
6.1. Experimental Study 1: Application of the DF and the DFI Methods on a SDOF System .....	81
6.2. Experimental Study 2: Application of the DFI method on a MDOF System.....	87
6.3. Experimental Study 3: Application of the DDF Method on a SDOF System .....	92
6.4. Experimental Study 4: Application of the DDF Method on a Stabilized Optic Platform .....	94
7. APPLICATION OF NONLINEAR IDENTIFICATION APPROACH TO CRACK DETECTION PROBLEMS.....	99
7.1. Damage Localization by Improved DF Method.....	99
7.2. Experimental Studies.....	99
7.2.1. Experimental Study 1: Localization of Damage in a 7 DOF Beam by Shaker Testing .....	99
7.2.2. Experimental Study 2: Localization of Damage in a 7 DOF Composite Beam by Impact Testing .....	105
7.2.3. Experimental Study 3: Localization of Damage in a 4 DOF Waveguide by Impact Testing .....	107
8. DISCUSSION AND CONCLUSIONS .....	111
9. RECOMMENDATIONS FOR FUTURE WORK.....	113
REFERENCES .....	114
APPENDICES	
A. COMMON RESTORING FORCE FUNCTIONS AND CORRESPONDING DESCRIBING FUNCTIONS .....	120
B. PUBLISHED ARTICLES DURING PHD .....	122
VITA .....	171



## CHAPTER 1

### INTRODUCTION

This introductory chapter aims at presenting the need of understanding nonlinear system identification and modeling from a structural dynamics point of view, in conjunction with the requirements of the national defense industry.

#### 1.1. Structural System Identification

Structural system identification consists of finding transfer function of the system which is established by finding the modal parameters of the structure such as, natural frequencies, damping, modal vectors and residues. This task is very difficult even for linear systems, yet sometimes it is not possible to neglect the nonlinearities in the structure.

Theoretically, every structure is nonlinear. Extent of the nonlinearity determines whether we should be worried about it. Usually, the modeling and testing errors of the linear system are so dominant that most of the effort is spend to correct them. The importance of nonlinear elements is highlighted when we cannot predict a correct response from the mathematical model even though the structure is correctly modeled in the linear sense.

Physically, there are three main sources of nonlinearities:

**Geometric nonlinearities:** When a structure experiences large deformations, its changing geometric configuration can cause nonlinear behavior. A good example for this is thin sheets of metal. When such a sheet has small deformations the response will be linear. However, when the deformation is high then the sheet will react with higher stiffness at high displacements and with lower stiffness at smaller displacements.

**Material nonlinearities:** A nonlinear stress-strain relationship, such as metal plasticity, rubber elasticity etc. is another source of nonlinearity.

**Contact:** Contact is a type of “changing status” nonlinearity, where an abrupt change in stiffness or damping (i.e. friction) occurs between two bodies.

Nonlinearity in a system is usually observed by having different FRF plots to different load levels. Nevertheless, the main indicators of nonlinearity in a structure can be summarized as:

- Superposition principle does not hold,
- Homogeneity is lost,
- Harmonic distortions due to higher harmonics occur on the response
- Reciprocity may not be established.

Structural assemblies, especially when there are moving bodies' give rise to nonlinearities. In industrial designs, usually the mechanical assemblies contain localized nonlinear elements, such as bearings, gears and other types of joints. Thus, most of the nonlinearity identification and modeling methods in the literature try to identify nonlinear elements which are localized. Furthermore, extent of detail in modeling the nonlinear element can vary. Although detailed nonlinear models exist in the literature, most of the time it suffices to use simple models such as those given in Figure 1-1. The RFs and corresponding DFs for nonlinear elements usually encountered in practice are given in appendix A.

A final comment on nonlinearities in structural assemblies is that most of the time the nonlinear locations contain more than a single nonlinearity. An example might be a simple revolute joint. The joint will have definitely friction and some amount of backlash yielding two nonlinear elements.

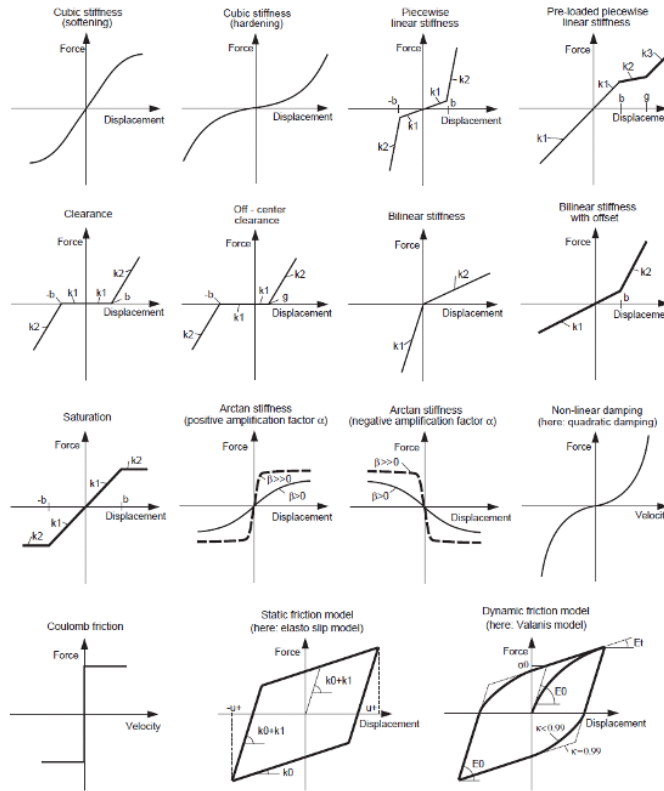


Figure 1-1. Idealized forms of various types of nonlinearities [1]

## 1.2. Motivation

ASELSAN Inc. is one of the leading military defense system designers, manufacturers and integrators in Turkey. In order to increase the performance and life of products, designed systems are thoroughly analyzed. One of the main research topics is the control of turret type weapon systems and integration based effects of these systems on platforms like helicopters and aircrafts (Figure 1-2).

Systems such as the ones shown in Figure 1-2 have moving parts which are controlled for various purposes. In order to correctly control such systems or integrate them without any interference to the platform, it is necessary to understand the dynamics of the system and the platform.

In order to show the nonlinear responses that are commonly encountered in structural assemblies that have moving bodies', some preliminary step sine tests were performed on a AB-204.B helicopter horizontal stabilizer (Figure 1-3-Figure 1-5).

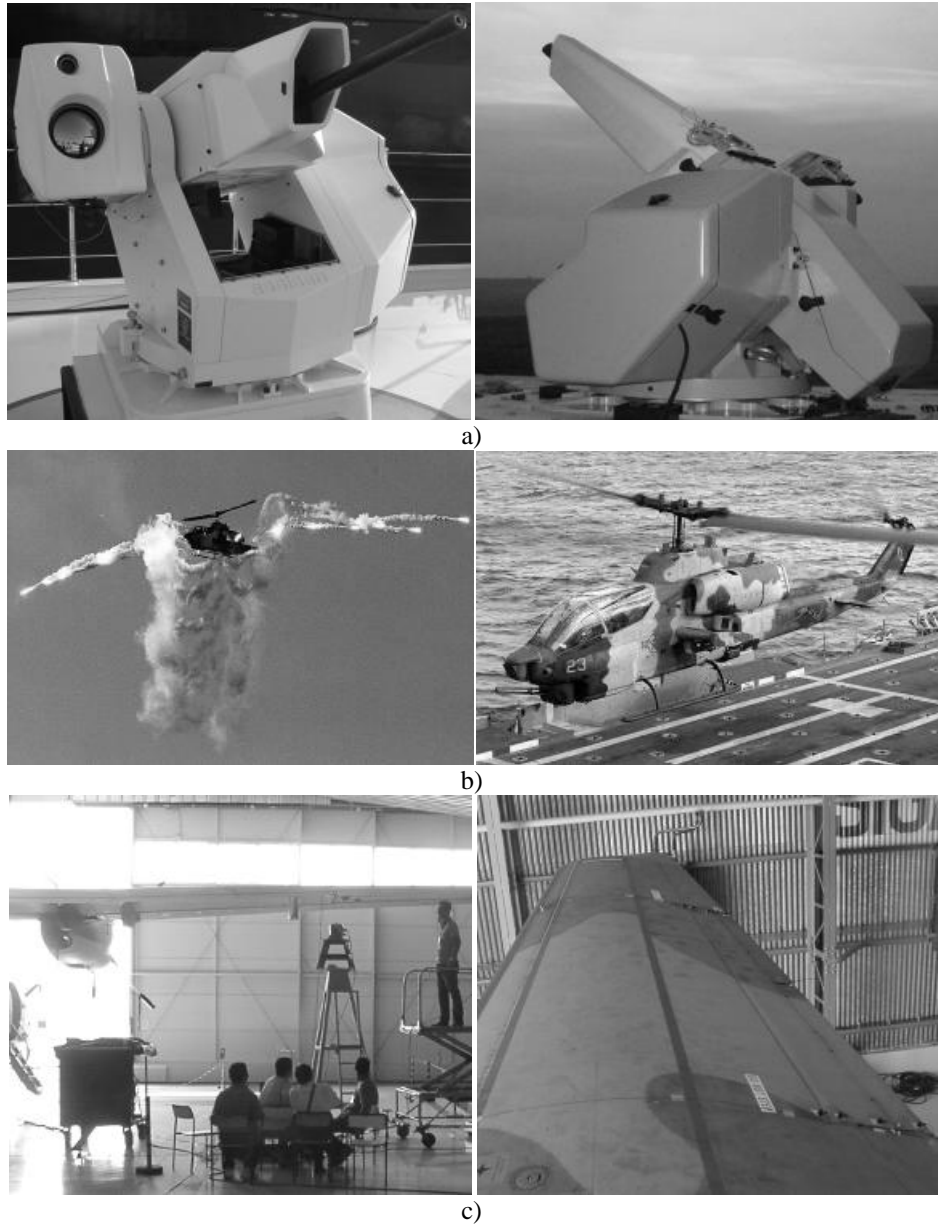


Figure 1-2. Different platforms where vibration is important, a) Weapon turret, b) Attack helicopter, and c) Aircraft control surface

For linear (low forcing, 0.5N amplitude sine) and nonlinear testing, a shaker (Dataphysics) was connected to one end of the stabilizer via a push-rod with a PCB 208C03 force transducer. The vibration responses were measured using six PCB 356A16 accelerometers. The frequency resolution was 0.02 Hz at frequencies close to the resonance and 0.1Hz for the rest. The closed loop control was achieved by the Dataphysics Abaqus data acquisition system. Tests were performed for four different load levels (0.5N, 1.5N, 3N, 4.5N) and the resulting driving point FRF's are given in Figure 1-6.

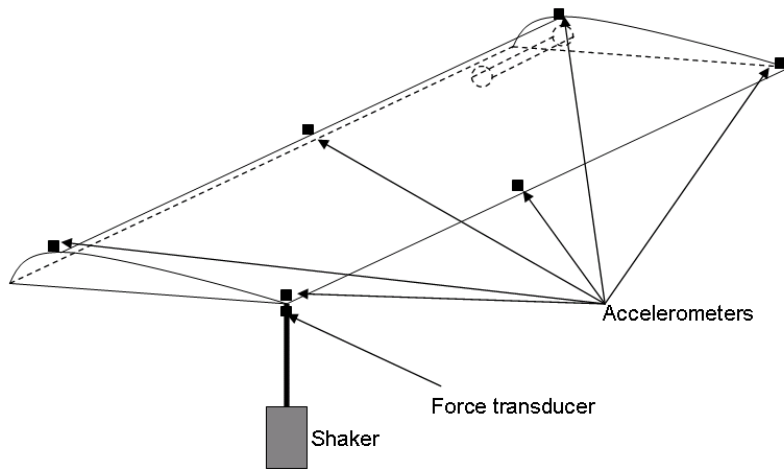


Figure 1-3. Representation of the modal tests performed on the helicopter horizontal stabilizer



Figure 1-4. Modal tests performed on the horizontal stabilizer

Two interesting results can be observed from Figure 1-6. The first shift seems to be of softening stiffness type whereas the second shift is more complicated. Most probably, this phenomenon is due to the existence of more than one type of nonlinearity present in the system.

The boundary condition, i.e. the attachment location, of the horizontal stabilizer is further investigated. Horizontal stabilizer is connected to the tail by a rod which is fitted into a bearing as shown in Figure 1-7.



Figure 1-5. Modal tests performed on the horizontal stabilizer with testing equipment

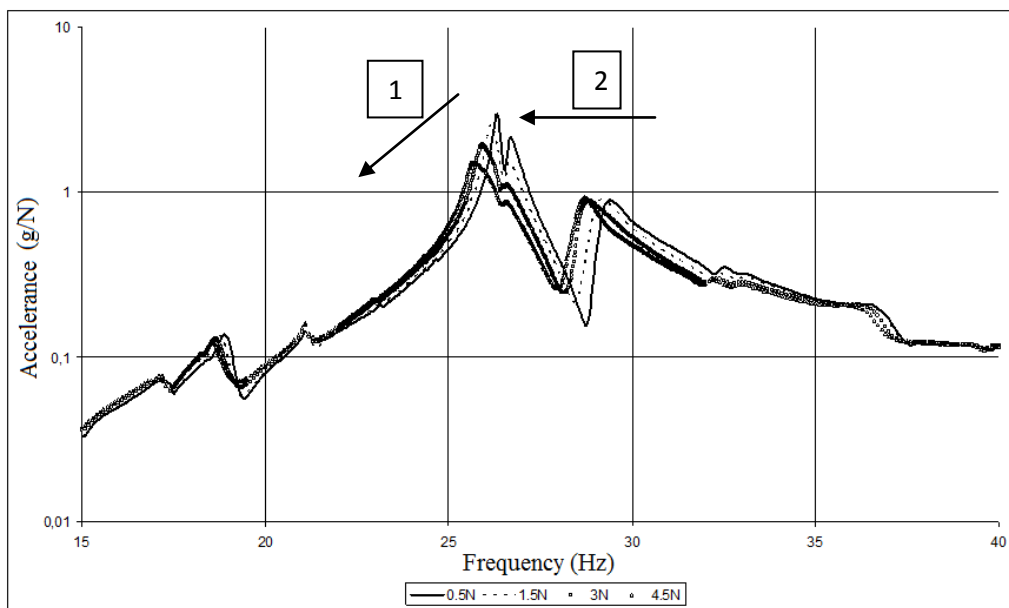


Figure 1-6. Constant force driving point FRF curves

The inner side of the helicopter revealed the simple mechanism which controls the horizontal stabilizer. A push rod controls the angle of the horizontal stabilizer by converting longitudinal motion into angular motion as shown in Figure 1-8.

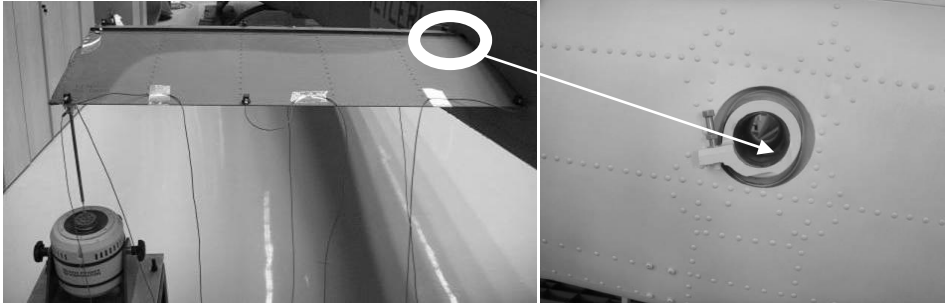


Figure 1-7. Attachment details of the horizontal stabilizer

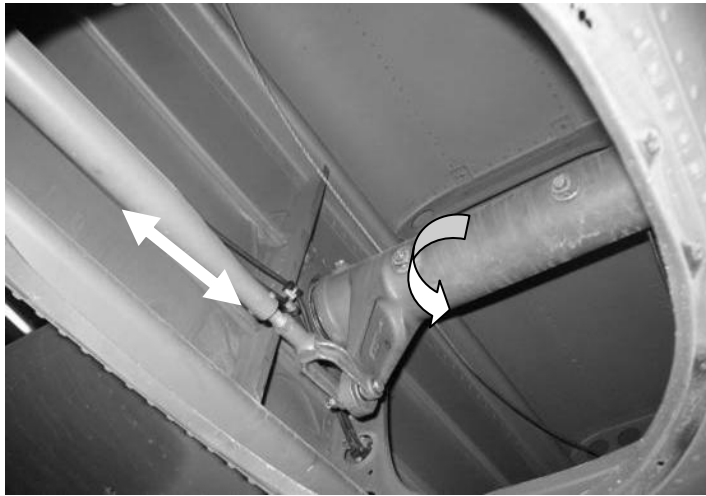


Figure 1-8. Control mechanism of the horizontal stabilizer

This configuration might be causing friction and backlash. Such engineering problems are the motivation behind this study.

### 1.3. Scope of Thesis

The common interest of nonlinear system identification is to identify the nonlinearity locations, types and parameters. Currently, there are several nonlinearity identification tools that provide this information up to different degrees of confidence.

The research presented in this thesis is mainly concerned with the nonlinear system identification from experimental measurements. The overall objective of the research presented in this thesis is to improve the performance of nonlinear system identification technique, Nonlinearity Identification by Describing Functions (DF method), developed by Özer *et al.* [2] for real structures, industrial systems and particularly to the problems associated with nonlinearity identification of experimental models. The specific objectives relevant to this work are:

- to extend the DF method to incomplete experimental models
- to develop a method for type and parameter identification of multiple nonlinearities
- to develop a new more efficient method for direct identification of the nonlinearity from nonlinear FRF measurements
- to apply the DF method to damage localization problems

The outline of each chapter is given below.

#### 1.4. Outline of Thesis

**Chapter 2** presents a comprehensive literature review of several sub topics concerning nonlinear identification.

**Chapter 3** reviews the DF method. Nonlinearity localization and parameter identification are discussed in this chapter with some remarks on the advantages and drawbacks of using of this method. However, although the problems faced by the method are pointed out, no attempt is made to try to solve them yet. Since the work also presents calculated nonlinear responses for the verification of the proposed identification method, single harmonic and multi-harmonic describing function (DF) formulations, and the procedure for nonlinear system response calculation is given. As the multi-harmonic DFs require a defined number of harmonics in the calculation, adaptive multi-harmonic solution method is proposed which adds higher harmonics into the calculations until a defined error criterion is met. Finally, spatial incompleteness in testing is introduced and a well known method is proposed to overcome this problem. Case studies are given with simulated experiments.

**Chapter 4** presents a new method, DFI method, which gives a solution to one of the drawbacks of the DF method. The DF method uses DF plots to determine the type and parameters of nonlinear element. In order to reduce the effort and avoid the limitations in using DF plots for identification of nonlinearity, DF inversion is used. Thus, it is made possible to identify the restoring force of more than one type of nonlinearity without any prior knowledge of the nonlinearities which may co-exist at the same location. If nonlinearities are required to be determined separately, then various possible nonlinear functions and their combinations should be tried to be fitted to the RF function obtained. Some engineering judgment will reduce the effort in trying different combinations. However, if nonlinearities are not required to be determined separately, then simply by curve fitting the RF plot, the coefficients of the total restoring force can be evaluated. Case studies are given with simulated experiments.

**Chapter 5** gives a new more efficient method, DDF, which can perform the nonlinear identification directly from a series of measured nonlinear FRFs without using linear FRFs which was required for the improved DF method. In general applications, the linear model of the system can be obtained by using FEM, and only for the identification of nonlinearity experiments can be made. Alternatively, the FRF of the underlying linear system can be obtained from FRF measurements in the system at very low forcing levels, where the nonlinear internal forces will be negligible. However, if the system has multiple nonlinearities including friction type of nonlinearity, it may be difficult to measure the FRFs of the underlying linear system experimentally, and using finite element model of the system seems to be the only alternative to obtain linear FRFs of the linear counterpart. The method eliminates the requirement of using linear FRFs, and therefore, it works in the presence of friction type nonlinearities by using only the experimental measurements, which is not possible with the improved DF method. Another outcome of this method is that, the true linear FRFs can be calculated using experimentally measured nonlinear FRFs. Case studies are given with simulated experiments.

**Chapter 6** presents validations of the formulations proposed on the previous chapters using experimental case studies. SDOF and MDOF experimental case studies are used with simple beams. The nonlinear elements of a real engineering product are also identified with the proposed methods and presented in this chapter. The accuracy of the identified nonlinear parameters is shown by regenerating the nonlinear responses.

**Chapter 7** discusses the applicability of the improved DF method for detecting and locating crack type structural damage. The verification of the method is demonstrated with experimental case studies using beams with different levels of cracks and a real engineering product.

**Chapter 8** presents the main conclusions derived in the previous chapters emphasizing the contributions and improvements made.

**Chapter 9** gives the suggestions for future work in order to improve the methods developed in this study.

## CHAPTER 2

### LITERATURE REVIEW AND SUMMARY OF THE THESIS

This chapter aims at reviewing the studies in the literature for nonlinear system identification and modeling. The advantages and disadvantages of the methods are discussed and the proposed methods are summarized. Furthermore, damage detection and localization methods are reviewed from a nonlinearity localization point of view.

#### 2.1. Nonlinear System Identification

System identification in structural dynamics has been thoroughly investigated over 30 years [3]. However, most of the studies were limited to the linear identification theories. This literature review does not cover linear identification theories which are well documented [4-5].

In the last decade, with the increasing need to understand nonlinear characteristics of complicated structures, there were several studies published on nonlinear system identification [1,2,6-15]. Nonlinearities can be localized at joints or boundaries or else the structure itself can be nonlinear. There are various types of nonlinearities, such as hardening stiffness, clearance, coulomb friction etc. [1].

Nonlinear system identification methods can be divided into two groups as time and frequency domain methods [2], and time domain methods can be further divided as discrete and continuous time methods [6]. Frequency domain techniques are either in the modal or the state space domain. Furthermore, the frequency domain techniques can include multi-harmonic terms in the response [16-20]. Some authors claim that the effect of such harmonics might be neglected in practice [7] and some add these harmonics to their solution [14,21-23]. The effect of harmonics in the response depends on the investigated frequency. If it is close to harmonics of resonances, then the harmonic terms may become important. However, it should be noted that the fundamental harmonic has the highest weight in the response and the weight of higher harmonics decrease drastically.

The common point of all of the methods is that, they try to detect, locate and identify the nonlinearity. The level of nonlinearity determines the applicability of the methods. The term weak (or light) or strong (or heavy) nonlinearity appears frequently in literature but a standardized terminology is not yet founded. Siller tried in his study [7] to derive the boundaries for weak, moderate and strong nonlinearities. Although the method proposed in his work sounds logical, the limits defined for the boundaries cannot be explained by the author. Therefore, it is difficult to determine the order of the nonlinearity and whether a certain method will work for every case.

The following discussions on the related literature are categorized in groups that will make it easier to visualize the differences between methods and their applicability to real world problems.

The first discussion topic is the excitation types that can be applied to nonlinear modal testing. Many researchers investigated the simplest excitation type, the sine wave. The application of this excitation has many advantages such as high signal to noise ratio and simplicity of control and application. However, the necessity to scan a frequency range with a specified frequency resolution (step sine testing) results in a long testing time which is the main disadvantage of this excitation type. Some methods found in the literature which rely on this type of excitation are presented in [1,2,7,8,11-15,24].

The requirement of long testing time of step sine testing does not usually satisfy the industrial needs. Thus, there are also many studies published [25-32] on random and sine sweep type excitations. The main handicap for random vibration testing is its uncontrolled (random) nature. All random tests performed by the authors resulted in not being able to successfully excite nonlinearity which is also addressed in the literature [6,27]. The reason for this phenomenon can be explained by the fact that the random signal has random levels of load which may not be enough to excite the nonlinearity for the investigated frequency range. The only random profile that can excite nonlinearities in a system may be white noise profile.

The sine sweep testing has also been used in the nonlinear system identification process. The main idea of this method is to combine the speed of sweep test and the controlled nature of sine test [25]. Although it is better than random excitation, sine sweep testing has its own disadvantages. Studies showed that the sweep rate influenced the identified nonlinearity level [26]. As the sweep rate is increased, the identified natural frequency is increased. Therefore, the sweep rate should be kept small in order to avoid this problem. But if the sweep rate is kept small then the main advantage, which is high speed, is lost.

The final type of excitation, transient excitation, has similar disadvantages as the random excitation [4,6]. Therefore, it is not usually preferred in nonlinear system identification.

Besides the type of excitation, an important feature of a nonlinear identification method is the amount of required foreknown data.

Most of the methods available require some foreknown data for the system. Some methods require all or part of mass, stiffness and damping values [8-10] whereas some methods [2,11-14] require the linear frequency response function (FRF) of the analyzed structure. In these methods nonlinearity type is usually foreknown or determined by inspecting the describing function footprints (DFF) visually. However, although the user interpretation may be possible for a single type of nonlinearity, it may not be so easy when there is more than one type of nonlinearity present [1].

The Restoring Force Surface (RFS) method, proposed by Masri *et al.* [10], constitutes one of the first attempts to identify nonlinear structures. A variant of this method was later independently developed by Crawley *et al.* [33,34] and was named as force-state mapping method. Masri *et al.* [35] extended the RFS method to MDOF systems in 1982.

The RFS method requires the time histories of the displacement and the applied force to be measured; however the derivatives of the displacement can also be calculated. Furthermore, sometimes the mass and damping matrices are required. In theory, the RFS method is applicable to MDOF systems. However, a number of practical considerations diminish this capability and its scope is, in fact, bound to systems with a few degrees of freedom only [36].

The RFS method has been studied experimentally for several systems with few degrees of freedom. Kerschen *et al.* [37] demonstrated experimental identification of impacting cantilever beams with symmetrical or asymmetrical piecewise linear stiffness using the RFS method. Another experimental application of the RFS method studied by Kerschen *et al.* [38] was the VTT Technical Research Center of Finland benchmark, which consists of wire rope isolators mounted between a load mass and a base mass. The RFS method was also used in vehicle suspension system characterization [39]. Recently, Noel *et al.* [36] demonstrated the application of RFS method for an elastomeric connection on a real life spacecraft structure. There are studies in the literature obtaining nonlinear RFS [40-41] using variants of RFS method or other similar approaches like neural networks and optimization [6,42]. Application of optimization methods in nonlinear system identification is rather a new and promising approach. The major disadvantage of these methods is generally long computational time requirements.

Nonlinearity identification methods presented in this study consist of four main stages. Firstly, existence of nonlinearity in the system is detected by performing step sine tests with different loads. Secondly, the location of the nonlinearity is determined by using incomplete FRF data. The next step is the determination of the type of nonlinearity which is achieved by investigating the restoring force function. Finally, in the parametric identification stage, the coefficients of the nonlinear elements are obtained by curve fitting techniques. The methods proposed in this study are mainly improved versions of the DF method. The improvements include using incomplete FRF data which makes the method applicable to large systems (Improved Nonlinearity Identification by DFs, improved DF method), and employing DF inversion (Nonlinearity Identification by DF Inversion, DFI) in order to reduce the effort in identification of nonlinearity. Furthermore, using DF inversion rather than DF graphs makes it possible to identify the total restoring force of more than one type of nonlinearity that might co-exist at the same location.

Another additional improvement is to perform the nonlinear identification directly from a series of measured nonlinear FRFs (Direct Nonlinearity Identification by DFs, DDF). The new method eliminates the requirement of linear FRFs and works in the presence of friction type nonlinearities in combination with other type of nonlinearity.

## **2.2. Damage Detection and Localization**

Structural damage is defined as a permanent change in the mechanical state of a structural material that may affect their performance [43]. Common sources of damage in materials and structural components include micro-structural defects (dislocations, voids, inclusions), corrosion (loss of material), residual stress, cracking (fatigue, matrix, ply), fastening fault (weld crack, bolt preload, broken rivet), adhesive fault (de-bonding, delamination, separation), and instability (thermo-mechanical buckling) [43].

Successful damage detection and localization in structures is essential for health monitoring and maintenance. Non-destructive testing methods which can identify damage can be used for this purpose. However, most of the non-destructive methods, such as ultrasonic methods require a suspected location for the damage, and furthermore, that location must be accessible. The methods which use vibration responses usually do not suffer from these limitations.

The basis of vibration response methods is that damage changes the dynamic behavior of the structure. Salawu [44] presented a review on damage detection methods which use the shift in natural frequencies. The measurement of natural frequency changes is very simple but less informative compared to the mode shapes and can lead to wrong crack locations. Thus, methods which use mode shapes and their derivatives for damage detection were developed [45-48]. Recently, Yan *et al.* [49] presented a review for the advances in vibration based damage detection methods. More recent vibration based methods use the basic dynamic information of structures such as FRFs [50] and modal parameters [51-55]. Some of the vibration methods use wavelet analysis [56-58] and some use neural network analysis [59-60]. These methods are based on linear models.

Damage can also add nonlinearity in structural systems which have otherwise linear responses [61]. The most common type of damage which introduces nonlinearity is breathing cracks which behave as bilinear stiffness elements. Many researchers have investigated different aspects of nonlinear damage identification using different approaches. These approaches include, for example, using nonlinear FRFs [62] NARMAX modeling [63], using nonlinear characteristics of forced response of structures [64], and bifurcation boundary analysis [65].

Damage detection method presented in this study consists of two main stages. Firstly, existence of damage in the system is detected by performing step sine tests with different loads. Secondly, the location of the damage is determined by using incomplete FRF data. The work presented in this study is mainly an experimental application of the method suggested by Aydođan [66] which was verified in his work only by simulated data. The approach is based on the improved DF method.



## CHAPTER 3

### IDENTIFICATION OF NONLINEARITY AND NONLINEAR RESPONSE CALCULATION BY USING DESCRIBING FUNCTIONS

This chapter discusses identification of nonlinearity and nonlinear response calculation by DF approach starting from the DF representation of nonlinearity. The renowned Harmonic Balance Method (HBM) which is widely used for approximate linearization of nonlinearities is also discussed in the second section. The last two sections highlight multi harmonic effects on the nonlinear response calculations and spatial incompleteness problem.

#### 3.1. DF Representation of Nonlinearity

DF representation of nonlinear elements [67-70] for linearization of nonlinear differential equations is the core of the methods proposed in this study. As these representations are used throughout this study, a brief introduction to DFs is given in this section.

The equation of motion for a nonlinear MDOF system under harmonic excitation can be written as

$$[M]\{\ddot{x}\} + [C]\{\dot{x}\} + [K]\{x\} + i[H]\{x\} + \{N(x, \dot{x})\} = \{f\} \quad (3.1)$$

where  $[M]$ ,  $[C]$ ,  $[K]$  and  $[H]$  stand for the mass, viscous damping, stiffness and structural damping matrices of the system, respectively. The term  $N(x(t), \dot{x}(t))$  contains all the nonlinear restoring forces which are dependent on response displacement and velocity, and  $\{f\}$  represents the harmonic forcing vector.

The nonlinear elements can be between a coordinate and ground and/or between two coordinates. Then, the elements of the nonlinear internal force vector,  $\{N\}$ , for an “ $n$ ” degrees of freedom system can be written as

$$N_r = \sum_{j=1}^n n_{rj} \quad r = 1, 2, 3 \dots n \quad (3.2)$$

where  $n_{rj}$  represents the nonlinear force element between coordinates  $r$  and  $j$  for  $j \neq r$ , and between the  $r^{\text{th}}$  coordinate and the ground for  $j = r$ . Equation (3.2) considers all possible connection for the nonlinear elements. However, practically, most elements will be zero due having localized nonlinearities. Consequently,  $n_{rj}$  is a function of the displacement  $x_r - x_j$  or  $x_r$  and/or velocity  $\dot{x}_r - \dot{x}_j$  or  $\dot{x}_r$ , according to the location of the nonlinear element. For the sake of simplicity assume that  $n_{rj}$  is a function of displacement only.

For non-grounded coordinates the response will be as

$$x_{rj} = x_r - x_j \quad j \neq r \quad (3.3)$$

Whereas for grounded coordinates the response is given as

$$x_{rj} = x_r \quad j = r \quad (3.4)$$

When the nonlinearity is excited by a harmonic input, then the nonlinear force vector can be expanded via Fourier series. If the responses of the non-grounded coordinates are used, the nonlinear force vector for “ $p$ ” harmonic terms can be represented as

$$n_{rj}(x_{rj}) = \sum_{m=0}^p (n_{rj}(x_{rj}))_m e^{im\omega t} \quad (3.5)$$

where

$$(n_{rj})_{m=0} = \frac{1}{2\pi} \int_0^{2\pi} n_{rj}(x_{rj})_{m=0} d\tau \quad (3.6)$$

$$(n_{rj})_{m \neq 0} = \frac{i}{\pi} \int_0^{2\pi} n_{rj}(x_{rj})_m e^{-im\tau} d\tau \quad (3.7)$$

$$\tau = \omega t \quad (3.8)$$

Furthermore, if the nonlinear element is assumed to be odd, then the dc term (equation (3.6)) diminishes, and if single harmonic response is assumed then equation (3.7) becomes

$$n_{rj}(x_{rj}) = \left( \frac{i}{\pi} \int_0^{2\pi} n_{rj}(x_{rj}) e^{-i\tau} d\tau \right) e^{i\omega t} \quad (3.9)$$

The nonlinear internal force can also be expressed as [71]

$$n_{rj}(x_{rj}) = v\left(\left|X_{rj}\right|\right) X_{rj} e^{i\omega t} \quad (3.10)$$

where

$v$  : DF of the nonlinearity

$X_{rj}$  : Complex amplitude of the nonlinear response

Thus, from equation (3.9) and (3.10), the DF of the nonlinearity,  $v(X_{rj})$ , is obtained as

$$v\left(\left|X_{rj}\right|\right) = \frac{i}{\pi \left|X_{rj}\right|} \int_0^{2\pi} n_{rj}(x_{rj}) e^{-i\tau} d\tau \quad (3.11)$$

Then, using equation (3.11) and (3.10), the nonlinear internal force elements of equation (3.2) can be calculated.

### 3.2. Harmonic Balance Method

HBM is a popular and simple method which is widely used for approximate linearization of nonlinearities. In order to observe the consequences of nonlinear elements when a system is harmonically excited, HBM is an effective method.

Consider the equation of motion for a SDOF nonlinear system as

$$m\ddot{x}(t) + c\dot{x}(t) + kx(t) + N(x(t), \dot{x}(t)) = f(t) \quad (3.12)$$

The nonlinear internal force can be represented by equation (3.5) where the response is assumed to consist of only the first fundamental harmonic as

$$n(x) = \sum_{m=0}^p (n(x))_m e^{im\omega t} \approx n(x)_1 e^{i\omega t} \quad (3.13)$$

$$x = \sum_{m=0}^{\infty} x_m = \sum_{m=0}^{\infty} X_m e^{im\omega t} \approx X_1 e^{i\omega t} \quad (3.14)$$

where  $m$  is the  $m^{\text{th}}$  harmonic and  $X_m$  is the  $m^{\text{th}}$  displacement response amplitude. Note that  $X$  is complex in order to accommodate phase information.

Furthermore, assuming a harmonic forcing such as  $f(t) = Fe^{i\omega t}$ , yields

$$(k - \omega^2 m + i\omega c) X_1 e^{i\omega t} = Fe^{i\omega t} - n(x)_1 e^{i\omega t} \quad (3.15)$$

If the complex response,  $X_1$ , forcing,  $F$ , and internal nonlinear force,  $n(x)_1$ , are written in open form, then the fundamental equation of HBM is obtained as

$$(k - \omega^2 m + i\omega c) (X_1 \sin(\omega t) + iX_1 \cos(\omega t)) = (F \sin(\omega t) + iF \cos(\omega t)) - \dots \quad (3.16)$$

$$\left( \left( \frac{i}{\pi} \int_0^{2\pi} n_{rj}(x_{rj}) e^{-ir} d\tau \right) \sin(\omega t) + i \left( \frac{i}{\pi} \int_0^{2\pi} n_{rj}(x_{rj}) e^{-ir} d\tau \right) \cos(\omega t) \right)$$

The solution of the response,  $X_1$ , is obtained by equating the coefficients of the fundamental harmonics. An application of HBM will be presented with symmetric Duffing's equation for the sake of clarity.

From the symmetric Duffing's equation, the nonlinear restoring force can be defined as

$$N(x(t), \dot{x}(t)) = k_2 x(t)^3 \quad (3.17)$$

where  $k_2$  is the nonlinear stiffness value. If equation (3.17) is substituted into equation (3.12), equation (3.18) is obtained as

$$m\ddot{x}(t) + c\dot{x}(t) + kx(t) + k_2 x(t)^3 = f(t) \quad (3.18)$$

The application of harmonic balance is based on the assumption that a harmonic excitation will result in a harmonic response. Thus, let the excitation be

$$f(t) = F \sin(\omega t - \theta) \quad (3.19)$$

and then the corresponding response can be assumed to be in the form of

$$x(t) = X \sin(\omega t) \quad (3.20)$$

The substitution of excitation and response expressions to equation (3.18) yields

$$-m\omega^2 X \sin(\omega t) + c\omega X \cos(\omega t) + kX \sin(\omega t) + k_2 X^3 \sin^3(\omega t) = F \sin(\omega t - \theta) \quad (3.21)$$

Using the trigonometric equivalent for  $\sin^3(\omega t)$  term we obtain

$$-m\omega^2 X \sin(\omega t) + c\omega X \cos(\omega t) + kX \sin(\omega t) + \dots \quad (3.22)$$

$$k_2 X^3 \left( \frac{3}{4} \sin(\omega t) - \frac{1}{4} \sin(3\omega t) \right) = F \sin(\omega t) \cos(\theta) - F \cos(\omega t) \sin(\theta)$$

By equating the coefficients of the fundamental harmonics ( $\sin(\omega t)$  and  $\cos(\omega t)$ ) equation (3.22) becomes

$$(-m\omega^2 X + kX + \frac{3}{4} k_2 X^3) = F \cos(\theta) \quad (3.23)$$

$$c\omega X = -F \sin(\theta) \quad (3.24)$$

If equation (3.23) and (3.24) are squared and summed, the following equation is obtained.

$$F^2 = X^2 \left[ (-m\omega^2 + k + \frac{3}{4}k_2 X^2)^2 + c^2 \omega^2 \right] \quad (3.25)$$

Further manipulations give

$$\left| \frac{X}{F} \right| = \frac{1}{\left[ (-m\omega^2 + k + \frac{3}{4}k_2 X^2)^2 + c^2 \omega^2 \right]^{1/2}} \quad (3.26)$$

$$\theta = \tan^{-1} \frac{-c\omega}{-m\omega^2 + k + \frac{3}{4}k_2 X^2} \quad (3.27)$$

From equation (3.26) and (3.27) it is evident that the receptance can be written as

$$\alpha(\omega) = \frac{1}{-m\omega^2 + k + \frac{3}{4}k_2 X^2 + ic\omega} \quad (3.28)$$

Hence, it can be concluded that the equivalent stiffness for the Duffing's equation is given as

$$k_{eq} = k + \frac{3}{4}k_2 X^2 \quad (3.29)$$

where the second terms is also the first order DF for the cubic stiffness nonlinearity.

In the above calculations the higher harmonics have been equated to zero. This is the main assumption of this method. However, the effect of higher harmonics can be included by assuming a response with higher order harmonics [6].

### 3.3. Calculation of Harmonic Response of Nonlinear Systems by Using DFs

Representation of nonlinear forces in matrix multiplication form using DFs has been developed and employed in response calculation of MDOF systems with structural nonlinearities by Tanrikulu *et al.* [71] and Ciğeroğlu *et al.* [72]. In this section the method will be briefly reviewed for the sake of completeness.

Let the equation of motion for a nonlinear MDOF system under harmonic excitation to be given as equation (3.1). When there is a harmonic excitation on the system in the form of

$$\{f\} = \{F\} e^{i\omega t} \quad (3.30)$$

The nonlinear internal force can be expressed as [71]

$$\{N(x, \dot{x})\} = [\Delta(|x|, |\dot{x}|)] \{X\} e^{i\omega t} \quad (3.31)$$

where  $[\Delta(|X|, |\dot{X}|)]$  is the response dependent “nonlinearity matrix” and its elements are given in terms of DFs,  $v$ , as follows:

$$\Delta_{rr} = v_{rr} + \sum_{\substack{j=1 \\ r \neq j}}^n v_{rj} \quad r = 1, 2, \dots, n \quad (3.32)$$

$$\Delta_{rj} = -v_{rj} \quad r \neq j \quad r = 1, 2, \dots, n \quad (3.33)$$

At this point, it should be noted that linearization via DF is equivalent to linearization using first order harmonic balance method [1], [3-6]. From the above equations it is possible to write the receptance matrix for the nonlinear system,  $[\alpha^{NL}]$ , as

$$[\alpha^{NL}] = (-\omega^2 [M] + i\omega [C] + i[H] + [K] + [\Delta])^{-1} \quad (3.34)$$

Thus, the nonlinear response of the system can be expressed as

$$\{X\} = [\alpha^{NL}] \{F\} \quad (3.35)$$

Therefore, the nonlinear response of a system for a harmonic excitation can be calculated by using equation (3.35). It should be noted that  $[\alpha^{NL}]$  is a function of displacement and/or velocity. Thus, solving equation (3.35) has to be iterative. The initial guess can start with the linear response and the nonlinear response can be calculated with the  $[\Delta]$  matrix constructed from linear response. Then, the new responses can be used for the calculation of  $[\Delta]$  matrix and a new nonlinear response can be calculated. This goes on until a specified error criterion is converged for the nonlinear response.

#### 3.4. Identification of Nonlinearity Using DFs

Harmonic response calculation method of nonlinear systems presented in the previous section is also used for detection, localization and parametrically identification of nonlinearity in structures. As the basic theory of the DF method is given in detail in reference [2], here it is briefly reviewed.

The receptance matrix of the linear counterpart of the nonlinear system discussed in previous section can be written as

$$[\alpha] = (-\omega^2 [M] + i\omega [C] + i[H] + [K])^{-1} \quad (3.36)$$

From equations (3.34) and (3.36), the nonlinearity matrix can be obtained as

$$[\Delta] = [\alpha^{NL}]^{-1} - [\alpha]^{-1} \quad (3.37)$$

Post multiplying both sides of equation (3.37) by  $[\alpha^{NL}]$  gives

$$[\Delta][\alpha^{NL}] = [I] - [Z][\alpha^{NL}] \quad (3.38)$$

where  $[Z]$  is the dynamic stiffness matrix of the linear part:

$$[Z] = [\alpha]^{-1} = (-\omega^2 [M] + i\omega [C] + i[H] + [K]) \quad (3.39)$$

In order to localize nonlinearity in a system, a parameter called “nonlinearity index” is used. The nonlinearity index (*NLI*) for a  $p^{th}$  coordinate is defined by taking any  $i^{th}$  column of  $[\alpha^{NL}]$  and the  $p^{th}$  row of  $[\Delta]$  from equation (3.38) as follows:

$$NLI_p = \Delta_{p1} \cdot \alpha_{1i}^{NL} + \Delta_{p2} \cdot \alpha_{2i}^{NL} + \dots + \Delta_{pn} \cdot \alpha_{ni}^{NL} \quad (3.40)$$

Here, theoretically, “ $i$ ” can be any coordinate; however, in practical applications it should be chosen as an appropriate coordinate at which measurement can be made and also be close to suspected nonlinear element. Equation (3.40) shows that any nonlinear element connected to the  $p^{th}$  coordinate will yield a nonzero  $NLI_p$ . On the other hand,  $NLI_p$  can be experimentally obtained by using the right hand side of equation (3.38), which requires the measurement of the receptances of the system at high and low forcing levels, presuming that low level forcing will yield FRFs of the linear part:

$$NLI_p = \delta_{ip} - Z_{p1} \cdot \alpha_{1i}^{NL} - Z_{p2} \cdot \alpha_{2i}^{NL} - \dots - Z_{pn} \cdot \alpha_{ni}^{NL} \quad (3.41)$$

As equation (3.41) is frequency dependent,  $NLI$  will also be frequency dependent, and therefore  $NLI$  for a coordinate will have different numerical values at every frequency. Yet, any nonlinearity at a coordinate  $p$  will depict itself as a nonzero  $NLI_p$  value at any frequency. However, it is found the best to use the sum of  $NLI_p$  values calculated at each frequency in the frequency range of interest, rather than using a single value determined at an arbitrary frequency. Throughout this study,  $NLI$  values given in plots for a coordinate are the sum of  $NLI$  values for that coordinate at each frequency in the frequency range of interest.

It can easily be seen from equation (3.41) that to calculate  $NLI$  for a coordinate, we need one column of dynamic stiffness matrix of the linear part of the system corresponding to measurement DOFs, and one row of the nonlinear receptance matrix corresponding to the same DOFs. If dynamic stiffness matrix is to be determined from the inversion of experimentally measured linear FRFs, then whole linear FRF matrix is required. On the other hand, as discussed in [2] in detail, in practical applications, dynamic stiffness matrices are sparse with several zero elements. Since  $NLI$  is a weighted summation of nonlinear receptances (weights being the elements of dynamic stiffness matrix), the nonlinear receptances that are multiplied with zero or small dynamic stiffness matrix elements do not need to be measured. Moreover, the  $NLI$  should be calculated only for coordinates around potential nonlinearities. As nonlinearities are usually due to joints, ground connections, etc., the number of coordinates at which nonlinear FRF measurements are required will be considerably small compared to total DOF of the system.

In order to identify nonlinearities from measured data, equation (3.38) has to be solved for the nonlinearity matrix,  $[\Delta]$ , using linear and nonlinear FRF's.

Assuming that nonlinearities exist between  $r^{th}$  and  $j^{th}$  coordinates, the nonlinearity matrix  $[\Delta]$  can be written as

$$[\Delta] = \begin{bmatrix} \dots & 0 & \dots \\ \vdots & \vdots & \vdots \\ \vdots & \vdots & \vdots \\ 0 & \begin{bmatrix} \nu & -\nu \\ -\nu & \nu \end{bmatrix} & 0 \\ \vdots & \vdots & \vdots \\ \vdots & \vdots & \vdots \\ \dots & 0 & \dots \end{bmatrix} \quad (3.42)$$

Furthermore, the nonlinearity matrix,  $[\Delta]$ , can be written as multiplication of two matrices as

$$[\Delta] = \{\delta_1\} \{\delta_2\}^T \quad (3.43)$$

where;

$$\{\delta_1\} = \begin{bmatrix} 0 \\ \vdots \\ \nu \\ -\nu \\ \vdots \\ 0 \end{bmatrix}, \quad \{\delta_2\} = \begin{bmatrix} 0 \\ \vdots \\ 1 \\ -1 \\ \vdots \\ 0 \end{bmatrix} \quad (3.44),(3.45)$$

The nonlinear response of the system can be expressed as

$$\{X\} = [\alpha^{NL}] \{F\} \quad (3.46)$$

Furthermore, if equation (3.34) is substituted into equation (3.46)

$$\{X\} = [Z + \{\delta_1\} \{\delta_2\}^T]^{-1} \{F\} \quad (3.47)$$

The Sherman-Morrison matrix inversion formula [2] is given as

$$[A + \{u\} \{v\}^T]^{-1} = [A]^{-1} - \frac{[A]^{-1} \{u\} \{v\}^T [A]^{-1}}{1 + \{v\}^T [A]^{-1} \{u\}} \quad (3.48)$$

where  $[A]$  is an  $N \times N$  matrix with full rank and  $\{u\}$  and  $\{v\}$  are  $N \times 1$  vectors. Rewriting equation (3.47) using equation (3.48)

$$\{X\} = \left( [\alpha] - \frac{[\alpha] \{\delta_1\} \{\delta_2\}^T [\alpha]}{1 + \{\delta_1\}^T [\alpha] \{\delta_2\}} \right) \{F\} \quad (3.49)$$

Performing the matrix multiplication the response of every coordinate can be obtained as

$$\begin{bmatrix} X_1 \\ \vdots \\ X_r \\ X_j \\ \vdots \\ X_n \end{bmatrix} = \begin{bmatrix} X_{lin_1} \\ \vdots \\ X_{lin_r} \\ X_{lin_j} \\ \vdots \\ X_{lin_n} \end{bmatrix} - \frac{[\alpha] \{\delta_1\} \{\delta_2\}^T}{1 + \{\delta_1\}^T [\alpha] \{\delta_2\}} \begin{bmatrix} X_{lin_1} \\ \vdots \\ X_{lin_r} \\ X_{lin_j} \\ \vdots \\ X_{lin_n} \end{bmatrix} \quad (3.50)$$

When the nonlinearity is located between the  $r^{th}$  and  $j^{th}$  coordinates, the response of the  $k^{th}$  coordinate can be written from equation (3.50) as;

$$X_k = X_{lin_k} - \frac{(\alpha_{kr} - \alpha_{kj})(X_{lin_r} - X_{lin_j})\nu}{1 + \nu(\alpha_{rr} - 2\alpha_{rj} + \alpha_{jj})} \quad (3.51)$$

and if the DF representation of the nonlinearity “ $\nu$ ” is solved from equation (3.51)

$$\nu = \frac{X_{lin_k} - X_k}{(X_k - X_{lin_k})(\alpha_{rr} - 2\alpha_{rj} + \alpha_{jj}) + (\alpha_{kr} - \alpha_{kj})(X_{lin_r} - X_{lin_j})} \quad (3.52)$$

The DF representation of the nonlinearity “ $\nu$ ” versus response amplitude graph gives a means to interpret the type of nonlinearity and to identify it by curve fitting.

### 3.5. Calculation of Multi-harmonic Response of Nonlinear Systems by Using DFs

The method given in section 3.3. considers the system response to be composed of the first harmonic term only. However, theoretically, the response has infinite harmonic terms in the response due to the nonlinear element. The effect of the higher harmonics in the response varies with the type of nonlinearity and its value. It is important to note that, the higher harmonic terms will not contribute to the response as much as the first harmonic term for weak nonlinear systems.

The response having higher harmonic terms such as  $\sin(2\omega t)$ ,  $\sin(3\omega t)$ , etc. also has the multiplications of these terms such as  $\sin(\omega t)\sin(2\omega t)$ ,  $\sin(\omega t)\sin(3\omega t)$ ,  $\sin(2\omega t)\sin(3\omega t)$ , etc. If the formulations do not include the multiplications, then this type of modeling is called higher harmonic solution. Whereas, when the formulations include these multiplications, this type of modeling is called multi-harmonic modeling [23,73].

The DF modeling which was introduced in section 3.1 used single harmonic DFs. Multi-harmonic response formulations require the DF to be also multi-harmonic. Therefore, the Fourier series expansion of the DF definition is used. The details of the formulations will be given in the next section which is based on the studies given in [23,73].

Finally, the classic multi-harmonic modeling procedure requires the number of harmonics that will be used in the solution to be predefined. An adaptive multi-harmonic solution method is proposed which adds harmonic terms to the response automatically until a predefined error criterion is satisfied. This control works for continuous type of nonlinearities (e.g. cubic stiffness) very well but for discrete type of nonlinearities such as free-play a further modification may be necessary.

#### 3.5.1. Multi-harmonic System Modeling Theory

The differential equation of motion of a MDOF system with nonlinear elements which is harmonically excited is defined as in equation (3.1). Then, up to equation (3.8) the formulations included higher harmonics. Thus, the following derivations will continue from equation (3.8) without removing the higher harmonic terms.

Considering the harmonic forcing,  $\{f\}$ , to be of sinusoidal form, it can be written as

$$\{f\} = \text{Im}(\{F\}e^{i\omega t}) \quad (3.53)$$

where,  $\{F\}$  is the amplitude vector of the forcing. The response to this harmonic force will not be a single sine as it was assumed in the single harmonic solution. But the response will still be periodic. Thus, the response for the grounded coordinates can be represented as a Fourier series by summing the harmonic terms as

$$x_r = \sum_{m=0}^{\infty} \{x_r\}_m = \sum_{m=0}^{\infty} \{X_r\}_m e^{im\omega t} \quad (3.54)$$

where  $m$  is the  $m^{\text{th}}$  harmonic and  $\{X_r\}_m$  is the  $m^{\text{th}}$  displacement response amplitude. Note that  $\{X_r\}$  is complex in order to accommodate phase information.

Thus, the grounded coordinate responses can be approximated to have “ $p$ ” harmonic terms ( $P=\{1,2,3,\dots,p\}$ ) as

$$\tilde{x}_r = \text{Im}\left(\sum_{m=0}^p \{X_r\}_m e^{im\omega t}\right) \quad (3.55)$$

The non-grounded responses ( $r$ - $j$  coordinates) can be obtained in a similar way as

$$x_{rj} = x_r - x_j = \sum_{m=0}^{\infty} \{x_{rj}\}_m = \sum_{m=0}^{\infty} \{X_{rj}\}_m e^{im\omega t} \quad (3.56)$$

The same approximation of restricting the number of harmonics to a set of “ $P$ ” can be applied and by taking the imaginary part of the response the following representation can be obtained.

$$\tilde{x}_{rj} = \text{Im} \left( \sum_{m=0}^P \{X_{rj}\}_m e^{im\omega t} \right) \quad (3.57)$$

where  $\{X_{rj}\}_m$  is the  $m^{\text{th}}$  displacement response amplitude.

Furthermore, nonlinear forces can be represented as harmonic functions of response at the same frequency.

$$n_{rj} = v_{rj} (x_r - x_j) \quad j \neq r \quad (3.58)$$

$$n_{rj} = v_{rj} x_r \quad j = r \quad (3.59)$$

where,  $v$  is the DF of the nonlinearity in the system such that it provides the best average of the true restoring force between coordinates  $r$  and  $j$  or between the coordinate  $r$  and the ground. Then, using equation (3.58) for multi-harmonic terms with the non-grounded coordinates yields

$$(n_{rj})_m = \sum_{l=1}^m (v_{rj})_{ml} (X_{rj})_l \quad j \neq r \quad (3.60)$$

Equation (3.60) can be expanded in matrix form as

$$\begin{Bmatrix} (n_{rj})_1 \\ (n_{rj})_2 \\ \vdots \\ (n_{rj})_m \end{Bmatrix} = \begin{bmatrix} (v_{rj})_{11} & (v_{rj})_{12} & \cdots & (v_{rj})_{1m} \\ (v_{rj})_{21} & (v_{rj})_{22} & \cdots & (v_{rj})_{2m} \\ \vdots & \vdots & \ddots & \vdots \\ (v_{rj})_{m1} & \cdots & \cdots & (v_{rj})_{mm} \end{bmatrix} \begin{Bmatrix} (X_{rj})_1 \\ (X_{rj})_2 \\ \vdots \\ (X_{rj})_m \end{Bmatrix} \quad (3.61)$$

which can be further expanded by using the response coordinate  $x$  as

$$\begin{Bmatrix} (n_r)_1 \\ (n_j)_1 \\ (n_r)_2 \\ (n_j)_2 \\ \vdots \\ (n_r)_m \\ (n_j)_m \end{Bmatrix} = \cdots \quad (3.62)$$

$$\begin{bmatrix} (v_{rj})_{11} & -(v_{rj})_{11} & (v_{rj})_{12} & -(v_{rj})_{12} & \cdots & (v_{rj})_{1m} & -(v_{rj})_{1m} \\ -(v_{rj})_{11} & (v_{rj})_{11} & -(v_{rj})_{12} & (v_{rj})_{12} & \cdots & -(v_{rj})_{1m} & (v_{rj})_{1m} \\ (v_{rj})_{21} & -(v_{rj})_{21} & (v_{rj})_{22} & -(v_{rj})_{22} & \cdots & (v_{rj})_{2m} & -(v_{rj})_{2m} \\ -(v_{rj})_{21} & (v_{rj})_{21} & -(v_{rj})_{22} & (v_{rj})_{22} & \cdots & -(v_{rj})_{2m} & (v_{rj})_{2m} \\ \vdots & \vdots & \vdots & \vdots & \ddots & \vdots & \vdots \\ (v_{rj})_{m1} & -(v_{rj})_{m1} & \cdots & \cdots & \cdots & (v_{rj})_{mm} & -(v_{rj})_{mm} \\ -(v_{rj})_{m1} & (v_{rj})_{m1} & \cdots & \cdots & \cdots & -(v_{rj})_{mm} & (v_{rj})_{mm} \end{bmatrix} \begin{Bmatrix} (X_r)_1 \\ (X_j)_1 \\ (X_r)_2 \\ (X_j)_2 \\ \vdots \\ (X_r)_m \\ (X_j)_m \end{Bmatrix}$$

Equation (3.62) can be written in compact form as

$$\begin{Bmatrix} (n_r)_m \\ (n_j)_m \end{Bmatrix} = \sum_{l=1}^m [\Delta]_{ml}^{rj} \begin{Bmatrix} (X_r)_l \\ (X_j)_l \end{Bmatrix} \quad (3.63)$$

where

$$[\Delta]_{ml}^{rj} = \begin{bmatrix} (v_{rj})_{ml} & -(v_{rj})_{ml} \\ -(v_{rj})_{ml} & (v_{rj})_{ml} \end{bmatrix} \quad (3.64)$$

In order to obtain the DF values,  $(v_{rj})_{ml}$ , equation (3.63) can be solved as

$$(v_{rj})_{ml} = \frac{n_{rj_m} (\tilde{x}_{rj})_l - n_{rj_m} (\tilde{x}_{rj})_{l-1}}{(X_{rj})_l} \quad (3.65)$$

Note that this solution method requires the knowledge of the nonlinearity type and parameters present in the system.

### 3.5.2. Multi-harmonic Nonlinear Response Calculation

The single harmonic nonlinear response calculation was discussed in section 3.3. If we extend the single harmonic response formulations to include multi harmonic DFs and the representation of nonlinear forces, we obtain

$$[\alpha]_m^{-1} \{X\}_m + \underbrace{\sum_{l=1}^m [\Delta]_{ml}}_N \{X\}_l = \{F\}_m \quad (3.66)$$

where

$$[\alpha]_m = (-(m\omega)^2 [M] + im\omega [C] + i[H] + [K])^{-1} \quad (3.67)$$

If m harmonics are used in the solution then equation (3.66) can be written as

$$\begin{pmatrix} [\alpha]_1^{-1} + [\Delta]_{11} & [\Delta]_{12} & \cdots & [\Delta]_{1m} \\ [\Delta]_{21} & [\alpha]_2^{-1} + [\Delta]_{22} & \cdots & [\Delta]_{2m} \\ \vdots & \vdots & \ddots & \vdots \\ [\Delta]_{m1} & [\Delta]_{m2} & \cdots & [\alpha]_m^{-1} + [\Delta]_{mm} \end{pmatrix} \begin{Bmatrix} \{X\}_1 \\ \{X\}_2 \\ \vdots \\ \{X\}_m \end{Bmatrix} = \begin{Bmatrix} \{F\}_1 \\ \{F\}_2 \\ \vdots \\ \{F\}_m \end{Bmatrix} \quad (3.68)$$

The nonlinear response can be obtained by taking the inverse of nonlinear receptance matrix as

$$\begin{Bmatrix} \{X\}_1 \\ \{X\}_2 \\ \vdots \\ \{X\}_m \end{Bmatrix} = \begin{pmatrix} [\alpha]_1^{-1} + [\Delta]_{11} & [\Delta]_{12} & \cdots & [\Delta]_{1m} \\ [\Delta]_{21} & [\alpha]_2^{-1} + [\Delta]_{22} & \cdots & [\Delta]_{2m} \\ \vdots & \vdots & \ddots & \vdots \\ [\Delta]_{m1} & [\Delta]_{m2} & \cdots & [\alpha]_m^{-1} + [\Delta]_{mm} \end{pmatrix}^{-1} \begin{Bmatrix} \{F\}_1 \\ \{F\}_2 \\ \vdots \\ \{F\}_m \end{Bmatrix} \quad (3.69)$$

Equation (3.69) is the extended version of equation (3.35) in terms of multi-harmonic components. Accordingly, the iterative solution procedure is similar to the one given in section 3.3.

### 3.5.3. Adaptive Multi-harmonic Solution Method

The multi-harmonic calculations require the number of multi-harmonic terms that will be included in the solution. As the multi-harmonic terms are usually significant at frequencies close to the harmonics of resonances and insignificant for the other frequencies, an error criterion based adaptive control has been proposed. A predefined error value is set and the solution starts with single harmonic solution. When the error increases then the code automatically adds a higher harmonic to the solution. This method reduces the calculation time as higher harmonics are added only at the frequencies close to the harmonics of resonances. The error criterion is based on the nonlinear force vector  $\{\tilde{N}(x_{rj}, \dot{x}_{rj})\}$ . The percent error for the multi-harmonic solution can be defined as;

$$\%Error = \sum_{k=1}^n \frac{\left| \left\{ \tilde{N}_k(\tilde{x}_{rj}, \dot{\tilde{x}}_{rj}) \right\}_m - \left\{ \tilde{N}_k(\tilde{x}_{rj}, \dot{\tilde{x}}_{rj}) \right\}_{m-1} \right|}{\left\{ \tilde{N}_k(\tilde{x}_{rj}, \dot{\tilde{x}}_{rj}) \right\}_m} \cdot 100 \quad (3.70)$$

where

$n$ : the degree of freedom,

$m$ : number of harmonics.

### 3.6. Case Study: Nonlinearity Identification and Multi-harmonic Response Calculation

The model used for demonstration of the DF method and multi-harmonic response calculation (Figure 3-1) is taken from [74]. The model parameters of the system are as follows

$$m_1 = 1 \text{ kg} \quad k_1 = k_2 = k_3 = 500 \text{ N/m}$$

$$m_2 = 5 \text{ kg} \quad c_1 = c_2 = c_3 = 5 \text{ Ns/m}$$

$$F = 50 \text{ N}$$

$$k'_1 = k'_2 = 80000 \text{ N/m}^3$$

The nonlinear elements at coordinate 1 - ground and coordinate 2 - ground are cubic stiffness type elements.

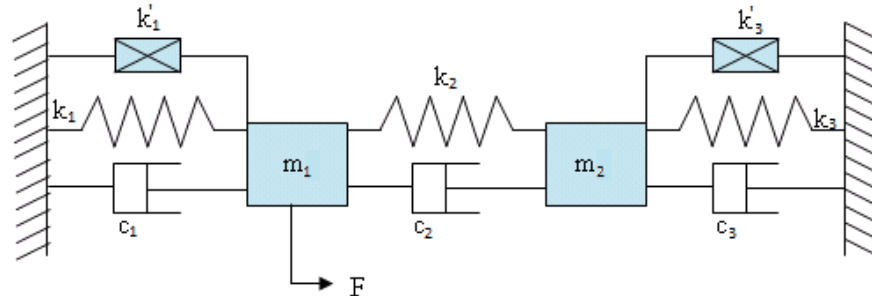


Figure 3-1. 2 DOF nonlinear system with two cubic stiffness nonlinear elements

The harmonic time response of the system is calculated with MATLAB by using the ordinary differential equation solver ODE45. The simulation was run for 32 seconds at each frequency to ensure that transients die out. The frequency range used during the simulations is between 0 and 10 Hz with frequency increments of 0.02 Hz. The above procedure is applied to obtain both linear and nonlinear responses. The linear FRFs are obtained by applying a very low sinusoidal forcing (0.1N) from the first coordinate as presented in Figure 3-1. The nonlinear FRFs are obtained by applying high sinusoidal forcing (50N) to the system from the first coordinate as shown in Figure 3-1.

The system investigated has two nonlinear elements at two separate coordinates which make the Sherman-Morrison solution method given in section 3.4. not applicable. Therefore, equations (3.40) and (3.41), have to be solved simultaneously for the DF,  $v$ , values.

The DF representation of the nonlinearity “ $v$ ” can be graphically shown as a function of response amplitude, which makes it possible to identify the type of nonlinearity and to make parametric identification by using curve fitting. Then the DF is plotted as a function of displacement amplitude (Figure 3-2).

As expected, the curve fitted to the experimental data describes cubic stiffness nonlinearity. The nonlinear stiffness value is obtained from the fitted curve (Figure 3-2) as  $80000 \text{ N/m}^3$ . After identifying the coefficient of the nonlinearity in the system, the multi-harmonic response of the nonlinear system as well as the nonlinear FRFs can be calculated by using the iterative solution method given in section 3.3.

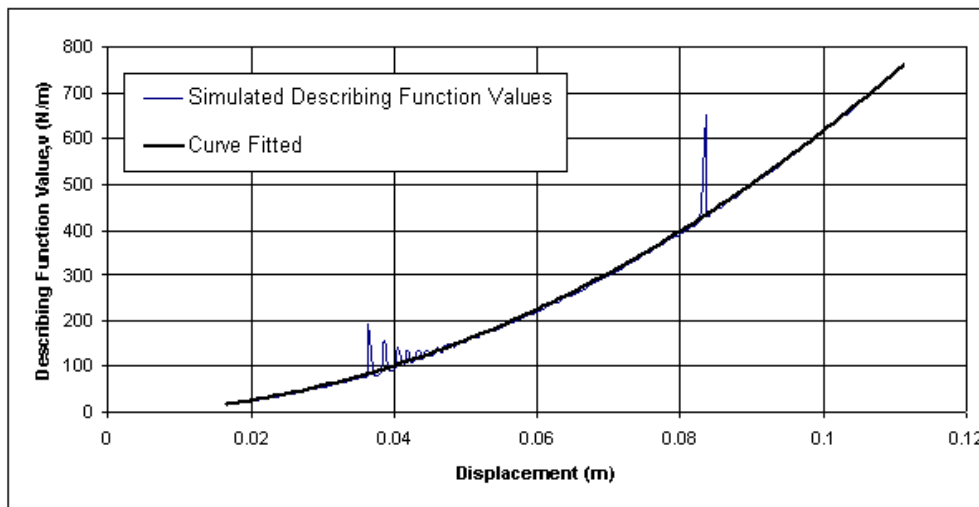


Figure 3-2. Simulated DF values and the fitted curve

The method discussed in section 3.5 is applied with 3 harmonics to show the effect of multi-harmonic terms on the system response. The response consists of the harmonics of  $\sin(\omega t)$ ,  $\sin(3\omega t)$  and  $\sin(5\omega t)$ . Figure 3-3 shows the comparison of FRFs obtained by single and multi-harmonic solution with the time integration results. The FRFs for time integration are obtained by dividing the FFT of the time response by the FFT of the forcing.

The single harmonic solution is not so accurate especially around natural frequencies (around 2.7 Hz and 6.6 Hz) and the sub-harmonic frequency (around 0.7 Hz). Figure 3-4 shows the sub-harmonic frequency region where the single harmonic solution fails to match the time integration solution.

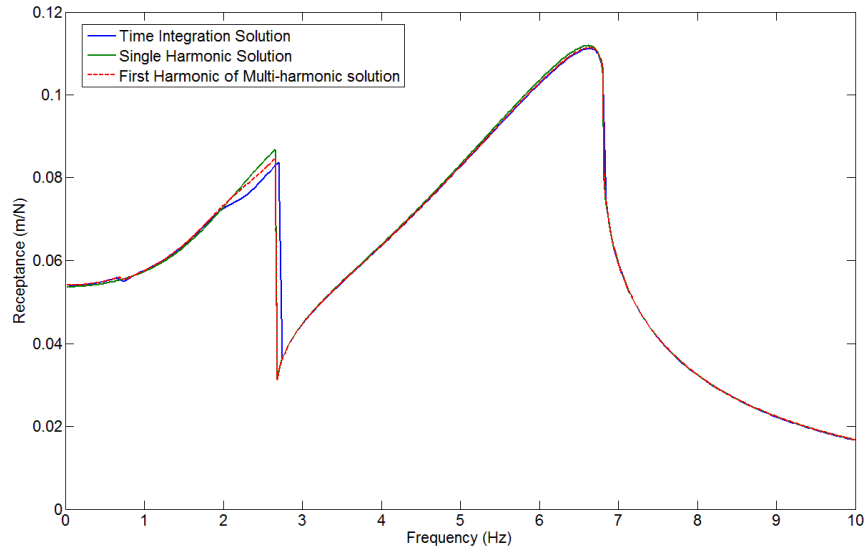


Figure 3-3. Nonlinear FRFs at 50N, blue: Time integration FRF, green: Single harmonic FRF, red: multi-harmonic 1<sup>st</sup> harmonic FRF (of 3 harmonics)

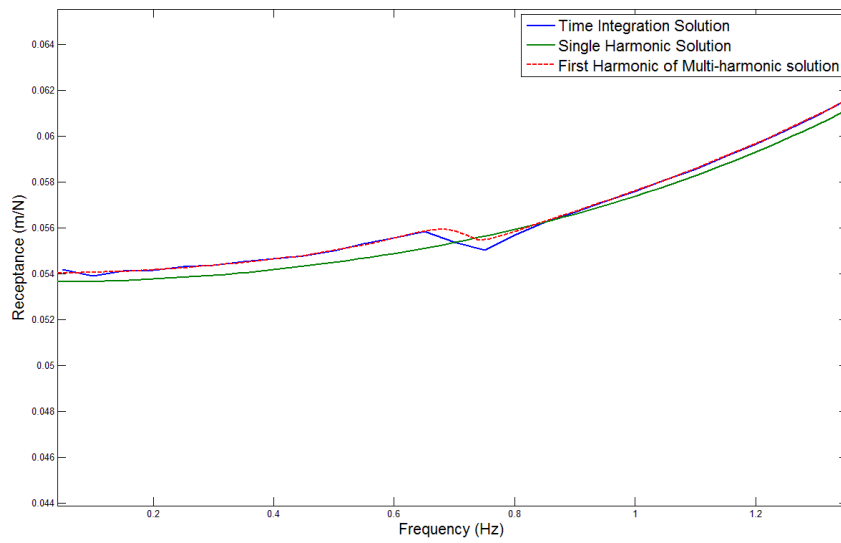


Figure 3-4. Nonlinear FRFs at 50N, one third of the first natural frequency, blue: Time integration FRF, green: Single harmonic FRF, red: multi-harmonic 1<sup>th</sup> harmonic FRF (of 3 harmonics)

The phase plot (Figure 3-5) shows also that there is a better correlation between multi-harmonic solution and time integration than the single harmonic solution.

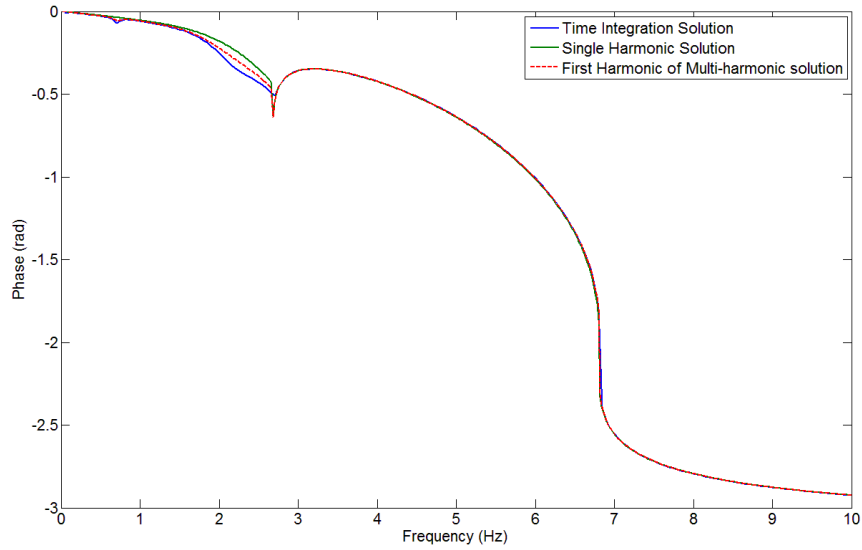


Figure 3-5. Nonlinear phases at 50N, blue: Time integration phase, green: Single harmonic phase, red: multi-harmonic 1<sup>th</sup> harmonic phase (of 3 harmonics)

Finally, a specific frequency of 2 Hz is chosen which is close to the first resonance (around 2.7 Hz at 50N forcing level) to compare the time responses of all the methods. Figure 3-6 shows the time integration, single and multi-harmonic responses. It is evident that as higher harmonic terms are included to the response, the solution will converge to response obtained by time integration. Considering these plots, it can be concluded that the response may not be accurately represented by the single harmonic component when the frequencies of interest are close to the resonances and/or harmonics of resonances.

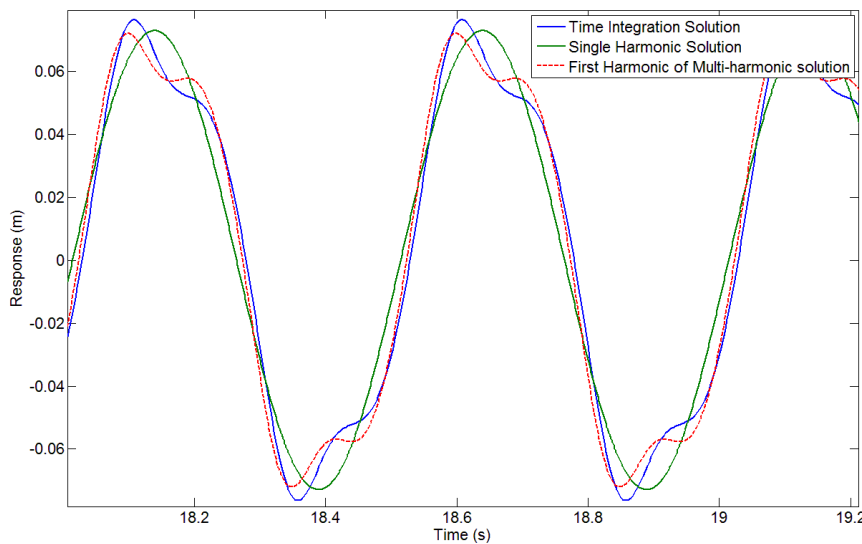


Figure 3-6. Nonlinear time responses at 2 Hz, blue: Time integration response, green: Single harmonic response, red: multi-harmonic total response (of 3 harmonics)

### 3.7. Spatial Incompleteness and FRF Synthesis with an Application

In modal testing of complicated structures usually a shaker is attached to a specific location on the test structure and measurements are made at several locations. These measurement locations must be chosen such that they are not on the nodal points of the mode shapes under interest. Figure 3-7 shows first two mode shapes of a beam and a nodal point. The beam example will be used to discuss the spatial incompleteness definition.

Usually test engineer excites the structure from 1 or 2 locations and measures responses from many points using accelerometers. This yields 1 or 2 columns of the FRF matrix. For example, for the beam example given in Figure 3-7, the receptance matrix, considering 3 measurement points, will be

$$[\alpha] = \begin{bmatrix} \alpha_{11} & ? & ? \\ \alpha_{21} & ? & ? \\ \alpha_{31} & ? & ? \end{bmatrix} \quad (3.71)$$

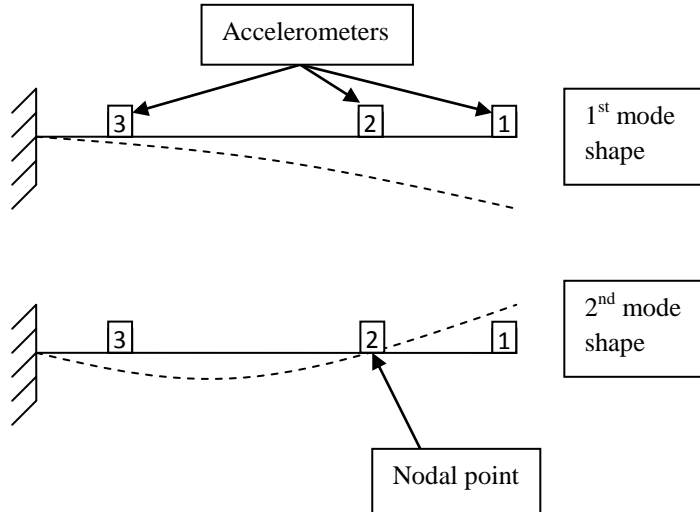


Figure 3-7. Nodal point representation

The number of unknown receptances can be reduced if reciprocity is used, which is one of the main assumptions of linearity. Then,

$$[\alpha] = \begin{bmatrix} \alpha_{11} & \alpha_{12} & \alpha_{13} \\ \alpha_{21} & ? & ? \\ \alpha_{31} & ? & ? \end{bmatrix} \quad (3.72)$$

where from reciprocity,

$$\begin{aligned} \alpha_{12} &= \alpha_{21} \\ \alpha_{13} &= \alpha_{31} \end{aligned} \quad (3.73)$$

However, there will be still unknown terms in the FRF matrix, especially the ones related with rotational degrees of freedom may be missing. Although there are various methods to obtain FRFs at rotational degrees of freedom [75], measuring FRFs for rotational degrees of freedom is usually found very difficult and it is avoided.

Having missing FRFs due to not exciting the structure from all coordinates is called as Spatial Incompleteness. The traditional way of dealing with spatial incompleteness is either to assume that those elements are insignificant or to create a numerical or analytical model of the test structure and update it using the spatially incomplete data. Then this updated model is used to obtain the full FRF matrix. This method is very difficult due to the trials needed to update the numerical model correctly.

Incomplete FRF matrix is indeed very troublesome to handle. Rotational degrees of freedom elimination is not as bad as not exciting the structure from all coordinates. The reason is that, when rotational degrees of freedoms are eliminated, the resulting FRF matrix is still square and mathematically usable. However, when the structure is not excited from all coordinates, the resulting FRF matrix is not square.

In order to obtain the missing elements of the experimentally obtained receptance matrix, the application of a well known method is proposed. Theoretically, if the modal parameters (natural frequency, damping ratio, modal constant, lower and upper residues) of a structure are obtained by linear modal identification, then missing elements of the receptance matrix can be synthesized.

Synthesis of the unmeasured elements of the FRF matrix can be summarized in the flow chart given in Figure 3-8.

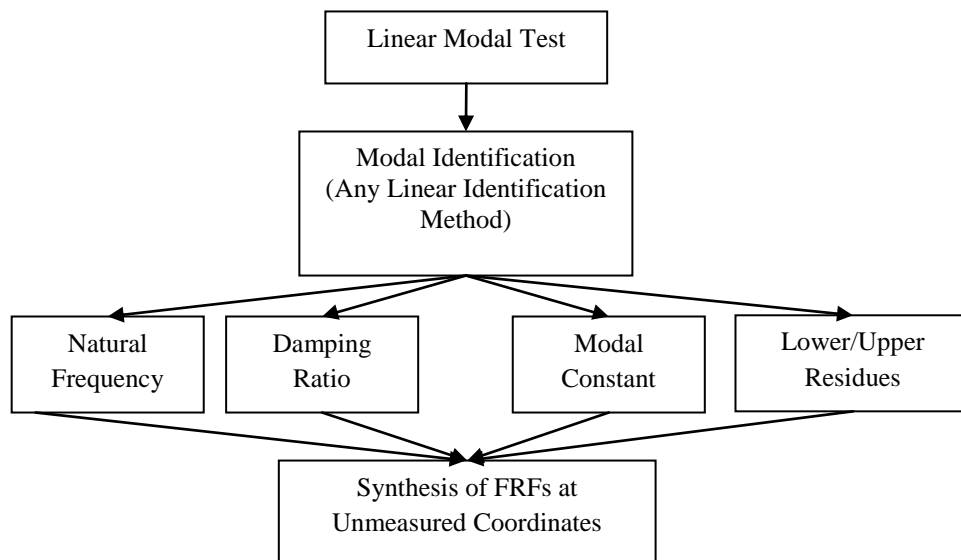


Figure 3-8. Synthesis process of the unmeasured coordinates

In this study the linear modal identification is performed in the LMS Test Lab software. LMS Test Lab software utilizes a further evolution of the least-squares complex frequency domain estimation method [76] which is called PolyMAX. The details of this method can be found in the manual of the software [77].

During this identification process natural frequencies, damping ratios and scaled modal constants are identified. Furthermore, during the identification a frequency band is selected so that lower and upper residues are also calculated. In order to synthesize the unmeasured FRFs, the scaled modal constants must be separated to modal constants and the scaling factor. The derivation of this process is given below.

LMS Test Lab uses the Laplace domain transfer function representation [4]. Therefore, derivation of the FRF of a SDOF system from Laplace transfer yields

$$\alpha(\omega) = \frac{A}{i(\omega - \omega_d) + \zeta\omega_n} + \frac{A^*}{i(\omega + \omega_d) + \zeta\omega_n} \quad (3.74)$$

where

$$\begin{aligned} \omega_n &: \text{Undamped natural frequency} \\ \omega_d &= \omega_n \sqrt{1 - \zeta^2} : \text{Damped natural frequency} \\ \zeta &: \text{Damping ratio} \end{aligned} \quad (3.75)$$

The complex conjugates  $A, A^*$  are defined as the scaled modal constants of the FRF and can be obtained as

$$A = \frac{1}{i2\omega_d m} \quad (3.76)$$

For a MDOF system the scaled modal constant  $A_{ij}^k$ , between  $i^{th}$  and  $j^{th}$  location of mode  $k$ , can be written as the product of a scaling factor  $a_k$  (independent of the location) and the modal vector components in both locations.

$$A_{ij}^k = a_k u_i^k u_j^k \quad (3.77)$$

where,

$$a_k = \frac{1}{i2\omega_d^k m^k} \quad (3.78)$$

$$\omega_d^k = \omega_n^k \sqrt{1 - (\zeta^k)^2} : \text{Damped natural frequency of mode } k \quad (3.79)$$

$m^k$ : Modal mass of mode  $k$

$\omega_n^k$ : Undamped natural frequency of mode  $k$

$\zeta^k$ : Damping ratio of mode  $k$

The damping type defines whether the modal vector will be real or complex. If the damping is proportional then the modal vectors will be real, thus the modal constants will be imaginary. Therefore the scaling factor will also be imaginary. If the damping is not proportional then modal vectors, modal constants and the scaling factor will be complex.

The most common scaling that is applied is the unit modal mass scaling (i.e. mass normalization).

$$m^k = 1 \quad (3.80)$$

Thus the scaling factor (equation (3.78)) becomes;

$$a_k = \frac{1}{i2\omega_d^k} \quad (3.81)$$

If this scaling factor is used;

$$A_{ij}^k = \frac{1}{i2\omega_d^k} \phi_i^k \phi_j^k \quad (3.82)$$

where,

$\phi$ : Modal Vector

Further manipulations yield modal constants as

$$\phi_i^k \phi_j^k = A_{ij}^k i2\omega_d^k \quad (3.83)$$

If the driving point scaled modal constant is used (i.e.  $i = j$ )

$$(\phi_i^k)^2 = A_{ii}^k i2\omega_d^k \quad (3.84)$$

Then, mass normalized complex eigenvector for the driving point can be found. The other eigenvectors can be simply found from equation (3.83) with the knowledge of the mass normalized complex eigenvector for the driving point.

The FRF formulation with the scaled modal constants for viscously damped systems can be defined as;

$$\alpha_{ij}(\omega) = \sum_{k=1}^N \frac{A_{ij}^k}{\omega_n^k \zeta^k + i(\omega - \omega_n^k \sqrt{1 - (\zeta^k)^2})} + \frac{(A_{ij}^k)^*}{\omega_n^k \zeta^k + i(\omega + \omega_n^k \sqrt{1 - (\zeta^k)^2})} \quad (3.85)$$

where,

$N$ : Number of modes considered

If we substitute equation (3.79) and (3.82) into equation (3.85), unmeasured receptance  $\alpha_{ij}(\omega)$  can be calculated as

$$\alpha_{ij}(\omega) = \sum_{k=1}^N \frac{\frac{1}{i2\omega_n^k \sqrt{1 - (\zeta^k)^2}} \phi_i^k \phi_j^k}{\omega_n^k \zeta^k + i(\omega - \omega_n^k \sqrt{1 - (\zeta^k)^2})} + \frac{(\frac{1}{i2\omega_n^k \sqrt{1 - (\zeta^k)^2}} \phi_i^k \phi_j^k)^*}{\omega_n^k \zeta^k + i(\omega + \omega_n^k \sqrt{1 - (\zeta^k)^2})} \quad (3.86)$$

Furthermore, if the upper and lower residuals are included into equation (3.86) we obtain the final form as

$$\alpha_{ij}(\omega) = \sum_{k=1}^N \frac{\frac{1}{i2\omega_n^k \sqrt{1 - (\zeta^k)^2}} \phi_i^k \phi_j^k}{\omega_n^k \zeta^k + i(\omega - \omega_n^k \sqrt{1 - (\zeta^k)^2})} + \dots \quad (3.87)$$

$$\frac{(\frac{1}{i2\omega_n^k \sqrt{1 - (\zeta^k)^2}} \phi_i^k \phi_j^k)^*}{\omega_n^k \zeta^k + i(\omega + \omega_n^k \sqrt{1 - (\zeta^k)^2})} + UR_{ij} - \frac{LR_{ij}}{\omega^2}$$

This formulation is the basis for the synthesis of the receptances for the unexcited coordinates. Once the modal parameters (natural frequency,  $\omega_n^k$ , damping ratio,  $\zeta^k$ , scaled modal constant,  $A_{ij}^k$ , lower/upper residues) are obtained from linear identification tools, equation (3.87) is used to obtain the unmeasured elements of the FRF matrix.

In order to show that FRF synthesis method is practical and applicable, a simulated “test” will be considered. The FRF synthesis method is performed on a four degree of freedom system, shown in Figure 3-9.

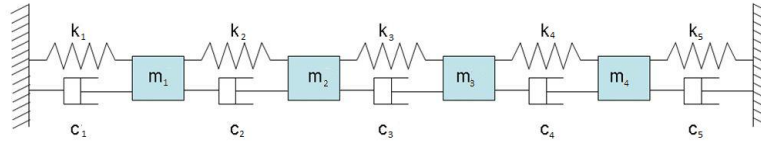


Figure 3-9. Four-DOF example model for FRF synthesis of a noise free system

where,

$$k_1 = k_2 = k_3 = k_4 = k_5 = 500 \text{ N/m}$$

$$c_1 = c_2 = c_3 = c_4 = c_5 = 5 \text{ Ns/m}$$

$$m_1 = 1 \text{ kg}, m_2 = 2 \text{ kg}, m_3 = 3 \text{ kg}, m_4 = 5 \text{ kg}$$

The simulated “test” FRF values are obtained by matrix inversion. Only the first column of the FRF matrix is used in the modal identification process (i.e.  $\alpha_{11}, \alpha_{21}, \alpha_{31}, \alpha_{41}$ ). The driving point FRF ( $\alpha_{11}$ ) is shown in Figure 3-10. In practical applications most of the time a specific frequency range is under consideration. The analysis frequency range should be chosen by considering the out-of-band effects. The out-of-band effects are caused by modes below and above the analysis band. The unmeasured modes can be compensated by upper and lower residuals. However such compensation cannot be made for the unmeasured FRFs. Thus, the frequency band should be wide enough so that the out-of-band effects are not disturbing the analysis. As it can be clearly seen from Figure 3-10, the modes are very close to each other. Therefore, the whole frequency band is chosen for modal identification. Otherwise, small errors that may seem insignificant in FRF plots may easily be magnified when FRF matrix is inverted to obtain the dynamic stiffness matrix. This may lead to errors in localization and identification of nonlinearity.

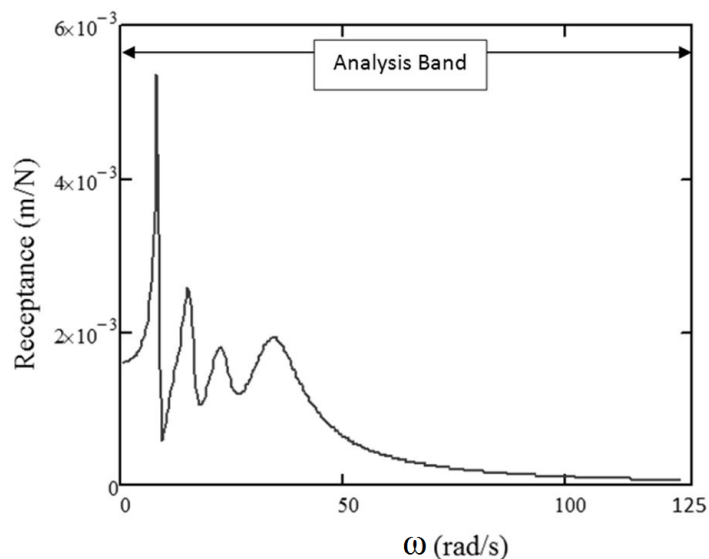


Figure 3-10. Driving point linear FRF

The modal parameters (natural frequency, damping ratio, and scaled modal constants) and lower/upper residuals were identified using receptances  $\alpha_{11}$ ,  $\alpha_{21}$ ,  $\alpha_{31}$  and  $\alpha_{41}$  by LMS Test Lab PolyMAX identification method as given below:

$$\omega_n^1 = 1.308 \text{ Hz}, \omega_n^2 = 2.482 \text{ Hz}, \omega_n^3 = 3.631 \text{ Hz}, \omega_n^4 = 5.417 \text{ Hz}$$

$$\zeta^1 = 0.0412, \zeta^2 = 0.0782, \zeta^3 = 0.1149, \zeta^4 = 0.1729$$

$$\phi^1 = \begin{bmatrix} 0.1646 + 0.00004145i \\ 0.3070 + 0.0001168i \\ 0.3663 + 0.0001771i \\ 0.2768 + 0.0001467i \end{bmatrix}, \phi^2 = \begin{bmatrix} -0.2681 + 0.0001203i \\ -0.4053 + 0.0001051i \\ -0.1461 - 0.00005879i \\ 0.3276 - 0.000128i \end{bmatrix},$$

$$\phi^3 = \begin{bmatrix} -0.3779 + 0.0002021i \\ -0.358 - 0.0001406i \\ 0.4169 - 0.0002271i \\ -0.1272 + 0.00008844i \end{bmatrix}, \phi^4 = \begin{bmatrix} 0.8709 + 0.00001343i \\ -0.3376 + 0.0004567i \\ 0.06667 - 0.0001865i \\ -0.006768 - 0.00002484i \end{bmatrix}$$

$$LR = \begin{bmatrix} 0.0000001222 \\ 0.0000001512 \\ 0.00000009833 \\ 0.00000005022 \end{bmatrix}, UR = \begin{bmatrix} 0.000001065 \\ 0.0000002104 \\ 0.0000001095 \\ 0.00000003525 \end{bmatrix}$$

These values are used in equation (3.87) to obtain  $\alpha_{11}$  as

$$\alpha_{11}(\omega) = \sum_{k=1}^4 \frac{1}{i2\omega_n^k \sqrt{1-(\zeta^k)^2} \omega_n^k \zeta^k + i(\omega - \omega_n^k \sqrt{1-(\zeta^k)^2})} \phi_1^k \phi_1^k + \dots$$

$$\frac{(\frac{1}{i2\omega_n^k \sqrt{1-(\zeta^k)^2}} \phi_1^k \phi_1^k)^*}{\omega_n^k \zeta^k + i(\omega + \omega_n^k \sqrt{1-(\zeta^k)^2})} + UR_{11} - \frac{LR_{11}}{\omega^2}$$
(3.88)

Substituting the corresponding values yields regenerated  $\alpha_{11}$ , which is compared with the original  $\alpha_{11}$  as shown in Figure 3-11.

Furthermore, the point receptance  $\alpha_{44}$  for the unexcited coordinate ( $\alpha_{44}$ ) is also synthesized by using equation (3.87). Original and synthesized  $\alpha_{44}$  curves are compared in Figure 3-12.

### 3.8. Nonlinearity Localization from Spatially Incomplete FRF Data

The main disadvantage of the DF method presented in section 3.4. is that in order to calculate the *NLI* the complete linear FRF matrix may be required (if instead of theoretically calculated dynamic stiffness matrix, inverse of experimentally measured receptance matrix is used). When this is the case, it may not be feasible to apply the method. In this study, it is proposed to use theoretically predicted values for unmeasured receptances calculated from the measured ones (improved DF method), and it is shown with case studies that this approach yields acceptable results.

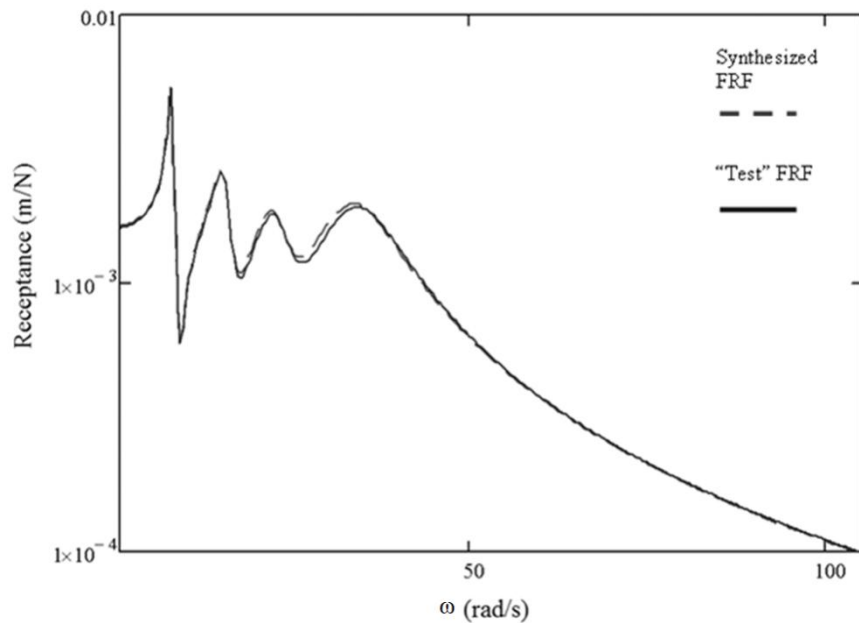


Figure 3-11. Driving point “test” and synthesized FRF

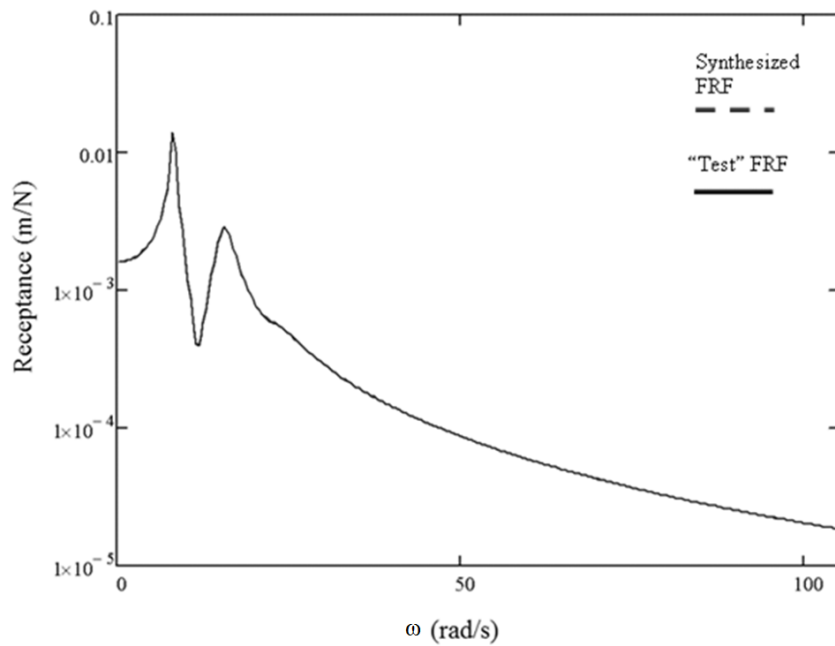


Figure 3-12.  $a_{44}$  “Test” and synthesized FRF

Nonlinearity localization by using the right hand side of equation (3.41) requires either the system matrices (that can be obtained from the FE model) or the complete receptance matrix of the linear part so that it can be inverted to find the dynamic stiffness matrix,  $[Z]$ . The flowchart of the FRF synthesis and its application for nonlinearity localization is given in Figure 3-13.

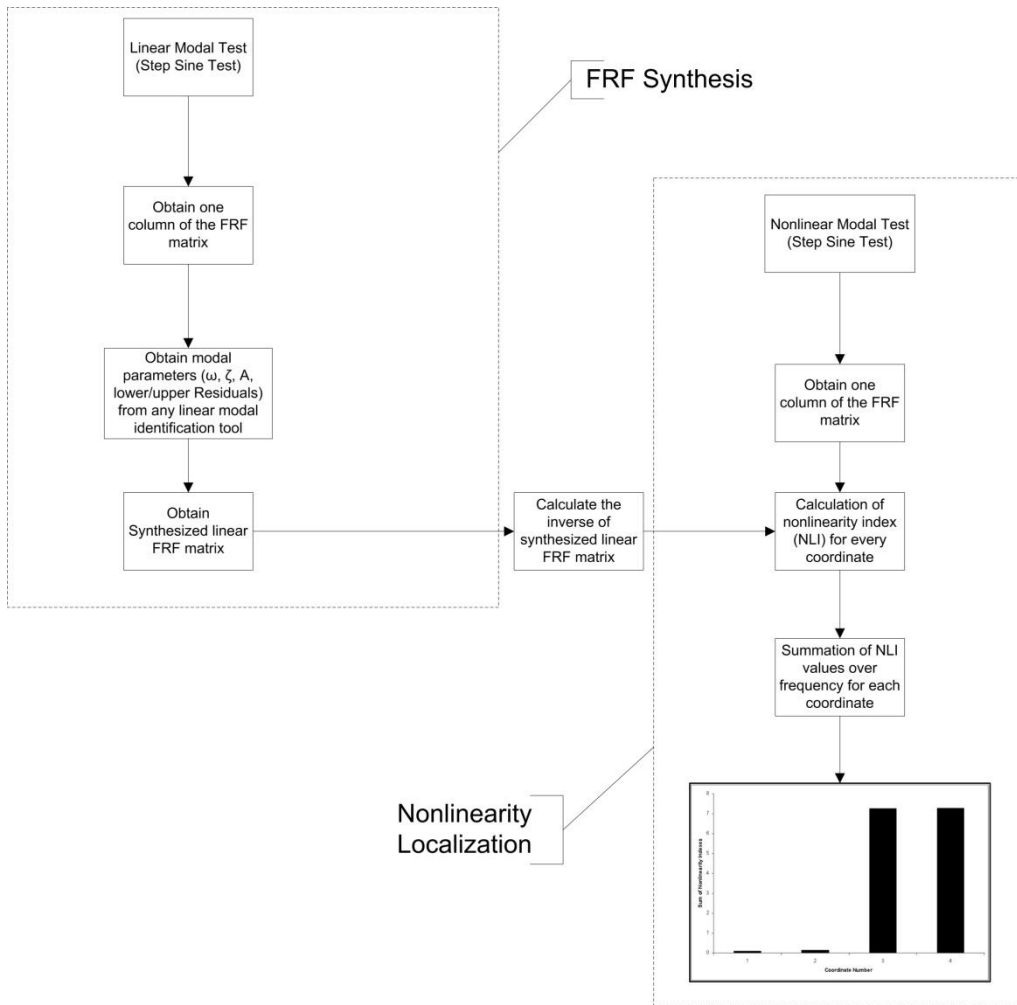


Figure 3-13. FRF synthesis and nonlinearity localization flow

### 3.8.1. Case Study 1: Nonlinearity Localization from Spatially Incomplete Noise Free FRFs

In order to demonstrate the application of the improved DF method, the numerical model given in Figure 3-9 with a nonlinear cubic hardening spring ( $k_4' = 10^6 \text{ N/m}^3$ ) between coordinates 3 and 4 is considered (Figure 3-14).

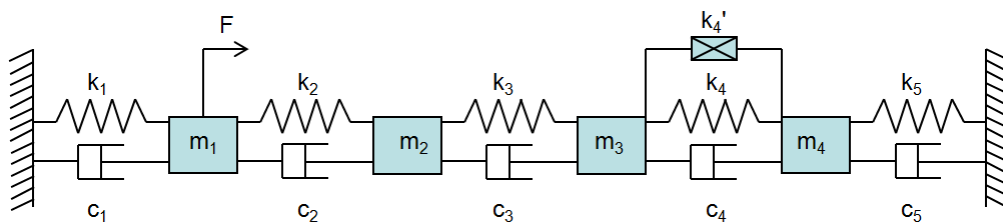


Figure 3-14. Four-DOF example model with nonlinear element for nonlinearity localization from spatially incomplete noise free FRFs

First, the time response of the system is calculated with MATLAB by using the ordinary differential equation solver ODE45. The simulation is run for 32 seconds at each frequency to ensure that transients die out. The frequency range used during the simulations is from 0 to 20 Hz with frequency increments of 0.0625 Hz. The above procedure is applied to obtain both linear and nonlinear responses. The linear FRFs are obtained by applying a very low sinusoidal forcing (0.1N) and nonlinear FRFs are obtained by applying high sinusoidal forcing (10N) to the system from the first coordinate as presented in Figure 3-14. A sample comparison for the linear and nonlinear FRFs of  $\alpha_{11}$  is given in Figure 3-15.

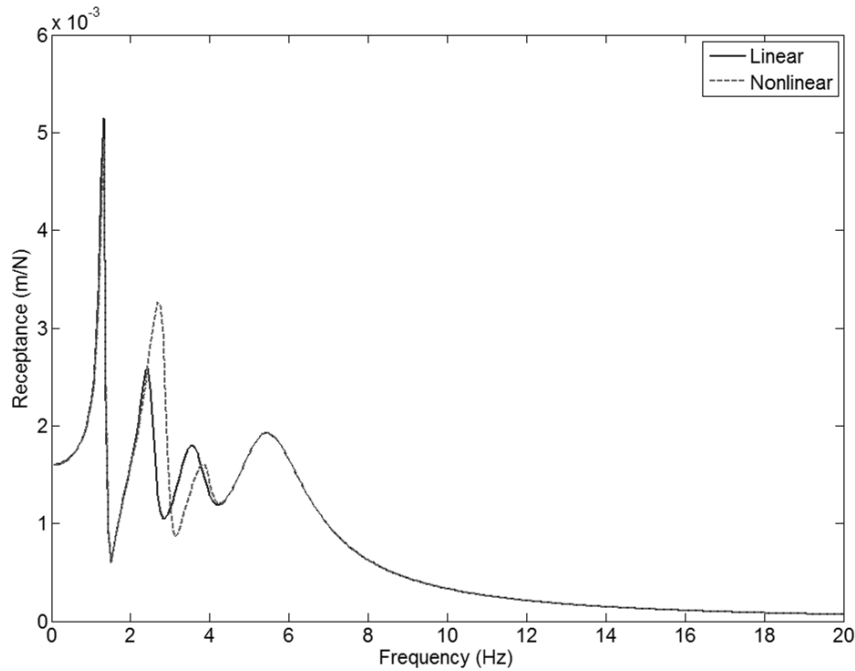


Figure 3-15. Nonlinear and linear FRF ( $\alpha_{11}$ ) comparison

The improved DF method is applied and the *NLI* for each coordinate is calculated and summed over the frequency interval 0 to 20 Hz where the linear FRF is synthesized by equation (3.87) using only the first column of linear FRFs. The sum of *NLI* for each coordinate is given in Figure 3-16.

The results show that there is a nonlinear element between coordinates 3 and 4 or there are two nonlinear elements at coordinates 3 and 4 respectively. This problem can be solved by physically checking the structure under consideration whether or not there is a connection between coordinate 3 and 4, etc. If there is a connection between two coordinates it may be a nonlinear element in between, otherwise it indicates nonlinear elements between 3 and ground, and between 4 and ground, etc. When this is not obvious, another approach would be to regenerate the nonlinear FRF with the identified nonlinearity and compare it with the measurement. A match will be obtained only for correct localization and identification. In order to compare the FRF synthesis method with the exact values, all of the linear FRFs are obtained by matrix inversion and *NLI* values are calculated. Then, the *NLI* values obtained from FRF synthesis method are compared with the *NLI* values obtained from the exact linear FRFs (Figure 3-17).

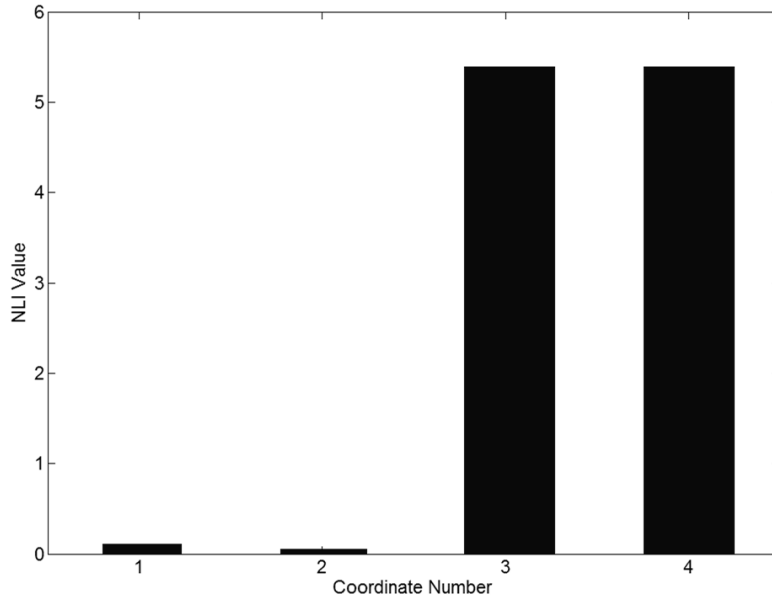


Figure 3-16. Sum of nonlinearity indexes for measurement coordinates

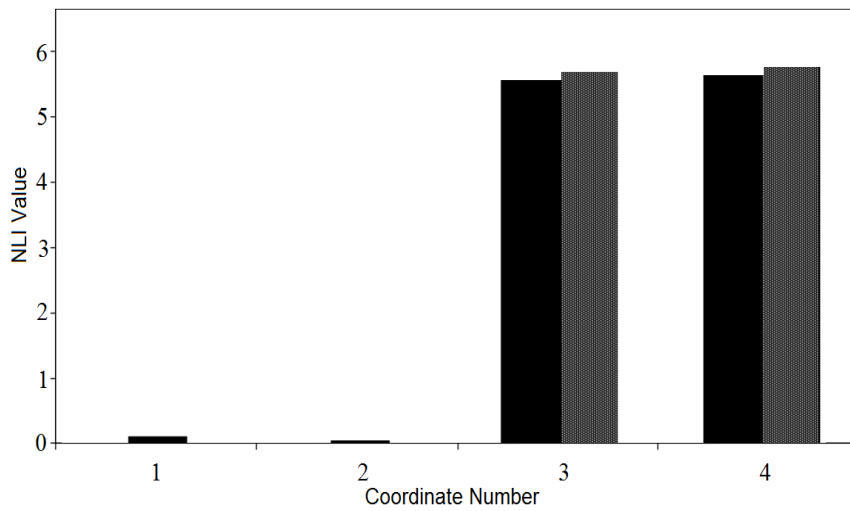


Figure 3-17. Comparison of the nonlinearity indexes obtained by using synthesized and exact FRF values. (Black: Using synthesized FRFs; Gray: Using exact FRFs)

### 3.8.2. Case Study 2: Nonlinearity Localization from Spatially Incomplete FRF Data with Noise #1

The improved DF method is also tested in the presence of random noise by using the “normrnd” function of MATLAB with zero mean, normal distribution and standard deviation of 0.0025 m which corresponds to 5% of the maximum response amplitude. The noise is added on the time responses before the FRF value is calculated. The corresponding linear and nonlinear FRF curves for  $\alpha_{11}$  are given in Figure 3-18.

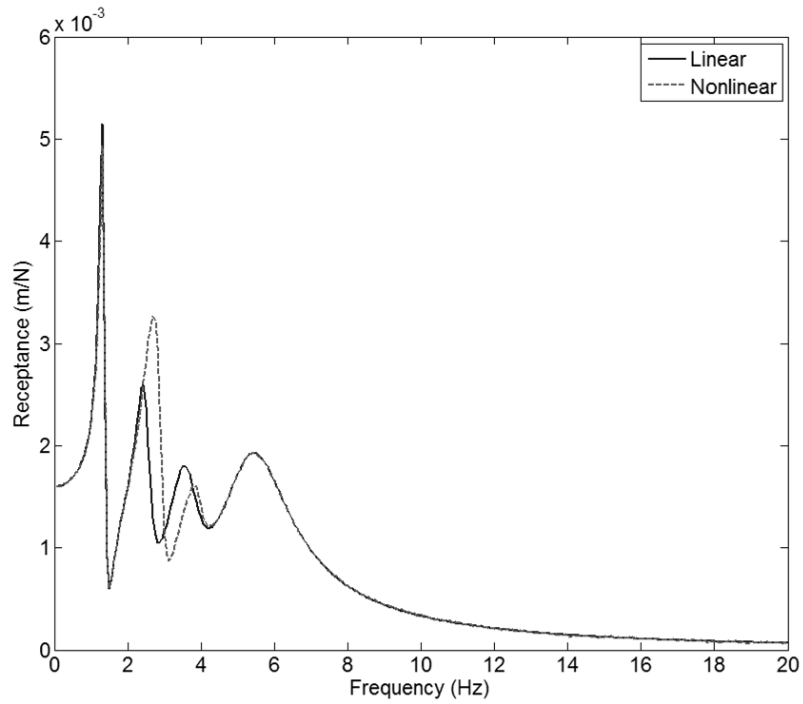


Figure 3-18. Comparison of nonlinear and linear FRFs ( $\alpha_{11}$ ) in the presence of noise #1

Then using the improved DF method again, the *NLI* for each coordinate is calculated and summed over the same frequency range, where again the linear FRFs are synthesized using equation (3.87). The sum of *NLI* for each coordinate is given in Figure 3-19.

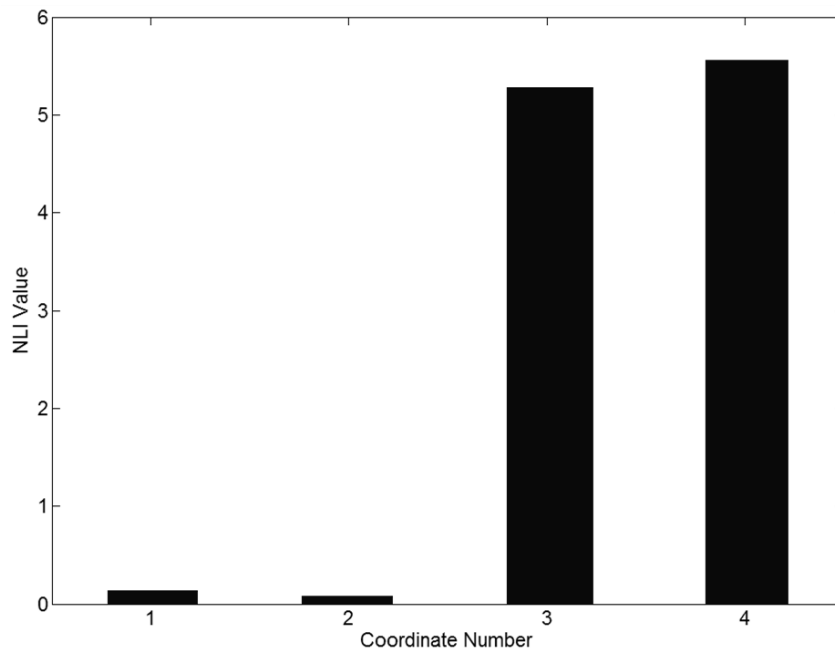


Figure 3-19. Nonlinearity indexes obtained with simulated noise #1

### 3.8.3. Case Study 3: Nonlinearity Localization from Spatially Incomplete FRF Data with Noise #2

Furthermore, another type of noise is added to the FRFs by multiplying a normal distribution noise, with unity mean and 0.025 standard deviation, with the linear and nonlinear FRFs. The driving point noisy FRF curves are given in Figure 3-20 and the sum of  $NLI$  for each coordinate is given in Figure 3-21. Thus, even with such high noise levels, the nonlinear element is successfully localized as being attached to coordinate 3 and 4.

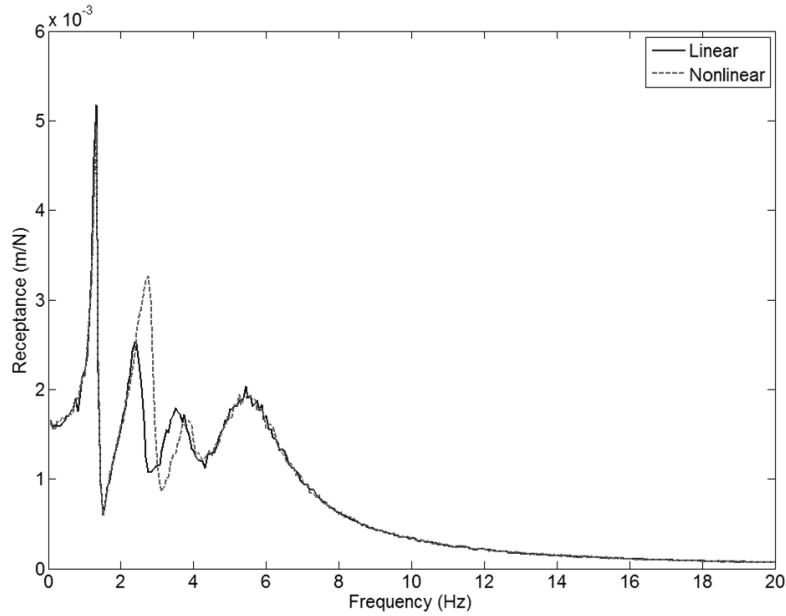


Figure 3-20. Comparison of nonlinear and linear FRFs ( $\alpha_{ij}$ ) in the presence of noise #2

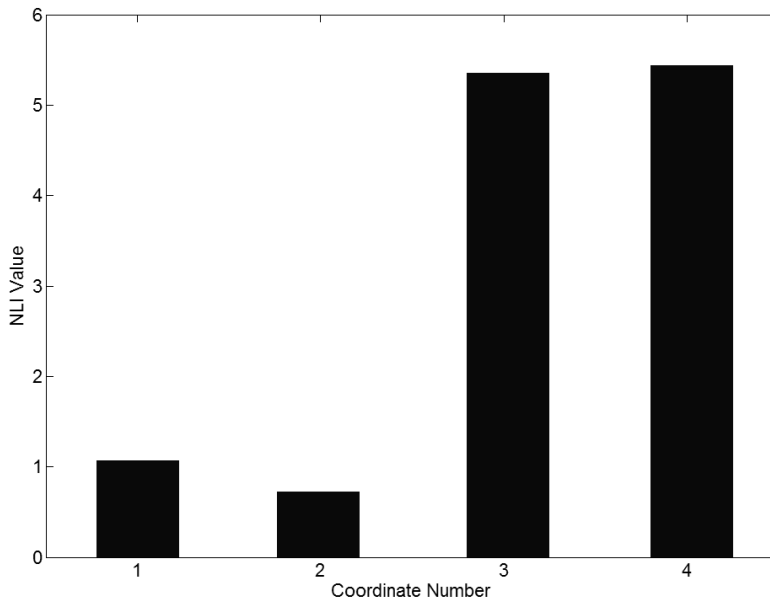


Figure 3-21. Nonlinearity indexes obtained with simulated noise #2

It is interesting to note that, the location of the nonlinearity changes the system FRFs considerably. A study where the nonlinearity is placed at different locations (0 “ground” coordinate-1<sup>st</sup> coordinate, 1<sup>st</sup>-2<sup>nd</sup> coordinate, 2<sup>nd</sup>-3<sup>rd</sup> coordinate, 3<sup>rd</sup>-4<sup>th</sup> coordinate, 4<sup>th</sup>- 0 “ground” coordinate) is performed, and the driving point FRFs are obtained as shown in Figure 3-22. However, the improved DF method works successfully for all cases.

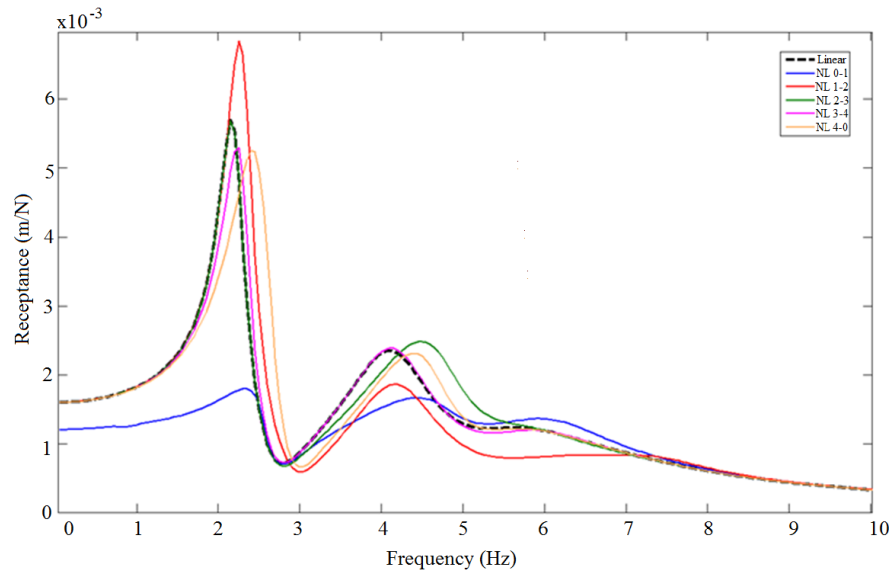


Figure 3-22. Linear and nonlinear FRFs for different nonlinear element locations; black: Linear, blue: 0 “ground” coordinate-1<sup>st</sup> coordinate, red: 1<sup>st</sup>-2<sup>nd</sup> coordinate, green: 2<sup>nd</sup>-3<sup>rd</sup> coordinate, purple: 3<sup>rd</sup>-4<sup>th</sup> coordinate, orange: 4<sup>th</sup>- 0 “ground” coordinate

#### 3.8.4. Case Study 4: Nonlinearity Localization from Spatially Incomplete FRF Data with Missing Coordinates

Another practical consideration that must be discussed is the unmeasured coordinates. In other words, consider the system given in Figure 3-14 and assume that the measurements are taken from coordinates 1, 2 and 4. The modal identification process will still identify 4 modes and corresponding modal parameters. The improved DF method is presented by using the noise-free FRF data. The sum of *NLI* for each coordinate is given in Figure 3-23. This time the nonlinear element seems to be located between coordinates 2 and 4.

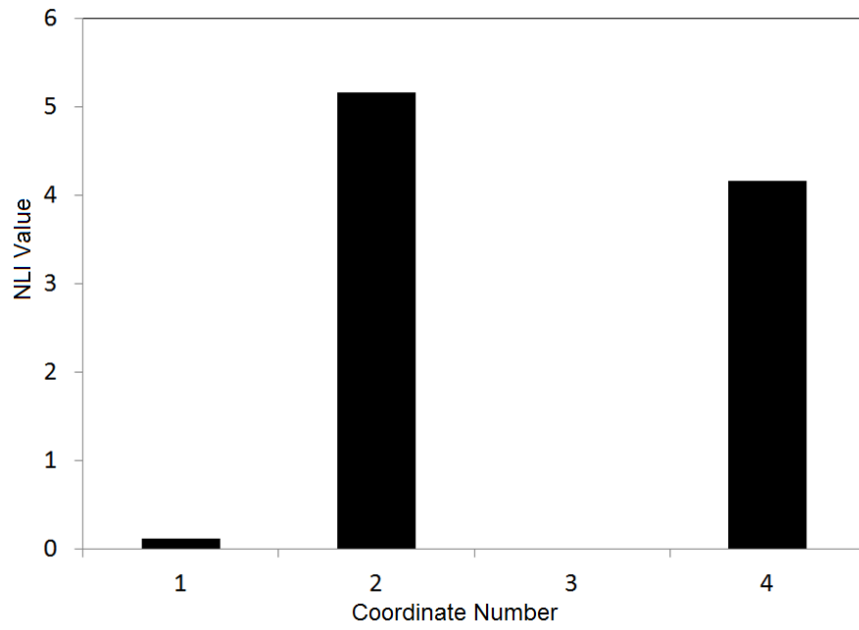


Figure 3-23. Nonlinearity indexes obtained with missing coordinates

The case studies given above show that, the improved DF method can successfully localize the nonlinear elements even with high noise levels.

## CHAPTER 4

### NONLINEARITY IDENTIFICATION BY RESTORING FORCE APPROACH

This chapter discusses the proposed nonlinearity identification method by restoring force approach using DF inversion.

#### 4.1. Introduction to Nonlinearity Identification Process Using DFs

The nonlinearity identification process consists of a series of processes. Kerschen *et al.* [3] describes the nonlinearity identification process as detection, characterization and parameter estimation. A simple flow chart is given in Figure 4-1.

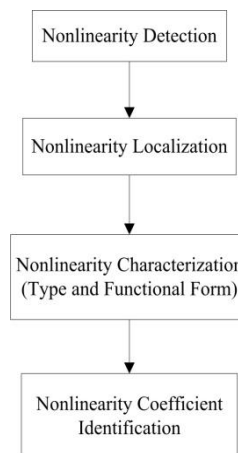


Figure 4-1. Nonlinearity identification process

The detection of the nonlinearity can be considered much easier compared to the other stages of the identification process. When a structure is excited at two different force levels the response should increase linearly resulting in an unchanged FRF. However if the system is not linear, then the FRF curve for different forcing levels will be different (Figure 4-2). This is the easiest way to detect whether or not nonlinearity is present in the structure.

In the second step, the locations of nonlinear elements in a structural system can be evaluated from nonzero *NLI* values. The next step, which is nonlinearity characterization, is more challenging.

First of all, equation (3.37) is used to evaluate the numerical values of DFs for each nonlinear element at various response levels. However, it should be noted that the method proposed requires measurement of nonlinear FRFs only at one high excitation level. The value of the DF, when there is single nonlinearity present in the system can be obtained from experimental data at different response amplitudes by using Sherman-Morrison formulation to avoid inversion (see section 3.4. for details).

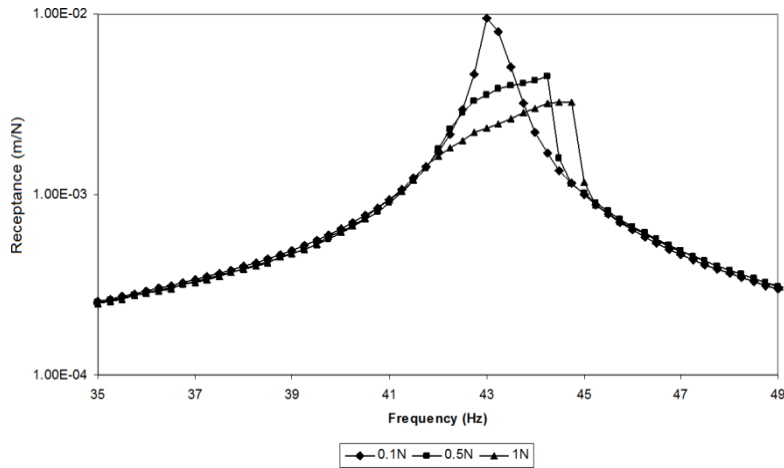


Figure 4-2. Driving point FRF curves of a nonlinear system for different constant forcing levels

However, when there are multiple nonlinearities present in the system, Sherman-Morrison formulation cannot be employed. Yet, simultaneous solution of all DF values is possible as long as the number of nonlinear elements do not exceed the total number of measurement coordinates, which would be rather unusual in practical applications.

Then, the value of each DF can be plotted at different response amplitudes for obtaining DFFs which can be used for determining the type of nonlinearity, as well as for parametric identification of nonlinear element(s).

Another common approach used for the same purpose is to obtain Restoring Force (RF) plots. Figure 4-3 presents RF and DFF plots for some common nonlinear elements. It is clear that RF plots contain more physical information compared to DFF plots.

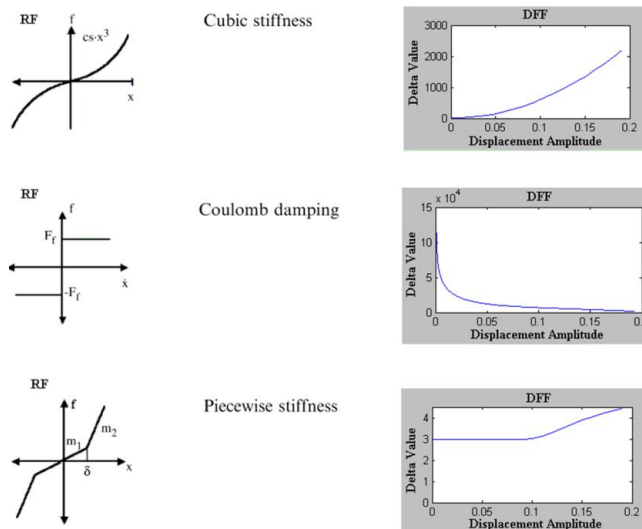


Figure 4-3. RFs and corresponding DFF plots

## 4.2. Nonlinearity Identification by DF Inversion (DFI Method)

In this study, DF calculated as discussed in the previous section is inverted to obtain RF function, which is graphically investigated to evaluate the type of nonlinearity. The DF inversion method works on the total DF and gives a RF for the total nonlinearity. The functional representation of nonlinear elements by RF is much simpler compared to the DF approach. However, if nonlinearities are required to be determined separately, then various possible nonlinear functions and their combinations should be tried to be fitted to the RF function obtained. Some engineering judgment will reduce the effort in trying different combinations. A flow chart of the nonlinear dynamic analysis process including the DFI method is given in Figure 4-4.

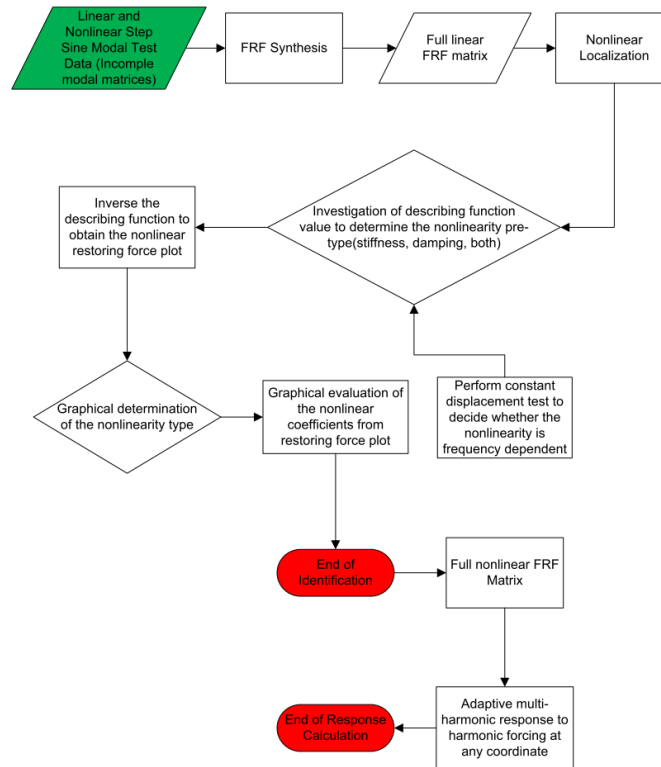


Figure 4-4. Nonlinear dynamic analysis process by DF inversion

### 4.2.1. Nonlinearity Characterization

Nonlinearities in a structural system are usually due to nonlinear stiffness (piecewise stiffness, hardening cubic stiffness, etc.) and/or nonlinear damping (coulomb friction, quadratic damping, etc.). DF formulation makes it possible to handle stiffness and damping nonlinearities separately [78]. The real part of the DF corresponds to stiffness nonlinearities whereas the imaginary part corresponds to damping nonlinearities. Therefore, a kind of indication about the type of the nonlinearity is available once DF is available. The case studies in the following sections will give a better insight on the indicator concept discussed.

If the nonlinearity is frequency dependent it is very difficult to distinguish the type of the nonlinearity. In order to determine the frequency dependency of the nonlinearity from experimental data, the method given in [78] can be used. According to the method, if the displacement is kept constant for the nonlinear element, this will give a linear system for the

given displacement and the real and imaginary parts of the nonlinearity matrix will remain constant throughout the frequency band. However, if the nonlinearity is frequency dependent then these terms will still change with frequency which will be the indicator that the nonlinearity is frequency dependent.

The DFI method requires inversion of the DF which has to be performed using different approaches for stiffness and damping nonlinearities when using experimental data with no knowledge on the type of the nonlinearity. Gibson [80] derived inverses for real, imaginary and mean parts of a DF. However, in this formulation the inversion of the real part and the mean of the DF require the information about the type of nonlinearity, but the inversion for the imaginary part works for any DF and it does not require information about the type of nonlinearity. The only limitation for the imaginary part is that the damping nonlinearity, which yields the imaginary part of DF, should not be frequency dependent. The derivation for the inverse of the imaginary part of the DF is given as follows [80]:

Let the nonlinearity in a system defined as

$$N(x) = f(x) \quad (4.1)$$

where  $f(x)$  can be double valued but not frequency dependent. If  $f(x)$  is double valued, it can be separated into two single valued functions as

$$\begin{aligned} f_1(x) & \quad \text{for} \quad \delta x < 0 \\ f_2(x) & \quad \text{for} \quad \delta x > 0 \end{aligned} \quad (4.2)$$

where  $\delta x$  is an increment of the independent variable.

If  $x$  from equation (4.1) is replaced by  $X \cos \alpha$ , where  $X$  is the amplitude of  $x$ ,  $N(\alpha)$  will become periodic with period  $2\pi$ . If  $N(\alpha)$  satisfies the Dirichlet conditions ( $N(\alpha)$  must be absolutely integrable over a period,  $N(\alpha)$  must have a finite number of extrema in any given interval,  $N(\alpha)$  must have a finite number of discontinuities in any given interval and  $N(\alpha)$  must be bounded), its Fourier expansion is given as

$$\begin{aligned} N(\alpha) = & M(X) + g_1(X) \cos \alpha + g_2(X) \cos 2\alpha + \dots \\ & + b_1(X) \sin \alpha + b_2(X) \sin 2\alpha + \dots \end{aligned} \quad (4.3)$$

where  $M(X)$ ,  $g_l(X)$ , and  $b_l(X)$  are the Fourier coefficients and are given as

$$\begin{aligned} g_1(X) &= \frac{1}{\pi X} \int_0^{2\pi} f(X \cos \alpha) \cos \alpha d\alpha \\ b_1(X) &= \frac{1}{\pi X} \int_0^{2\pi} f(X \cos \alpha) \sin \alpha d\alpha \\ M(X) &= \frac{1}{2\pi X} \int_0^{2\pi} f(X \cos \alpha) d\alpha \end{aligned} \quad (4.4)$$

Over the integral  $0$  to  $\pi$ ,  $\delta x$  is negative, and it is positive over the integral  $\pi$  to  $2\pi$ . Therefore, using equations (4.2), equation (4.4) can be rewritten as

$$\begin{aligned}
g(X) &= \frac{1}{\pi X} \left[ \int_0^{\pi} f_1(X \cos \alpha) \cos \alpha d\alpha + \int_{\pi}^{2\pi} f_2(\cos \alpha) \cos \alpha d\alpha \right] \\
b(X) &= \frac{1}{\pi X} \left[ \int_0^{\pi} f_1(X \cos \alpha) \sin \alpha d\alpha + \int_{\pi}^{2\pi} f_2(\cos \alpha) \sin \alpha d\alpha \right] \\
M(X) &= \frac{1}{2\pi X} \left[ \int_0^{\pi} f_1(X \cos \alpha) d\alpha + \int_{\pi}^{2\pi} f_2(\cos \alpha) d\alpha \right]
\end{aligned} \tag{4.5}$$

Moreover, all single valued functions can be replaced by the sum of an even and an odd function. Therefore,  $f_1(x)$  and  $f_2(x)$  can be written as

$$\begin{aligned}
f_1(x) &= p_1(x) + q_1(x) \\
f_2(x) &= p_2(x) + q_2(x)
\end{aligned} \tag{4.6}$$

where

$$\begin{aligned}
p_1(x) &= p_1(-x) & q_1(x) &= -q_1(-x) \\
p_2(x) &= p_2(-x) & q_2(x) &= -q_2(-x)
\end{aligned} \tag{4.7}$$

If equations (4.6) and (4.7) are substituted into equation (4.5)

$$\begin{aligned}
g(X) &= \frac{1}{\pi E} \left[ \int_0^{\pi} p_1(X \cos \alpha) \cos \alpha d\alpha + \int_{\pi}^{2\pi} p_2(X \cos \alpha) \cos \alpha d\alpha \dots \right. \\
&\quad \left. \int_0^{\pi} q_1(X \cos \alpha) \cos \alpha d\alpha + \int_{\pi}^{2\pi} q_2(X \cos \alpha) \cos \alpha d\alpha \right] \\
b(X) &= \frac{1}{\pi E} \left[ \int_0^{\pi} p_1(X \cos \alpha) \sin \alpha d\alpha + \int_{\pi}^{2\pi} p_2(X \cos \alpha) \sin \alpha d\alpha \dots \right. \\
&\quad \left. \int_0^{\pi} q_1(X \cos \alpha) \sin \alpha d\alpha + \int_{\pi}^{2\pi} q_2(X \cos \alpha) \sin \alpha d\alpha \right] \\
M(X) &= \frac{1}{2\pi E} \left[ \int_0^{\pi} p_1(X \cos \alpha) d\alpha + \int_{\pi}^{2\pi} p_2(X \cos \alpha) d\alpha \dots \right. \\
&\quad \left. \int_0^{\pi} q_1(X \cos \alpha) d\alpha + \int_{\pi}^{2\pi} q_2(X \cos \alpha) d\alpha \right]
\end{aligned} \tag{4.8}$$

Then if the following change of variable in all the integrals that are integrated over the interval  $\pi$  to  $2\pi$  is performed:

$$\alpha = \beta + \pi \tag{4.9}$$

Then equation (4.8) becomes

$$\begin{aligned}
g(X) &= \frac{1}{\pi E} \left\{ \int_0^\pi p_1(X \cos \alpha) \cos \alpha d\alpha + \int_0^\pi p_2[X \cos(\beta + \pi)] \cos(\beta + \pi) d\beta \cdots \right. \\
&\quad \left. + \int_0^\pi q_1(X \cos \alpha) \cos \alpha d\alpha + \int_0^\pi q_2[X \cos(\beta + \pi)] \cos(\beta + \pi) d\beta \right\} \\
b(X) &= -\frac{1}{\pi X} \left\{ \int_0^\pi p_1(X \cos \alpha) \sin \alpha d\alpha + \int_0^\pi p_2[X \cos(\beta + \pi)] \sin(\beta + \pi) d\beta \cdots \right. \\
&\quad \left. + \int_0^\pi q_1(X \cos \alpha) \sin \alpha d\alpha + \int_0^\pi q_2[X \cos(\beta + \pi)] \sin(\beta + \pi) d\beta \right\} \\
M(X) &= \frac{1}{2\pi X} \left\{ \int_0^\pi p_1(X \cos \alpha) d\alpha + \int_0^\pi p_2[X \cos(\beta + \pi)] d\beta \cdots \right. \\
&\quad \left. + \int_0^\pi q_1(X \cos \alpha) d\alpha + \int_0^\pi q_2[X \cos(\beta + \pi)] d\beta \right\}
\end{aligned} \tag{4.10}$$

where

$$\begin{aligned}
\cos(\beta + \pi) &= -\cos \beta \\
\sin(\beta + \pi) &= -\sin \beta
\end{aligned} \tag{4.11}$$

If these substitutions are made in equation (4.10), the result becomes

$$\begin{aligned}
g(X) &= \frac{1}{\pi X} \left[ \int_0^\pi P(X \cos \alpha) \cos \alpha d\alpha + \int_0^\pi Q(X \cos \alpha) \cos \alpha d\alpha \right] \\
b(X) &= -\frac{1}{\pi X} \left[ \int_0^\pi P(X \cos \alpha) \sin \alpha d\alpha + \int_0^\pi Q(X \cos \alpha) \sin \alpha d\alpha \right] \\
M(X) &= \frac{1}{2\pi X} \left[ \int_0^\pi P'(X \cos \alpha) d\alpha + \int_0^\pi Q'(X \cos \alpha) d\alpha \right]
\end{aligned} \tag{4.12}$$

where

$$\begin{aligned}
P(x) &= p_1(x) - p_2(x) \\
Q(x) &= q_1(x) + q_2(x) \\
P'(x) &= p_1'(x) + p_2'(x) \\
Q'(x) &= q_1'(x) - q_2'(x)
\end{aligned} \tag{4.13}$$

$p_1(x)$  and  $p_2(x)$  are even functions and  $q_1(x)$  and  $q_2(x)$  are odd functions, then  $P(x)$  and  $P'(x)$  are also even functions and  $Q(x)$  and  $Q'(x)$  are odd functions.

Furthermore if the interval is separated into two parts in equations (4.12), such as the first integral to be integrated from 0 to  $\pi/2$  and the second integral to be integrated from  $\pi/2$  to  $\pi$ , and the change of variables  $\alpha = \pi - \beta$  is performed for the integrals that are integrated from  $\pi/2$  to  $\pi$ , then equation (4.12) becomes

$$\begin{aligned}
g(X) &= \frac{1}{\pi X} \left\{ \int_0^{\pi/2} P(X \cos \alpha) \cos \alpha d\alpha - \int_{\pi/2}^0 P(X \cos(\pi - \beta)) \cos(\pi - \beta) d\beta \dots \right. \\
&\quad \left. + \int_0^{\pi/2} Q(X \cos \alpha) \cos \alpha d\alpha - \int_{\pi/2}^0 Q(X \cos(\pi - \beta)) \cos(\pi - \beta) d\beta \right\} \\
b(X) &= \frac{1}{\pi X} \left\{ \int_0^{\pi/2} P(X \cos \alpha) \sin \alpha d\alpha - \int_{\pi/2}^0 P(X \cos(\pi - \beta)) \sin(\pi - \beta) d\beta \dots \right. \\
&\quad \left. + \int_0^{\pi/2} Q(X \cos \alpha) \sin \alpha d\alpha - \int_{\pi/2}^0 Q(X \cos(\pi - \beta)) \sin(\pi - \beta) d\beta \right\} \\
M(X) &= \frac{1}{2\pi X} \left\{ \int_0^{\pi/2} P'(X \cos \alpha) d\alpha - \int_{\pi/2}^0 P'(X \cos(\pi - \beta)) d\beta \dots \right. \\
&\quad \left. + \int_0^{\pi/2} Q'(X \cos \alpha) d\alpha - \int_{\pi/2}^0 Q'(X \cos(\pi - \beta)) d\beta \right\}
\end{aligned} \tag{4.14}$$

where

$$\begin{aligned}
\cos(\pi - \beta) &= -\cos \beta \\
\sin(\pi - \beta) &= \sin \beta
\end{aligned} \tag{4.15}$$

Therefore, equations (4.14) are reduced to

$$\begin{aligned}
g(X) &= \frac{2}{\pi} \int_0^{\pi/2} Q(X \cos \alpha) \cos \alpha d\alpha \\
b(X) &= \frac{2}{\pi} \int_0^{\pi/2} P(X \cos \alpha) \sin \alpha d\alpha \\
M(X) &= \frac{1}{\pi} \int_0^{\pi/2} P'(X \cos \alpha) d\alpha
\end{aligned} \tag{4.16}$$

Returning back to the original variable  $x$  in equation (4.16):

$$X \cos(\alpha) = x \tag{4.17}$$

The final result becomes

$$\begin{aligned}
g(X) &= \frac{2}{\pi X^2} \int_0^x \frac{xQ(x)}{\sqrt{X^2 - x^2}} dx \\
b(X) &= \frac{2}{\pi X^2} \int_0^x P(x) dx \\
M(X) &= \frac{1}{\pi X} \int_0^x \frac{P'(x)}{\sqrt{X^2 - x^2}} dx
\end{aligned} \tag{4.18}$$

The next step is to solve equations (4.18). The solution for  $b(X)$  is clear, and the remaining two equations are special cases of Volterra's integral equation of the first kind. The solutions of equations (4.18) are given as

$$\begin{aligned}
Q(x) &= \frac{1}{x} \frac{d}{dx} \left[ \int_0^x \frac{z^3 g(z)}{\sqrt{x^2 - z^2}} dz \right] \\
P(x) &= \frac{\pi}{2} \frac{d}{dx} \left[ x^2 b(x) \right] \\
P'(x) &= 2 \frac{d}{dx} \left[ \int_0^x \frac{z^2 M(z)}{\sqrt{x^2 - z^2}} dz \right]
\end{aligned} \tag{4.19}$$

Here  $Q(x)$  gives the inverse of the real part of the DF,  $P'(x)$  gives the inverse of the mean part of the DF, and  $P(x)$  in equation (4.19) gives the inverse of the imaginary part of the DF which can be calculated without any knowledge of the nonlinearity function.

Now let us consider the inversion of the real part of the DF. In order to obtain the DF inversion for the real part, the approximate inversion equations suggested by Gelb and Vander Velde [78] are used. The derivation for the inverse of the real part of the DF is given as follows:

The DF representation for general dynamic nonlinearity can be defined as

$$v(X, \dot{X}) = \frac{i}{\pi X} \int_0^{2\pi} N(x, \dot{x}) e^{-i\tau} d\tau \tag{4.20}$$

where the response is assumed to be of the form;

$$x(t) = X \sin(\omega t + \theta) = X \sin(\tau) \tag{4.21}$$

$$\tau = \omega t + \theta \tag{4.22}$$

Equation (4.20) can be rewritten in real and imaginary terms as

$$v_r(X, \dot{X}) = \frac{1}{\pi X} \int_0^{2\pi} N(x, \dot{x}) \sin\tau d\tau \tag{4.23}$$

$$v_i(X, \dot{X}) = \frac{1}{\pi X} \int_0^{2\pi} N(x, \dot{x}) \cos\tau d\tau \tag{4.24}$$

Further simplifications to equation (4.20) are possible if the nonlinearity is independent of velocity (frequency independence) and no memory (real DFs) assumptions are made;

$$v(X) = \frac{2}{\pi X} \int_{-\pi/2}^{\pi/2} N(x) \sin\tau d\tau \tag{4.25}$$

Gelb and Vander Velde [78] derived approximate analytic solution to the DF integral. The derivation starts with equation (4.25).

Using the transformations

$$u = \sin\tau \tag{4.26}$$

$$du = \cos\tau d\tau \tag{4.27}$$

Equation (4.25) can be written as

$$v(X) = \frac{2}{\pi X} \int_{-1}^1 N(Xu) \frac{udu}{\sqrt{1-u^2}} \quad (4.28)$$

The approximate evaluation of a similar integral form is as follows;

$$\int_{-1}^1 g(u) \frac{du}{\sqrt{1-u^2}} \approx \frac{\pi}{6} [g(1) + g(-1) + 2g(0.5) + 2g(-0.5)] \quad (4.29)$$

From equation (4.28) and (4.29);

$$v(X) \approx \frac{1}{3X} \left[ N(X) - N(-X) + N\left(\frac{X}{2}\right) - N\left(-\frac{X}{2}\right) \right] \quad (4.30)$$

For odd nonlinear restoring function, ( $N(-X) = -N(X)$ ), equation (4.30) becomes,

$$v(X) \approx \frac{2}{3X} \left[ N(X) + N\left(\frac{X}{2}\right) \right] \quad (4.31)$$

Furthermore, evaluating the DF values at  $2^n$  multiples of  $X$  ( $n=0,1,2,3\dots$ ) yields

$$\begin{aligned} v(X) &\approx \frac{2}{3X} \left[ N(X) + N\left(\frac{X}{2}\right) \right] \\ v(2X) &\approx \frac{1}{3X} \left[ N(2X) + N(X) \right] \\ v(4X) &\approx \frac{1}{6X} \left[ N(4X) + N(2X) \right] \\ &\dots \end{aligned} \quad (4.32)$$

Solving the above equations for  $N(X)$  gives

$$N(X) \approx 3X \sum_{i=0}^{\infty} (-2)^i v(2^{i+1} X) \quad \text{for } v(X) \text{ increasing with } X \quad (4.33)$$

Similarly, the DF could be evaluated at  $2^{-n}$  multiples of  $X$  ( $n=1,2,3\dots$ ) which would give

$$\begin{aligned} v(X) &\approx \frac{2}{3X} \left[ N(X) + N\left(\frac{X}{2}\right) \right] \\ v\left(\frac{X}{2}\right) &\approx \frac{4}{3X} \left[ N\left(\frac{X}{2}\right) + N\left(\frac{X}{4}\right) \right] \\ v\left(\frac{X}{4}\right) &\approx \frac{8}{3X} \left[ N\left(\frac{X}{4}\right) + N\left(\frac{X}{8}\right) \right] \\ &\dots \end{aligned} \quad (4.34)$$

Solving the above equations for  $N(X)$  gives

$$N(X) \approx \frac{3X}{2} \sum_{i=0}^{\infty} \left(-\frac{1}{2}\right)^i v\left(\frac{X}{2^i}\right) \quad \text{for } v(X) \text{ decreasing with } X \quad (4.35)$$

The major drawback of these formulations is that when the DF is inversely proportional to  $X$ , for instance due to Coulomb friction, the summation gives alternating series and a correct result cannot be obtained. However for damping the imaginary part of the DF is to be inverted and this is achieved analytically as explained above.

Consequently, in this study it is proposed to use equation (4.33) or (4.35) for the real part of DF, which is due to stiffness type of nonlinearity, and  $P(x)$  of equation (4.19) for the imaginary part of DF, which is due to damping type of nonlinearity. In order to overcome the problems encountered due to obtaining noisy DFs because of experimental noise, a common smoothing function is applied to DF before inversion.

#### **4.2.2. Nonlinearity Coefficient Identification**

There are numerous ways to calculate parametric values for DF and RF functions. Optimization and black box methods such as neural networks provide promising results if they are well guided. More direct approaches like graphical methods require the engineer to be experienced.

In this study the parametric values of the nonlinearity are obtained from RF plots by curve fitting. It is also possible to obtain the coefficients from DF when the type of nonlinearity is known. However, for most of the nonlinearity types, DF representation is far more complicated than the corresponding RF function. It should be noted that when the RF representation of nonlinearity is already obtained, most of the time it is of little importance what the coefficients of RF function are. All the required information about nonlinear element is stored in the RF function itself which can be further employed in dynamic analysis for different inputs. Determining RF function, rather than DF may be more important when there is more than one type of nonlinearity at the same location, in which case it will be very difficult if not impossible to make parametric identification for each nonlinearity by using DF.

#### **4.3. Accuracy of Approximate DF Inversion**

In order to demonstrate the accuracy of the approximate DF inversion method for some well-known structural nonlinearities, the following three numerical cases are given.

##### **4.3.1. Cubic Stiffness**

DF of the cubic stiffness expressed as  $F_k' = 80000x^3$  N is plotted in Figure 4-5a. The restoring force obtained with approximate inversion for this case is compared with the exact force-deflection curve in Figure 4-5b. It can be seen from the comparison of two curves in Figure 4-5b that a very close match is obtained. This is an expected result because the DFI method is based on continuous and polynomial type DFs.

##### **4.3.2. Coulomb Friction**

DF of the coulomb friction expressed as  $F_c' = 100\text{sgn}(\dot{x})$  N is given in Figure 4-6a. The restoring force obtained with approximate inversion for this case is compared with the exact force-deflection curve in Figure 4-6b. It can be seen from the comparison of two curves in Figure 4-6b that a very close match is obtained.

##### **4.3.3. Piecewise Stiffness**

DF of the piecewise stiffness expressed as  $F_k' = 3x$   $x < 0.05$  N and  $F_k' = 7x - 0.2$   $x \geq 0.05$  N is plotted in Figure 4-7a. The restoring force obtained with approximate inversion for this case is compared with the exact force-deflection curve in Figure 4-7b. It can be seen from the comparison of two curves in Figure 4-7b that the match is not as good as the previous nonlinearities due to the fact that piecewise stiffness is not continuous.

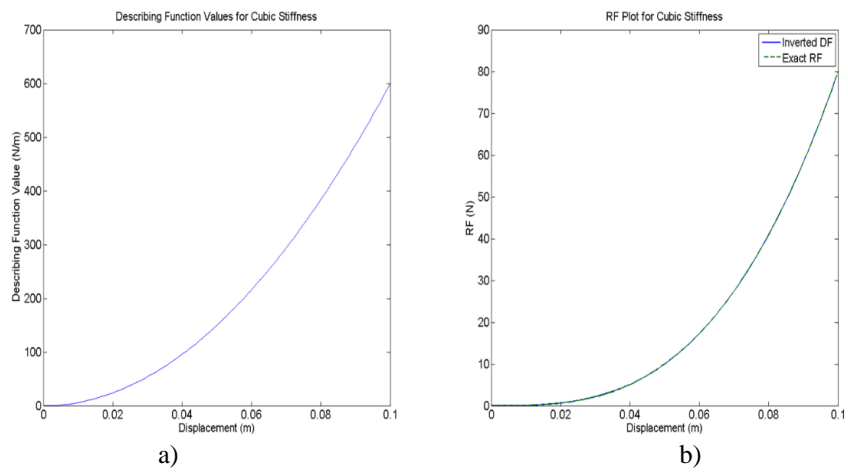


Figure 4-5. Cubic Stiffness, a)DF, b)RF plots

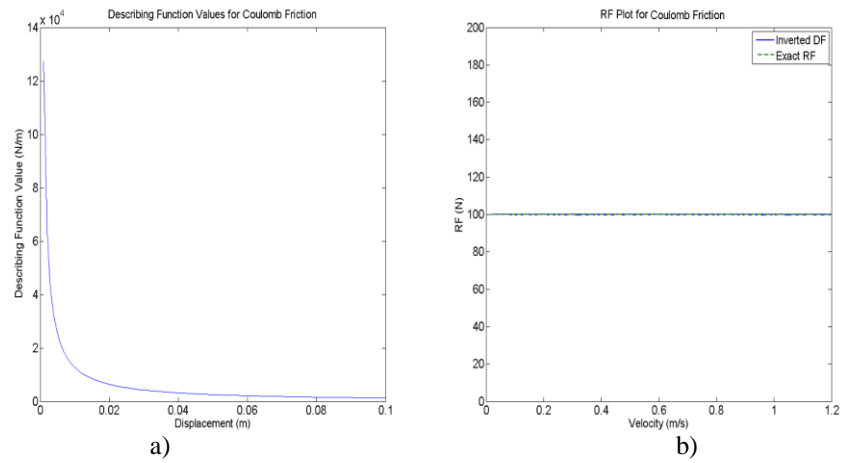


Figure 4-6. Coulomb Friction, a)DF, b)RF plots

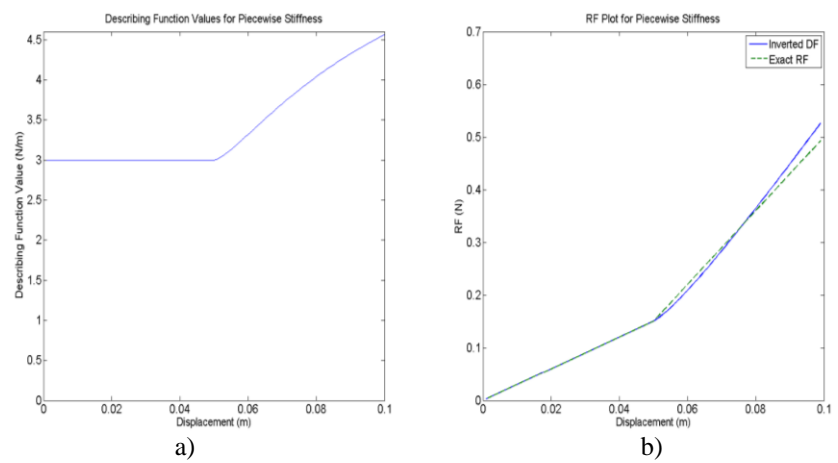


Figure 4-7. Piecewise Stiffness, a)DF, b)RF plots

#### 4.3.4. Backlash

DF of the backlash expressed as  $F_b'=0 \quad x < 0.05 \text{ N}$  and  $F_b'=2x-0.1 \quad x \geq 0.05 \text{ N}$  is plotted in Figure 4-8a. The restoring force obtained with approximate inversion for this case is compared with the exact force-deflection curve in Figure 4-8b. It can be seen from the comparison of two curves in Figure 4-8b that the match is not as good as the first two nonlinearities, again due to the fact that backlash is not continuous.

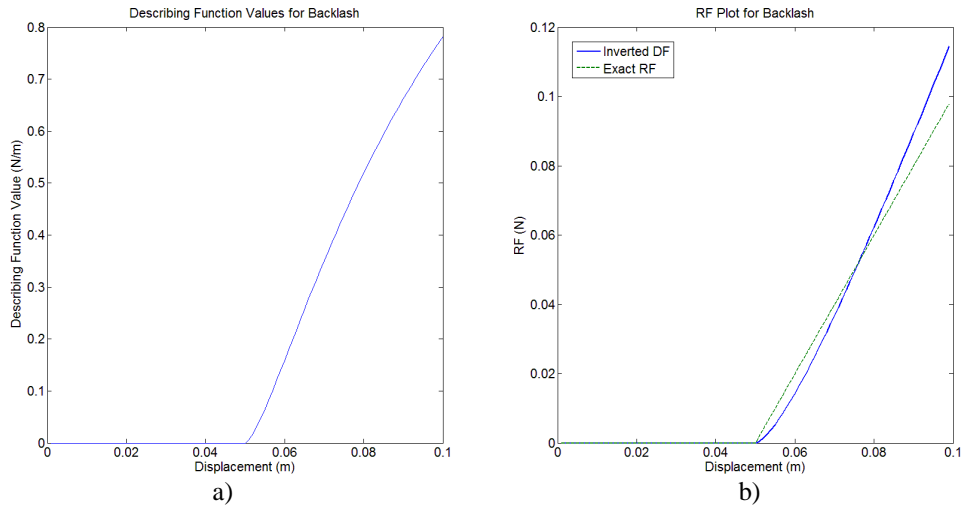


Figure 4-8. Backlash, a)DF, b)RF plots

#### 4.4. Case Studies

##### 4.4.1. Case Study 1: Nonlinear Elements at Different Locations

The DFI method proposed in this study is applied to a 4 DOF discrete system. In this first case study a nonlinear elastic element represented by  $k_1'$  (a linear stiffness of 100 N/m with a backlash of 0.005 m) between ground and coordinate 1, and a nonlinear hardening cubic stiffness represented by  $k_4'$  ( $= 10^6 x^2 \text{ N/m}$ ) between coordinates 3 and 4, as shown in Figure 4-9, are considered. The numerical values of the linear system elements are given as follows:

$$k_1 = k_2 = k_3 = k_4 = k_5 = 500 \text{ N/m}$$

$$c_1 = c_2 = c_3 = c_4 = c_5 = 5 \text{ Ns/m}$$

$$m_1 = 1 \text{ kg}, m_2 = 2 \text{ kg}, m_3 = 3 \text{ kg}, m_4 = 5 \text{ kg}$$

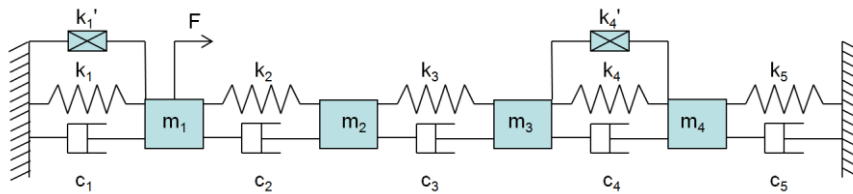


Figure 4-9. Four DOFs discrete system with two nonlinear elements at different locations

The time response of the system to sinusoidal forcing is calculated with MATLAB by using the ordinary differential equation solver ODE45. The simulation was run for 32 seconds at each frequency to ensure that transients die out. The frequency range of the harmonic excitation that is used during the simulations is from 0.0625 to 16 Hz with frequency increments of 0.0625 Hz. The linear FRFs are obtained by applying a very low sinusoidal forcing (0.1N) from first coordinate. The nonlinear FRFs are obtained by applying high sinusoidal forcing (10N) to the system from the first coordinate. Before using the calculated FRFs as simulated experimental data, they are polluted by using the “normrnd” function of MATLAB with zero mean, normal distribution and standard deviation of 5% of the maximum amplitude of the FRF value. A sample comparison for the nonlinear and linear FRFs ( $\alpha_{11}$ ) is given in Figure 4-10.

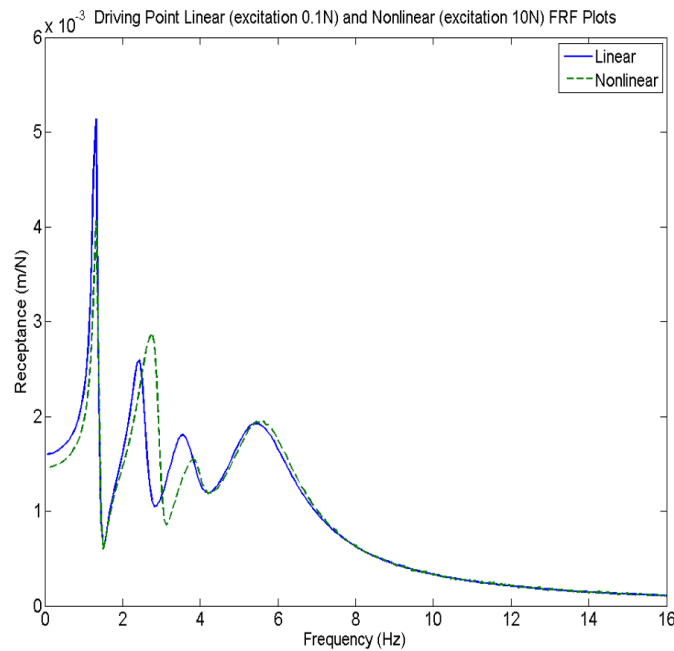


Figure 4-10. Driving point linear (for F=0.1N) and nonlinear (for F=10N) FRF plots

It is assumed in this case study that only the first columns of the linear and nonlinear receptance matrices are measured. Then, firstly the missing elements of the linear FRF matrix are calculated by using FRF synthesis, and the NLI values are calculated and shown in Figure 4-11a. From Figure 4-11a it can easily be concluded that there are nonlinear elements between ground and coordinate 1, and between coordinates 3 and 4. Furthermore, since the nonlinearity can be stiffness and/or damping type, it is possible to make this distinction at this stage by investigating the real and imaginary parts of the DF. The real and imaginary parts of the DFs can be summed over the frequency range and compared with each other. Figure 4-11b reveals that system has stiffness type of nonlinearity since DFs has much higher real parts compared to imaginary parts.

Using the improved DF method, the DFs representing these nonlinear elements are calculated and are plotted in Figure 4-12a as functions of response amplitudes. From the general pattern of the curves it may be possible to identify the types of nonlinearity. Fitting a curve to the calculated values makes the parametric identification easier. Although identification of backlash may not be so easy from DFF, it is quite straightforward to identify the type of cubic stiffness from Figure 4-12b.

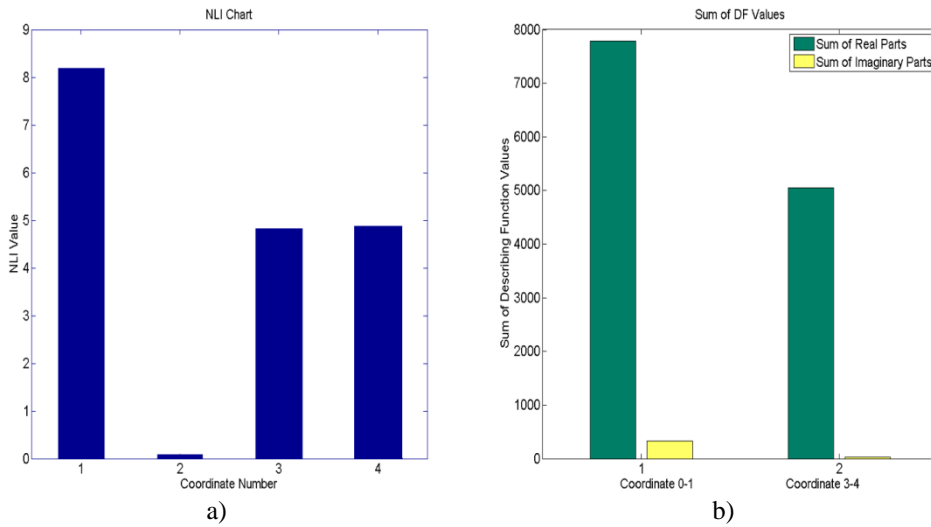


Figure 4-11. a) Nonlinearity index chart, b) Sums of real and imaginary parts of DF values at high forcing excitation

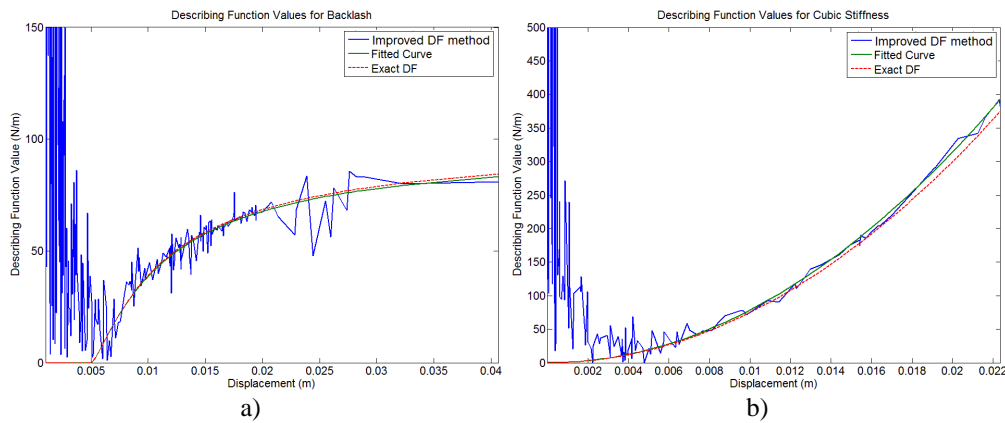


Figure 4-12. Calculated, fitted and exact DFs. a) For nonlinear element between coordinate 1 and ground, b) For nonlinear element between coordinates 3 and 4

Alternatively, the types of nonlinear elements can be identified more easily if the DFI method is used. The inversion of DFs are obtained for this case study by using the formulation given in section 4.2.1., and RF plots obtained are presented in Figure 4-13. Figure 4-13a gives the RF plot for the nonlinearity between the first coordinate and ground, whereas Figure 4-13b shows the RF plot for the nonlinearity between coordinates 3 and 4. By first fitting curves to the calculated RF plots, parametric identification can easily be made.

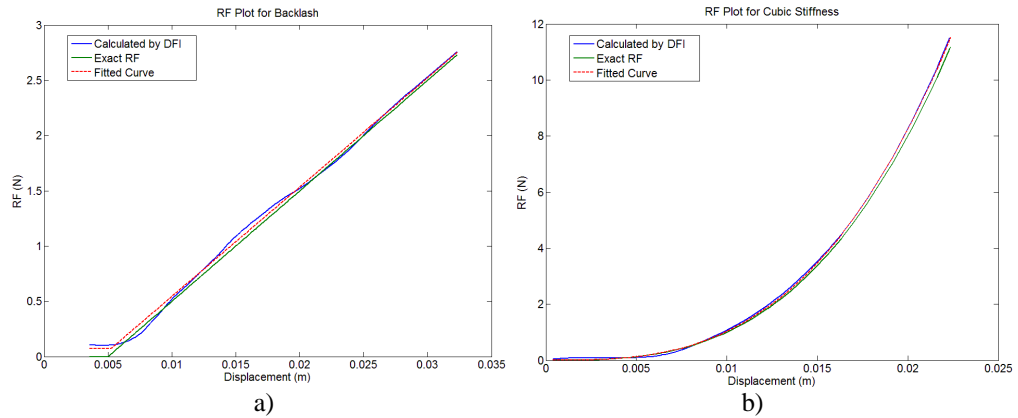


Figure 4-13. Calculated, exact and fitted RF plots. a) For nonlinear element between coordinate 1 and ground, b) For nonlinear element between coordinates 3 and 4

The parametric identification results with the DFI and improved DF methods for the nonlinear elements are tabulated in Table 4-1. As it can be seen from the table, the identified values do not deviate from the actual values more than 4% for the DFI method and %5 for improved DF method. However, it should be noted that the improved DF method cannot identify the backlash value as the fitted DF is not defined for displacement values smaller than 0.005 m. Furthermore, the DF forms must be known to perform improved DF method for parametric identification. The nonlinear FRFs are regenerated by using the method given in section 3.3. with the identified nonlinearities from the DFI and improved DF methods (Figure 4-14). As the errors in parametric identification are very small for all methods, a good match is obtained.

Table 4-1. Parametric identification results for the nonlinear elements

	Actual	Identified by DFI method		Identified by improved DF method	
		Value	Error %	Value	Error %
Backlash (m)	0.0050	0.0052	4	-	-
$k_1'$ (Linear stiffness part) N/m	100	99	-1	99	-1
$k_4'$ (cubic stiffness constant) N/m <sup>3</sup>	$10^6$	$1.03 \cdot 10^6$	3	$1.05 \cdot 10^6$	5

Although the DFI method is based on polynomial type DFs, it is shown in this case study that they work, at an acceptable level, for discontinuous DFs such as backlash as well. Furthermore, with this case study it is illustrated that accurate identification can be made even if only the first harmonic of the nonlinear internal forces are used.

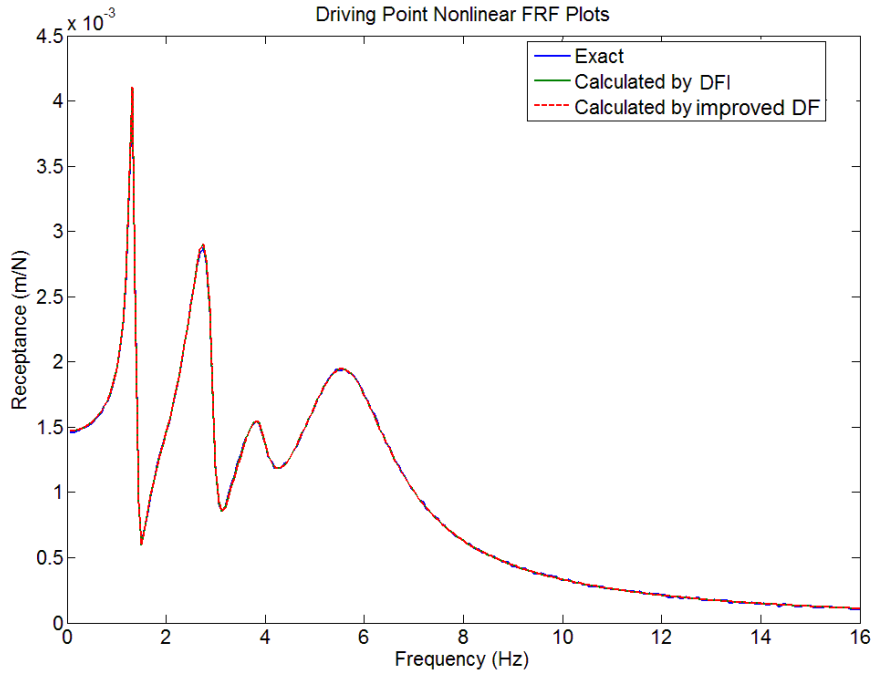


Figure 4-14. Nonlinear driving point FRFs, (blue: exact values; green: calculated by the DFI method; dashed red: calculated by improved DF method)

#### 4.4.2. Case Study 2: Two Different Nonlinear Elements at the Same Location

In the second case study, the nonlinear elastic element represented by  $k_1'$  (a linear stiffness of 100 N/m with a backlash of 0.005 m) is again taken between the ground and coordinate 1, and also a nonlinear hardening cubic stiffness represented by  $k_1''$  ( $= 10^6 x^2$  N/m) is added between ground and coordinate 1, as shown in Figure 4-15, are considered.

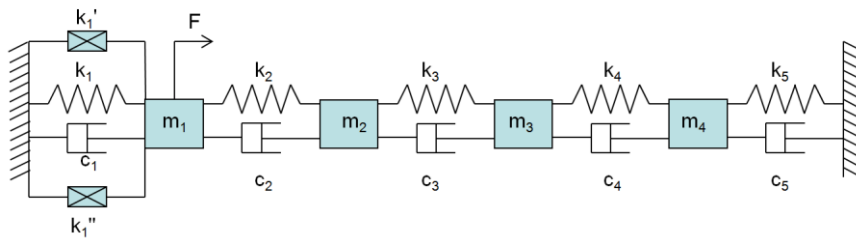


Figure 4-15. Four DOFs discrete system with two nonlinear elements at the same coordinate

The numerical values of the linear system elements and the FRF calculation procedure are the same as in case study 1. A sample comparison for the linear and nonlinear FRFs ( $\alpha_{11}$ ) is given in Figure 4-16. Linear and nonlinear FRFs are found for harmonic forcing with amplitudes of 0.1N and 10N, respectively.

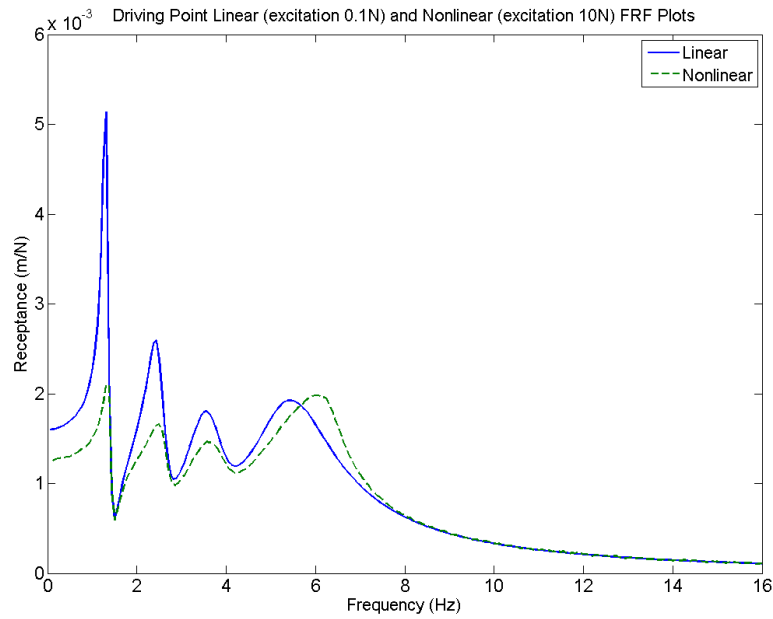


Figure 4-16. Driving point linear (for  $F=0.1N$ ) and nonlinear (for  $F=10N$ ) FRF plots

The calculated  $NLI$  values are shown in Figure 4-17a. From Figure 4-17a it can easily be concluded that there are nonlinear elements between ground and coordinate 1. Furthermore, Figure 4-17b reveals that system has stiffness type of nonlinearity since DF has much higher real part compared to its imaginary part.

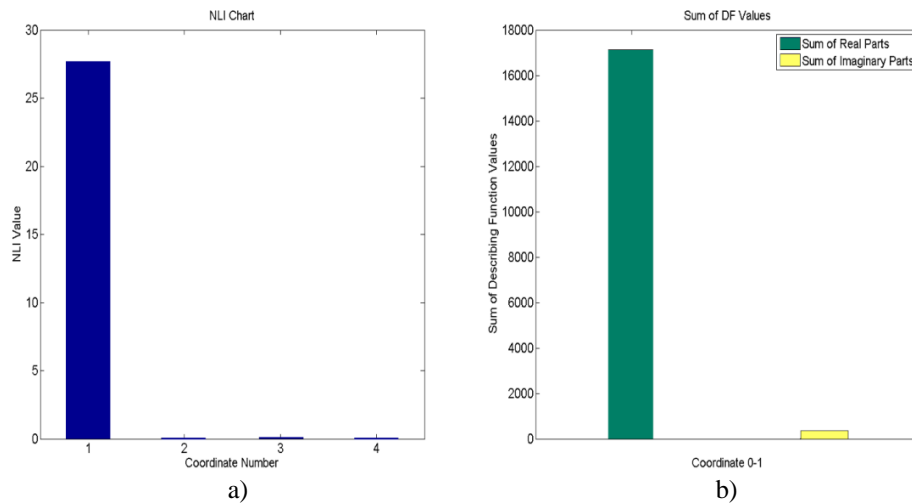


Figure 4-17. a) Nonlinearity index chart, b) Sums of real and imaginary parts of DF values at high forcing excitation

The DFs representing these nonlinear elements are calculated at different response amplitudes and are plotted in Figure 4-18. This time it is not possible to identify the types of nonlinearity

from the general pattern of the curve. Thus, improved DF method is not applicable to this case study.

The inversion of DFs are obtained for this case study by using the DFI method, and RF plots obtained are presented in Figure 4-19. By first fitting a curve to the calculated RF plot, parametric identification can easily be made.

As there are two stiffness type nonlinearities at the same location, parametric identification is not straightforward. The RF plot again reveals the backlash value as 0.0052 m. Then, the RF curve is curve fitted to polynomial functions where a linear and cubic function gives the best fit. The parametric identification results for the nonlinear elements are tabulated in Table 4-2. As can be seen from the table, the identified values do not deviate from the actual values more than 5%.

Table 4-2. Parametric identification results for the nonlinear elements

	Actual	Identified by the DFI method	Error %
Backlash (m)	0.0050	0.0052	4
$k_1'$ (Linear stiffness part) N/m	100	95	-5
$k_1''$ (cubic stiffness constant) N/m <sup>3</sup>	$10^6$	$0.99 \cdot 10^6$	-1

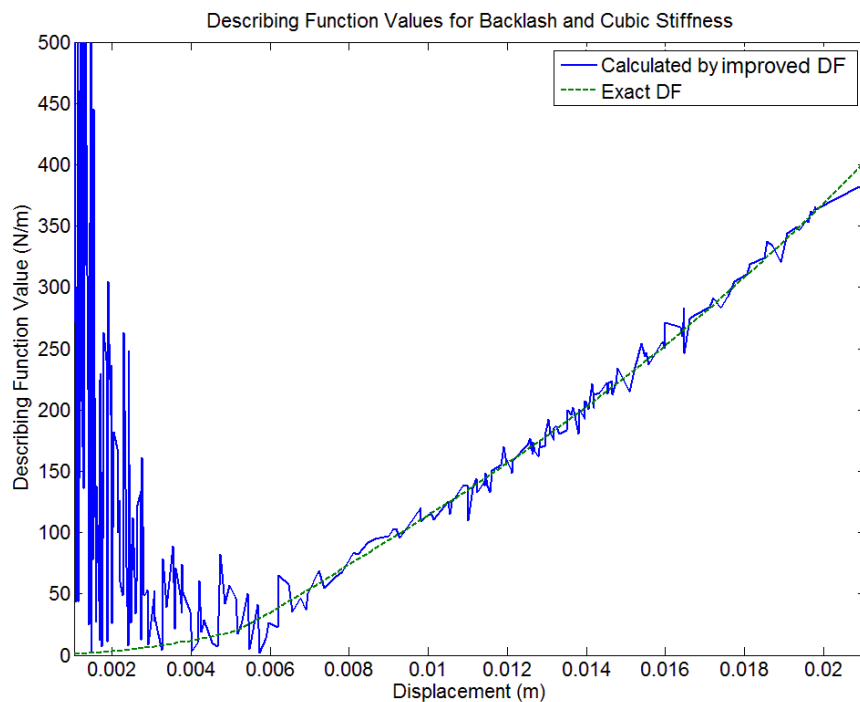


Figure 4-18. Calculated and exact DFs for nonlinear element between coordinate 1 and ground

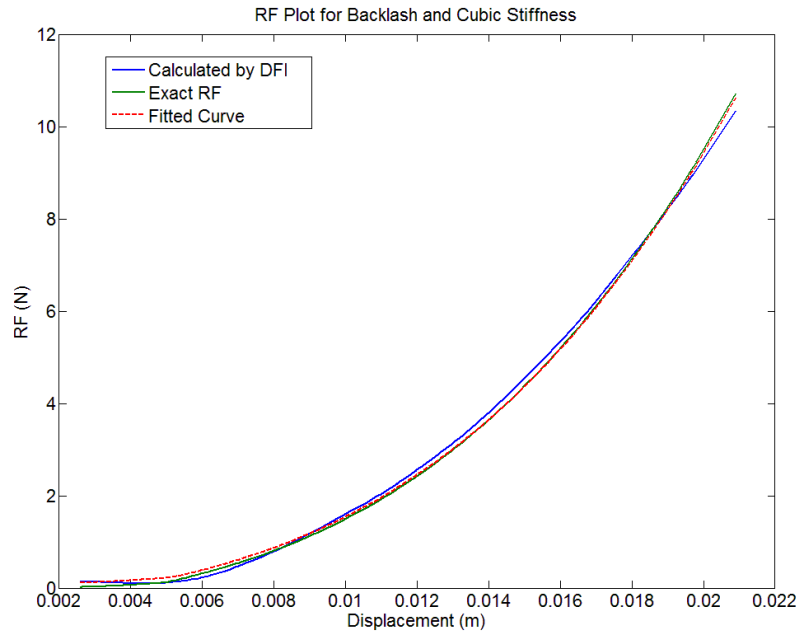


Figure 4-19. Calculated, exact and fitted RF plots for nonlinear element between coordinate 1 and ground

The nonlinear FRFs are regenerated by using the method given in section 3.3. with the identified nonlinearities from the DFI method (Figure 4-20). As the errors in parametric identification are very small for the DFI method, a good match is obtained. The power of this method can be seen in this case study where two or more nonlinear elements can be successfully identified.

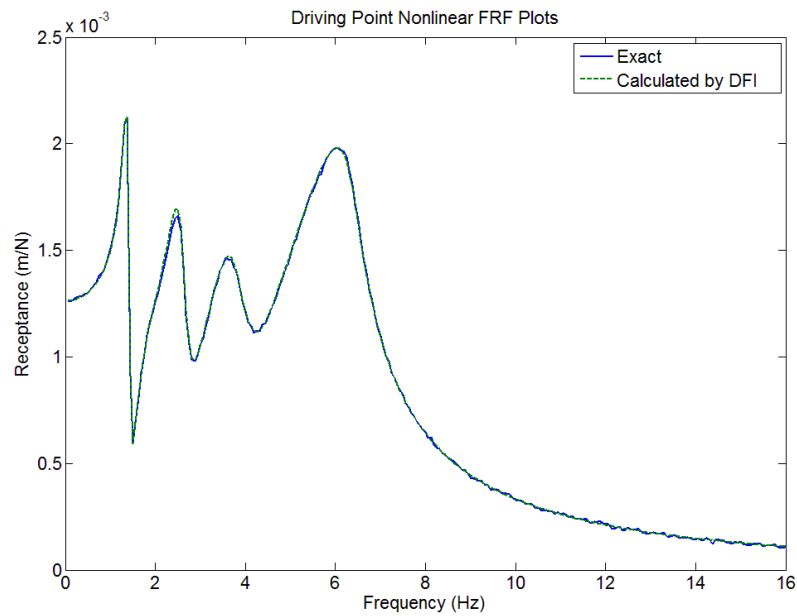


Figure 4-20. Nonlinear driving point FRFs, (blue: exact values; green: calculated by the DFI method)

#### 4.4.3. Case Study 3: Two Different Nonlinear Elements at the Same Location-Finite Element Model

In the third case study, a cantilever beam with two nonlinear elements is considered. In order to demonstrate the application of the DFI method to systems with several DOFs, the beam is modeled by using finite element formulation and the nonlinear responses calculated at 8 coordinates are used in this simulated experimental case study. The beam elements are chosen as BEAM188 [81] with 6 DOF at each node (x, y, z directions and rotations around these axes). The beam has a square cross section (8mm x 8mm) and a length of 0.42 m. The beam is produced from steel where the material properties are taken as 210 GPa for the Modulus of Elasticity and 7800 kg/m<sup>3</sup> for the density. The harmonic forcing is applied from the tip of the beam in the y direction. Two nonlinear elements are assumed at the free end of the beam in y direction. The first element is a linear stiffness of 1000 N/m with a backlash of 0.00025 m, ( $k_1'$ ). The second element is a nonlinear hardening cubic stiffness represented by  $k_1'' (= 6 \cdot 10^7 x^2 \text{ N/m})$  (Figure 4-21).

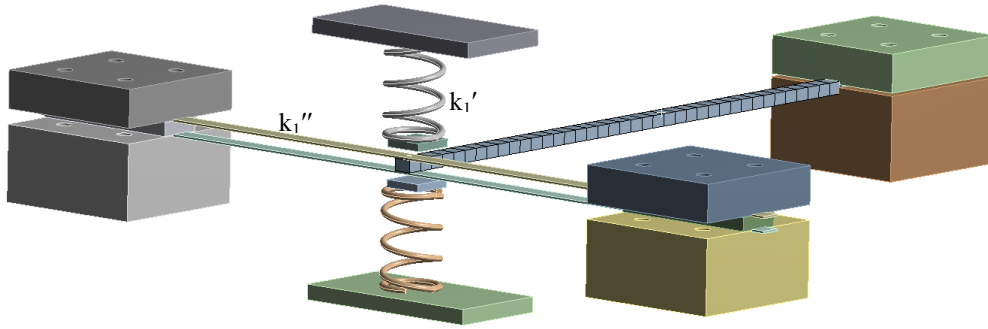


Figure 4-21. 360 DOFs discrete system with two nonlinear elements at the same coordinate

The stiffness and mass matrices are taken from the 360 DOF finite element model. The damping matrix is generated by assuming Rayleigh damping model [81] with negligible mass damping. The coefficients required to calculate the Rayleigh damping matrix are not generally known directly, but are calculated from modal damping ratio which is taken 0.03 for this case study. The nonlinear responses at each DOF are calculated by using the nonlinear analysis method given in section 3.3. The responses at 8 points are calculated in y direction. The locations of these points are shown in Figure 4-22. Then these calculated responses are polluted and used as measured nonlinear responses. The noise is added to the FRFs by multiplying a normal distribution noise, with unity mean and 0.01 standard deviation, with the linear and nonlinear FRFs. A sample comparison for the linear and nonlinear FRFs is given in Figure 4-23 for  $\alpha_{11}$ . Linear and nonlinear FRFs are found for harmonic forcing with amplitudes of 0.01N and 1N, respectively.

It is assumed in this case study that only the first columns of the linear and nonlinear receptance matrices are measured. Then, firstly the missing elements of the linear FRF matrix are calculated by using FRF synthesis method. The calculated *NLI* values are shown in Figure 4-24a. From Figure 4-24a it can easily be concluded that there is a nonlinear element between ground and coordinate 1. Furthermore, Figure 4-24b reveals that system has stiffness type of nonlinearity since DF has much higher real part compared to its imaginary part.

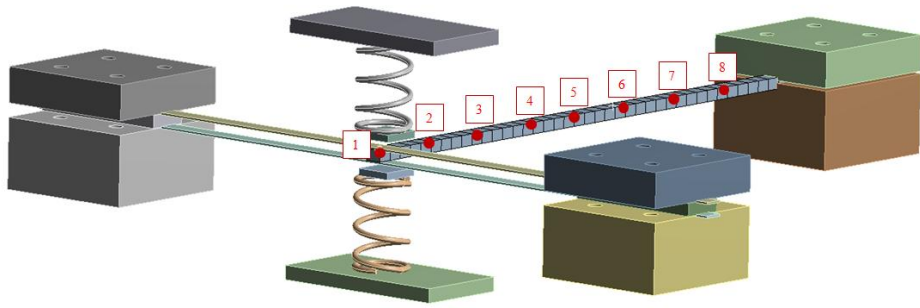


Figure 4-22. 8 equidistant measurement nodes

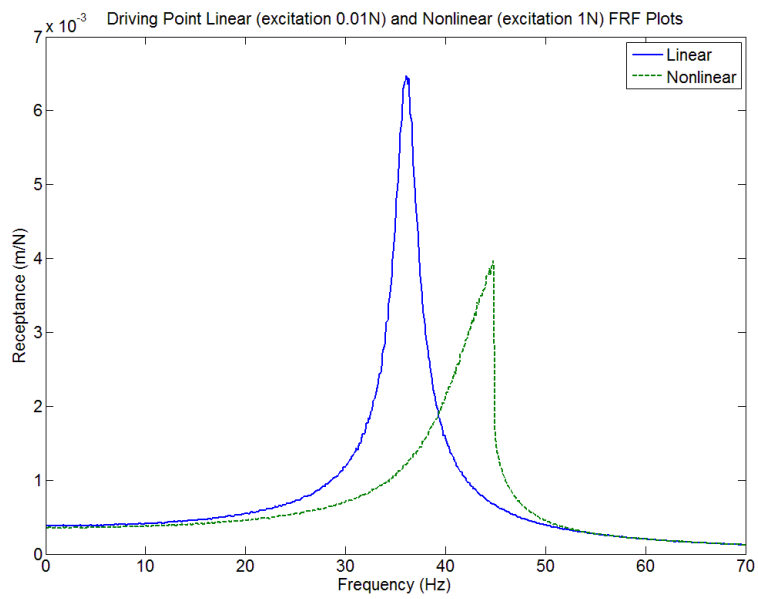


Figure 4-23. Driving point linear (for  $F=0.01N$ ) and nonlinear (for  $F=1N$ ) FRF plots

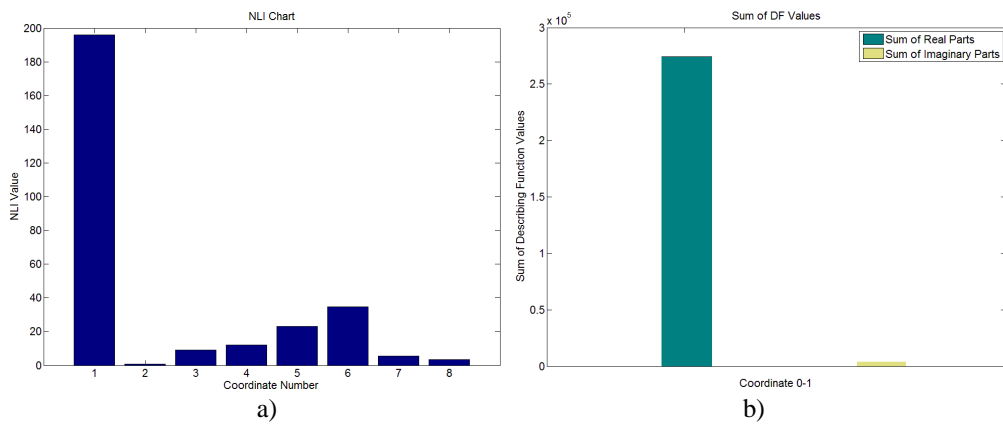


Figure 4-24. a) Nonlinearity index chart, b) Sums of real and imaginary parts of DF values at high forcing excitation

The DF representing these nonlinear elements is calculated at different response amplitudes and is plotted in Figure 4-25. This time it is not possible to identify the type of nonlinearity from the general pattern of the curve. The reason is not having a single nonlinear element but two nonlinear elements with completely different behavior. Obviously, improved DF method will not be helpful in identifying the type of the nonlinearity.

The inversion of DF is obtained for this case study by using the DFI method, and RF plot obtained is presented in Figure 4-26. By first fitting a curve to the calculated RF plot, parametric identification can easily be made. In order to show the accuracy of the method in predicting nonlinear RF, the exact RF curve is also shown in the same figure.

As there are two stiffness type nonlinearities at the same location, parametric identification is not straightforward. The RF plot reveals the backlash value as 0.0002511 m. Then, the RF values are curve fitted to polynomial functions in order to obtain the coefficients of the nonlinear elements. The least error is obtained for a linear and cubic function. The parametric identification results for the nonlinear elements are tabulated in Table 4-3. As can be seen from the table, the identification is very successful and the identified values do not deviate from the actual values more than 1.7%.

Table 4-3. Parametric identification results for the nonlinear elements

	Actual	Identified by the DFI method	Error %
Backlash (m)	0.00025	0.0002511	0.4
$k_1'$ (Linear stiffness part) N/m	1000	990	-1
$k_1''$ (cubic stiffness constant) N/m <sup>3</sup>	$6 \cdot 10^7$	$6.1 \cdot 10^7$	1.7

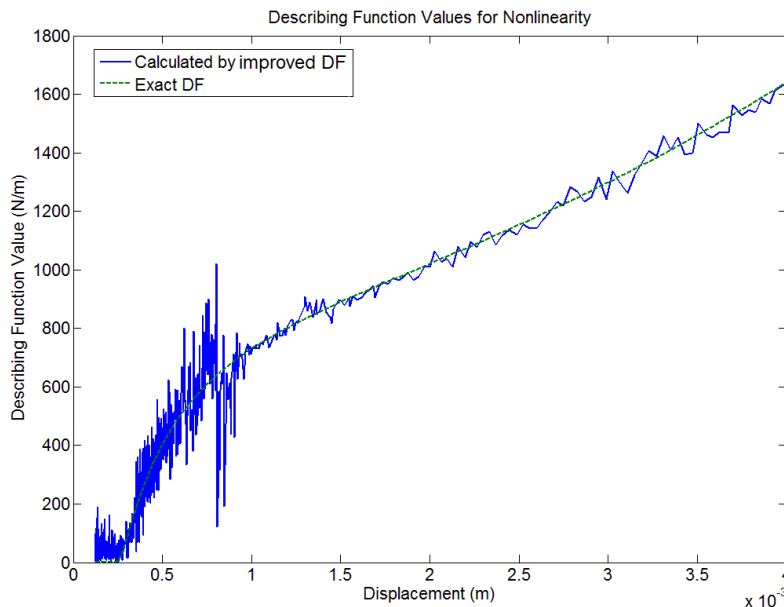


Figure 4-25. Calculated and exact DFs for nonlinear element between coordinate 1 and ground

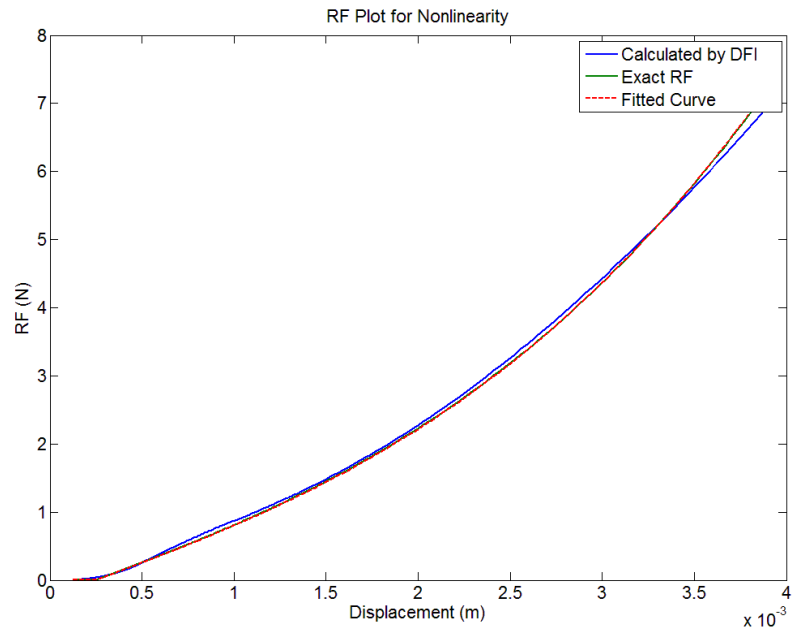


Figure 4-26. Calculated, exact and fitted RF plots for nonlinear element between coordinate 1 and ground

The nonlinear FRFs are regenerated by using the method given in section 3.3. with the identified nonlinearities from the DFI method (Figure 4-27) for a forcing level of 1N. As the errors in parametric identification are very small for the DFI method, a good match is obtained. The power of this method can be seen in this case study where two or more nonlinear elements can be successfully identified.

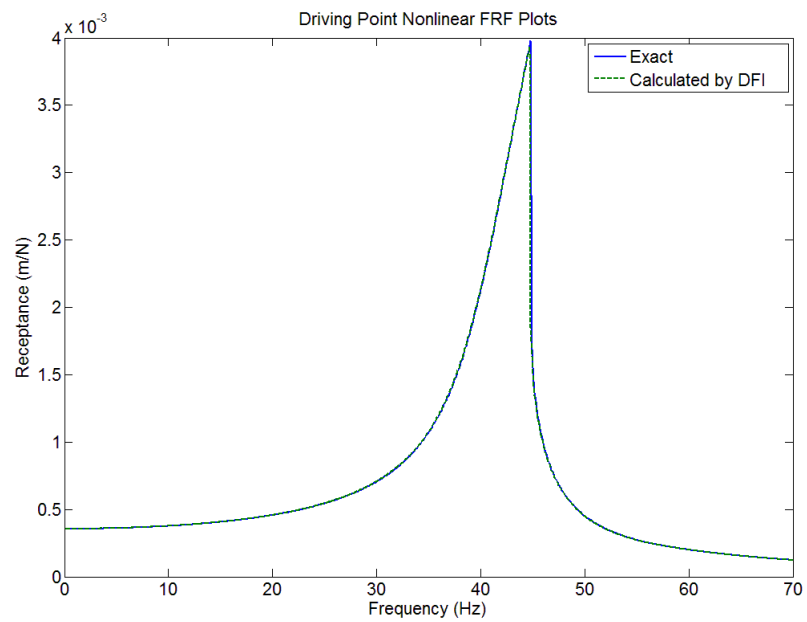


Figure 4-27. Nonlinear driving point FRFs at 1N forcing level, (blue: exact values; green: calculated by the DFI method)

#### 4.4.4. Case Study 4: Stiffness and Friction Nonlinear Elements at Different Locations

In the last case study, a nonlinear coulomb friction element represented by  $c_2'$  ( $= 0.001$  N/ms) is taken between the coordinate 1 and coordinate 2, and a nonlinear hardening cubic stiffness represented by  $k_4'$  ( $= 0.8 \cdot 10^6 x^2$  N/m) is added between coordinate 3 and coordinate 4, as shown in Figure 4-28, are considered.

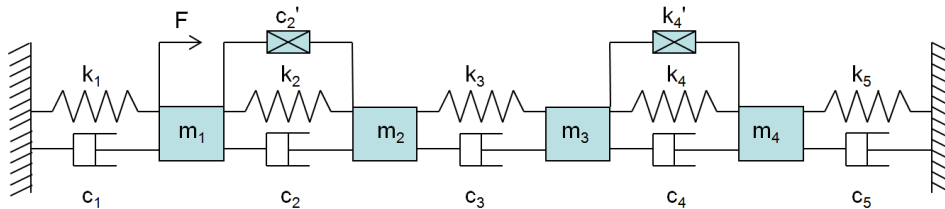


Figure 4-28. Four DOFs discrete system with two nonlinear elements at different coordinates

The numerical values of the linear system elements and the FRF calculation procedure are the same as in case study 1. Since the system has both coulomb friction and nonlinear hardening spring elements, the linear FRFs cannot be obtained by applying low forcing. The coulomb friction element is dominant at low forcing and the nonlinear hardening spring dominates at high forcing. Therefore the linear FRFs cannot be obtained by applying low forcing to the system. Thus, the first column of the linear FRF matrix is obtained by matrix inversion. A sample comparison for the linear and nonlinear FRFs ( $\alpha_{11}$ ) is given in Figure 4-29. Nonlinear FRFs are found for harmonic forcing with amplitudes of 0.1N (low forcing) and 50N (high forcing), respectively.

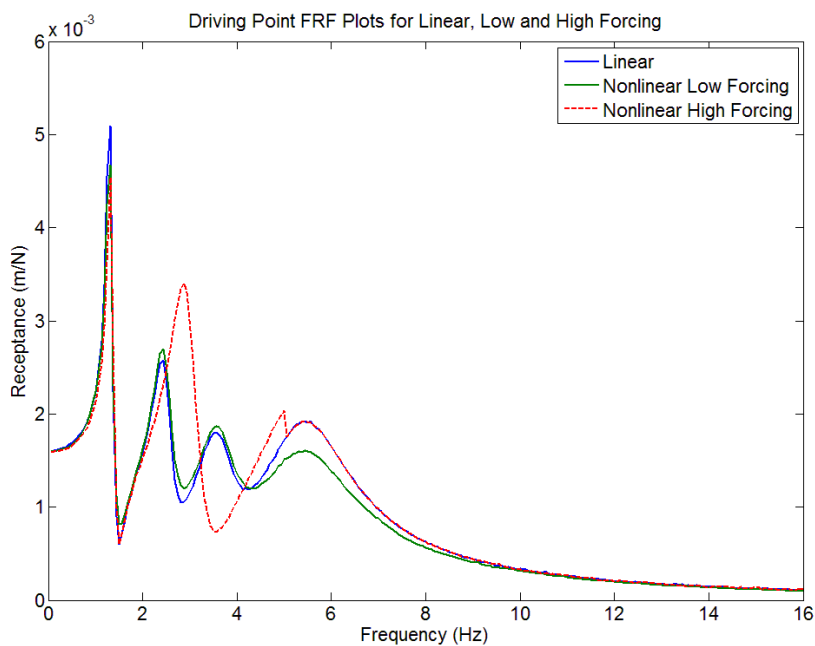


Figure 4-29. Driving point linear, low forcing (for  $F=0.1$ N) and high forcing (for  $F=50$ N) FRF plots

The calculated *NLI* values are shown in Figure 4-30a. From Figure 4-30a it can easily be concluded that there are nonlinear elements between coordinate 1 - coordinate 2 and coordinate 3 - coordinate 4. Furthermore, Figure 4-30b reveals that the nonlinear element between coordinate 3 - coordinate 4 is stiffness type of nonlinearity since DF has much higher real part compared to its imaginary part and the nonlinear element between coordinate 1 - coordinate 2 is damping type of nonlinearity since DF has higher imaginary part compared to its real part.

Using the improved DF method, the DFs representing these nonlinear elements are calculated and are plotted in Figure 4-31a as functions of response amplitudes. From the general pattern of the curves it may be possible to identify the types of nonlinearity. Fitting a curve to the calculated values makes the parametric identification easier.

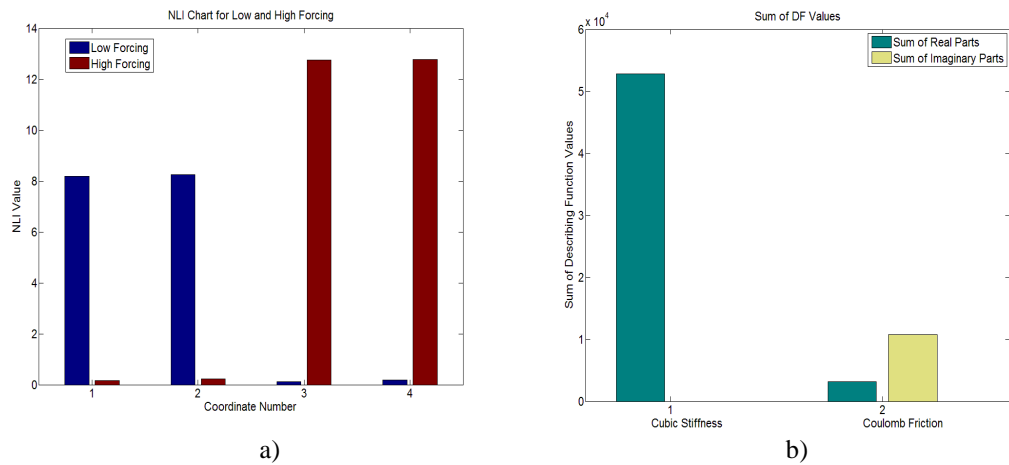


Figure 4-30. a) Nonlinearity index chart, b) Sums of real and imaginary parts of DF values

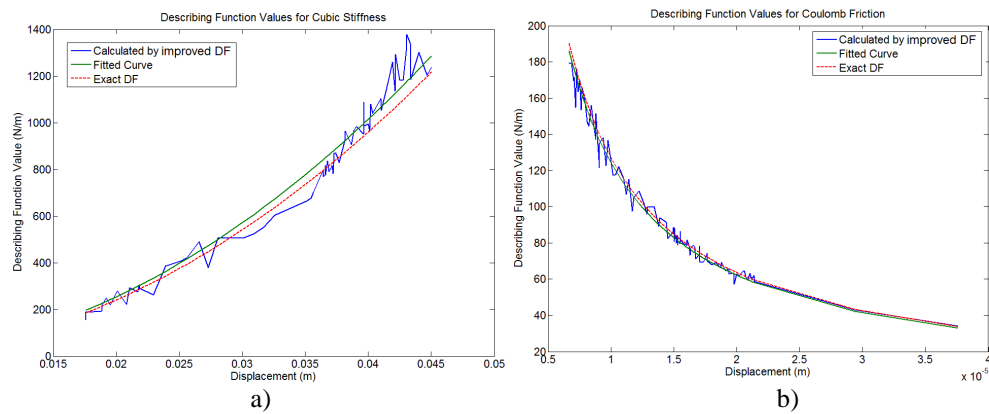


Figure 4-31. Calculated, fitted and exact DFs. a) For nonlinear element between coordinate 3 and coordinate 4, b) For nonlinear element between coordinates 1 and 2

Alternatively, the types of nonlinear elements can be identified more easily if the DFI method is used. The inversion of DFs is obtained in this case study by using the DFI method, and RF plots obtained are presented in Figure 4-32. Figure 4-32a gives the RF plot for the nonlinearity between the third coordinate and fourth coordinate, whereas Figure 4-32b shows the RF plot

for the nonlinearity between coordinates 1 and 2. By first fitting curves to the calculated RF plots, parametric identification can easily be made.

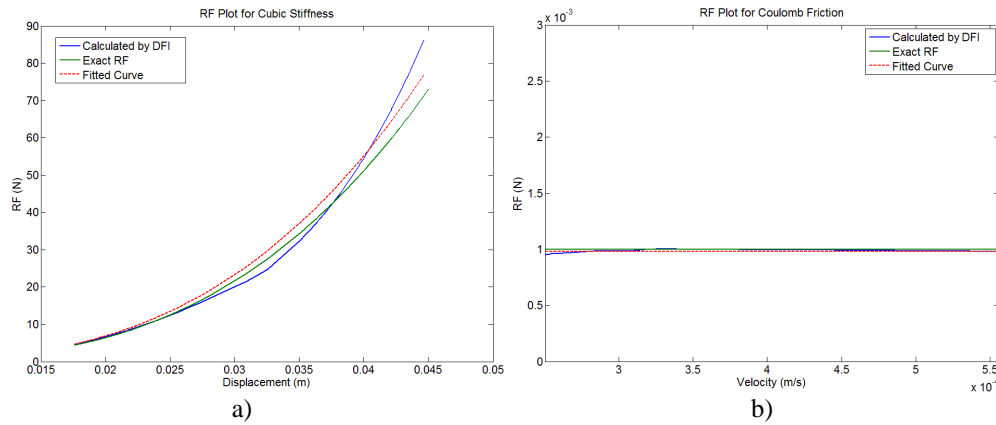


Figure 4-32. Calculated, exact and fitted RF plots. a) For nonlinear element between coordinate 3 and 4, b) For nonlinear element between coordinates 1 and 2

The parametric identification results with the DFI and improved DF methods for the nonlinear elements are tabulated in Table 4-4. As it can be seen from the table, the identified values do not deviate from the actual values more than 6% in the DFI and improved DF methods. However, the DF forms must be known to perform improved DF method for parametric identification. The nonlinear FRFs are regenerated for high forcing level by using the method given in section 3.3. with the identified nonlinearities from the DFI and improved DF methods (Figure 4-33). As the errors in parametric identification are very small for all methods, a good match is obtained.

Table 4-4. Parametric identification results for the nonlinear elements

	Actual	Identified by the DFI method		Identified by the improved DF method	
		Value	Error %	Value	Error %
$c_2'$ (coulomb friction constant) Ns/m	0.00100	0.00098	-2	0.00098	-2
$k_4'$ (cubic stiffness constant) N/m <sup>3</sup>	$0.8 \cdot 10^6$	$0.85 \cdot 10^6$	6	$0.85 \cdot 10^6$	6

The last case study was presented to show the weak point of the improved DF method. The method relies on the assumption that somehow the linear FRFs can be obtained. If this is not possible, as it is in this case study due to coulomb friction, then the dynamic stiffness matrix for the linear part of the system has to be theoretically calculated to find the linear FRFs.

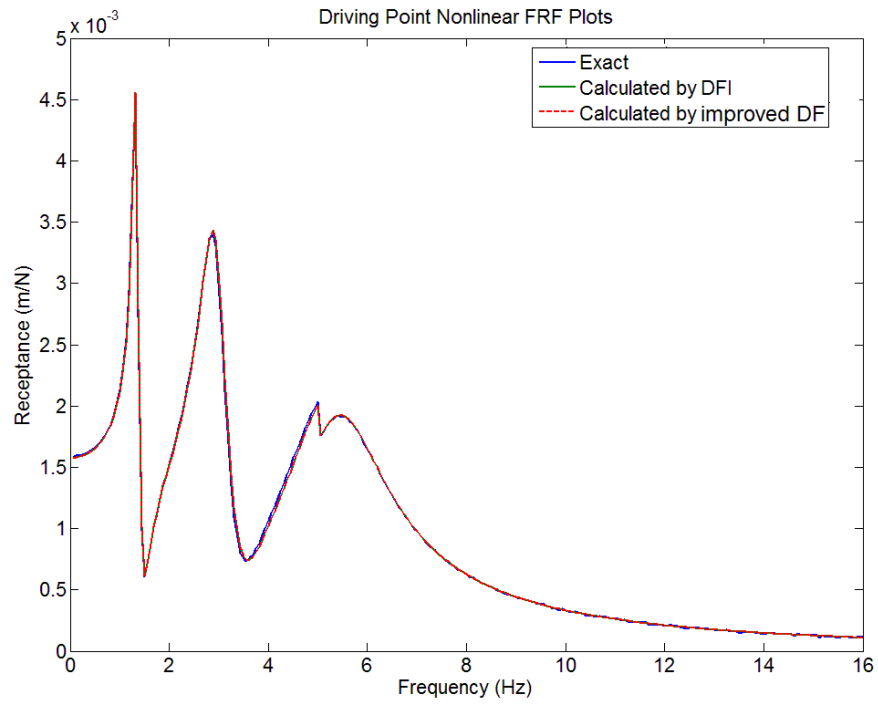


Figure 4-33. Nonlinear driving point FRFs for high forcing level, (blue: exact values; green: calculated by the DFI method; dashed red: calculated by the improved DF method)



## CHAPTER 5

### IDENTIFICATION OF RESTORING FORCE SURFACES IN NONLINEAR MDOF SYSTEMS FROM FRF DATA USING NONLINEARITY MATRIX

The approach proposed in this chapter aims to perform the nonlinear identification directly from a series of measured nonlinear FRFs. The proposed method uses only the nonlinear FRFs, thus, it also works when friction is present in the structure. It is shown that Restoring Force Surfaces (RFS) can be identified more accurately by employing this approach.

#### 5.1. Nonlinearity Matrix Evaluation

In general applications, the linear model of the system can be obtained by using FEM, and only for the identification of nonlinearity experiments can be made. Alternatively, the FRF of the underlying linear system can be obtained from FRF measurements in the system at very low forcing levels, where the nonlinear internal forces will be negligible. However, when there is only friction type of nonlinearity, FRFs measured at low amplitude of vibration will not represent FRFs of the underlying system; on the contrary, the FRFs measured at high response levels will represent FRFs of the linear counterpart. Comparison of FRFs measured at different response levels will reveal whether there is only friction type of nonlinearity, so that FRFs measured at high response level can be taken as the FRFs for the underlying linear system. Yet, if the system has multiple nonlinearities including friction type of nonlinearity, it may be difficult to measure the FRFs of the underlying linear system experimentally, and using finite element model of the system seems to be the only alternative to obtain linear FRFs of the linear counterpart.

In an attempt to obtain the nonlinearity matrix from experimental measurements, the following methodology is proposed;

Let  $[\Delta]$  represent the nonlinearity matrix at forcing  $F_1$ . Then

$$[\Delta_1] = [\alpha_1^{NL}]^{-1} - [\alpha]^{-1} \quad (5.1)$$

Changing the forcing to another level  $F_2$ , equation (5.1) becomes;

$$[\Delta_2] = [\alpha_2^{NL}]^{-1} - [\alpha]^{-1} \quad (5.2)$$

Subtracting equation (5.2) from equation (5.1) yields

$$[\Delta_2] - [\Delta_1] = [\alpha_2^{NL}]^{-1} - [\alpha_1^{NL}]^{-1} \quad (5.3)$$

Equation (5.3) is now independent of the linear FRF matrix. The nonlinearity matrices will be functions of the displacement only if a displacement dependent nonlinearity is assumed. Furthermore, the nonlinearity matrix for first level of forcing and second level of forcing will be of the same functional form. The only difference will be the displacement values used. Therefore, if a polynomial form is assumed for elements of the nonlinearity matrix and two nonlinear FRF matrices are measured from experiments, the coefficients for the function that describes the nonlinearity can be achieved.

$$v(X) = \sum_{i=1}^{\infty} c_i X^i \quad (5.4)$$

Equation (5.3) requires the complete nonlinear FRF matrix. However, as the nonlinear elements are usually at connections, measurement is required only at before and after the connection which yields a 2x2 matrix for each DOF. If a coordinate has more DOFs, then every DOF at that coordinate will have a 2x2 matrix. The only difficulty in application of this method to MDOF systems is that when exciting the coordinates before and after the connection, the displacement of the nonlinear element has to be same. Thus, the forcing levels have to be chosen appropriately. In the next chapter, the application of the proposed Direct Nonlinearity by Describing Functions (DDF) method will be presented.

## 5.2. Application of the DDF Method

The first step to be performed is to test the nonlinear structure at two excitation levels. Equation (5.3) requires having the inverses of the nonlinear FRF matrices which is sensitive to noise. In order to minimize this effect, the excitation levels can be chosen high enough or averaging can be performed. However, if the forcing levels are high then friction type nonlinearities lose their effect. In order to identify this effect, a low forcing test is also performed. Moreover,  $[\Delta_2] - [\Delta_1]$  from equation (5.3) will have complex elements, whose real part represents the stiffness nonlinearity and the imaginary part represents the damping nonlinearity.

The application of DDF will be presented on a SDOF system for the sake of clarity. Extension of this application to MDOF systems is straightforward.

For a SDOF system, equation (5.3) reduces to;

$$\Delta_2 - \Delta_1 = \frac{1}{\alpha_2^{NL}} - \frac{1}{\alpha_1^{NL}} \quad (5.5)$$

In order to solve equation (5.5) we need as many equations as the order of the polynomial. These equations can be generated from the nonlinear FRF values, which have distinct displacement values for each frequency. In other words, if we assume a polynomial up to the third order for the nonlinearity, we will need at least three equations.

$$(c_1 X_2 + c_2 X_2^2 + c_3 X_2^3) - (c_1 X_1 + c_2 X_1^2 + c_3 X_1^3) = \frac{1}{\alpha_2^{NL}} - \frac{1}{\alpha_1^{NL}} \quad (5.6)$$

$$\begin{bmatrix} X_2 - X_1 & X_2^2 - X_1^2 & X_2^3 - X_1^3 \end{bmatrix} \begin{bmatrix} c_1 \\ c_2 \\ c_3 \end{bmatrix} = \frac{1}{\alpha_2^{NL}} - \frac{1}{\alpha_1^{NL}} \quad (5.7)$$

$$\begin{bmatrix} X_2(\omega_1) - X_1(\omega_1) & X_2^2(\omega_1) - X_1^2(\omega_1) & X_2^3(\omega_1) - X_1^3(\omega_1) \\ X_2(\omega_2) - X_1(\omega_2) & X_2^2(\omega_2) - X_1^2(\omega_2) & X_2^3(\omega_2) - X_1^3(\omega_2) \\ X_2(\omega_3) - X_1(\omega_3) & X_2^2(\omega_3) - X_1^2(\omega_3) & X_2^3(\omega_3) - X_1^3(\omega_3) \end{bmatrix} \begin{bmatrix} c_1 \\ c_2 \\ c_3 \end{bmatrix} = \dots \quad (5.8)$$

$$\begin{bmatrix} \frac{1}{\alpha_2^{NL}(\omega_1)} - \frac{1}{\alpha_1^{NL}(\omega_1)} \\ \frac{1}{\alpha_2^{NL}(\omega_2)} - \frac{1}{\alpha_1^{NL}(\omega_2)} \\ \frac{1}{\alpha_2^{NL}(\omega_3)} - \frac{1}{\alpha_1^{NL}(\omega_3)} \end{bmatrix}$$

The FRF values at each frequency give us one equation. Most of the time we will have more FRF values than that is required to solve the coefficients. We will use this property for our benefit to have a better fit of coefficients for the whole frequency bandwidth. Thus if we have “n” frequencies equation (5.8) can be expanded as;

$$\begin{bmatrix} X_2(\omega_1) - X_1(\omega_1) & X_2^2(\omega_1) - X_1^2(\omega_1) & X_2^3(\omega_1) - X_1^3(\omega_1) \\ X_2(\omega_2) - X_1(\omega_2) & X_2^2(\omega_2) - X_1^2(\omega_2) & X_2^3(\omega_2) - X_1^3(\omega_2) \\ X_2(\omega_3) - X_1(\omega_3) & X_2^2(\omega_3) - X_1^2(\omega_3) & X_2^3(\omega_3) - X_1^3(\omega_3) \\ \vdots & \vdots & \vdots \\ X_2(\omega_n) - X_1(\omega_n) & X_2^2(\omega_n) - X_1^2(\omega_n) & X_2^3(\omega_n) - X_1^3(\omega_n) \end{bmatrix} \begin{bmatrix} c_1 \\ c_2 \\ c_3 \end{bmatrix} = \dots \quad (5.9)$$

$$\begin{bmatrix} \frac{1}{\alpha_2^{NL}(\omega_1)} & \frac{1}{\alpha_1^{NL}(\omega_1)} \\ \frac{1}{\alpha_2^{NL}(\omega_2)} & \frac{1}{\alpha_1^{NL}(\omega_2)} \\ \frac{1}{\alpha_2^{NL}(\omega_3)} & \frac{1}{\alpha_1^{NL}(\omega_3)} \\ \vdots & \vdots \\ \frac{1}{\alpha_2^{NL}(\omega_n)} & \frac{1}{\alpha_1^{NL}(\omega_n)} \end{bmatrix}$$

Equation (5.9) can be solved by pseudo inversion which will give us a least square fit for the polynomial coefficients for the whole frequency bandwidth. After successful identification of high forcing effective nonlinearities we can evaluate the linear FRF from equation (5.1). After evaluating the linear FRF, equation (5.1) is solved with the low forcing nonlinear FRF by which the nonlinearity DF values for low forcing nonlinearities such as friction can be obtained.

In the previous chapter the DFI method was introduced. The DFI method can be easily applied after the DDF method. The following case studies and experimental studies will show the effectiveness of this method.

### 5.3. Case Studies

#### 5.3.1. Case Study 1: Backlash and Coulomb Friction Nonlinear Elements at the Same Location

The DDF is applied to a SDOF discrete system with a nonlinear elastic element represented by  $k_1'$  (a linear stiffness of 1000 N/m with a backlash of 0.005 m) and a coulomb friction element  $c_1'$  ( $= 0.001 \text{ sgn}(\dot{x}) \text{ N}$ ), as shown in Figure 5-1. The numerical values of the linear system elements are given as follows:

$$k_1 = 500 \text{ N/m}$$

$$c_1 = 5 \text{ Ns/m}$$

$$m_1 = 1 \text{ kg}$$

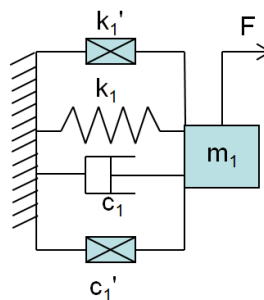


Figure 5-1. SDOF discrete system with two nonlinear elements

The time response of the system to sinusoidal forcing is calculated with MATLAB by using the ordinary differential equation solver ODE45. The simulation was run for 32 seconds at each frequency to ensure that transients die out. The frequency range of the harmonic excitation that is used during the simulations is from 0.0625 to 16 Hz with frequency increments of 0.0625 Hz. Three forcing levels (0.01N, 3N, 20N) are used, in turn, in the simulations. Before using the calculated FRFs as simulated experimental data, they are polluted by using the “normrnd” function of MATLAB with zero mean, normal distribution and standard deviation of 5% of the maximum amplitude of the FRF value. A sample comparison for the nonlinear and linear FRFs ( $\alpha_{11}$ ) is given in Figure 5-2.

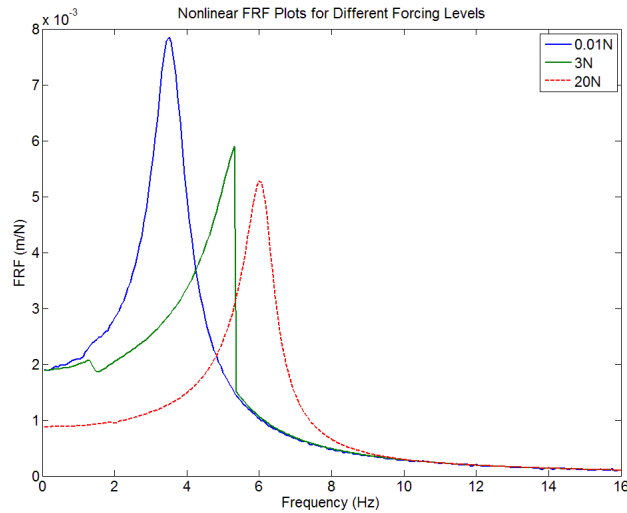


Figure 5-2. Driving point FRFs; blue: 0.01N, green: 3N, red: 20N

Using the DDF method, the DFs representing these nonlinear elements are calculated from simulated experimental results and are plotted in Figure 5-3. Figure 5-3a is plotted using the real part of the DF and Figure 5-3b is plotted using the imaginary part of the DF.

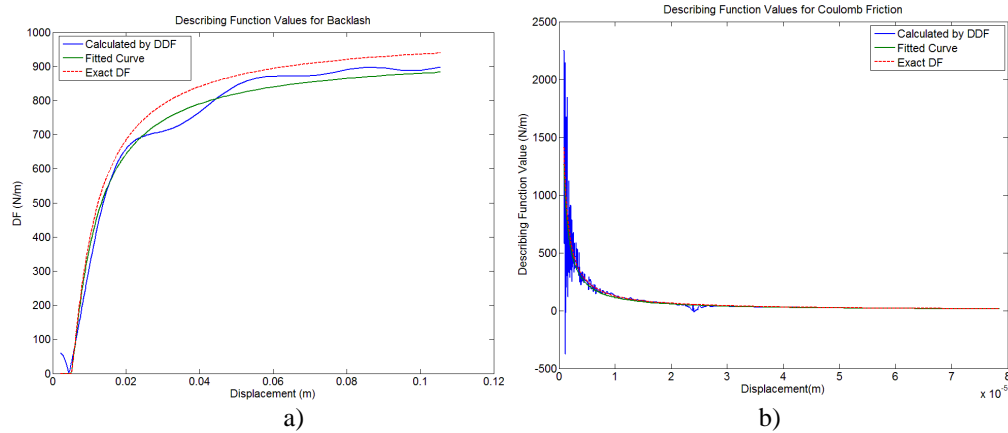


Figure 5-3. Calculated, fitted and exact DFs, a) stiffness type (backlash) nonlinear element, b) damping type (friction) nonlinear element

Alternatively, the types of nonlinear elements can be identified more easily if the DFI method proposed in the previous chapter is used. The calculated RF plots are presented in Figure 5-4. By first fitting curves to the calculated RF plots, parametric identification can easily be made.

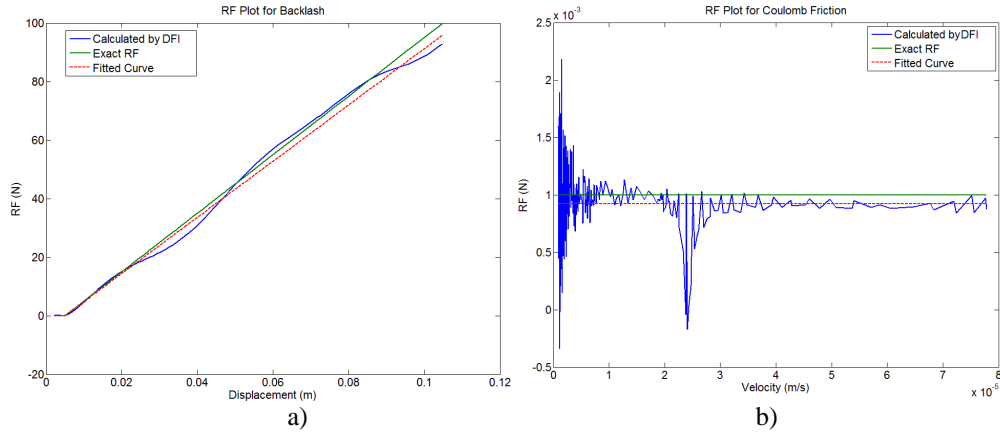


Figure 5-4. Calculated, exact and fitted RFs, a) stiffness type (backlash) nonlinear element, b) damping type (friction) nonlinear element

The parametric identification results with the DFI method and using DF fitted curves as suggested in the DF method for the nonlinear elements are tabulated in Table 5-1. As it can be seen from the table, the identified values do not deviate from the actual values more than 8% for the DFI method and %10 for the DF method. However, the DF forms must be known to perform the DF method for parametric identification. The nonlinear FRFs are regenerated for 20N forcing level by using the method given in section 3.3. with the identified nonlinearities from the DFI and DF methods (Figure 5-5). As the DFI method is slightly better in identification, the match of the DFI method is better than DF method.

Table 5-1. Parametric identification results for the nonlinear elements

	Actual	Identified by the DFI method		Identified by the DF method	
		Value	Error %	Value	Error %
Backlash (m)	0.0050	0.0050	0	-	-
$k_1'$ (Linear stiffness part) N/m	1000	960	-4	940	-6
$c_1'$ (coulomb friction constant) Ns/m	0.0010	0.00092	-8	0.0009	-10

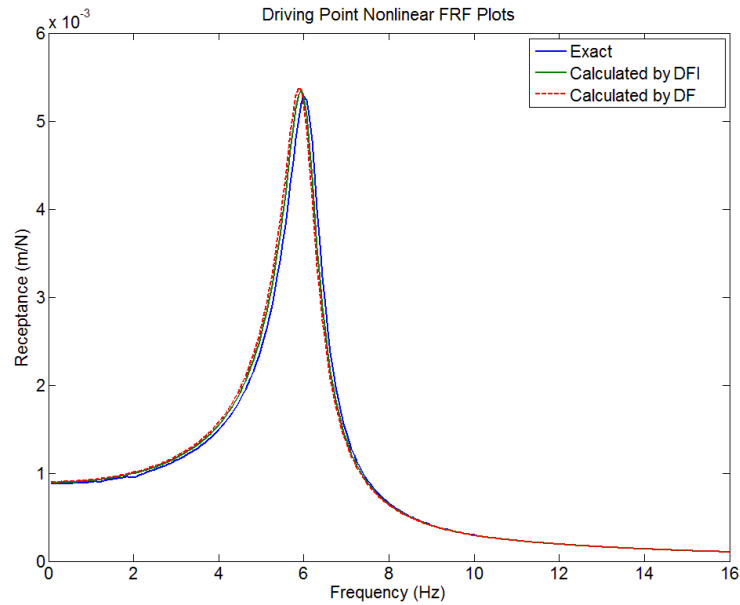


Figure 5-5. Nonlinear driving point FRFs for high forcing level, (blue: exact values; green: calculated using the nonlinear parameters from the DFI method; dashed red: calculated using the nonlinear parameters from the DF method)

### 5.3.2. Case Study 2: Cubic Stiffness and Coulomb Friction Nonlinear Elements at the Same Location

The DDF method is again applied to the same SDOF discrete system with a nonlinear elastic element represented by  $k_1'$  (a nonlinear hardening cubic spring =  $10^6 x^2$  N/m) and a coulomb friction element  $c_1'$  ( $= 0.001 \text{ sgn}(\dot{x})$  N), as shown in Figure 5-1. The nonlinear FRFs ( $\alpha_{11}$ ) are given in Figure 5-6 for three different forcing levels. Following the DDF method we obtain the DFs representing these nonlinear elements as given in Figure 5-7.

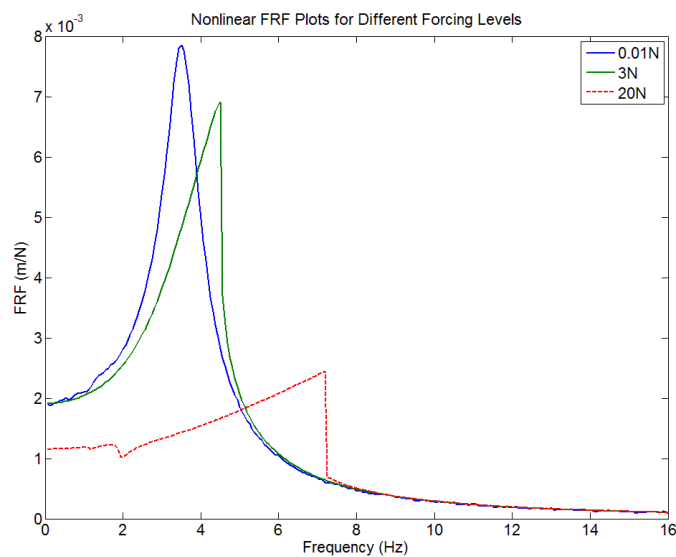


Figure 5-6. Driving point FRFs; blue: 0.01N, green: 3N, red: 20N

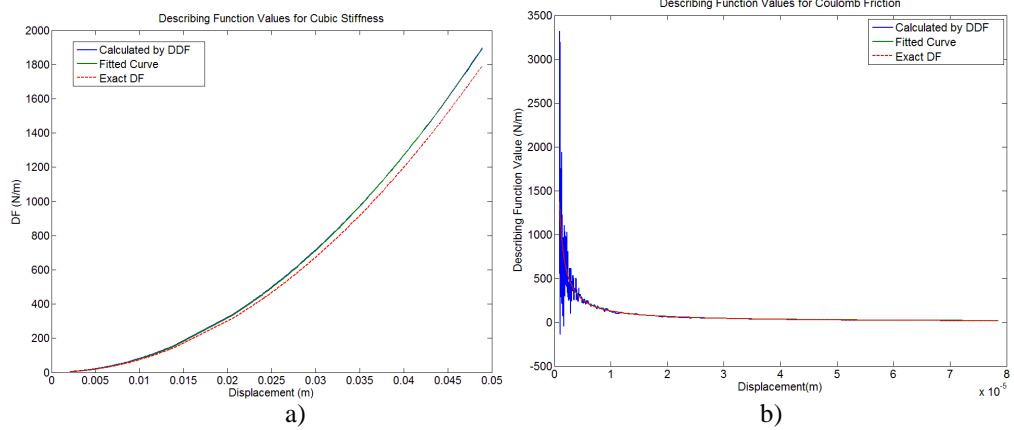


Figure 5-7. Calculated, fitted and exact DFs, a) stiffness type (cubic stiffness) nonlinear element, b) damping type (friction) nonlinear element

Similarly, the types of nonlinear elements can be identified more easily if the DFI method is used. These plots are given in Figure 5-8.

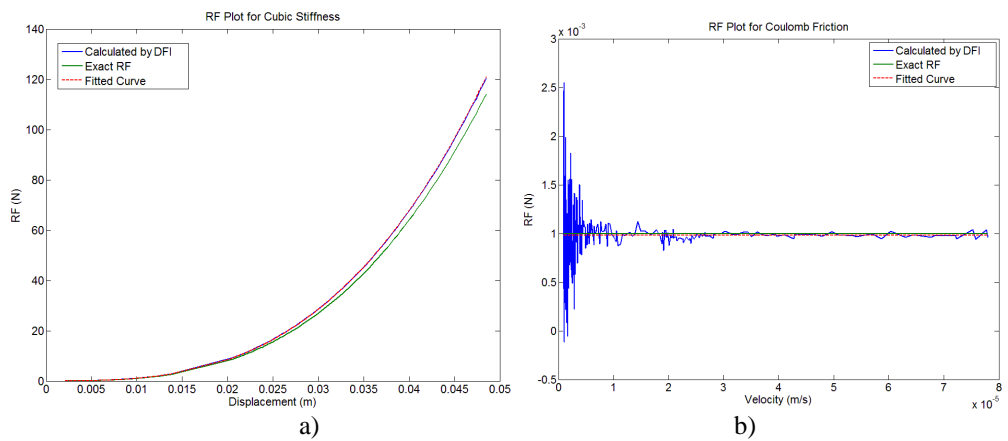


Figure 5-8. Calculated, exact and fitted RF, a) stiffness type (cubic stiffness) nonlinear element, b) damping type (friction) nonlinear element

The parametric identification results with the DFI and using DF fitted curves as suggested in the DF method for the nonlinear elements are tabulated in Table 5-2. As it can be seen from the table, the identified values do not deviate from the actual values more than 6% for the DFI and DF methods. The nonlinear FRFs are regenerated for 3N forcing level by using the method given in section 3.3. with the identified nonlinearities from the DFI and DF methods (Figure 5-9). As the errors in parametric identification are very small for all methods, a good match is obtained for both methods.

Table 5-2. Parametric identification results for the nonlinear elements

	Actual	Identified by the DFI method		Identified by the DF method	
		Value	Error %	Value	Error %
$k_1'$ (cubic stiffness constant) $\text{N/m}^3$	$10^6$	$1.06 \cdot 10^6$	-6	$1.06 \cdot 10^6$	-6
$c_1'$ (coulomb friction constant) $\text{Ns/m}$	0.0010	0.00098	-2	0.001	0

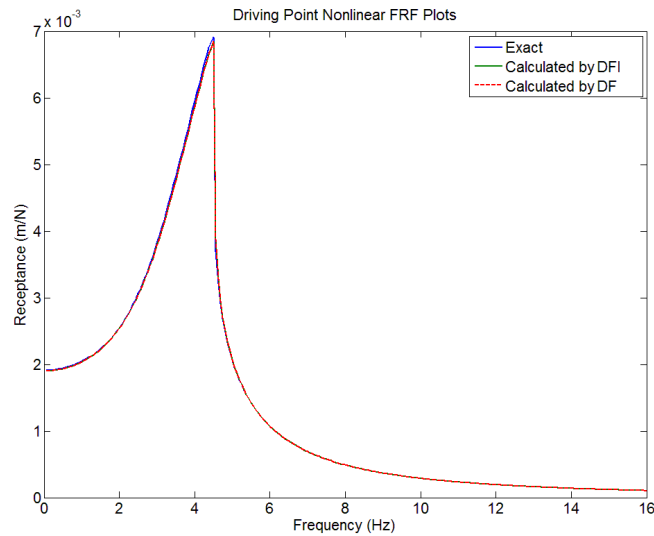


Figure 5-9. Nonlinear driving point FRFs for high forcing level, (blue: exact values; green: using the nonlinear parameters from the DFI method; dashed red: using the nonlinear parameters from the DF method)

### 5.3.3. Case Study3: Cubic Stiffness and Backlash Nonlinear Elements at the Same Location

The DDF method is applied to a 4 DOF discrete system with a nonlinear elastic element represented by  $k_4'$  (a linear stiffness of 100 N/m with a backlash of 0.005 m) and a nonlinear hardening cubic spring  $k_4'' (= 10^6 x^2 \text{ N/m})$  between coordinates 3 and 4, as shown in Figure 5-10.

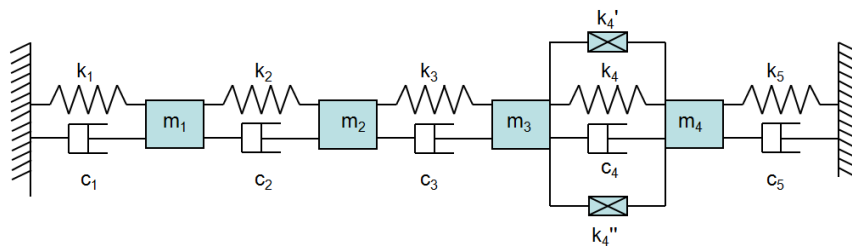


Figure 5-10. Four DOFs discrete system with two nonlinear elements at the same location

The numerical values of the linear system elements are given as follows:

$$k_1 = k_2 = k_3 = k_4 = k_5 = 500 \text{ N/m}$$

$$c_1 = c_2 = c_3 = c_4 = c_5 = 5 \text{ Ns/m}$$

$$m_1 = 0.5 \text{ kg}, m_2 = 1 \text{ kg}, m_3 = 1.5 \text{ kg}, m_4 = 3 \text{ kg}$$

A sample comparison for the nonlinear and linear FRFs ( $\alpha_{33}$ ) is given in Figure 5-11.

In this case study, first the low (10N) and high forcing (20N) levels are applied from 3<sup>rd</sup> coordinate, and then from 4<sup>th</sup> coordinate. Employing the DDF method and by using FRFs of the 3<sup>rd</sup> and 4<sup>th</sup> coordinates only ( $\alpha_{33}$ ,  $\alpha_{43}$ ,  $\alpha_{44}$ ,  $\alpha_{34}$ ), the DFs representing these nonlinear elements are obtained as given in Figure 5-12. This time it is not possible to identify the types of nonlinearity from the general pattern of the curve. Thus, the DF method is not applicable to this case study. As it is the case in the previous examples, the total restoring force of nonlinear elements can be identified more easily when the DFI method is used.

As there are two stiffness type nonlinearities at the same location, parametric identification is not straightforward. The RF plot reveals the backlash value as 0.005m. The remaining RF curve is simply curve fitted to polynomials and a linear and cubic function gives the best fit. The parametric identification results for the nonlinear elements are tabulated in Table 5-3. As it can be seen from the table, the identified values do not deviate from the actual values more than 10%.

The nonlinear FRFs are regenerated by using the method given in section 3.3. with the identified nonlinearities from the DFI method (Figure 5-13). As the errors in parametric identification are small for the DFI method, a good match is obtained. The power of this method can be seen in this case study where two or more nonlinear elements can be successfully identified.

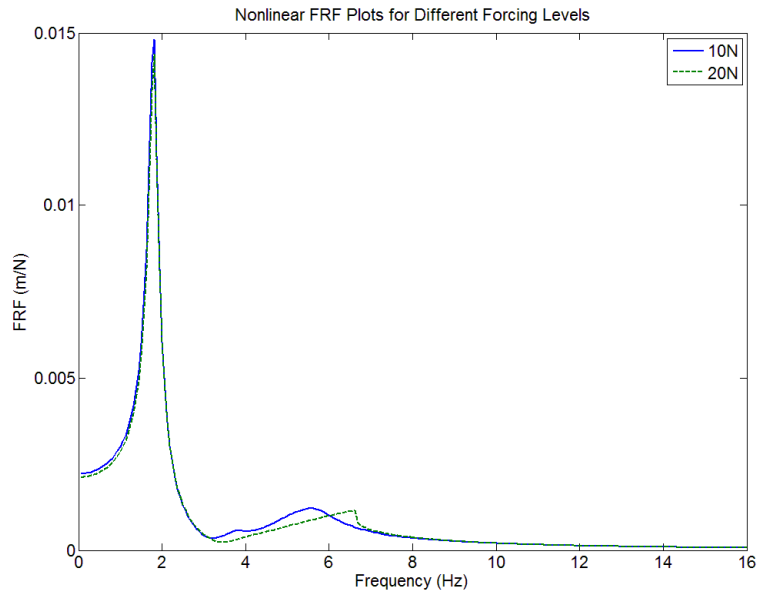


Figure 5-11. Nonlinear FRFs; blue: 10N, green: 20N

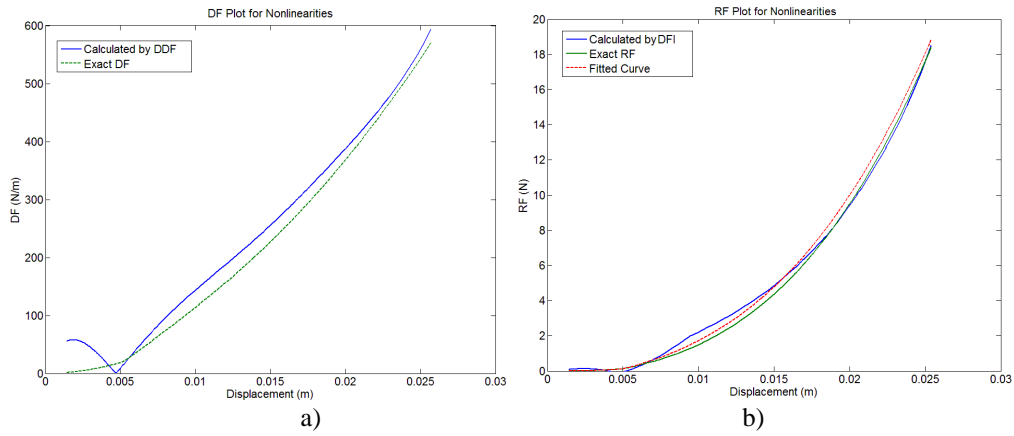


Figure 5-12. a) Calculated and exact DFs, b) calculated, exact and fitted RFs

Table 5-3. Parametric identification results for the nonlinear elements

	Actual	Identified by the DFI method	Error %
Backlash (m)	0.005	0.005	0
$k_1'$ (Linear stiffness part) N/m	100	110	10
$k_1''$ (cubic stiffness constant) N/m <sup>3</sup>	$10^6$	$0.96 \times 10^6$	-4

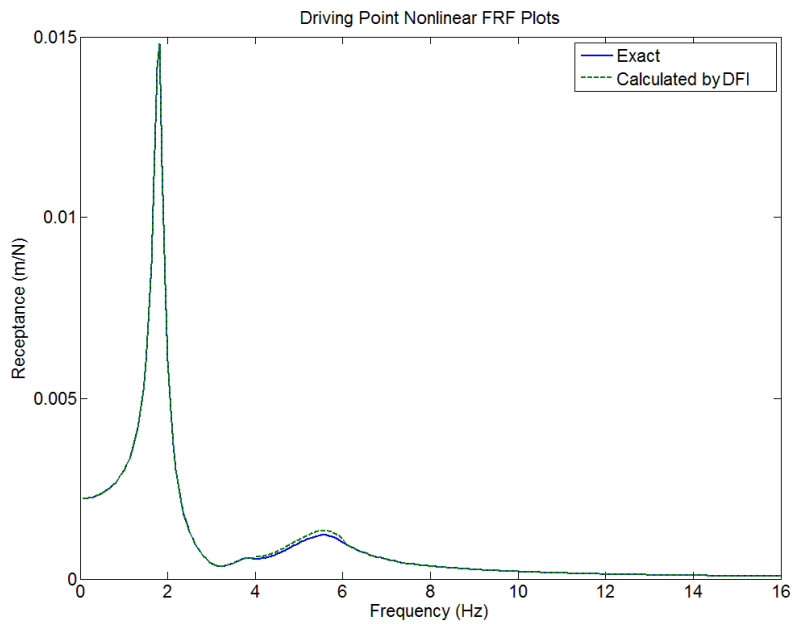


Figure 5-13. Nonlinear driving point ( $\alpha_{33}$ ) FRFs, (blue: exact values; green: calculated by the DFI method)

The last case study was presented to show the weak point of the DDF method. The method requires the nonlinear FRF matrix for MDOF systems which is very difficult and time consuming. The nonlinear elements are usually at connections, thus, measurement is required only for before and after the connection which yields a 2x2 matrix. Still this may be difficult to achieve. Therefore, if there is negligible amount of friction in the system, the improved DF and the DFI methods should be used.



## CHAPTER 6

### EXPERIMENTAL WORK AND VERIFICATION OF THE NONLINEAR IDENTIFICATION METHODS

#### 6.1. Experimental Study 1: Application of the DF and the DFI Methods on a SDOF System

For the implementation and validation of the DF and the DFI methods, linear and nonlinear modal tests were performed on a nonlinear structure. The test rig similar to the one first used by Ferreira [82], and then also by Siller [7] is used in this study (Figure 6-1). Dimensions and technical details of the rig manufactured for this study are given in Figure 6-2.

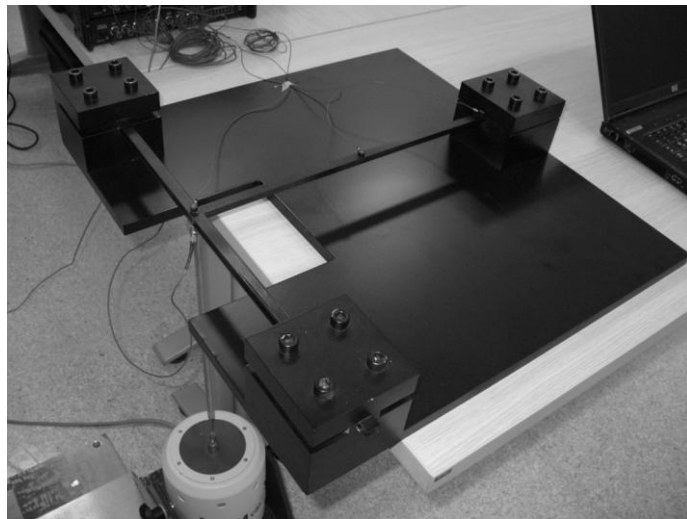


Figure 6-1. Test rig used in experimental study 1

This test rig is preferred for its simplicity in modeling the dynamic system since the structural configuration causes hardening stiffness nonlinearity only. The test rig consists of a linear cantilever beam with its free end held between two thin identical beams which generate cubic spring effect. The cantilever beam and the thin nonlinear beams were manufactured from St37 steel. The modal test setup configuration with its elements is shown in Figure 6-3.

For linear and nonlinear testing, a shaker (TIRA) was connected to the free end of the cantilever beam via a push-rod with a PCB 208C03 force transducer. The vibration responses were measured using three miniature PCB 352A24 accelerometers. The frequency resolution was 0.25 Hz due to the limitation of the software used with data acquisition system. Cubic nonlinearity in the system causes jump in the frequency response around resonance frequencies. Ability to observe this phenomenon is closely related to the frequency resolution employed in the harmonic vibration tests. Even though it was possible in the experimental study to capture the jump in the frequency response, it is believed that better results could have been obtained with a higher frequency resolution. The closed loop control was achieved by the Dataphysics Vector-1 shaker controller.

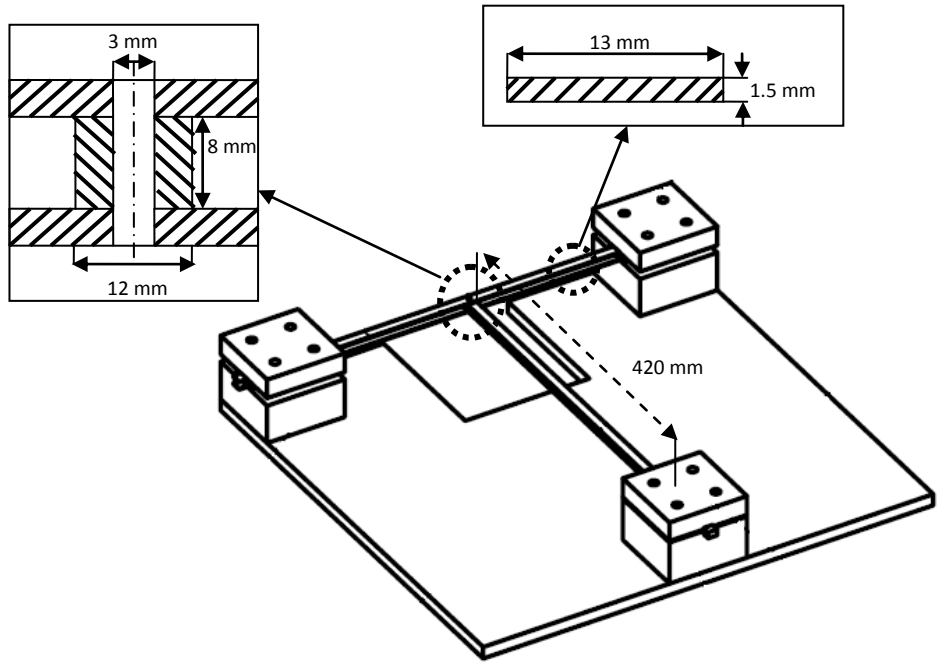


Figure 6-2. Dimensions of the test rig used in experimental study 1

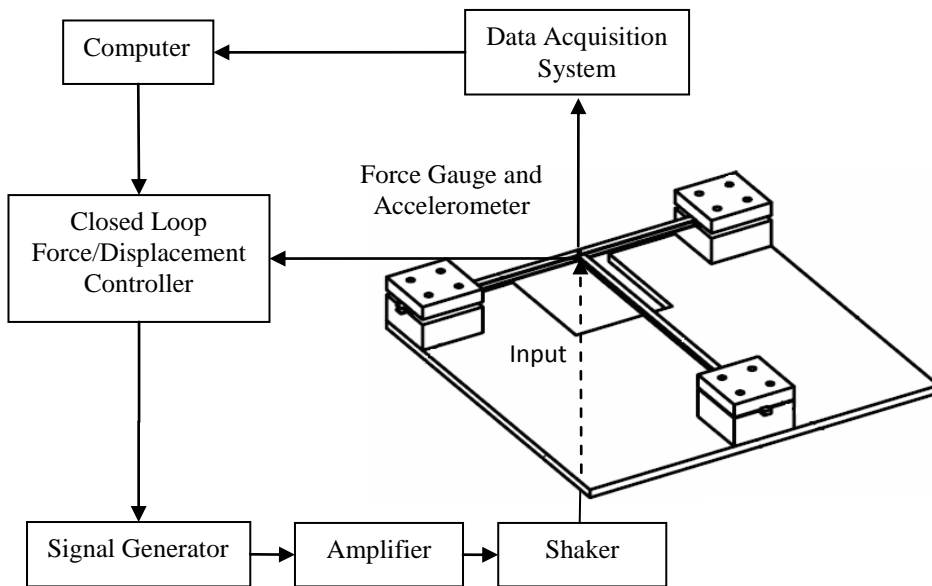


Figure 6-3. Experimental test setup used in experimental study 1

The linear and nonlinear modal tests are performed according to the work of Arslan *et al.* [79]. In [79], the application of the DF method and a new identification method which used constant displacement modal tests was presented. Furthermore, the application of the DF method used the smallest constant displacement modal test result as the linear FRF of the structure. Therefore for this case study, the modal tests are divided into two groups: constant force testing and constant displacement testing. Only the driving point FRFs are measured in these tests, which are sufficient to verify the identification methods.

The FRF results obtained for the constant force and constant displacement tests are shown in Figure 6-4 and Figure 6-5, respectively.

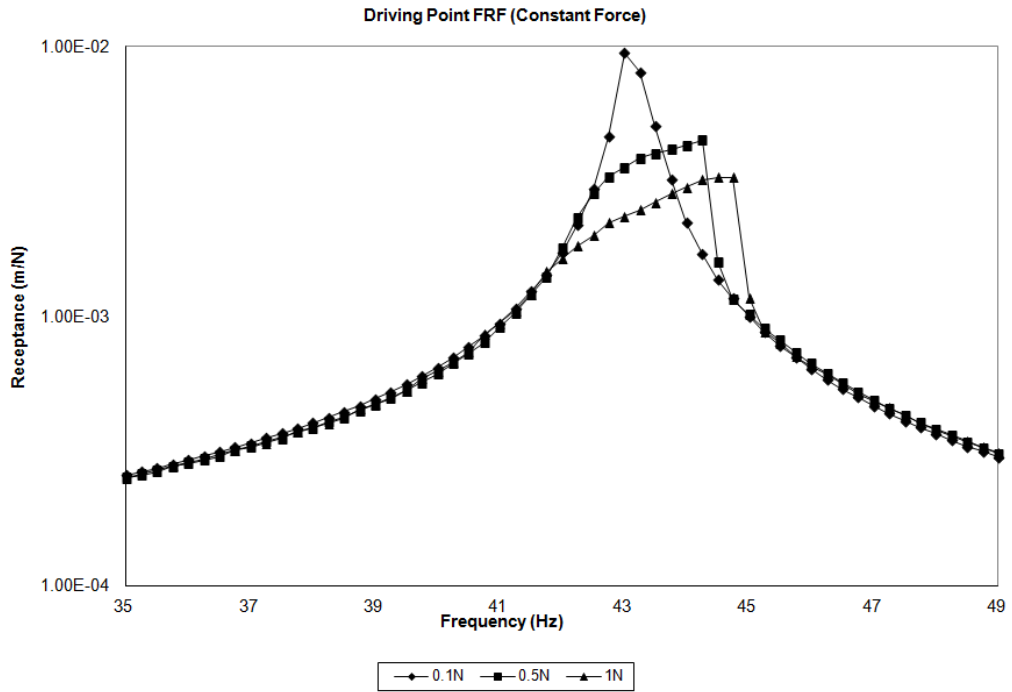


Figure 6-4. Constant force driving point FRF curves - experimental results

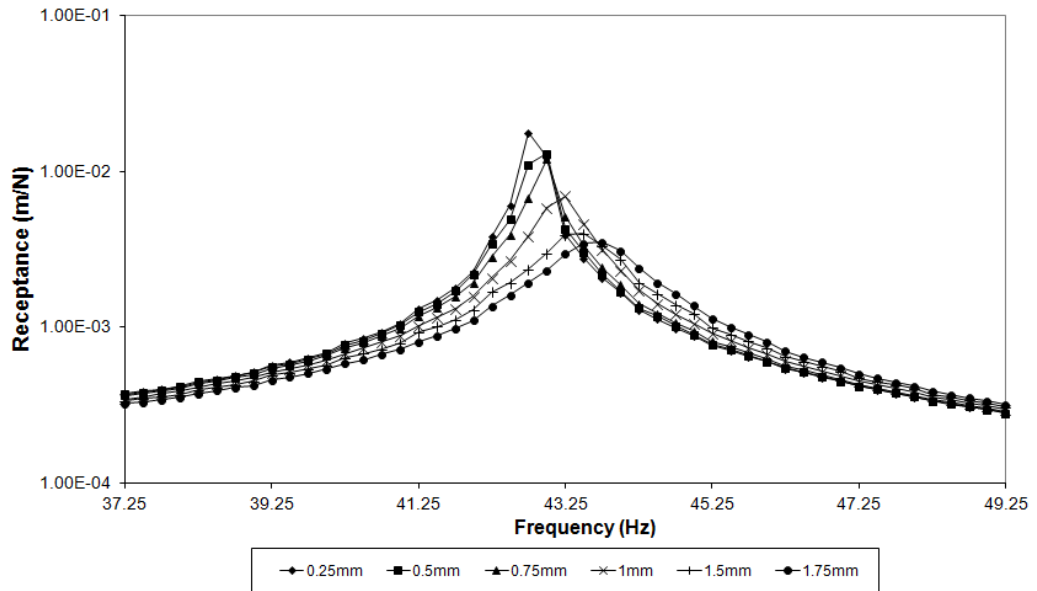


Figure 6-5. Constant displacement driving point FRF curves - experimental results

The FRF curve obtained by using constant displacement control with 0.25 mm of vibration amplitude is taken as the reference linear FRF since the nonlinear part of the elastic force is negligible compared to the linear part for this value of displacement. This is also the minimum displacement limit of the setup with the hardware used.

For a single degree of freedom system the nonlinearity matrix reduces to the DF defining the nonlinearity,

$$\Delta = \nu = \frac{\alpha - \alpha^{NL}}{\alpha^{NL} \alpha} \quad (6.1)$$

The nonlinear coefficient for the hardening cubic stiffness is obtained by a static test. In the static test a load cell is used to measure force, and a linear variable differential transformer is used to measure displacement for stepped loadings with 5 N increments. The force is applied at the point where the cantilever beam is attached to thin beams. The deflection is also measured at the same point. The results of this test are presented as a force versus deflection curve in Figure 6-6.

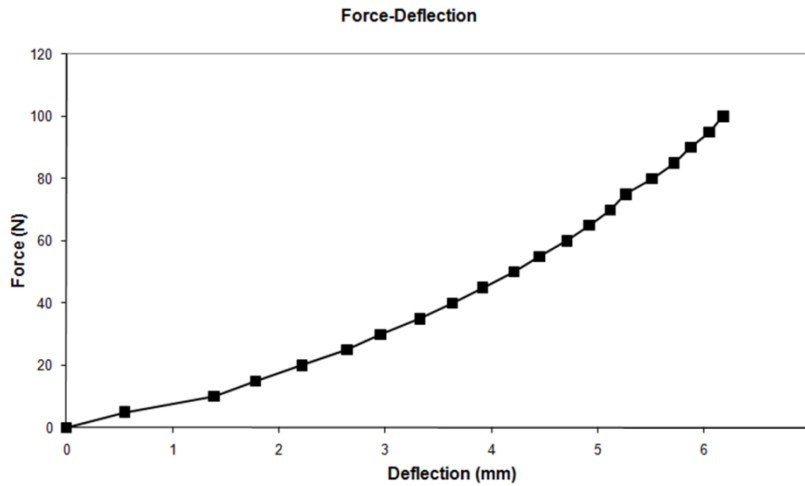


Figure 6-6. Static force-deflection curve for the cubic stiffness.

Furthermore, the DF representation of the nonlinearity ( $\nu$ ) can be graphically shown as a function of response amplitude, which makes it possible to identify the type of nonlinearity and to make parametric identification by using curve fitting. It is important to note that equation (6.1) requires the linear FRF. In general applications, the linear model of the system can be obtained by using FEM and only for the identification of nonlinearity experiments can be used, or alternatively the linear model can also be obtained from modal analysis of the system at very low forcing levels, where the nonlinear internal forces will be negligible unless there is frictional nonlinearity. In this case study, the linear FRF of the system obtained by using constant displacement control with 0.25 mm of vibration amplitude is taken as the linear FRF of the system, since the nonlinear part of the elastic force is negligible compared to the linear part at this value of displacement.

Then, by using the DF and the DFI methods for nonlinear identification, both DF and RF plots are obtained for the nonlinear element between the tip point of the cantilever beam and the ground (Figure 6-7 and Figure 6-8). The cubic stiffness constants identified by using the DF and the DFI methods are  $2.667 \cdot 10^8 \text{ N/m}^3$  and  $2.656 \cdot 10^8 \text{ N/m}^3$ , respectively. The cubic stiffness

constant obtained from static test, on the other hand is  $2.437 \cdot 10^8 \text{ N/m}^3$ . For visual comparison, force deflection curves obtained from static test and the DFI methods are compared with the force deflection characteristics obtained from the DF method in Figure 6-8. As can be seen, the DF and the DFI methods yield very close results. The difference between the identified nonlinear stiffness property and the one obtained using static deflection test may be partly due to using single harmonic assumption in formulations.

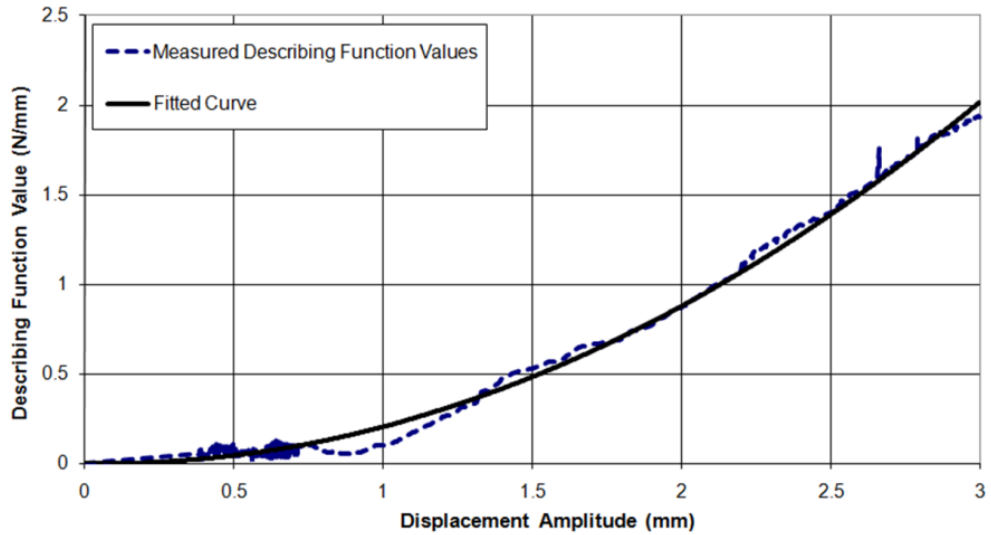


Figure 6-7. Measured DF values and the fitted curve

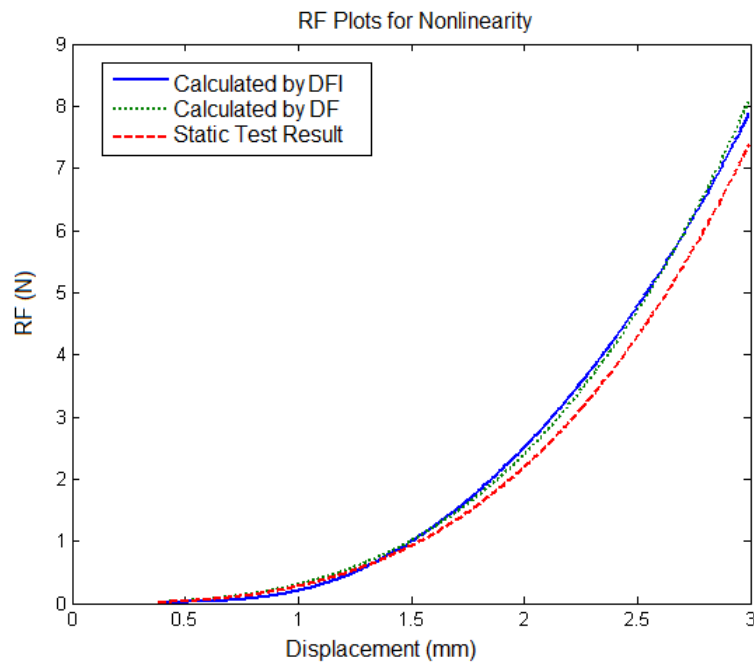


Figure 6-8. RF plots of nonlinearity for experimental study 1; blue: calculated by the DFI method, green: calculated by the DF method, red: static test result

Thus, it can be concluded that the accuracy in parametric identification of nonlinearity by the DFI method is comparable to that of the DF method. However, the main advantage of the DFI method is that it gives better insight into the type of the nonlinearity. Furthermore, when the RF function is obtained by the DFI method, it may be directly used in nonlinear model of the system when time domain analysis is to be used. Then, it will be possible to identify the restoring force of more than one type of nonlinearity which may co-exist at the same location. After identifying nonlinearity in the system, the harmonic response of the nonlinear system as well as the nonlinear FRFs can be calculated by using the method given in section 3.3.

The nonlinear FRFs calculated using the nonlinear coefficients from the DF and the DFI methods at forcing levels of 0.1 N, 0.5 N and 1 N are compared with experimentally measured values in Figure 6-9-Figure 6-11, respectively. As can be seen from the figures, very good agreements are obtained between experimental and predicted responses.

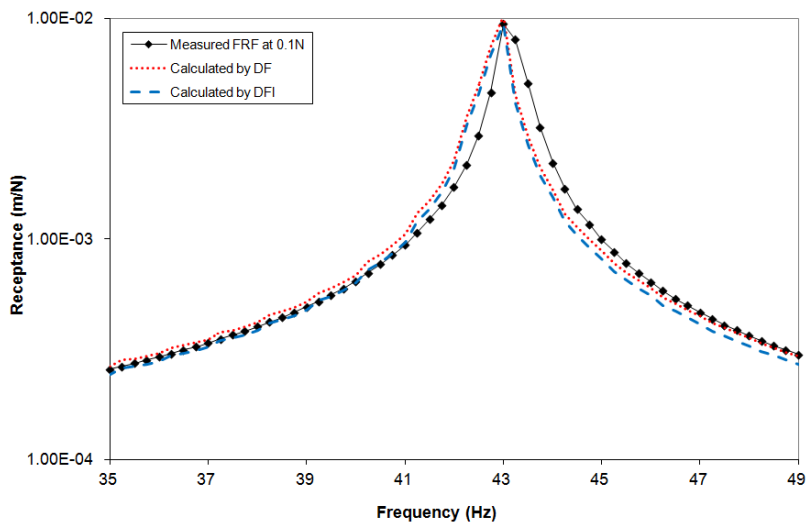


Figure 6-9. Calculated and measured FRF values at 0.1 N

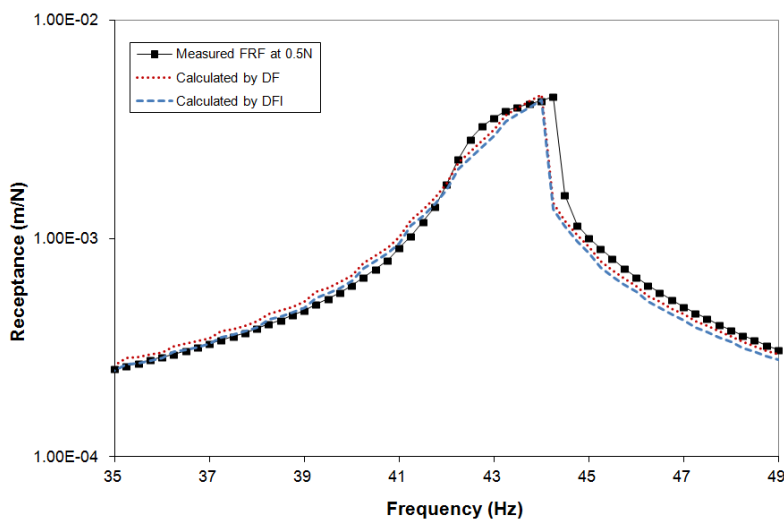


Figure 6-10. Calculated and measured FRF values at 0.5 N

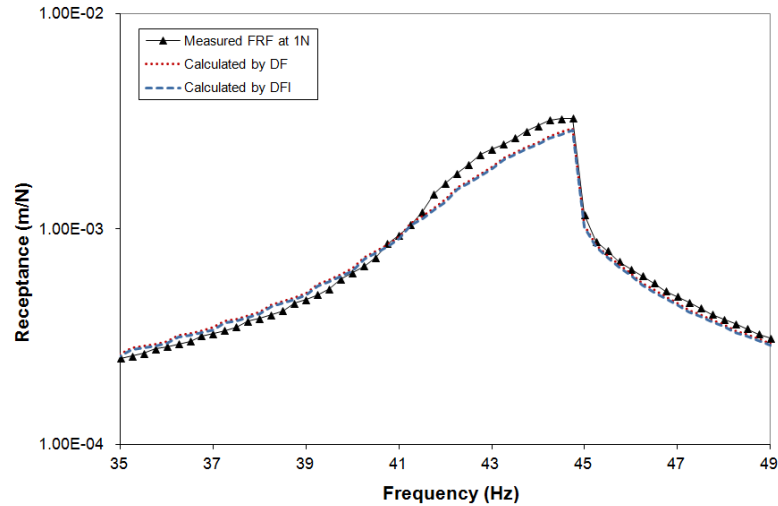


Figure 6-11. Calculated and measured FRF values at 1 N

## 6.2. Experimental Study 2: Application of the DFI method on a MDOF System

For the implementation and validation of the DFI method on a MDOF system, linear and nonlinear modal tests were performed on a nonlinear structure. The test rig manufactured for this study, dimensions and technical details are given in Figure 6-12 and Figure 6-13, respectively. This test rig is preferred for its simplicity in modeling the dynamic system since the structural configuration causes hardening stiffness nonlinearity only. The test rig consists of a two linear cantilever beams with their free ends held between two thin identical beams which cause cubic stiffness. The cantilever beams and the thin nonlinear beams were manufactured from St37 steel. The modal test setup configuration with its elements is shown in Figure 6-14. For linear and nonlinear testing, a shaker (PCB) was connected to the free end of the cantilever beam via a push-rod with a PCB 208C01 force transducer. The vibration responses were measured using three miniature PCB 352C65 accelerometers. The frequency resolution was 0.1 Hz. Cubic nonlinearity in the system causes jumps in the frequency response around resonance frequencies. Ability to observe this phenomenon is closely related to the frequency resolution employed in the harmonic vibration tests. The force closed loop control was achieved by the SCADAS-III data acquisition system.

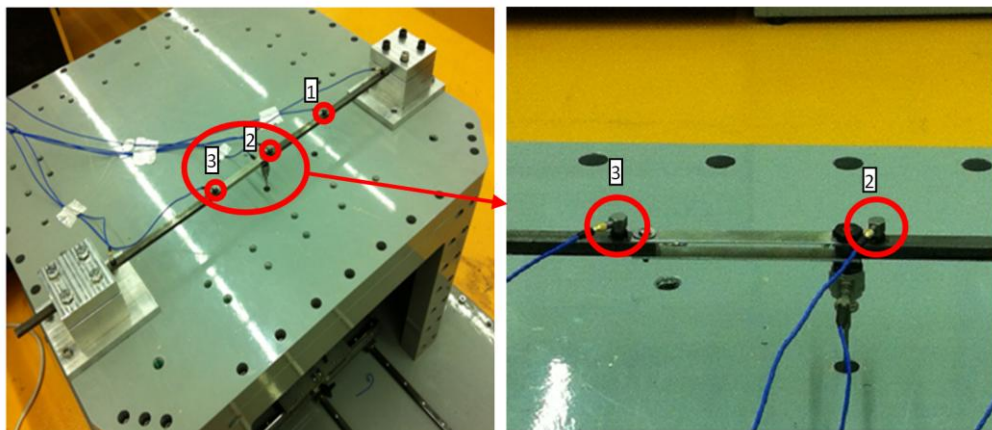


Figure 6-12. Setup used in the experimental study 2

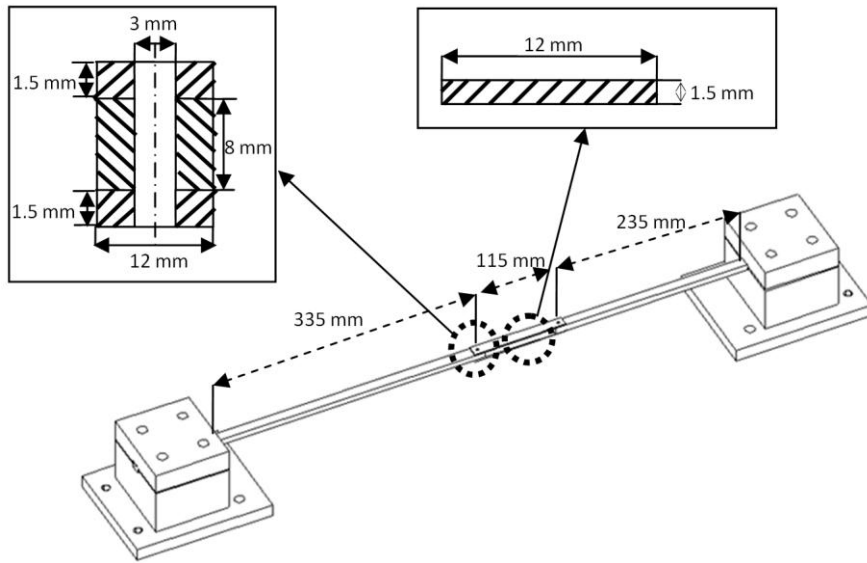


Figure 6-13. Dimensions of experimental study 2

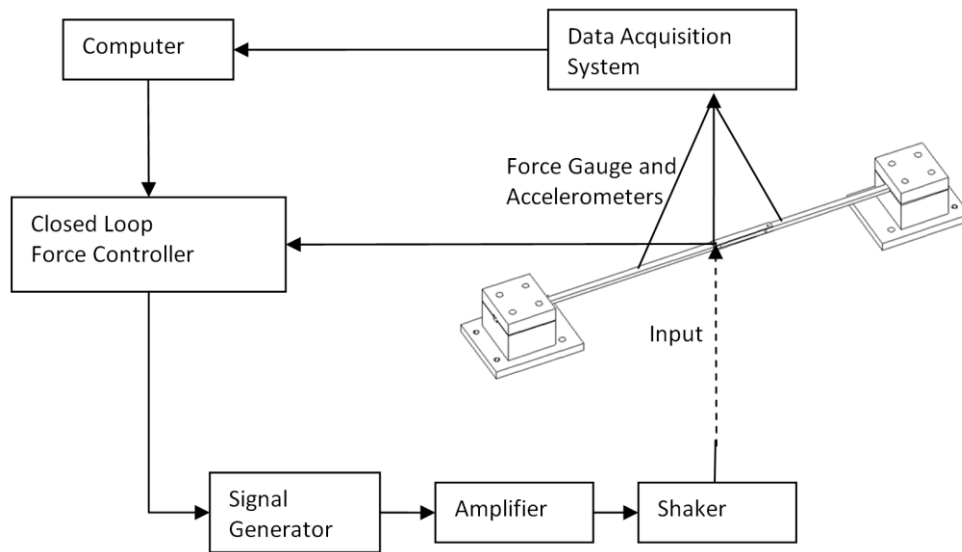


Figure 6-14. Test setup of experimental study 2

The modal tests are performed using harmonic forcing with amplitudes of 0.01N and 0.4N. The FRFs obtained for the constant amplitude force tests are shown in Figure 6-15. The FRFs obtained with 0.01N amplitude harmonic forcing are taken as linear FRFs of the system.

In this experimental study, only the first columns of the linear (0.01N forcing) and nonlinear receptance (0.4N forcing) matrices are measured. Then, firstly the missing elements of the linear FRF matrix are calculated by using FRF synthesis method, and the *NLI* values are calculated for each coordinate. The calculated *NLI* values are shown in Figure 6-16a. From Figure 6-16a it can easily be concluded that there are nonlinear elements between coordinate 2 and 3. Furthermore, Figure 6-16b reveals that system has stiffness type of nonlinearity since DF is almost real with a negligible imaginary part.

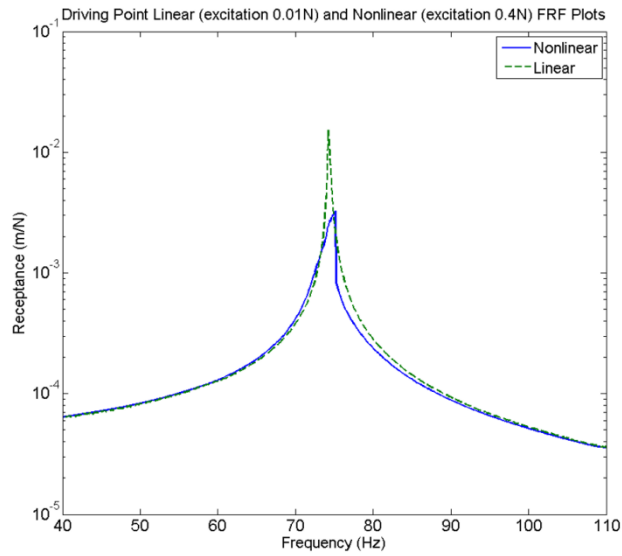


Figure 6-15. Measured constant force driving point FRF curves; green: 0.01N, blue: 0.4N

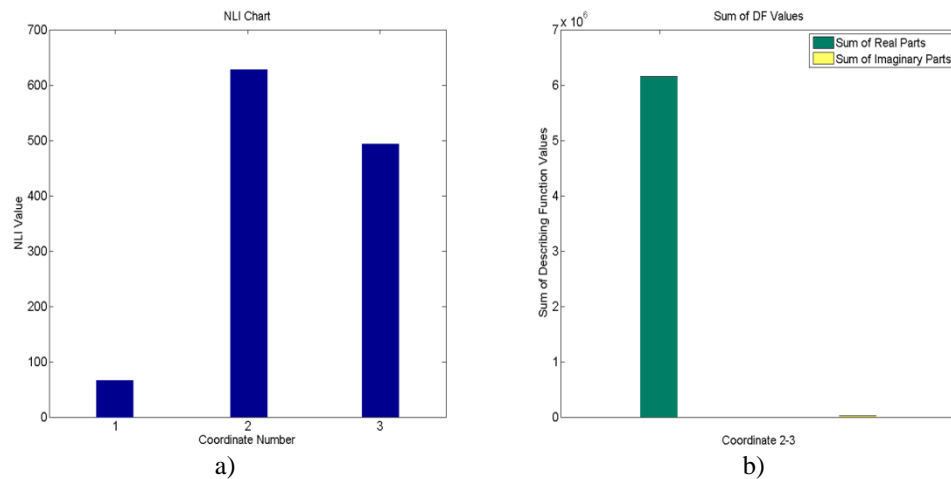


Figure 6-16. a) Nonlinearity index chart, b) Sums of real and imaginary parts of DF values at high forcing excitation

Firstly, by using the measured FRFs, the DF representing the nonlinear element is calculated by improved DF method at different response amplitudes and is plotted in Figure 6-17a. From the general pattern of the curve it may be possible to identify the type of nonlinearity. Fitting a curve to the calculated values makes the parametric identification easier. However, when there are more than single nonlinearity at the same coordinate this may not be possible. Therefore, the inverse of the DF is calculated using the DFI method. The RF plot obtained is presented in Figure 6-17b. By first fitting a curve to the calculated RF plot, parametric identification can easily be made.

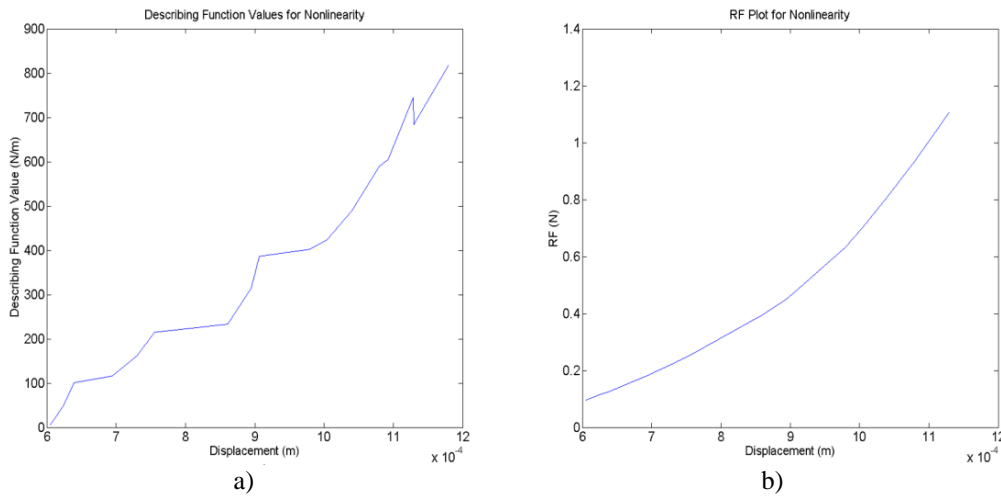


Figure 6-17. a) Calculated DF by improved DF method, b) Calculated RF by the DFI method for nonlinear element between coordinate 2 and 3

The correct assembly of beam setup is very important. Slight misalignments can cause unsymmetrical bending which leads to addition of second order ( $x^2$ ) nonlinear terms to overall stiffness. This has also been observed by Josefsson *et al.* [27]. In the restoring force plot, firstly a pure cubic function is fitted as seen in Figure 6-18 and a cubic coefficient of  $7 \cdot 10^8 \text{ N/m}^3$  is obtained.

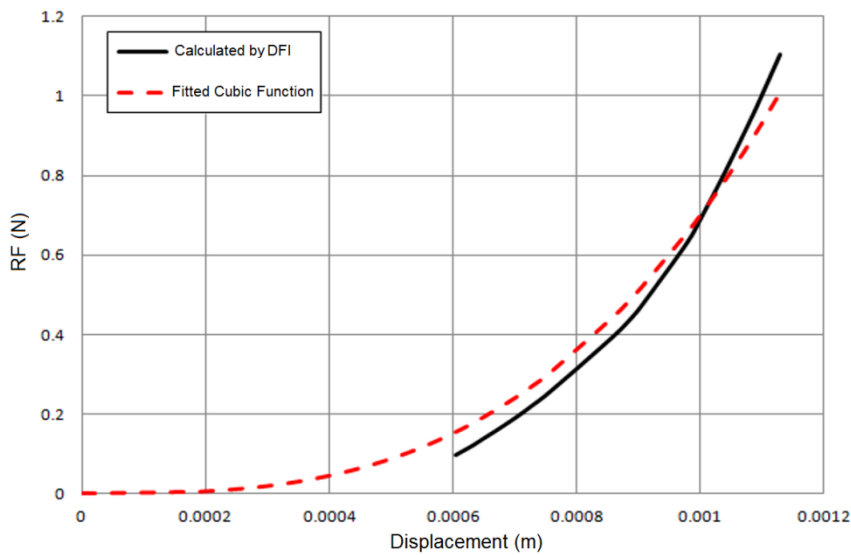


Figure 6-18. Fitted cubic curve and RF for nonlinear element between coordinate 2 and 3

Then a quadratic and cubic function is fitted as shown in Figure 6-19 and a cubic coefficient of  $10 \cdot 10^8 \text{ N/m}^3$  and  $-2.925 \cdot 10^5 \text{ N/m}^2$  is obtained.

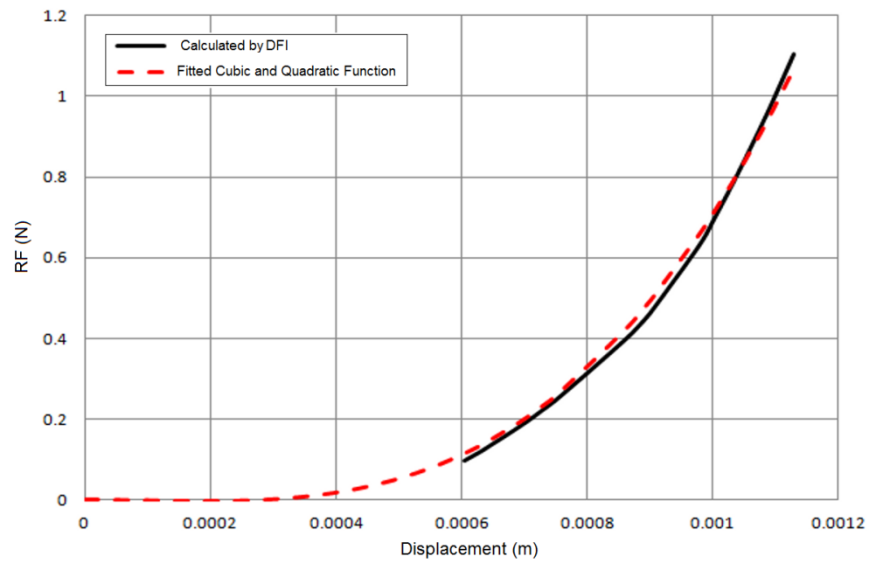


Figure 6-19. Fitted quadratic and cubic curve and RF for nonlinear element between coordinate 2 and 3

After identifying nonlinearity in the system, the harmonic response of the nonlinear system can be calculated by using the iterative solution method given in section 3.3. The driving point FRFs calculated at forcing level of 0.4 N are compared with experimentally measured values in Figure 6-20. As expected, the combined nonlinear element gives slightly better results.

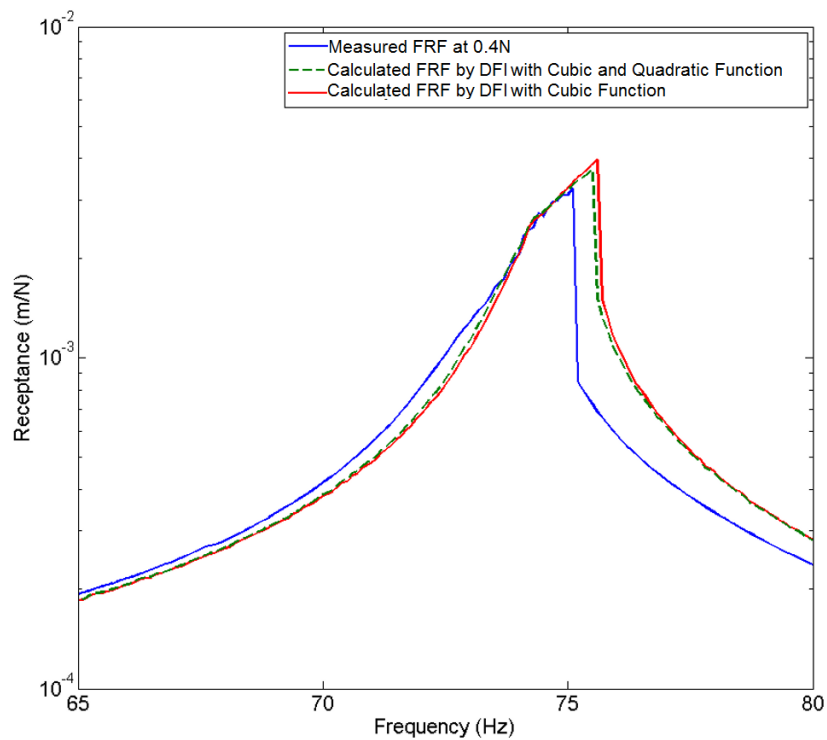


Figure 6-20. Calculated and measured FRF values at 0.4 N

### 6.3. Experimental Study 3: Application of the DDF Method on a SDOF System

The DDF method is also tested on the experimental setup used in experimental study 1. The tests carried out in previous study were repeated with better frequency resolution (0.1 Hz) and force control. The experimental setup and FRF plots obtained with constant amplitude harmonic forces are given in Figure 6-21 and Figure 6-22, respectively.

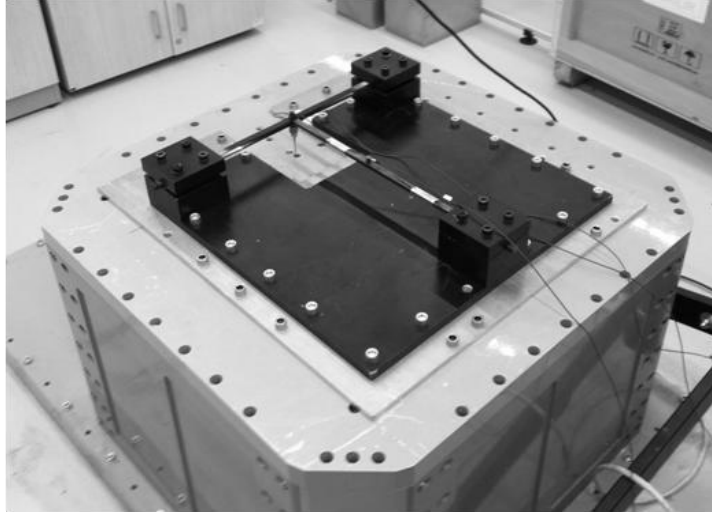


Figure 6-21. Setup used in the experimental study 3

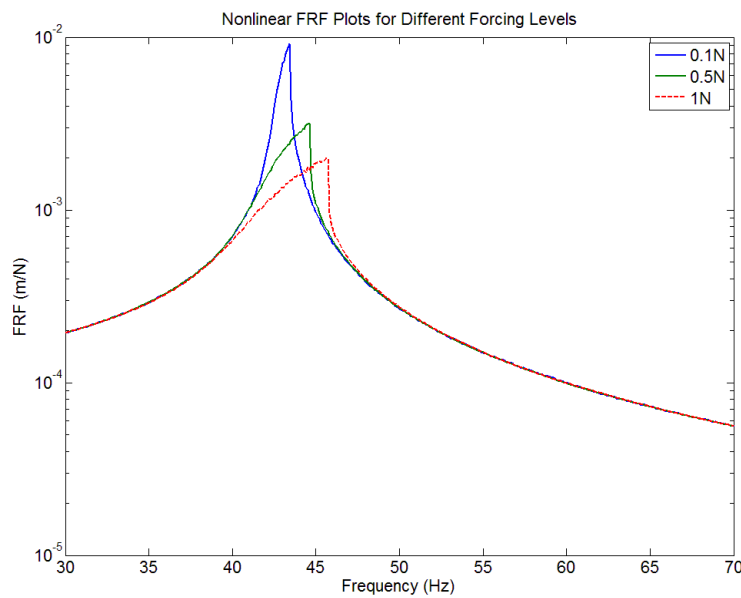


Figure 6-22. Measured driving point FRFs; blue: 0.1N, green: 0.5N, red: 1N

As discussed in section 3.4., the method requires the linear FRFs. Thus, we may assume that the lowest force level that we can achieve gives the linear FRF. However, the DDF method

shows that the linear FRF may not always be obtained accurately by low forcing even though there is no friction type of nonlinearity (Figure 6-23).

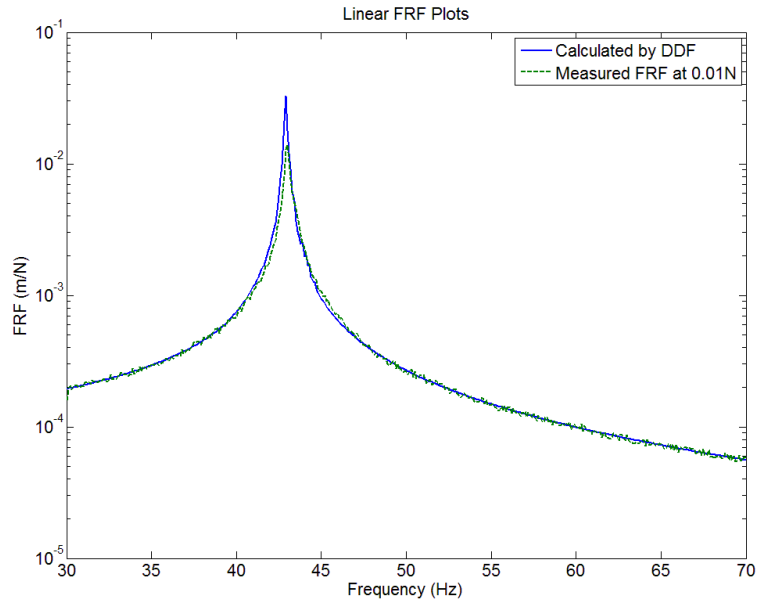


Figure 6-23. Linear FRF curves; blue: Calculated by the DDF method, green: measured at 0.01N

If we cannot apply sufficiently low forcing level or if there is friction type of nonlinearity in the system then the approach proposed becomes more valuable. The DF representation of the nonlinearity ( $v$ ) can be graphically shown as a function of response amplitude, which makes it possible to identify the type of nonlinearity and to make parametric identification by using curve fitting (Figure 6-24a). Figure 6-24a shows the DF curves calculated by the DDF and the DF methods. The restoring force plot is also given in Figure 6-24b. From Figure 6-24b the nonlinearity coefficient is found by curve fitting as  $6.18 \cdot 10^8 \text{ N/m}^3$ .

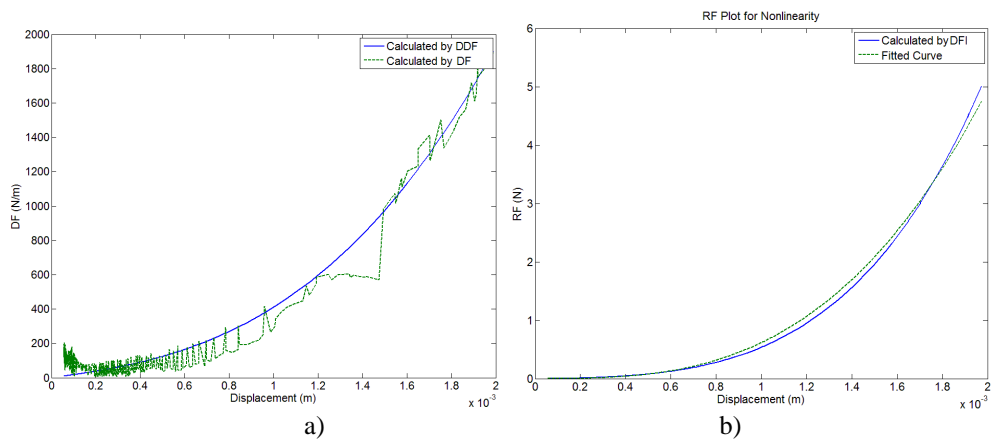


Figure 6-24. a) DF curves calculated by the DDF and the DF methods, b) RF curve calculated by the DFI using the DF calculated by the DDF and fitted curve

The nonlinear FRFs are regenerated using the method discussed in section 3.3. using the identified nonlinearity coefficient at forcing levels of 0.5 N and 1 N and are compared with experimentally measured values in Figure 6-25. As can be seen from the figure, better agreements are obtained between experimental and predicted responses with the DDF method.

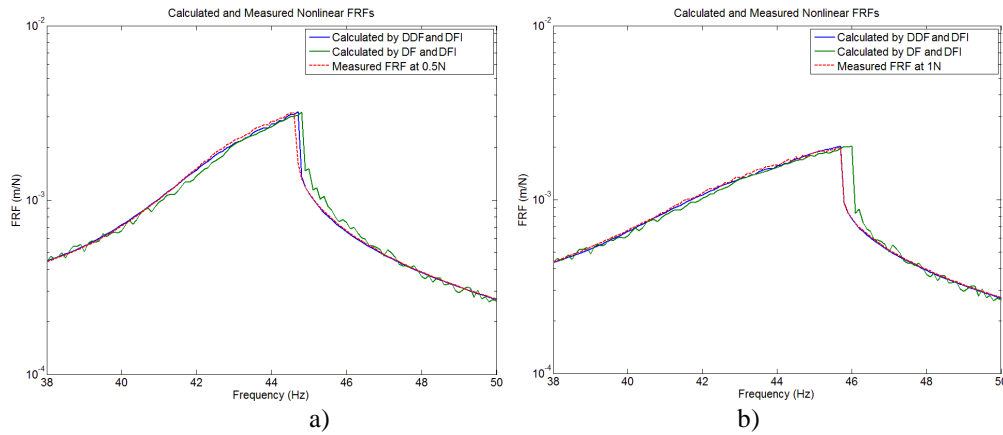


Figure 6-25. Calculated and measured nonlinear FRF curves at forcing level of a) 0.5N, b) 1N

#### 6.4. Experimental Study 4: Application of the DDF Method on a Stabilized Optic Platform

The DDF method is also tested on a stabilized optic platform (SOP). The mission of the SOP is to guide weapon systems to the target. It has stabilization in the elevation and the yaw axis. The SOP used in this study and FRF plots obtained with constant amplitude harmonic forces are given in Figure 6-26 and Figure 6-27, respectively. The SOP has two direct drive motors guided with double bearings. For linear and nonlinear testing, a shaker (PCB) was connected to point 9 via a push-rod with a PCB 208C01 force transducer. The vibration responses were measured using 20 triaxial PCB 356A16 accelerometers. The frequency resolution was 0.1 Hz. The force closed loop control was achieved by the SCADAS-III data acquisition system.

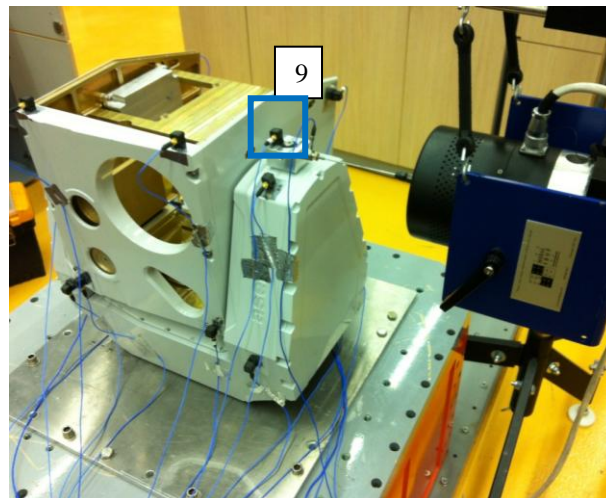


Figure 6-26. Modal tests on the SOP

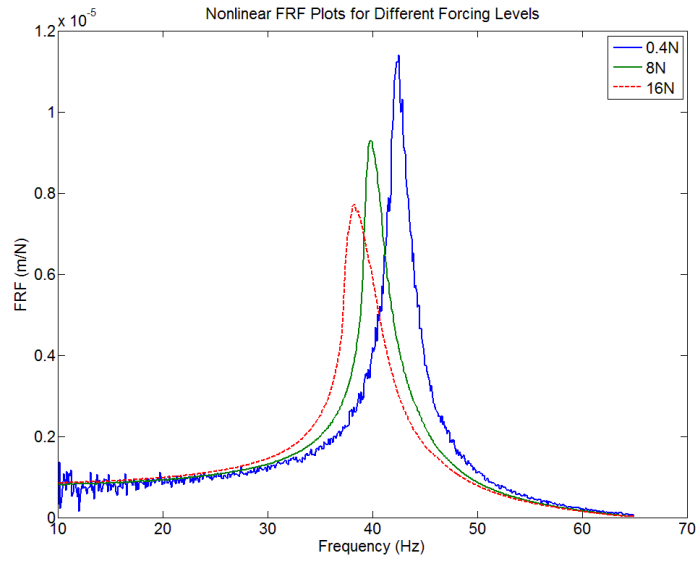


Figure 6-27. Driving point FRFs; blue: 0.4N, green: 8N, red: 16N

In order to visualize the behavior of the system at this resonance linear modal identification is performed by using LMS Test Lab software. The mode shape of the SOP at this resonance is given in Figure 6-28.

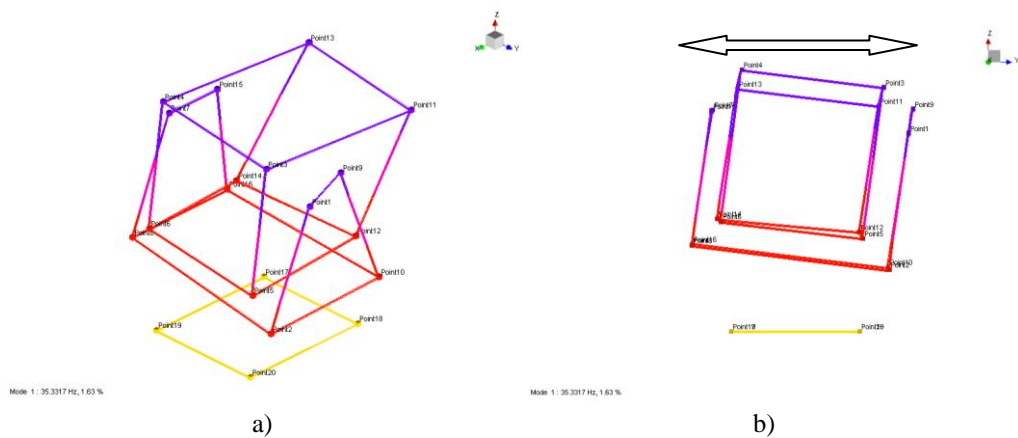


Figure 6-28. Mode shapes of the SOP for the first resonance, a) isometric view, b) front view

Thus, as the SOP rigidly oscillates in the y axis around its yaw axis connection, the nonlinear element must be at this location. Nevertheless, the DDF method is applied simplifying the system as a SDOF system and using the driving point FRF just to identify the nonlinear element. Figure 6-29a shows the real part of DF curves calculated by the DDF method and Figure 6-29b shows the imaginary part of the DF curve calculated by the DDF method. Then, by using the DFI method the restoring force values for stiffness and friction nonlinearity are calculated and are given in Figure 6-30a and Figure 6-30b, respectively. From Figure 6-30a and Figure 6-30b the nonlinearity coefficients are found by curve fitting using polynomials up to the third order. The coefficients of the restoring force curves are given in Table 6-1.

Table 6-1. Parametric identification results for the nonlinear elements

	Linear	Quadratic	Cubic
Real Part of RF	$-1.8362 \cdot 10^4$	$-5.4134 \cdot 10^9$	$1.3373 \cdot 10^{13}$
Imaginary Part of RF	$3.5901 \cdot 10^4$	$2.1355 \cdot 10^8$	$1.15324 \cdot 10^{12}$

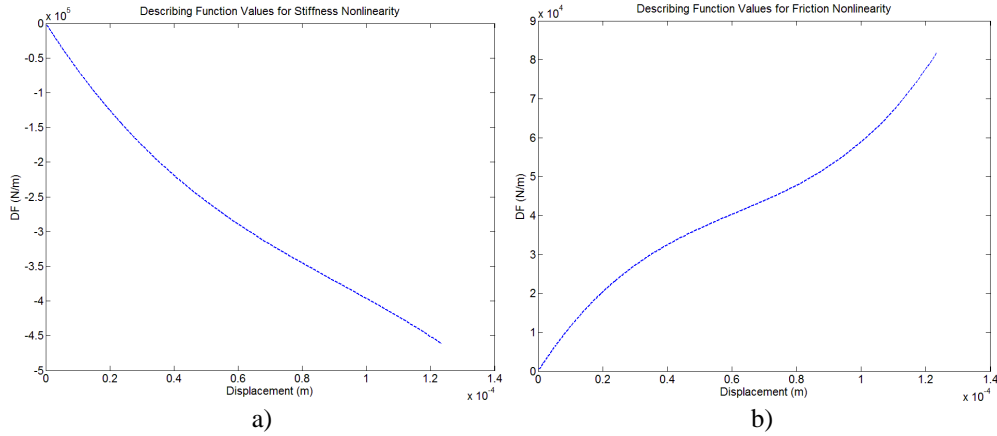


Figure 6-29. Calculated DFs by the DDF method, a) stiffness DF, b) friction DF

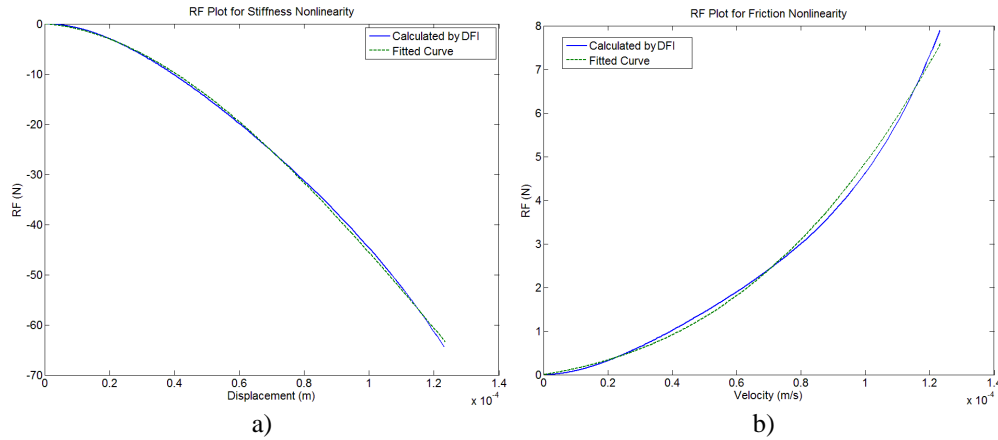


Figure 6-30. Calculated RFs by the DFI method, a) stiffness RF, b) friction RF

The nonlinear FRFs are regenerated using the method discussed in section 3.3. using the identified nonlinearity coefficient at forcing levels of 8 N and 16 N and are compared with experimentally measured values in Figure 6-31 and Figure 6-32, respectively. Note that, during the identification process the type and functional form of the nonlinearity was not known. The coefficients of the nonlinearities are obtained simply by curve fitting the RF values. Then, while regenerating the nonlinear FRFs, the describing function representations of polynomial functions are used.

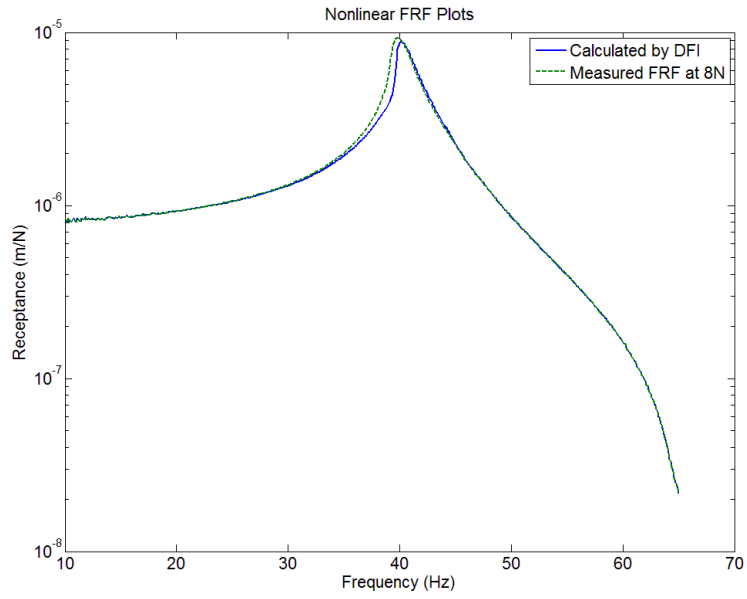


Figure 6-31. Calculated and measured nonlinear FRF curves at forcing level of 8N

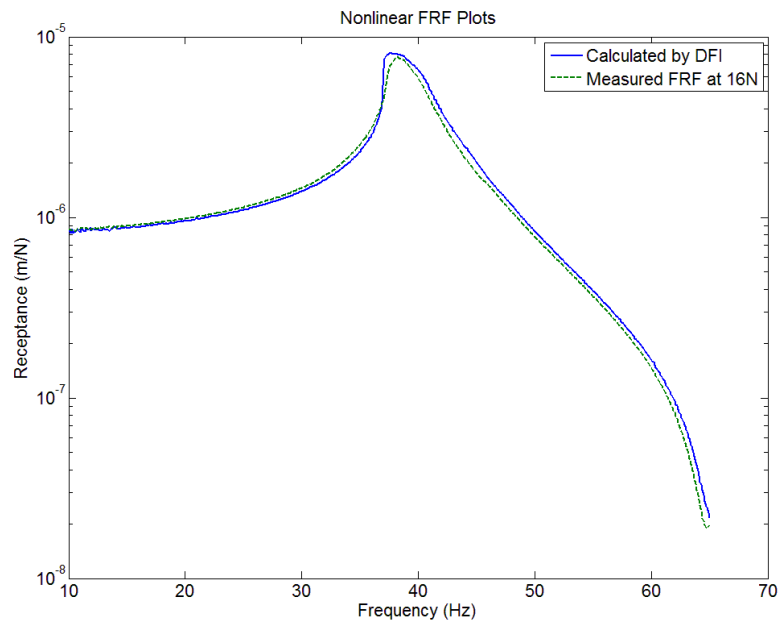


Figure 6-32. Calculated and measured nonlinear FRF curves at forcing level of 16N

As can be seen from the figure, a good match is obtained between experimental and predicted responses with the DDF method.



## CHAPTER 7

### APPLICATION OF NONLINEAR IDENTIFICATION APPROACH TO CRACK DETECTION PROBLEMS

Structural damages usually introduce nonlinearity to the system. The nonlinearity localization part of improved DF method is employed to detect crack type structural damage. The method requires the measurement of FRFs at various points in order to locate the damage. The method makes it also possible to determine the extent of damage by identifying the level of nonlinearity.

Damage detection method presented in this study consists of two main stages. Firstly, existence of damage in the system is detected by performing step sine tests with different loads. Secondly, the location of the damage is determined by using incomplete FRF data. The work presented in this study is mainly an experimental application of the method suggested by Aydoğan [66] which was verified only by simulated data.

#### 7.1. Damage Localization by Improved DF Method

In this chapter, the damage locations are determined from NLI values calculated from vibration tests. In order to calculate the NLI values, improved DF method is used which is thoroughly discussed in chapter 3. Before going into the experimental studies, some important points about interpreting the NLI values for damage localization are discussed below.

Theoretically, if a nonlinear element is between a coordinate and ground, we would expect to have high NLI value for that coordinate only, and if a nonlinear element is between two coordinates, we would expect to have high NLI values at these two coordinates. In the simulated cantilever beam case studies given in [66], it is concluded that, in order to observe such characteristics we need to measure the rotational coordinates which are affected the most from crack type nonlinearities. If translational coordinates are measured, then this method gives us an indication of the crack location by yielding a high peak only at the coordinate right after the crack closer to the fixed boundary. When this is the case, further investigations should be carried out by NDT methods around the coordinate with high NLI to pinpoint the crack.

#### 7.2. Experimental Studies

##### 7.2.1. Experimental Study 1: Localization of Damage in a 7 DOF Beam by Shaker Testing

For the implementation and validation of the method given above, step sine tests with different load levels are performed with four hollow square beams which are all manufactured from aluminum. The beams have 2.5 mm, 5.5 mm and 7.5 mm cracks, respectively. In order to see the effect of measurement noise on NLI values calculated from experimental measurements, a fourth beam with no crack is also tested. The cracks are produced by creating an indentation of 1mm first with a saw and then bending the beam several times until the desired crack is obtained. The test rig manufactured for this study, dimensions and technical details are given in Figure 7-1 and Figure 7-2, respectively. This test rig is preferred for its simplicity. The test rig consists of a cantilever beam with a crack between 4th and 5th coordinates. The modal test setup configuration with its elements is shown in Figure 7-3. For step sine testing, a shaker (PCB) is connected to the free end (point 1) of the cantilever beam via a push-rod with a PCB 208C01 force transducer. The vibration responses are measured using six miniature PCB 352C65 and one PCB 352A24 accelerometers. The frequency resolution is 0.1 Hz. The crack in the system causes changes in the frequency response around resonance frequencies. Ability to observe this phenomenon is closely related to the frequency resolution employed in the

harmonic vibration tests. The force closed loop control is achieved by the SCADAS-III data acquisition system.

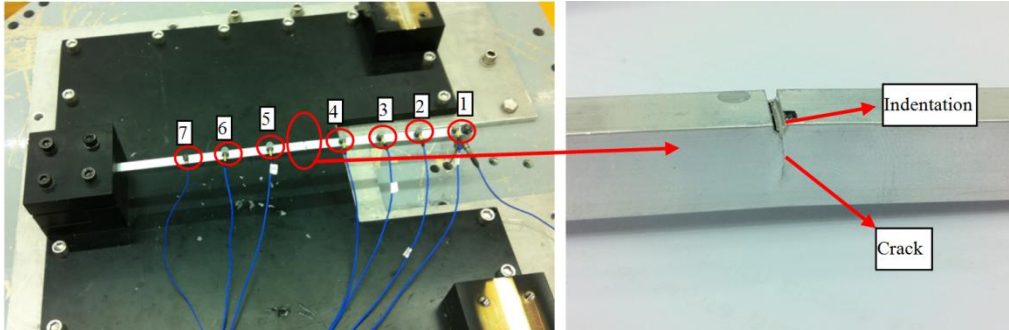


Figure 7-1. Setup used in the experimental study 1

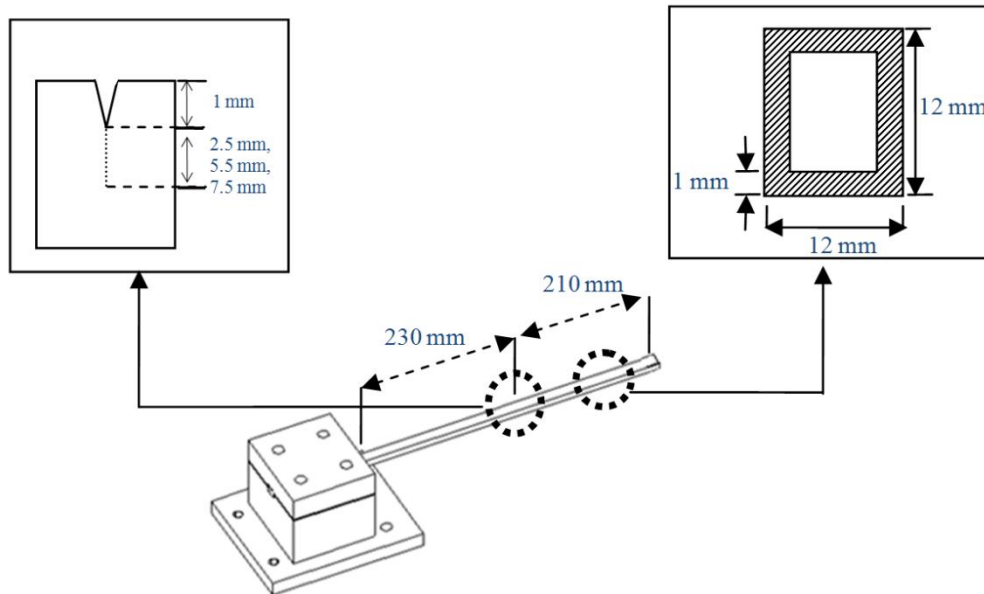


Figure 7-2. Dimensions of experimental study 1

The modal tests are performed using harmonic forcing with amplitudes of 0.01N and 0.05N at point 1 and measuring responses from 7 points. The FRFs obtained for the constant amplitude force tests with an undamaged beam and with three different crack lengths ( $h=2.5$  mm, 5.5 mm and 7.5 mm) are shown in Figure 7-4-Figure 7-7. The FRFs obtained with 0.01N amplitude harmonic forcing are taken as linear FRFs of the system.

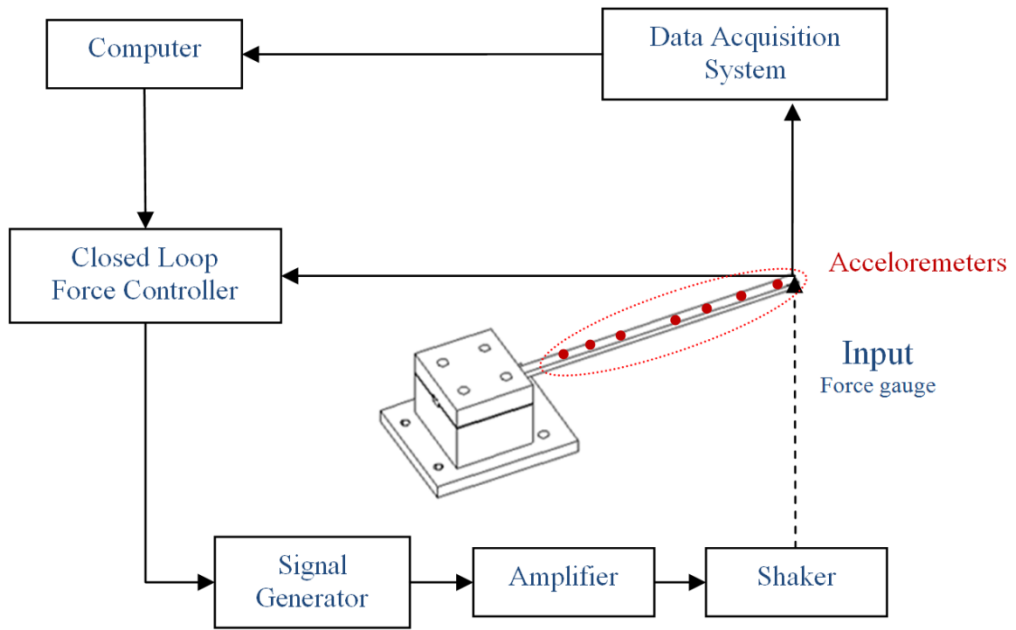


Figure 7-3. Test setup of experimental study 1

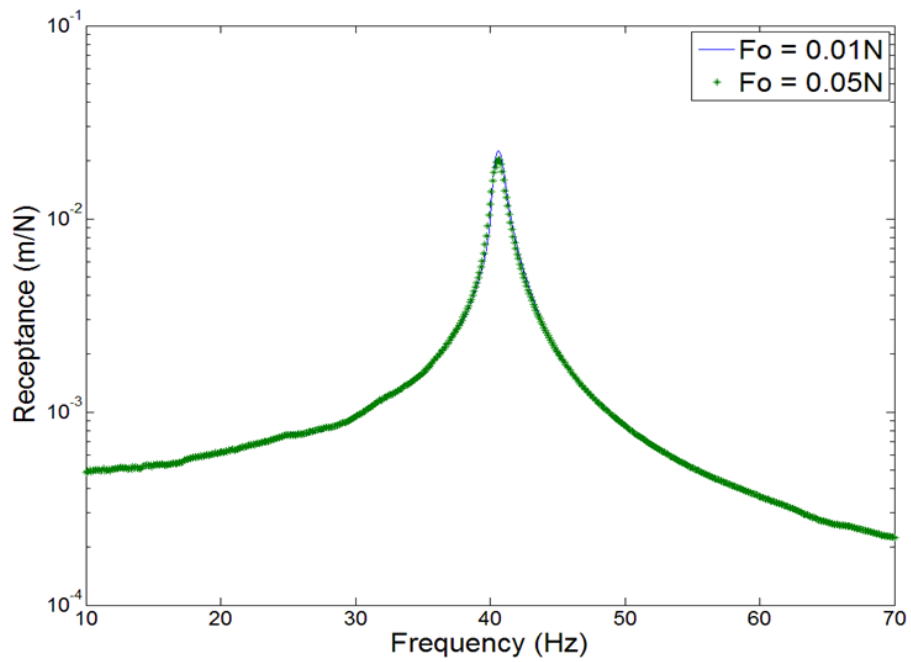


Figure 7-4. Linear and nonlinear direct point FRFs at point 1 (undamaged)

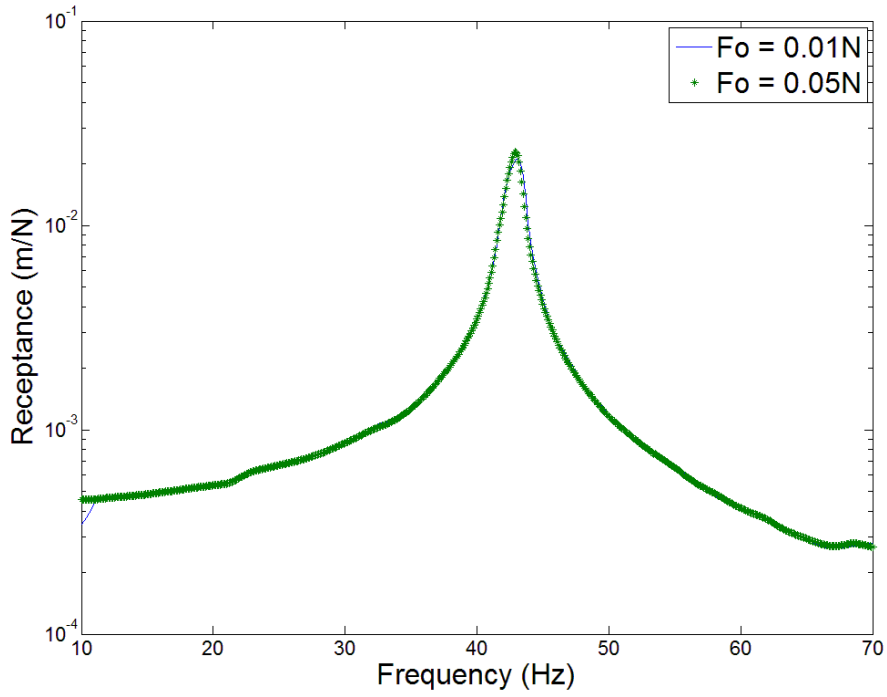


Figure 7-5. Linear and nonlinear direct point FRFs at point 1 ( $h= 2.5$  mm)

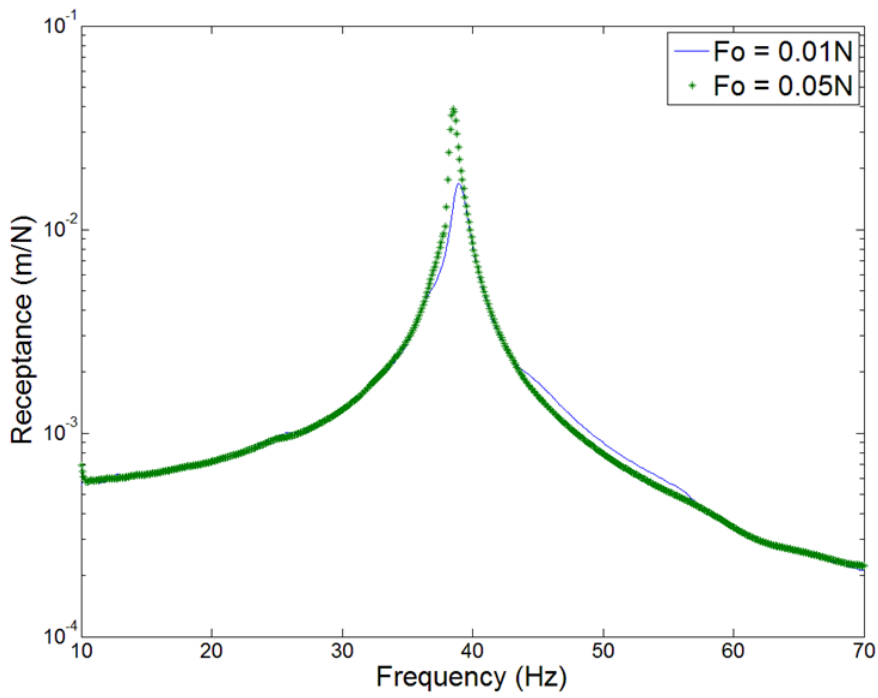


Figure 7-6. Linear and nonlinear direct point FRFs at point 1 ( $h= 5.5$  mm)

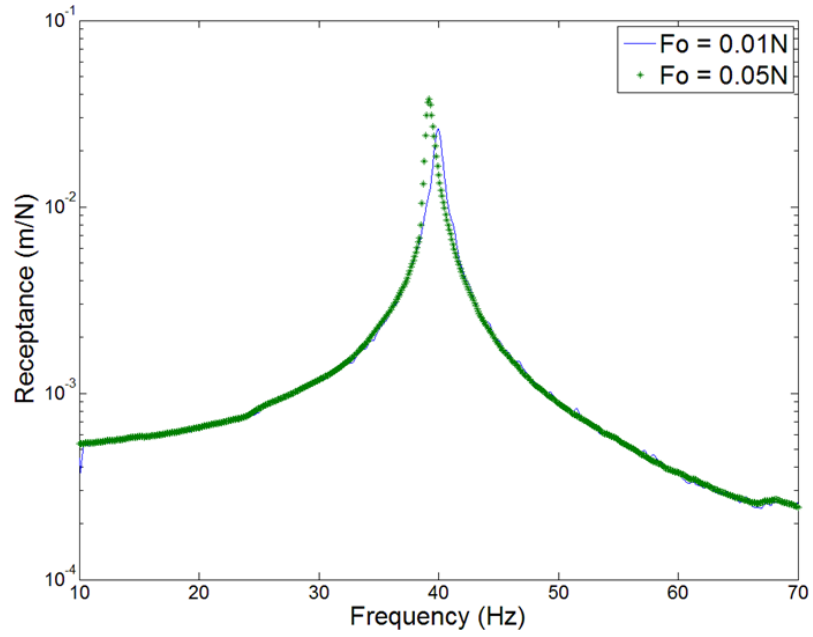


Figure 7-7. Linear and nonlinear direct point FRFs at point 1 ( $h= 7.5$  mm)

In this experimental study, only the first columns of the linear (0.01N forcing) and nonlinear receptance (0.05N forcing) matrices are measured. Then, firstly the missing elements of the linear FRF matrix are calculated by FRF synthesis method, and the *NLI* values are calculated for each coordinate. Note that here only translational DOFs are used. The calculated *NLI* values are shown in Figure 7-8 to Figure 7-11.

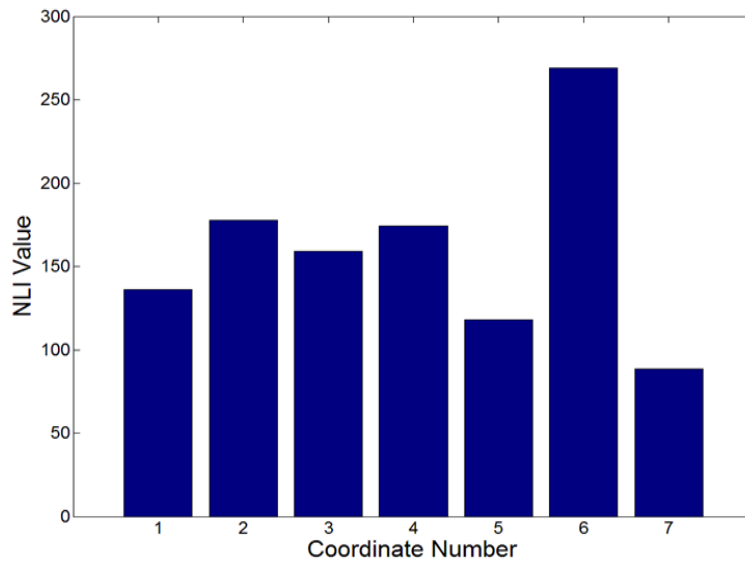


Figure 7-8. Undamaged Nonlinearity Index Chart

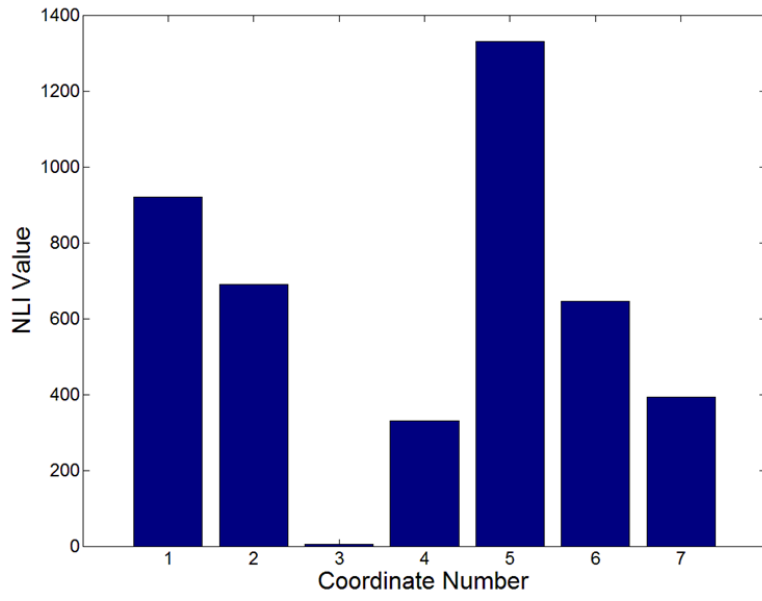


Figure 7-9. 2.5 mm Nonlinearity Index Chart

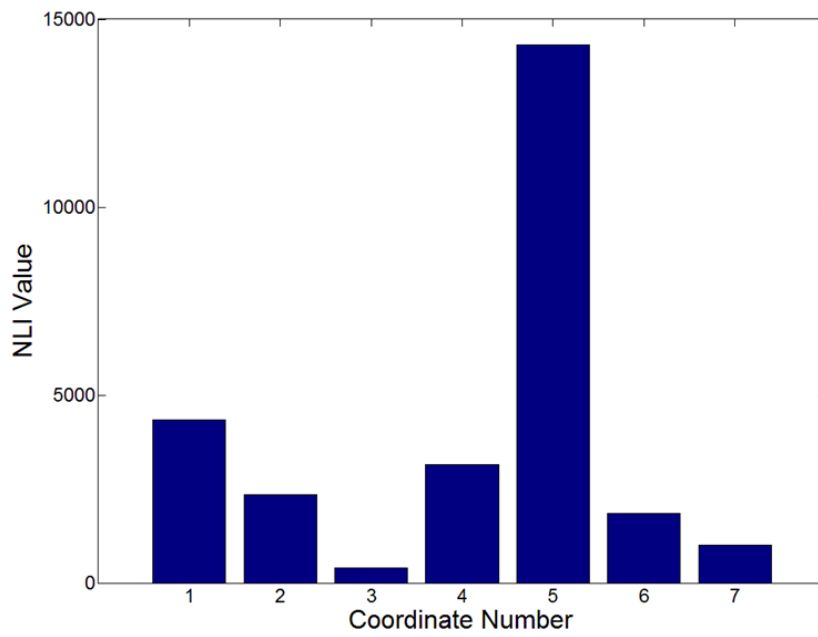


Figure 7-10. 5.5 mm Nonlinearity Index Chart

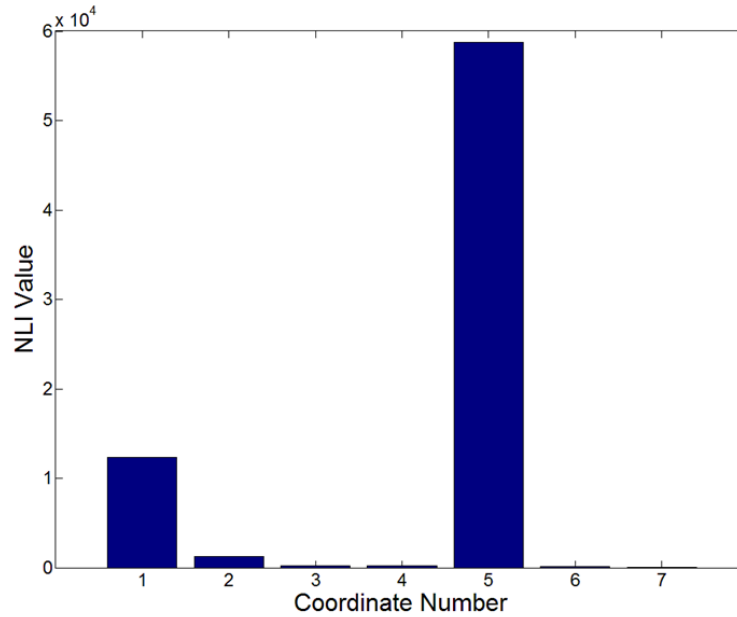


Figure 7-11. 7.5 mm Nonlinearity Index Chart

The coordinates which are affected from nonlinearity can be determined from the *NLI* values obtained for each coordinate. The crack is located between the 4<sup>th</sup> and 5<sup>th</sup> coordinates so one expects to find two high peaks at these coordinates. In the simulated case studies given in [66], it is stated that, in order to observe such a chart we have to measure FRFs at the rotational coordinates which are affected the most from the nonlinearity. If translational coordinates are measured, then this method gives us an indication about the crack location by giving a high peak only at the coordinate right after the crack closer to the fixed boundary. The results obtained verify this expectation: We have high peaks at 5<sup>th</sup> coordinate. However, the *NLI* values obtained for the other coordinates are not much smaller than that of coordinate 5, unless the crack gets deeper (when we have deeper cracks the *NLI* value of 5<sup>th</sup> coordinate increases considerably, compared to other *NLI* values).

### 7.2.2. Experimental Study 2: Localization of Damage in a 7 DOF Composite Beam by Impact Testing

In the first experimental study step sine testing with a shaker was preferred for the validation of the improved DF method for damage localization. With this case study it is intended to demonstrate that this method can also be used with impact testing. However, it must be noted that the change in the FRFs with different impact levels will not be as much as that observed in closed loop shaker testing since it is more difficult to apply considerably higher force levels in impact testing. In this experimental study, the test specimen is changed to E-Glass reinforced plastic (E-GFRP). The damage is located between the same coordinates but this time the extent of damage is not known since the damage is created by simply bending the sheet. The test rig manufactured for this study, dimensions and technical details are given in Figure 7-12 and Figure 7-13, respectively. For impact testing, an impact hammer (PCB 086C01) is used and the structure is hit at the 7<sup>th</sup> coordinate. The vibration responses are measured using six miniature PCB 352C65 and one PCB 352A24 accelerometers. The frequency resolution is 0.3125 Hz. The crack in the system causes changes in the frequency response around resonance frequencies. Ability to observe this phenomenon is closely related to the frequency resolution employed in the harmonic vibration tests.

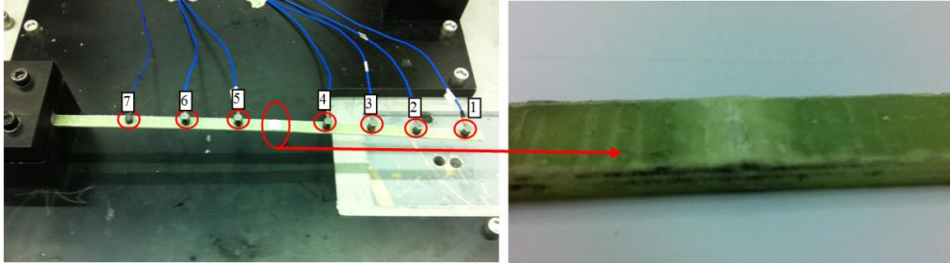


Figure 7-12. Setup used in the experimental study 2

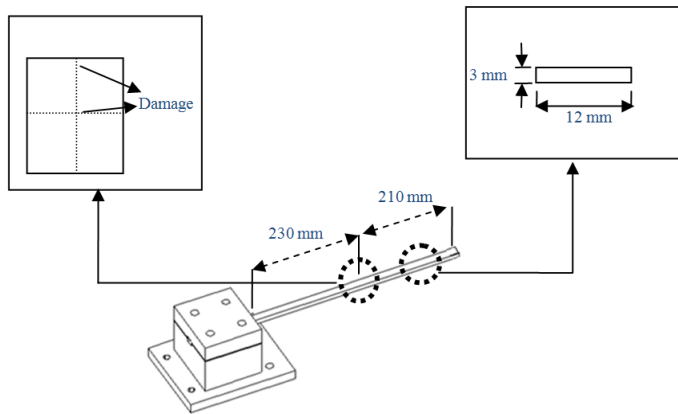


Figure 7-13. Dimensions of experimental study 2

The modal tests are performed by hitting the structure with low and high impact forces. The FRFs obtained for two load levels are shown in Figure 7-14. The FRFs obtained with low amplitude forcing are taken as linear FRFs of the system.

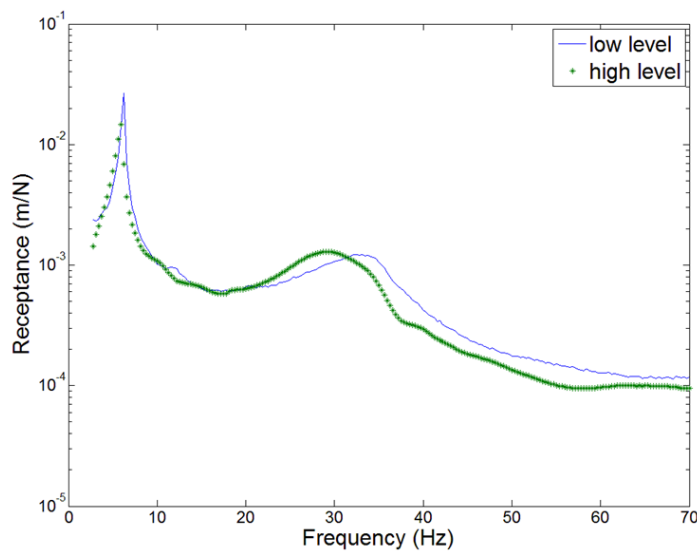


Figure 7-14. E-GFRP impact tests, tip point FRF curves

In this experimental study, only the first columns of the linear (low forcing) and nonlinear receptance (high forcing) matrices are measured. Then, firstly the missing elements of the linear FRF matrix are calculated by using FRF synthesis method, and the *NLI* values are calculated. The calculated *NLI* values are shown in Figure 7-15. The *NLI* chart shows the coordinates which are affected from nonlinearity. High *NLI* values at 4th and 5th coordinates indicate the damage between these coordinates. Relatively high value obtained for *NLI* at 6th coordinate may be due to the damage that might be extended to that coordinate. However, we observe from the experimental results that the method proposed may yield nonzero *NLI* values at some other coordinates as well, although they are not adjacent to damaged region. This is most probably due to using only translational FRFs and not including those related with rotational DOF in the computation of *NLI* values. Fortunately, these nonzero *NLI* values are not as high as the ones obtained at damaged locations.

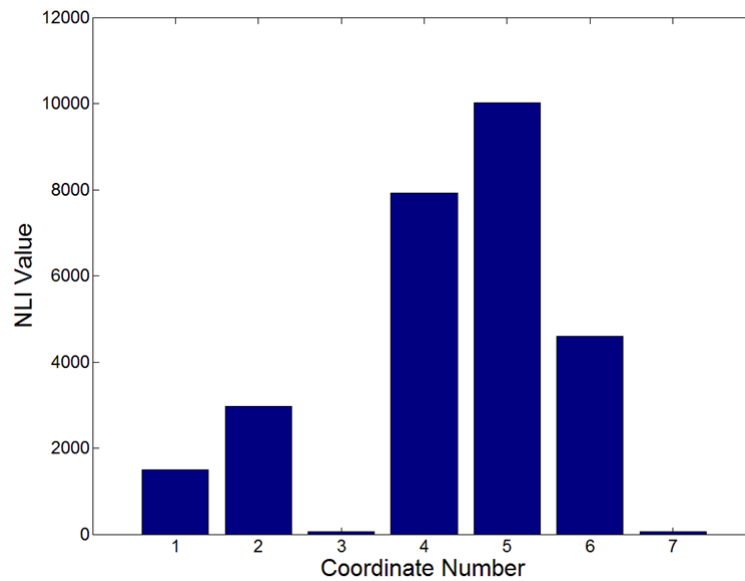


Figure 7-15. E-GFRP Nonlinearity Index Chart

### 7.2.3. Experimental Study 3: Localization of Damage in a 4 DOF Waveguide by Impact Testing

In this experimental study, the localization of the defects of a brazing process on a waveguide is presented. A waveguide is an engineering structure which guides waves (electromagnetic or sound waves). There are different types of waveguides for each type of wave. In this case study, it is intended to demonstrate that this method can also be used on real engineering structures with impact testing. However, it must be noted that the change in the FRFs with different impact levels will not be as much as that observed in closed loop shaker testing since it is more difficult to apply considerably higher force levels in impact testing. The waveguide and measurement locations are given in Figure 7-16 and Figure 7-17, respectively. For impact testing, an impact hammer (PCB 086C01) is used and the structure is hit at the 1<sup>th</sup> coordinate. The vibration responses are measured using four miniature PCB 352C65 accelerometers. The frequency resolution is 0.3125 Hz. The crack in the system causes changes in the frequency response around resonance frequencies. Ability to observe this phenomenon is closely related to the frequency resolution employed in the harmonic vibration tests.

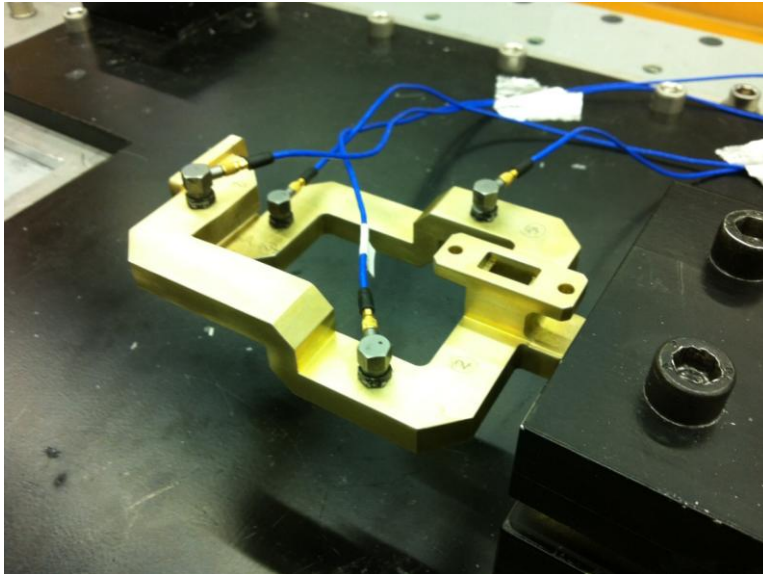


Figure 7-16. Setup used in the experimental study 3

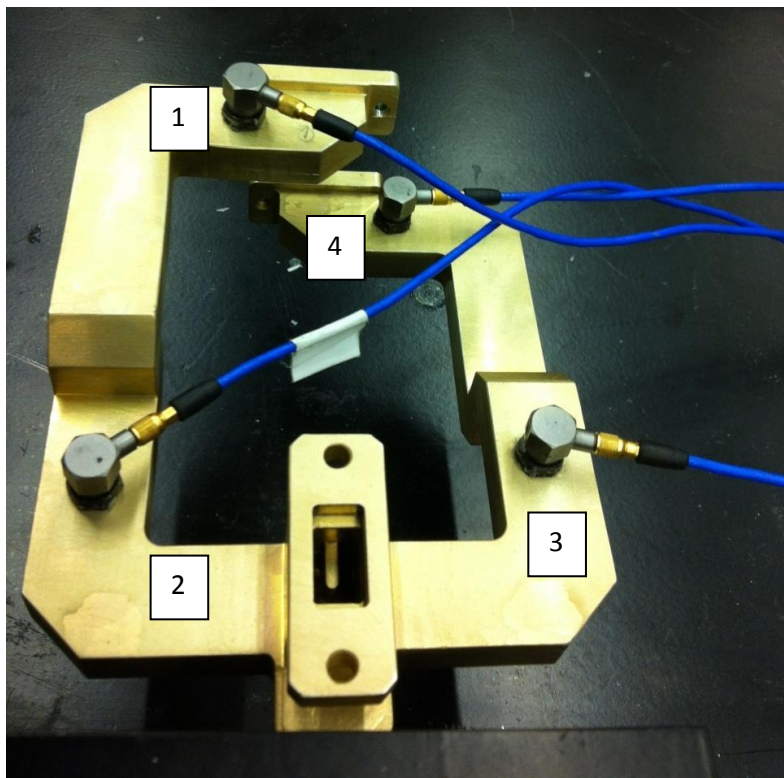


Figure 7-17. Measurement locations

The modal tests are performed by hitting the structure with low and high impact forces. The FRFs obtained for two load levels are shown in Figure 7-18. The FRFs obtained with low amplitude forcing are taken as linear FRFs of the system.

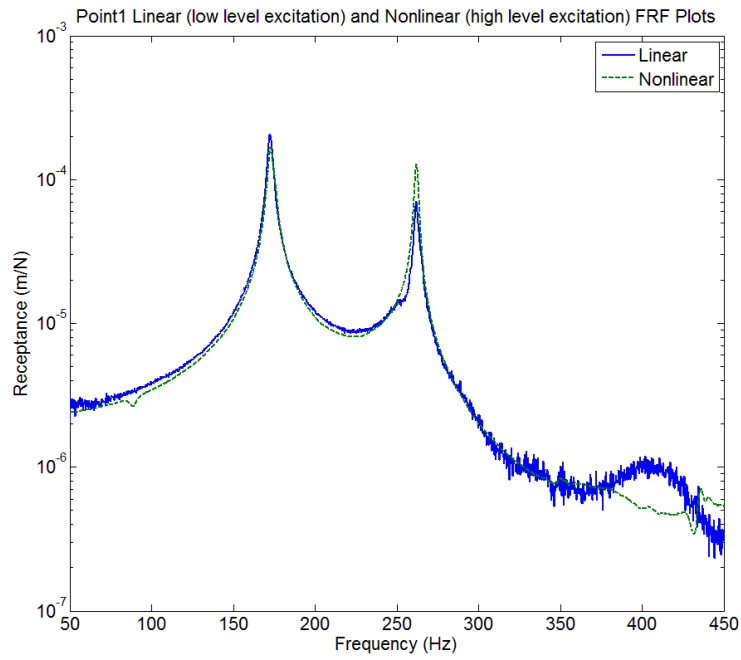


Figure 7-18. Waveguide impact tests, tip point FRF curves

In this experimental study, only the first columns of the linear (low forcing) and nonlinear receptance (high forcing) matrices are measured. Then, firstly the missing elements of the linear FRF matrix are calculated by using FRF synthesis method, and the *NLI* values are calculated. The calculated *NLI* values are shown in Figure 7-19. The *NLI* chart shows the coordinates which are affected from nonlinearity. High *NLI* values at 1<sup>th</sup> and 2<sup>nd</sup> coordinates indicate the damage between these coordinates.

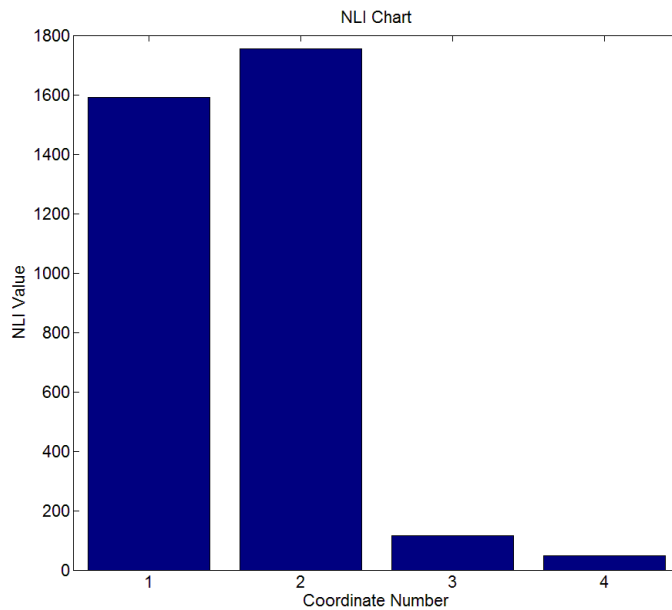


Figure 7-19. Waveguide Nonlinearity Index Chart

Although the parts seem that they are brazed correctly from quality control perspective, the performance of the waveguide is not as predicted. Thus, vibration tests show that the two branches are not identical as they should be. A closer inspection to the waveguide reveals a thin line between the brazed parts which is successfully localized by the improved DF method. The damage in this part is along the brazing line consisting of several micro cracks.



Figure 7-20. Waveguide damaged region

## CHAPTER 8

### DISCUSSION AND CONCLUSIONS

It was recently shown [78] with an experimental case study that the DF method developed by Özer *et al.* [2] for detecting, localizing and parametrically identifying nonlinearity in MDOF systems is a promising method that can be used in industrial applications. In this study, improvements to the DF method (improved DF method) and two new methods, the DFI and the DDF methods are given which eliminate the practical limitations of the DF method. The improvements made along with numerical and experimental studies for verification can be summarized as follows:

The DF method requires dynamic stiffness matrix of the linear part of the system which can be obtained by constructing a numerical model for the system and updating it using experimental measurements or else measuring the complete receptance matrix at low level of forcing to obtain the receptance matrix of the linear part of the system. In this study, however, it is proposed to make linear modal identification by using one column of the receptance matrix of the system which is experimentally measured at low forcing level, and then to calculate the missing elements of the complete FRF matrix so that the dynamic stiffness matrix required for the identification can be obtained (improved DF method). Note that low forcing testing will not give the linear receptances if nonlinearity is due to dry friction, since its effect will be dominant at low level vibrations. For this type of nonlinearity, experiments with high level forcing will yield approximate values for the linear receptances. Having frictional nonlinearity with other types of nonlinearities makes it difficult to determine linear FRFs experimentally. Therefore, when frictional nonlinearity exists with other types of nonlinearities, the approach proposed can be applied only if linear FRFs are theoretically obtained. The improved DF method suggested is applied to lumped parameter systems, SDOF and MDOF experiments including the cases where the nonlinear element is also between two coordinates, and it is shown that detection, localization and identification of nonlinear elements can successfully be achieved.

Secondly, it is proposed in this study to use RF plots that can be obtained from DF inversion for parametric identification, instead of using DF plots, in order to avoid the limitations in using footprint graphs (the DFI method). It is found easier to determine the type of nonlinearity by using RF plots rather than DF plots, especially for discontinuous nonlinear functions such as backlash. The application of the DFI method proposed is also demonstrated on three real structural test systems, and it is concluded that the accuracy in parametric determination of nonlinearity by DF inversion is comparable to that of improved DF method, and since RF plots give better insight into the type of nonlinearity, this approach may be preferred in several applications to identify the type of nonlinearity. Furthermore, once the RF function is obtained, it may be directly used in nonlinear model of the system if time domain analysis is to be made. Using DF inversion rather than footprint graphs makes it possible to identify total restoring force of more than one type of nonlinearity that may co-exist at the same location. Thus, DF inversion yields an equivalent RF function that can be used in further calculations without any need to identify each nonlinearity separately.

Furthermore, obtaining the nonlinearity matrix directly from nonlinear FRFs is presented which eliminates the need for obtaining linear FRFs (the DDF method). The DF method requires dynamic stiffness matrix of the linear part which can be obtained by low forcing measurements. However, low forcing testing may not always give the linear FRFs accurately when nonlinearity is high, and furthermore, if nonlinearity is due to dry friction, low forcing level testing will not give linear FRFs at all, since its effect will be dominant at low level vibrations. In order to overcome such problems, in the DDF method developed, it is proposed to test the structure at two forcing levels and calculate the nonlinearity matrix directly from

these measurements. The DFI method can be easily applied after obtaining the DFs by the DDF method. The suggested DDF method is first applied to lumped parameter systems and it is shown that identification of nonlinear elements can successfully be achieved even when there is more than one nonlinear element with different characters at the same coordinate. The application of the proposed DDF method is also demonstrated on two real structural test systems, and it is concluded that the accuracy in parametric determination of nonlinearity by the DDF method gives better results than the DF method where low forcing tests are used to obtain linear FRFs. It is concluded in this study that the proposed DDF method is very promising to be used in practical systems, especially when there are multiple nonlinear elements at the same location.

Finally, it is shown that the improved DF method for detecting, localizing and parametrically identifying nonlinearity in MDOF systems can also be used for damage detection and localization for the type of damages which introduce nonlinearity to the structure. The suggested improved DF method is first applied to an aluminum beam with a breathing crack and it is shown that detection and localization of damage can be achieved by exciting the system from only one point and measuring the responses at all other coordinates (or only at the coordinates around which there might be a crack). Furthermore, it is shown in this study that the improved DF method can also be employed to localize damage by using impact testing, which is more practical. The tests are conducted on a composite sheet and it is concluded that the accuracy in damage localization with impact testing is comparable to that of a shaker testing. Impact testing has many advantages over shaker testing as the most important one being the reduction of setup preparation time and test duration. Moreover, the possibility of damaging the specimen during localization tests is much less in impact testing. The nonzero and relatively high *NLI* values obtained at coordinates not adjacent to damaged locations are believed to be due to measuring only translational FRFs and not including those related with rotational DOF. As a final case study, a real engineering structure, a waveguide is tested with great success. Consequently, it can be said that the proposed improved DF method is applicable to damage detection studies, but still open to further improvements.

## CHAPTER 9

### RECOMMENDATIONS FOR FUTURE WORK

Although in this study a variety of topics concerning nonlinear identification are covered, there are still several aspects that need further investigation.

First of all, multi-harmonic identification is one of the important topics that may be researched. In order to perform multi-harmonic identification, the formulations used for describing function should be multi-harmonic. Furthermore, the step sine tests conducted should be also modified to capture the multi harmonic responses.

Secondly, as the step sine tests require long testing time, the accuracy of random excitation and impact testing in nonlinearity identification using describing functions should be investigated.

Another improvement that can be accomplished in the DFI method is, instead of using only polynomial type functions using more complicated functions to fit DFs, which will definitely improve the quality of RFs.

Finally, the methods proposed can be extended to include rotational DOFs which will improve identification results especially for more complicated structures.

## REFERENCES

- [1] D. Göge, M.U. Sinapius, U. Füllekrug, M. Link, Detection and Description of Non-Linear Phenomena in Experimental Modal Analysis via Linearity Plots, *International Journal of Non-linear Mechanics* 40 (2005) 27-48.
- [2] M.B. Özer, H.N. Özgüven, T.J. Royston, Identification of Structural Non-Linearities Using Describing Functions and The Sherman–Morrison Method, *Mechanical Systems and Signal Processing* 23 (2009) 30-44.
- [3] G. Kerschen, K. Worden, A.F. Vakakis, J.C. Golinval, Past, present and future of nonlinear system identification in structural dynamics, *Mechanical Systems and Signal Processing* 20 (2006) 505-592.
- [4] N.M.M. Maia, J.M.M. Silva, *Theoretical and Experimental Modal Analysis*, Research Studies Press LTD., Baldock, Hertfordshire, England, 1997.
- [5] D.J. Ewins, *Modal Testing: Theory and Practice*, Research Studies Press LTD., Baldock, Hertfordshire, England, 1995.
- [6] K. Worden, G.R. Tomlinson, *Nonlinearity in Structural Dynamics*, Institute of Physics Publishing, Bristol, 2001.
- [7] H.R.E. Siller, *Non-linear Modal Analysis Methods for Engineering Structures*, PhD Thesis in Mechanical Engineering, Imperial College London/University of London, 2004.
- [8] S. Narayanan, P. Sekar, A Frequency Domain Based Numeric–Analytical Method for Non-Linear Dynamical Systems, *Journal of Sound and Vibration* 211 (1998) 409-424.
- [9] A.A. Muravyov, S.A. Rizzi, Determination of Nonlinear Stiffness with Application to Random Vibration of Geometrically Nonlinear Structures, *Computers and Structures* 81 (2003) 1513-1523.
- [10] S.F. Masri, T.K. Caughey, A nonparametric identification Technique for Nonlinear Dynamic Problems, *Transaction of ASME Journal of Applied Mechanics* 46 (1979) 433-445.
- [11] H. Elizalde, M. İmregun, An Explicit Frequency Response Function Formulation for Multi-Degree-Of-Freedom Non-Linear Systems, *Mechanical Systems and Signal Processing* 20 (2006) 1867-1882.
- [12] M. Thothadri, R.A. Casas, F.C. Moon, R. D’andrea, C. R. Johnson Jr., Nonlinear System Identification of Multi-Degree-of-Freedom Systems, *Nonlinear Dynamics* 32 (2003) 307-322.
- [13] P. Cermelj, M. Boltezar, Modeling Localized Nonlinearities Using the Harmonic Nonlinear Super Model, *Journal of Sound and Vibration* 298 (2006) 1099-1112.
- [14] P.W.J.M. Nuij, O.H. Bosgra, M. Steinbuch, Higher-Order Sinusoidal Input Describing Functions for the Analysis of Non-Linear Systems With Harmonic Responses, *Mechanical Systems and Signal Processing* 20 (2006) 1883-1904.

- [15] D.E. Adams, R.J. Allemang, A New Derivation of the Frequency Response Function Matrix for Vibrating Non-Linear Systems, *Journal of Sound and Vibration* 227 (1999) 1083-1108.
- [16] Ö. Tanrikulu, H.N. Özgüven, A new method for the identification of non-linearities in vibrating structures, in: *Proceedings of the Fourth International Conference on Recent Advances in Structural Dynamics*, Southampton, England, July 15–18, 1991.
- [17] A.F. Vakakis, D.J. Ewins, Effects of weak non-linearities on modal analysis, *Proceedings of IMAC 10* (1992) 72–78.
- [18] R.M. Lin, D.J. Ewins, Location of localised stiffness non-linearity using measured data, *Mechanical Systems and Signal Processing* 9 (3) (1995) 329–339.
- [19] K.Y. Şanlıtürk, D.J. Ewins, Modelling two dimensional friction contact and its application using harmonic balance method, *Journal of Sound and Vibration* 193 (2) (1996) 511–523.
- [20] M.B. Özer, H.N. Özgüven, A new method for localization and identification of non-linearities in structures, in: *Proceedings of the ESDA 2002: Sixth Biennial Conference on Engineering Systems Design and Analysis*, ASME, İstanbul, Turkey, July 8–11, 2002.
- [21] T. C. Kim, T. E. Rook, R. Singh, Super- and Sub-Harmonic Response Calculations for a Torsional System With Clearance Nonlinearity Using the Harmonic Balance Method, *Journal of Sound and Vibration* 281 (2005) 965-993.
- [22] B. Kuran, H. N. Özgüven, A Modal Superposition Method for Non-Linear Structures, *Journal of Sound and Vibration* 189 (1996) 315–339.
- [23] J. V. Ferreira, D. J. Ewins, Algebraic Nonlinear Impedance Equation Using Multi-Harmonic Describing Function, *Proceedings of the XV International Modal Analysis Conference-IMAC 96*, Orlando, USA, February 1997.
- [24] P. A. Atkins, J. R. Wright, An Extension of Force Appropriation to the Identification of Non-Linear Multi-Degree of Freedom Systems, *Journal of Sound and Vibration* 237 (2000) 23-43.
- [25] G. Gloth, M. Sinapius, Analysis of Swept-Sine Runs During Modal Identification, *Mechanical Systems and Signal Processing* 18 (2004) 1421-1441.
- [26] G. Gloth, M. Sinapius, Influence and Characterization Of Weak Non-Linearities In Swept-Sine Modal Testing, *Aerospace Science and Technology* 8 (2004) 111-120.
- [27] A. Josefsson, M. Magnevall, K. Ahlin, On Nonlinear Parameter Estimation with Random Noise Signals, *Proceedings of the SEM IMAC XXV Conference*, Orlando, FL USA, 2007.
- [28] C. R. Pickrel, Airplane Ground Vibration Testing Correlation With Nominal Modal Model, *Sound and Vibration* 36 (2002) 18-23.
- [29] P. Verboven, P. Guillaume, S. Vanlanduit, B. Cauberghe, Assessment Of Nonlinear Distortions in Modal Testing and Analysis of Vibrating Automotive Structures, *Journal of Sound and Vibration* 293 (2006) 299-319.
- [30] S. Bellizzi, R. Bouc, Analysis of Multi-Degree of Freedom Strongly Non-Linear Mechanical Systems With Random Input Part I: Non-Linear Modes And Stochastic Averaging, *Probabilistic Engineering Mechanics* 14 (1999) 229-244.

- [31] S. Bellizzi, R. Bouc, Analysis of Multi-Degree of Freedom Strongly Non-Linear Mechanical Systems with Random Input Part II: Equivalent Linear System with Random Matrices and Power Spectral Density Matrix, *Probabilistic Engineering Mechanics* 14 (1999) 245-256.
- [32] S. M. Spottswood, R. J. Allemang, Identification of Nonlinear Parameters for Reduced Order Models, *Journal of Sound and Vibration* 295 (2006) 226-245.
- [33] E.F. Crawley, A.C. Aubert, Identification of nonlinear structural elements by force-state mapping, *AIAA Journal* 24 (1986) 155–162 (Sections 3.2, 6.1).
- [34] E.F. Crawley, K.J. O'Donnell, Identification of nonlinear system parameters in joints using the force-state mapping technique, *AIAA Paper* 86-1013 (1986) 659–667 (Sections 3.2, 6.1).
- [35] S.F. Masri, H. Sass, T.K. Caughey, A Nonparametric Identification of Nearly Arbitrary Nonlinear Systems, *Journal of Applied Mechanics* 49 (1982) 619-628.
- [36] J.P. Noel, G. Kerschen, Newerla, Application of the Restoring Force Surface Method to a Real-life Spacecraft Structure, *Proceedings of the SEM IMAC XXX Conference 3*, Jacksonville, FL USA, 2012.
- [37] G. Kerschen, J.C. Golinval, Theoretical and Experimental Identification of a Nonlinear Beam, *Journal of Sound and Vibration* 244(4) (2001) 597-613.
- [38] G. Kerschen, V. Lenaerts, J.C. Golinval, VVT Benchmark: Application of the Restoring Force Surface Method, *Mechanical Systems and Signal Processing* 17(1) (2003) 189-193.
- [39] K. Worden, D. Hickey, M. Haroon, D.E. Adams, Nonlinear System Identification of Automotive Dampers: A Time and Frequency-domain Analysis, *Mechanical Systems and Signal Processing* 23 (2009) 104-126.
- [40] C. Xueqi, L. Qiuhai, H. Zhichao, G. Tieneng, A Two-step Method to Identify Parameters of Piecewise Linear Systems, *Journal of Sound and Vibration* 320 (2009) 808-821.
- [41] M. Haroon, D.E. Adams, Y.W. Luk, A.A. Ferri, A time and Frequency Domain Approach for Identifying Nonlinear Mechanical System Models in the absence of an Input Measurement, *Journal of Sound and Vibration* 283 (2005) 1137-1155.
- [42] Y.C. Liang, D.P. Feng., J.E. Cooper, Identification of Restoring Forces in Non-linear Vibration Systems Using Fuzzy Adaptive Neural Networks, *Journal of Sound and Vibration* 242(1) (2001) 47-58.
- [43] D.E. Adams, *Health Monitoring of Structural Materials and Components*, John Wiley and Sons, Chichester, 2007.
- [44] O.S. Salawu, Detection of structural damage through changes in frequency: a review, *Engineering Structures* 19(9) (1997) 718–723.
- [45] A. K. Pandey, M. Biswas, M. M. Samman, Damage detection from changes in curvature mode shapes, *Journal of Sound and Vibration* 145(2) (1991) 321–332.
- [46] C. P. Ratcliffe, Damage detection using a modified Laplacian operator on mode shape data, *Journal of Sound and Vibration* 204(3) (1997) 505–517.

- [47] N. M. M. Maia, J. M. M. Silva, E. A. M. Almas, Damage detection in structures: from mode shape to frequency response function methods, *Mechanical Systems and Signal Processing* 17(3) (2003) 489–498.
- [48] T. M. Whalen, The behavior of higher order mode shape derivatives in damaged beam-like structures, *Journal of Sound and Vibration* 309(3–5) (2008) 426–64.
- [49] Y. J. Yan, L. Cheng, Z. Y. Wu, L. H. Yam, Development in vibration-based structural damage detection technique, *Mechanical Systems and Signal Processing* 21(2007) 2198-2211.
- [50] D. Huynh, J. He, D. Tran, Damage location vector: A non-destructive structural damage detection technique, *Computers & Structures* 83 (2005) 2353-2367.
- [51] D. D. Rizos, S. D. Fassois, Z. P. Marioli-Riga, A. N. Karanika, Vibration-based skin damage statistical detection and restoration assessment in a stiffened aircraft panel, *Mechanical Systems and Signal Processing* 22 (2008) 3151-337.
- [52] M. Radzienski, M. Krawczuk, M. Palacz, Improvement of damage detection methods based on experimental modal parameters, *Mechanical Systems and Signal Processing* 25 (2011) 2169-2190.
- [53] J. Wang, P. Qiao, On irregularity-based damage detection method for cracked beams, *Solids and Structures* 45 (2008) 688-704.
- [54] Q. Huang, P. Gardoni, S. Hurlbaeus, A probabilistic damage detection approach using vibration-based nondestructive testing, *Structural Safety* 38 (2012) 11-21.
- [55] P. Qiao, K. Lu, W. Lestari, J. Wang, Curvature mode shape-based damage detection in composite laminated plates, *Composite Structures* 80 (2007) 409-428.
- [56] J. Xiang, M. Liang, A two-step approach to multi-damage detection for plate structures, *Engineering Fracture Mechanics* 91 (2012) 73-86.
- [57] N. Wu, Q. Wang, Experimental Studies on damage detection of beam structures with wavelet transform, *International Journal of Engineering Science* 49 (2011) 253-261.
- [58] W. Fan, P. Qiao, A 2-D continuous wavelet transform of mode shape data for damage detection of plate structures, *International Journal of Solids and Structures* 46 (2009) 4379-4395.
- [59] N. Bakhary, H. Hao, A. J. Deeks, Damage detection using artificial neural network with consideration of uncertainties, *Engineering Structures* 29 (2007) 2806-2815.
- [60] L. Yu, L. Cheng, L. H. Yam, Y. J. Yan, J. S. Jiang, Experimental validation of vibration-based damage detection for static laminated composite shells partially filled with fluid, *Composite Structures* 79 (2007) 288-299.
- [61] J. M. Nichols, M. Seaver, S. T. Trickey, M. D. Todd, C. Olson, L. Overbey, Detecting nonlinearity in structural systems using the transfer entropy, *Physical Review* E72 (2005) 046217.
- [62] Z.Q. Lang, G. Park, C. R. Farrar, M. D. Todd, Z. Mao, L. Zhao, K. Worden, Transmissibility of non-linear output frequency response functions with application in detection and location of damage in MDOF structural systems, *International Journal of Non-Linear Mechanics* 46 (2011) 841-853.

- [63] Z. K. Peng, Z. Q. Lang, C. Wolters, S. A. Billings, K. Worden, Feasibility study of structural damage detection using NARMAX modeling of Nonlinear Output Frequency Response Function based analysis, *Mechanical Systems and Signal Processing* 25 (2011) 1045-1061.
- [64] U. Andreaus, P. Baragatti, Experimental damage detection of cracked beams by using nonlinear characteristics of forced response, *Mechanical Systems and Signal Processing* 31 (2012) 382-404.
- [65] S. A. Eftekhari, F. Bakhtiari-Nejad, E. H. Dowell, Bifurcation boundary analysis as a nonlinear damage detection feature: does it work?, *Journal of Fluids and Structures* 27 (2011) 297-310.
- [66] M. Ö. Aydoğan, Damage Detection in structures using vibration measurements, MSc. Thesis in Mechanical Engineering, Middle East Technical University, 2003.
- [67] B. Van der Pol, Forced Oscillations in a Circuit with Non-linear Resistance, *The London, Edinburgh, and Dublin Philosophical Magazine and Journal of Science* 3, (1927) 65–80.
- [68] N. N. Bogoliubov, Y. A. Mitropolsky, *Asymptotic Methods in the Theory of Non-linear Oscillations*, Hindustan Publishing Company, Delhi, 1961.
- [69] Y. H. Ku1, C. F. Chen, A New Method for Evaluating the Describing Function of Hysteresis-type Nonlinearities, *Journal of the Franklin Institute* 273, (1962) 226–241.
- [70] K. Watanabe, H. Sato, A Modal Analysis Approach to Nonlinear Multi-degrees-of-freedom Systems, *ASME Journal of Vibrations, Stress, and Reliability in Design* 189-3, (1988) 110–410.
- [71] Ö. Tanrikulu, B. Kuran, H.N. Özgüven, M. İmregun, Forced Harmonic Response Analysis of Non-linear Structures, *AIAA Journal* 31 (1993) 1313 – 1320.
- [72] E. Ciğeroğlu, H.N. Özgüven, “Non-linear Vibration Analysis of Bladed Disks with Dry Friction Dampers”, *Journal of Sound and Vibration*, 295 (2006) 1028-1043.
- [73] D. Abat, Harmonic Vibration Analysis of Large Structures with Local Nonlinearity, MSc. Thesis in Mechanical Engineering, Middle East Technical University, 2009.
- [74] B. Kuran. Dynamic Analysis of harmonically excited non-linear structures by using iterative modal method, MSc. Thesis in Mechanical Engineering, Middle East Technical University, 1992.
- [75] M.L.M. Duarte, Experimentally-Derived Structural Models for Use in Further Dynamic Analysis, PhD Thesis in Mechanical Engineering, Imperial College London, 1996.
- [76] W. Heylen, S. Lammens, P. Sas, *Modal Analysis Theory and Testing*, Katholieke Universiteit Leuven, 1997.
- [77] LMS Test.Lab Modal Analysis Manual, 2010.
- [78] A. Gelb, W.E. Vander Velde, *Multiple-Input Describing Functions and Nonlinear System Design*, McGraw Hill, New York, 1968.
- [79] Ö. Arslan, M. Aykan, H.N. Özgüven, Parametric Identification of Structural Nonlinearities from Measured Frequency Response Data, *Mechanical Systems and Signal Processing* 25 (2011) 1112-1125.

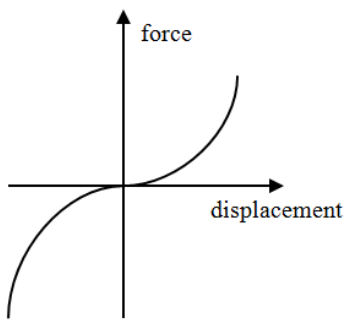
- [80] J.E. Gibson, Nonlinear Automatic Control, McGraw-Hill Book Company, Inc., New York, 1963.
- [81] ANSYS Classic 14.0 Help Manual
- [82] J.V. Ferreira, Dynamic response analysis of structures with nonlinear components, PhD. Thesis, Department of Mechanical Engineering, Imperial College London, 1998.

## APPENDIX A

### COMMON RESTORING FORCE FUNCTIONS AND CORRESPONDING DESCRIBING FUNCTIONS

The RFs and corresponding DFs for nonlinear elements usually encountered in practice are given in Figure A-1 and A-2.

#### Hardening Cubic Stiffness



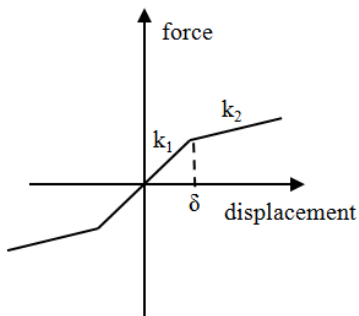
#### RF representation

$$N = bx^3$$

#### DF representation

$$v = \frac{3}{4}bX^2$$

#### Piecewise Linear Stiffness



#### RF representation

$$N = k_1x, \quad |x| < \delta$$

$$N = (k_1 - k_2)\delta + k_2x, \quad |x| \geq \delta$$

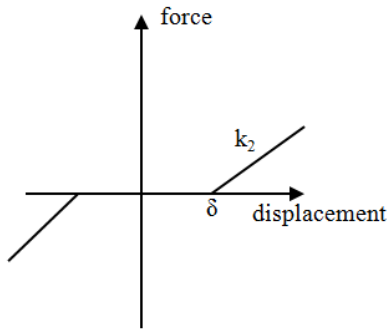
#### DF representation

$$v = k_1, \quad X < \delta$$

$$v = \frac{2(k_1 - k_2)}{\pi} \left[ \sin^{-1} \left( \frac{\delta}{X} \right) + \left( \frac{\delta}{X} \right) \sqrt{1 - \left( \frac{\delta}{X} \right)^2} \right] + k_2, \quad X \geq \delta$$

Figure A-1. RF and DF representations of nonlinear elements

**Backlash**



**RF representation**

$$N = 0, \quad |x| < \delta$$

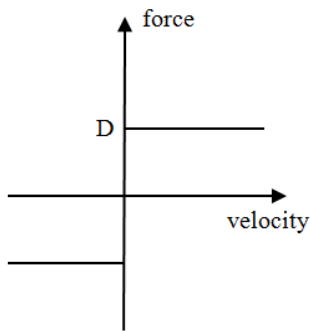
$$N = k_2(x - \delta), \quad |x| \geq \delta$$

**DF representation**

$$v = 0, \quad X < \delta$$

$$v = -\frac{2k_2}{\pi} \left[ \sin^{-1} \left( \frac{\delta}{X} \right) + \left( \frac{\delta}{X} \right) \sqrt{1 - \left( \frac{\delta}{X} \right)^2} \right] + k_2, \quad X \geq \delta$$

**Coulomb Friction**



**RF representation**

$$N = \text{sgn}(\dot{x})$$

**DF representation**

$$v = \frac{4D}{\pi X}$$

Figure A-2. RF and DF representations of nonlinear elements

## APPENDIX B

### PUBLISHED PAPERS DURING PHD

Mechanical Systems and Signal Processing 25 (2011) 1112–1125



Contents lists available at ScienceDirect

Mechanical Systems and Signal Processing

journal homepage: [www.elsevier.com/locate/jnlabr/ymssp](http://www.elsevier.com/locate/jnlabr/ymssp)



## Parametric identification of structural nonlinearities from measured frequency response data

Özge Arslan<sup>a</sup>, Murat Aykan<sup>b</sup>, H. Nevzat Özgüven<sup>a,\*</sup>

<sup>a</sup> Department of Mechanical Engineering, Middle East Technical University, Ankara 06531, Turkey

<sup>b</sup> Defense Systems Technologies Division, ASELSAN A.Ş., Ankara 06172, Turkey

### ARTICLE INFO

#### Article history:

Received 23 June 2010  
Received in revised form  
12 October 2010  
Accepted 14 October 2010  
Available online 21 October 2010

#### Keywords:

Nonlinear structural dynamics  
Nonlinear identification  
Nonlinear modal model  
Nonlinear modal analysis  
Nonlinear modal testing  
Experimental verification

### ABSTRACT

Structural nonlinearity is a common phenomenon encountered in engineering structures under dynamic loading. In several cases, linear theory can suffice to analyze nonlinear systems to some extent. However, there are cases where nonlinear effects and therefore nonlinear analysis become unavoidable. In most of the engineering applications it is usually very difficult if not impossible to model nonlinearity theoretically, especially for nonlinear effects stemming from structural connections. Then it becomes necessary to detect, localize and parametrically identify nonlinear elements from measured vibration data. In this study, two different methods, one being a method suggested recently by two of the authors of this paper, and the other being again a method developed in an earlier work, are implemented on a test rig containing a nonlinear element. Both methods are capable of parametrically identifying nonlinearities from measured frequency response functions. It is aimed in this paper to assess the validity of each method by applying them to a real test structure and thus parametrically identifying the nonlinear element in the system to obtain a mathematical model, and then employing the model in harmonic response analysis of the system in order to compare predicted responses with measured ones.

© 2010 Elsevier Ltd. All rights reserved.

### 1. Introduction

Although modal identification of mechanical systems is thoroughly investigated for several years, the need to obtain accurate values for modal parameters is still very important. Most of the researches performed so far are generally limited to linear identification. However, in the last two decades, with the increasing need to make more accurate analysis, several researchers were focused on modeling and analyzing nonlinear structures.

Nonlinearities are usually localized at joints and boundaries, or the structure itself can be nonlinear. Structural joints set a self-explanatory example in this perspective since they may exhibit a remarkable amount of nonlinearity and they should be properly modeled as nonlinear elements. First studies on nonlinearity in structural dynamics were mostly focused on detection of nonlinearity [1–5]. In these studies, presence of nonlinearity was sought mainly by examining FRF plots under different forcing conditions. Following researches were concentrated on localization of nonlinearity [6–8]. Most recent studies are focused on nonlinear system modeling and identification, including quantification of nonlinearity. An important feature of an identification method is the required pre-known data. Some methods require mass, stiffness and damping values of the linear part [1,9,10], whereas some methods require the FRF of the linear counterpart of the structure to be

\* Corresponding author. Tel.: +90 312 2102103; fax: +90 312 2101105.  
E-mail address: [ozguven@metu.edu.tr](mailto:ozguven@metu.edu.tr) (H. Nevzat Özgüven).

analyzed [11–17]. Parametric identification methods usually use the describing function approach which requires prior information about the nonlinearity type [9,18–24]. For instance, in studies [21–23], the nonlinear system is subjected to a series of static tests initially, which are used to derive an expression for the nonlinear restoring force. There also exist studies using time domain techniques for nonlinear system identification [25–29]. However, as in the previously mentioned studies, the accuracy of the results relies on the accuracy of the prior information about the type of nonlinearity.

The textbook by Worden and Tomlinson [30] on nonlinear structural dynamics and the review paper by Kerschen et al. [31] in which more than 400 references were cited are two reference publications on nonlinear system identification in structural dynamics. An interested reader is urged to refer to these publications for a more general survey on nonlinear system identification and/or for the theories of some of these methods and approaches.

The methods considered in this study offer functional solutions for modeling nonlinear structures by using experimentally measured frequency responses. As mentioned above, former studies mostly require prior information about the nonlinearity present in the system. Methods presented in this paper aim to overcome this difficulty by directly processing the frequency response functions of the structure to obtain a nonlinear model. The first method suggested here [32,33] is based on the fact that nonlinear structures behave linearly under specific conditions. This fact has been explored in earlier studies on nonlinear identification [3]. However, identification and then the use of “displacement amplitude dependent modal parameters” in response prediction of nonlinear structures is a new concept suggested by Arslan and Özgüven [32]. This concept was also very recently used by Carrella and Ewins [34] in their nonlinear identification method. Their method has the advantage of using standard vibration tests, but is applicable to single degree of freedom models only. The second method is developed by Özer et al. [12] and is based on expressing the nonlinear forcing vector in a matrix multiplication form in the differential equation of motion of a multi-degree of freedom (MDOF) nonlinear system with harmonic excitation. The study is an extension of a previously developed method by the first two authors for localization and quantification of nonlinearity. The same theoretical formulation presented in [12] has also been very recently used by Gondhalekar et al. [35].

The theory of the first method, the method based on response amplitude dependent modal parameter identification [32], is given below in detail, whereas the theory of the second method, the method based on describing function representation of nonlinear elements [12], is briefly summarized here, as it has already been documented in detail. Then the implementation and experimental verification of these methods are demonstrated on a nonlinear test structure by first identifying the nonlinear system and afterwards by using the identified nonlinear dynamic model to calculate the frequency responses of the test structure at various forcing levels in order to compare them with experimental ones.

## 2. Theory

### 2.1. Method 1: modal model of a nonlinear structure from measured frequency responses

This method has recently been proposed [32] and verified with case studies based on simulated experiments. Here, the theory of the method is given in more detail and then it is verified using experimental data. The method is applicable to structures where there is local nonlinearity that can be modeled as a single nonlinear element.

While frequency response functions (FRFs) are independent of the amplitude of the forcing applied in a linear system, in a nonlinear system this is not so, and therefore we will have forcing (or response) amplitude dependent FRFs. For instance, when a nonlinear system is excited with a constant amplitude harmonic force in a frequency range, nonlinear stiffness and/or nonlinear damping matrices will have different values at each frequency since they are response level dependent and the response changes at each frequency. Therefore, FRFs will depend on the external forcing level and moreover depict nonlinear behaviors. However, when the response amplitude is kept constant while obtaining the frequency response function experimentally, nonlinear elements will behave like equivalent linear springs and/or dampers; hence, the frequency response function of the nonlinear system will be given by the FRF of the equivalent linear system for that specific response amplitude level. Note that this approach is valid for displacement dependent nonlinearities, which is the case in several practical applications.

This method basically exploits the idea that linear modal identification can be applied to pseudo-linear data obtained by keeping the response amplitude constant and a set of modal parameters can be obtained for each response level [3]. Earlier studies have shown that linear identification of constant force measurements present unreliable results [36,37] since modal parameters change with changing response amplitudes. Furthermore, variation of modal parameters of a nonlinear system with respect to response amplitude is not random but follows a continuous pattern according to the type of nonlinearity in the system [3]. So, one can successfully use these variations in constructing a modal model for a nonlinear system. Modal parameter variations of nonlinear systems were studied earlier by Chong and İmregün [21–23].

Consider the equation of motion of a nonlinear MDOF system under harmonic excitation:

$$[M]\{\ddot{x}\} + [C]\{\dot{x}\} + [K]\{x\} + \{i[H]\{x\} + \{N(x, \dot{x})\}\} = \{f\} \quad (1)$$

where  $[M]$ ,  $[C]$ ,  $[K]$  and  $[H]$  stand for the mass, viscous damping, stiffness and structural damping matrices of the system, respectively. The response of the system and the external force applied on it are shown by vectors  $\{x\}$  and  $\{f\}$ , respectively.  $\{N\}$  represents the nonlinear internal force in the system, and it is a function of the displacement and/or velocity response of the system, depending on the type of nonlinearity present in the system.

Considering harmonic forcing and assuming harmonic response at the same frequency, both expressions can be written as follows:

$$\{f\} = \{F\}e^{i\omega t} \quad (2)$$

$$\{x\} = \{X\}e^{i\omega t} \quad (3)$$

Note that  $\{X\}$  is complex in order to accommodate phase information. The elements of the nonlinear internal force vector can be written as

$$N_r = \sum_j^n n_{rj} \quad (4)$$

where  $n_{rj}$  represents the nonlinear force element between coordinates  $r$  and  $j$  for  $j \neq r$ , and between the  $r$ th coordinate and the ground for  $j=r$ . Consequently,  $n_{rj}$  is a function of the displacement  $x_r-x_j$  or  $x_r$  only, according to the location of the nonlinear element.

As the response is assumed harmonic at the same frequency of the forcing, nonlinear forces can also be represented as harmonic functions at the same frequency as follows:

$$n_{rj} = v_{rj}(x_r-x_j), \quad j \neq r \quad (5)$$

$$n_{rj} = v_{rj}x_r, \quad j = r \quad (6)$$

Here,  $v$  is the describing function of the nonlinearity in the system such that it provides the best average of the true restoring force between coordinates  $r$  and  $j$  or between the coordinate  $r$  and the ground. Derivation of  $v$  for various nonlinearities can be found in several references, for instance see [38]. By using Eq. (4), the vector  $\{N\}$  can be written as

$$\{N(x, \dot{x})\} = [A(x, \dot{x})]\{X\}e^{i\omega t} \quad (7)$$

where  $[A(x, \dot{x})]$  is the response dependent “nonlinearity matrix” and its elements are given in terms of describing functions  $v_{rj}$  as follows:

$$A_{rr} = v_{rr} + \sum_{j=1}^{r-1} v_{rj}, \quad r = 1, 2, \dots, n \quad (8)$$

$$A_{rj} = -v_{rj}, \quad r \neq j, \quad r = 1, 2, \dots, n \quad (9)$$

As a result, nonlinear forces in the system can be expressed in a matrix form. This representation has been first presented by Budak and Özgüven [39] in their studies analyzing harmonic vibrations of nonlinear MDOF systems, and then the method is generalized for any type of nonlinearity by Tanrikulu et al. [40] by using describing functions.

For the sake of clearness, the remaining part of the method will be first explained through a single degree of freedom (SDOF) example. Consider the equation of motion of a viscously damped SDOF system with cubic stiffness

$$m\ddot{x} + c\dot{x} + kx + \beta x^3 = f \quad (10)$$

In this example, nonlinearity is a cubic stiffness for which the nonlinear force vector can be written as follows:

$$n(x, \dot{x}) = \beta x^3 \quad (11)$$

and the describing function for this type of nonlinearity is given by [38]

$$v(x, \dot{x}) = \frac{3}{4}\beta X^2 \quad (12)$$

where  $X$  is the response amplitude of the harmonic oscillations. Note that the describing function is only a function of  $X$ , hence the nonlinear element will act like an additional stiffness to the system, of which value is changing with changing response amplitude.

Substituting Eq. (12) in Eq. (10) and arranging it, the equation of motion becomes

$$m\ddot{x} + c\dot{x} + \left(k + \frac{3}{4}\beta X^2\right)x = f \quad (13)$$

From Eq. (13), natural frequency and damping ratio of this system can be extracted as follows:

$$\omega_n = \sqrt{\frac{k + \frac{3}{4}\beta X^2}{m}} \quad (14)$$

$$\zeta = \frac{c}{2\sqrt{(k + \frac{3}{4}\beta X^2)m}} \quad (15)$$

As it can be seen from Eqs. (14) and (15), system properties are functions of the response amplitude, provided that the describing function for the nonlinearity is a function of the response amplitude only. Then it can be concluded that, response controlled harmonic vibration tests provide linear FRFs. Linear identification of these FRFs will result in sets of modal parameters of the system, each set corresponding to the response value at which the FRF is measured. As these parameters vary with changing response amplitude of the system, they can be expressed as functions of the response amplitude as follows:

$$\omega_n = \omega_n(X) \tag{16}$$

$$\zeta = \zeta(X) \tag{17}$$

$$A = A(X) \tag{18}$$

where  $A$  is the modal constant. Then the receptance expression of the system can be written in terms of these functions as

$$\theta(X, \omega) = \frac{A(X)}{(\omega_n(X))^2 - \omega^2 + 2i\zeta(X)\omega\omega_n(X)} \tag{19}$$

Here,  $\theta$  is the response level dependent receptance of the system. Note that  $\theta$  should better be called “pseudo-receptance”, since it is not possible to talk about receptance of a nonlinear system. This model can then be used in harmonic response prediction of the same system at various desired forcing levels by using an iterative solution method.

For a harmonic excitation with an amplitude  $F$  and frequency  $\omega$ , the response amplitude of the system will be

$$X = |\theta(X, \omega)|F \tag{20}$$

However, as  $\theta$  is a function of the response amplitude  $X$ , the solution of Eq. (20) for a specific  $\omega$  value requires iteration. In this study, fixed point iteration method with a weighting coefficient is used. The algorithm for the solution can be expressed as

$$(X)_{p+1} = |\theta(\omega, (X)_p)|F \tag{21}$$

where  $(X)_{p+1}$  is the response amplitude of the nonlinear coordinate at  $(p+1)$ th iteration step and  $\theta(\omega, (X)_p)$  is the pseudo-receptance expression at frequency  $\omega$  and  $p$ th iteration step. In Eq. (21), all the modal parameters corresponding to the  $p$ th iteration step are used in the calculation.

Up to this point, the methodology is presented through a SDOF system. Yet the method is also applicable to MDOF systems with local nonlinearity that can be modeled as a single nonlinear element. Consider a nonlinear MDOF system whose equation of motion is given by Eq. (1). Let us assume that the nonlinearity in this system can be modeled as a single element between the  $r$ th coordinate and the ground. Then the nonlinearity matrix,  $[A]$ , includes a single nonzero element,  $A_{rr}$ . If the nonlinearity exists between any two coordinates, say  $r$  and  $j$ , then the nonlinearity matrix, with other elements being zero, includes a sub-matrix in the following form:

$$\begin{bmatrix} A_{rr} & A_{rj} \\ A_{jr} & A_{jj} \end{bmatrix} \tag{22}$$

In order to produce pseudo-linear FRFs, the dynamic stiffness matrix is to be kept constant by keeping the elements nonlinearity matrix constant. This can be achieved by performing response controlled harmonic tests in which the relative response between the two ends of the nonlinear element is kept constant by using a closed loop controller for the displacement signal which can be obtained from an accelerometer. In a SDOF nonlinear system, naturally there exists a single nonlinear element. Thus a single set of harmonic tests in which the amplitude of the nonlinear element is kept constant at each measurement is sufficient for obtaining the complete model of the system that can be used to predict the response of the system under different levels of harmonic forcing.

Let us examine a single set of tests where the harmonic force is applied at the  $j$ th coordinate and the response is measured at the  $i$ th coordinate on a MDOF system with grounded nonlinear element. In this case, each harmonic test is performed by keeping the harmonic displacement amplitude of the nonlinear element,  $X_i$ , constant at a specific response level. Once the obtained linear-behaving FRFs are analyzed with linear identification methods, modal parameters of the structure can be expressed analogous to Eqs. (16)–(18):

$$\omega_r = \omega_r(X_i) \tag{23}$$

$$\zeta_r = \zeta_r(X_i) \tag{24}$$

$${}_rA_{ij} = {}_rA_{ij}(X_i) \tag{25}$$

Then, the pseudo-receptance expression is written as

$$\theta_{ij}(X_i, \omega) = \sum_{r=1}^Q \frac{{}_rA_{ij}(X_i)}{(\omega_r(X_i))^2 - \omega^2 + 2i\zeta_r(X_i)\omega\omega_r(X_i)} \tag{26}$$

where  $Q$  is the number of modes identified. Then the amplitude of the response at  $i$  due to harmonic force at  $j$  can be obtained as

$$X_i = |\theta_{ij}(\omega, X_i)| F_j \quad (27)$$

where  $X_i$  is the harmonic response amplitude,  $\omega$  is the frequency,  $F_j$  is the amplitude of the harmonic force applied at  $j$ th coordinate and  $\theta_{ij}$  is the response level dependent receptance value.

It is possible to obtain other receptance values by inserting the convergent response amplitude value in the modal parameter functions. However, it should be recalled that these pseudo-receptance values will be valid only when the harmonic force with amplitude  $F_j$  is applied at  $j$ th coordinate.

Eq. (27) is also an implicit equation as Eq. (21) and it is solved in the same way as Eq. (21) is solved. The pseudo-receptance expression is updated at every iteration step. Iterations are to be repeated until a specified tolerance is reached. In this study the convergence criteria is specified as

$$e_p = \frac{|(X)_{p+1} - (X)_p|}{|(X)_p|} \times 100 \quad (28)$$

$$e_p = \frac{|(X_i)_{p+1} - (X_i)_p|}{|(X_i)_p|} \times 100 \quad (29)$$

for SDOF and MDOF systems, respectively. Here,  $e_p$  is the percentage relative error between two successive iterations.

The initial response amplitude value for the iterations is taken as the linear solution of the system at the first frequency point. For the following frequencies, the convergent response amplitude value corresponding to the previous frequency point is used as the initial value. Similarly the solution is also carried out starting from the last frequency point and continuing with decreasing frequency values. If the nonlinearity in the system causes a jump in the FRF, jumps can be observed in the system when the solution of the implicit equation is used for frequency sweep in both directions.

At the frequencies where the system shows linear behavior convergence is achieved rapidly. However, at other frequencies which are near resonance convergence may be difficult to obtain with fixed point iteration. In such cases, convergence is obtained by using a weighted average displacement,  $(X_i)_{p+1}^*$ , instead of  $(X_i)_{p+1}$ , in calculating  $(\theta_{ij})_{p+1} \cdot (X_i)_{p+1}^*$  is defined as

$$(X_i)_{p+1}^* = \lambda(X_i)_{p+1} + (1-\lambda)(X_i)_p \quad (30)$$

In Eq. (30),  $\lambda$  is a weighting factor that is assigned a value between 0 and 0.5, so that the previous value is weighted more.

The method explained in this section is also extended to dynamic analyses of coupled and/or modified systems [32]. When a nonlinear system is to be coupled with a linear one, the constructed modal model can be employed in the classical receptance coupling method. Receptance values for the linear system, found experimentally or computationally by linear modal analysis tools, can be coupled with the pseudo-receptance values of the nonlinear system, calculated from the modal model explained above. Similarly, the method can also be used when a nonlinear system whose modal model is constructed is modified. Details of the implementation of the method in structural coupling and modification analyses can be found in Ref. [33].

## 2.2. Method 2: detection, localization and parametric identification of nonlinearity by using nonlinearity index and describing functions

Representation of nonlinear forces in matrix multiplication form using describing functions has also been employed in identification of structural nonlinearities. Özer et al. [12] developed a method starting from the formulation given in their earlier work, to detect, localize and parametrically identify nonlinearity in structures. As the theory is given in detail in Ref. [12], here the method is briefly reviewed just for the completeness.

Starting with the equation of motion of a MDOF system given by Eq. (1), and substituting Eqs. (2), (3) and (7) in (1), the following equation is obtained for harmonic excitation:

$$(-\omega^2[M] + i\omega[C] + i[H] + [K] + [A])(X) = \{F\} \quad (31)$$

or in compact form,

$$\{X\} = [\theta]\{F\} \quad (32)$$

where

$$[\theta] = (-\omega^2[M] + i\omega[C] + i[H] + [K] + [A])^{-1} \quad (33)$$

and is called the pseudo-receptance, as discussed in the previous section. The receptance matrix of the linear counterpart of the nonlinear system written can be written as

$$[\alpha] = (-\omega^2[M] + i\omega[C] + i[H] + [K])^{-1} \quad (34)$$

From Eqs. (33) and (34) the nonlinearity matrix can be obtained as

$$[A] = [\theta]^{-1} - [\alpha]^{-1} \quad (35)$$

Post multiplying both sides of Eq. (35) by  $[\theta]$  gives

$$[\Delta][\theta] = [I] - [Z][\theta] \quad (36)$$

where  $[Z]$  is the dynamic stiffness matrix of the linear part of the structure

$$[Z] = [x]^{-1} = (-\omega^2[M] + i\omega[C] + i[H] + [K]) \quad (37)$$

In order to localize nonlinearity in a system a parameter called “nonlinearity index” is used. Nonlinearity index (NLI) for an  $r$ th coordinate is defined by taking any  $i$ th column of  $[\theta]$  and the  $r$ th row of  $[\Delta]$  as follows:

$$NLI_r = \Delta_{r1}\theta_{1i} + \Delta_{r2}\theta_{2i} + \dots + \Delta_{rn}\theta_{ni} \quad (38)$$

Here, theoretically,  $i$  can be any coordinate; however, in practical applications it should be chosen as an appropriate coordinate at which measurement can be made and also close to suspected nonlinear element. It can be seen from Eq. (38) that any nonlinear element connected to  $r$ th coordinate will yield a nonzero  $NLI_r$ . On the other hand,  $NLI_r$  can experimentally obtained by using the right hand side of Eq. (36), which requires the measurement of the receptances of the system at high and low forcing levels. After finding the location of the nonlinear element(s), the value of describing function at different response amplitudes can be plotted for the parametric identification of nonlinear element(s) (for details see [12]). Very recently, Gondhalekar et al. [35] used the same formulation for detection, localization and identification of nonlinear elements. However, they used genetic algorithm optimization, rather than visual inspection by using a look up table to identify the type of the nonlinearity.

### 3. Case study

#### 3.1. Experimental setup

For the implementation and validation of the identification methods given above, linear and nonlinear modal tests were performed on a nonlinear structure. The test rig similar to the one first used by Ferreira [41], and then also by Siller [42] is used in this study (Fig. 1). Dimensions and technical details of the rig manufactured for this study are given in Fig. 2.

This test rig is preferred for its simplicity in modeling the dynamic system since the structural configuration causes hardening stiffness nonlinearity only. The test rig consists of a linear cantilever beam with its free end held between two thin identical beams which generate cubic spring effect. The cantilever beam and the thin nonlinear beams were manufactured from St37 steel. The modal test setup configuration with its elements is shown in Fig. 3.

For linear and nonlinear testing, a shaker (TIRA) was connected to the free end of the cantilever beam via a push-rod with a PCB 208C03 force transducer. The vibration responses were measured using three miniature PCB 352A24 accelerometers. The frequency resolution was 0.25 Hz due to the limitation of the software used with data acquisition system. Cubic nonlinearity in the system causes jump in the frequency response around resonance frequencies. Ability to observe this phenomenon is closely related to the frequency resolution employed in the harmonic vibration tests. Even though it was possible in the

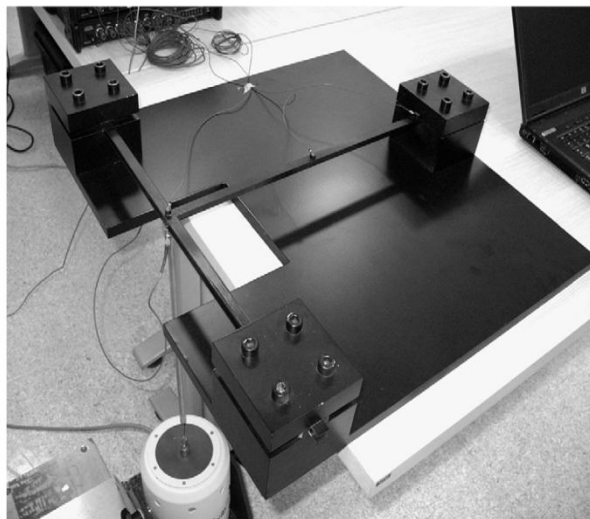


Fig. 1. Test rig used in the modal tests.

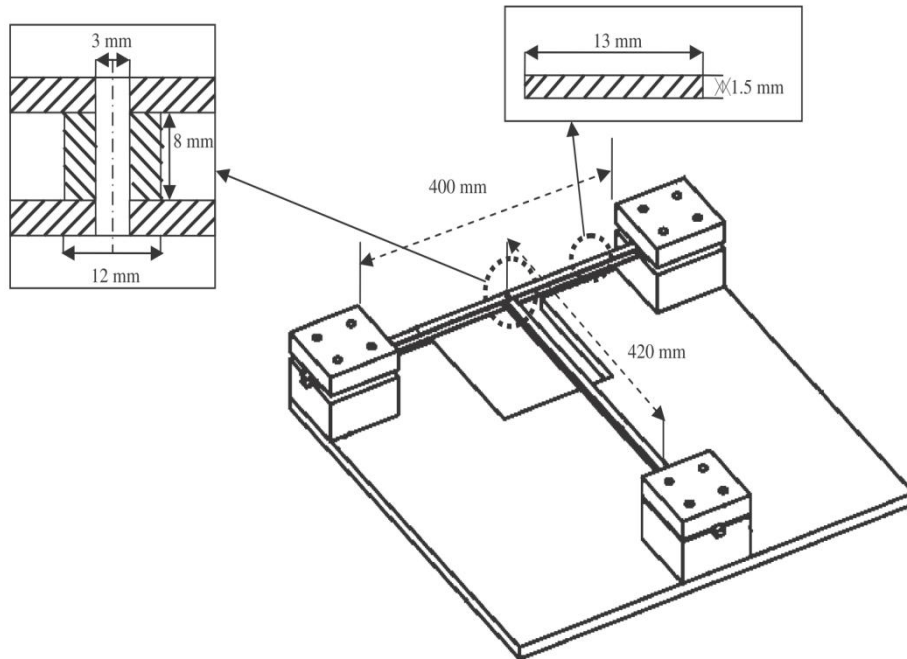


Fig. 2. Dimensions of the test rig.

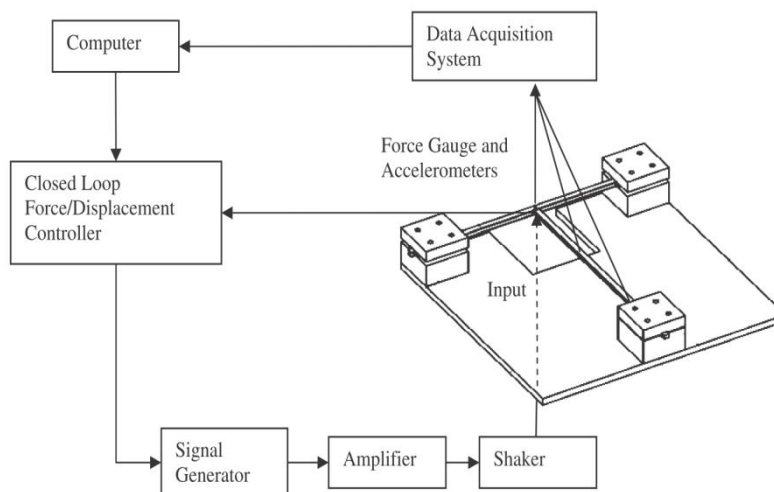


Fig. 3. Experimental test setup.

experimental study to capture the jump in the frequency response, it is believed that better results could have been obtained with a higher frequency resolution. The closed loop control was achieved by the Dataphysics Vector-1 shaker controller.

### 3.2. Modal tests

The modal tests are divided into two groups: constant force testing and constant displacement testing. Only the driving point FRFs are measured in these tests, which are sufficient to verify the identification methods.

The FRF results obtained for the constant force and constant displacement tests are shown in Figs. 4 and 5, respectively.

The FRF curve obtained by using constant displacement control with 0.25 mm of vibration amplitude is taken as the reference linear FRF since the nonlinear part of the elastic force is negligible compared to the linear part for this value of displacement. This is also the minimum displacement limit of the setup with the hardware used.

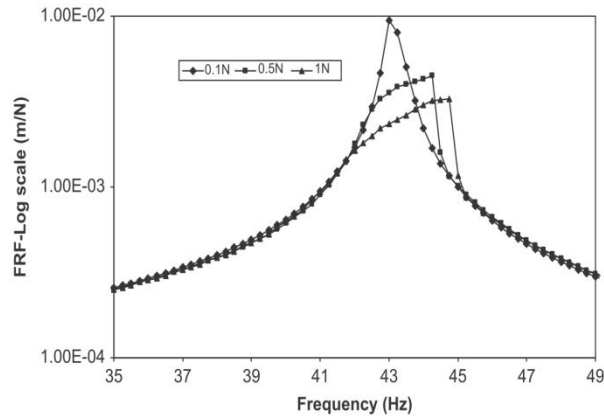


Fig. 4. Constant force driving point FRF curves—experimental results.

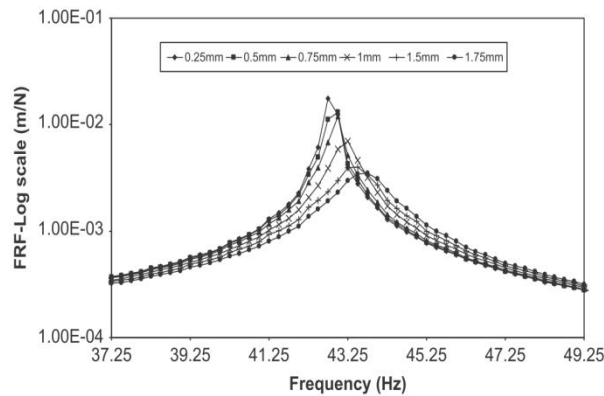


Fig. 5. Constant displacement driving point FRF curves—experimental results.

Table 1

Modal parameters obtained by identification of constant displacement FRFs.

Displacement amplitude (mm)	Natural frequency (rad/s)	Damping ratio (structural damping model)	Modal constant	Phase angle (deg)
0.25	269.2	0.00316	6.539	-0.80
0.50	269.5	0.00487	6.518	-1.04
0.75	270.1	0.00764	6.518	-1.27
1.00	271.4	0.01173	6.532	-1.49
1.50	272.8	0.02168	6.594	-1.95
1.75	274.3	0.02414	6.610	-2.04

### 3.3. Application of the first method

FRFs obtained by displacement controlled tests were used to identify the modal parameters of the system at different response levels. Six tests were performed with different displacement amplitudes, ranging from 0.25 to 1.25 mm. Modal parameters corresponding to each response level are given in Table 1. Parameters are obtained using the method of rational fraction polynomials [43]. A good agreement is obtained between the measured FRFs and regenerated FRFs with identified parameters.

Least square curve fitting is used to fit curves to the modal parameters identified at six different displacement amplitudes, as shown in Figs. 6–9.

After obtaining modal model of the nonlinear system, it was used to predict the frequency response of the system at different forcing amplitudes, and the calculated FRFs are compared with those experimentally obtained with force controlled tests. The FRFs were calculated at forcing levels 0.1, 0.5 and 1 N. The results are presented in Figs. 10–12. Although there are

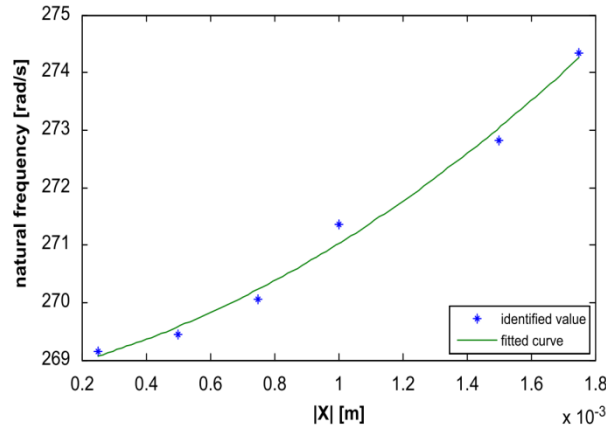


Fig. 6. Variation of natural frequency with response amplitude.

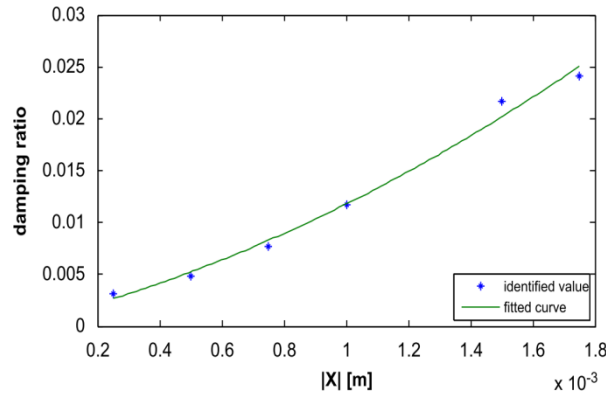


Fig. 7. Variation of damping ratio with response amplitude.

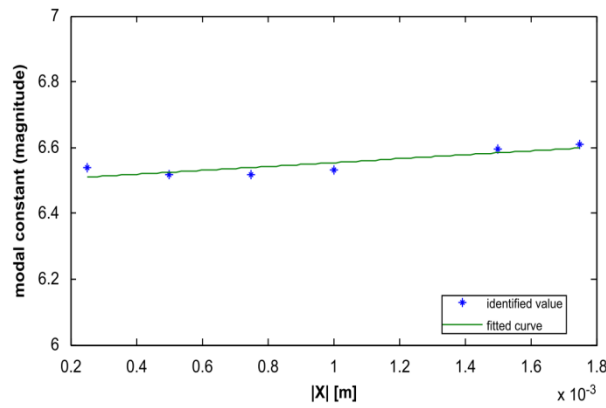


Fig. 8. Variation of modal constant magnitude with response amplitude.

slight shifts in the FRFs obtained from the modal model, which are believed due to force dropouts that were encountered during constant force tests at the resonance zone, it can be concluded that the identified modal model of the nonlinear system can successfully represent the basic nonlinear behavior of the system, which is especially important at high forcing levels where the effect of nonlinear element is dominant.

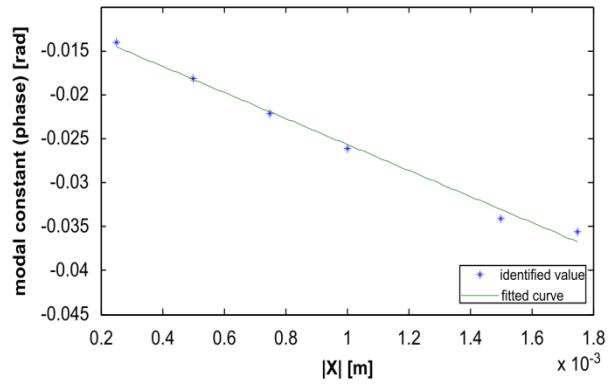


Fig. 9. Variation of phase of the modal constant with response amplitude.

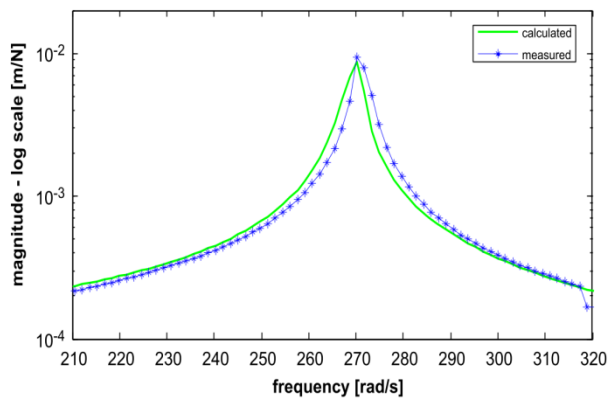


Fig. 10. Calculated and measured FRF values at F=0.1 N.

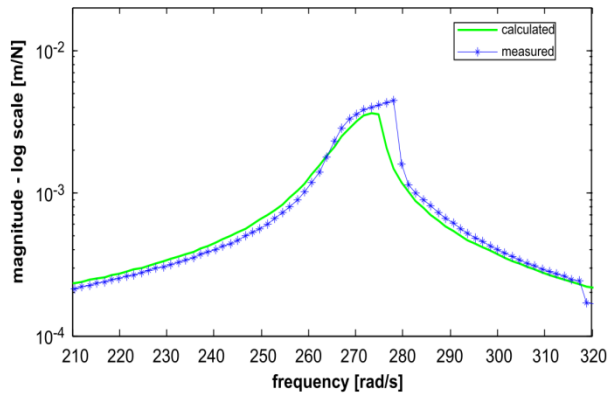


Fig. 11. Calculated and measured FRF values at F=0.5 N.

3.4. Application of the second method

For a single degree of freedom system the nonlinearity matrix reduces to the describing function defining the nonlinearity,

$$\Delta = v = \frac{\alpha - \theta}{\theta \alpha} \tag{39}$$

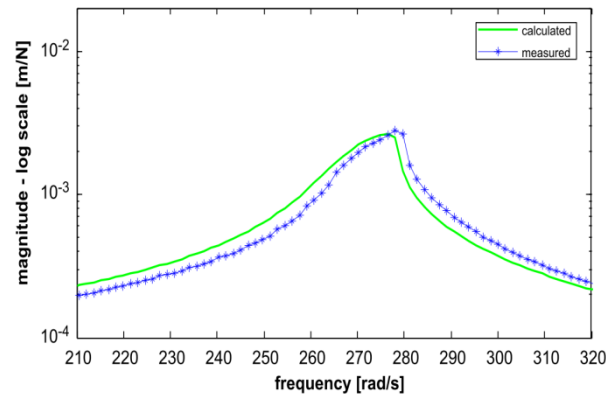


Fig. 12. Calculated and measured FRF values at  $F=1$  N.

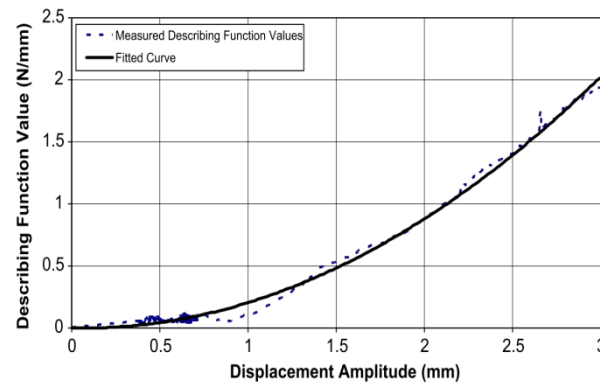


Fig. 13. Measured describing function values and the curve fitted.

where  $\theta$  is the “pseudo-receptance” of the nonlinear SDOF system. The describing function representation of the nonlinearity ( $v$ ) can be graphically shown as a function of response amplitude, which makes it possible to identify the type of nonlinearity and to make parametric identification by using curve fitting.

In order to identify the nonlinearity parametrically, harmonic vibration tests at different force levels are performed. The measured response values are used to obtain the value of the describing function from Eq. (39). Then the describing function is plotted as a function of displacement amplitude (Fig. 13). As expected, the curve fitted to the experimental data describes cubic stiffness nonlinearity.

The nonlinear stiffness value,  $\beta$ , is obtained from the curve fitted (Fig. 13) as  $2.667 \times 10^8$  N/m<sup>3</sup>. After identifying nonlinearity in the system, the harmonic response of the nonlinear system as well as the pseudo FRFs (FRFs defined at a given force level, since the system is nonlinear) can be calculated by using an iterative solution method [12].

In general applications, the linear model of the system can be obtained by using FEM, and only for the identification of nonlinearity experiments can be made. Alternatively, the FRF of the underlying linear system can be obtained from FRF measurements in the system at very low forcing levels, where the nonlinear internal forces will be negligible. However, when there is only friction type of nonlinearity, FRF measured at low amplitude of vibration will not represent FRF of the underlying system; on the contrary, the FRF measured at high response levels will represent FRF of the linear counterpart. Comparison of FRFs measured at different response levels will reveal whether or not there is only friction type of nonlinearity so that FRF measured at high response level can be taken as the FRF for the underlying linear system. Yet, if the system has multiple nonlinearities including friction type of nonlinearity, it may be difficult to measure the FRF of the underlying linear system experimentally, and using finite element model of the system seems to be the only alternative to obtain linear FRF of the linear counterpart. In this case study, the linear FRF of the system obtained by using constant displacement control with 0.25 mm of vibration amplitude is taken as the linear FRF of the system, since the nonlinear part of the elastic force is negligible compared to the linear part at this value of displacement.

The pseudo-FRFs calculated at forcing levels of 0.1, 0.5 and 1 N are compared with experimentally measured values in Figs. 14–16, respectively. As can be seen from the figures, very good agreements are obtained between experimental and predicted responses.

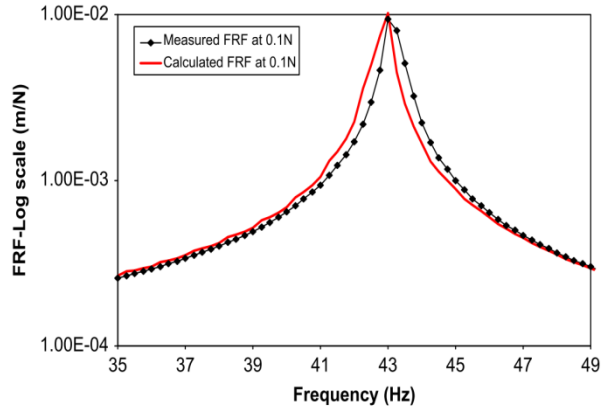


Fig. 14. Calculated and measured FRF values at 0.1 N.

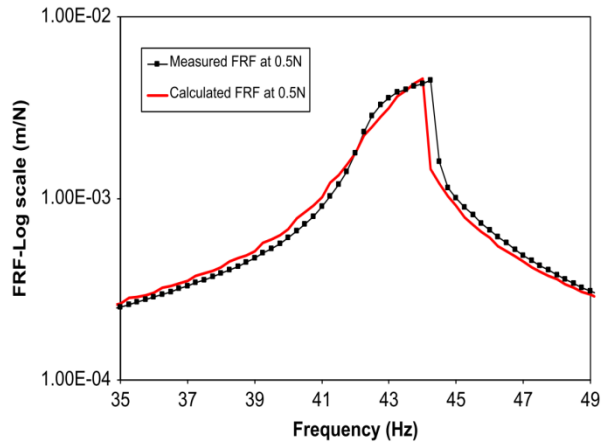


Fig. 15. Calculated and measured FRF values at 0.5 N.

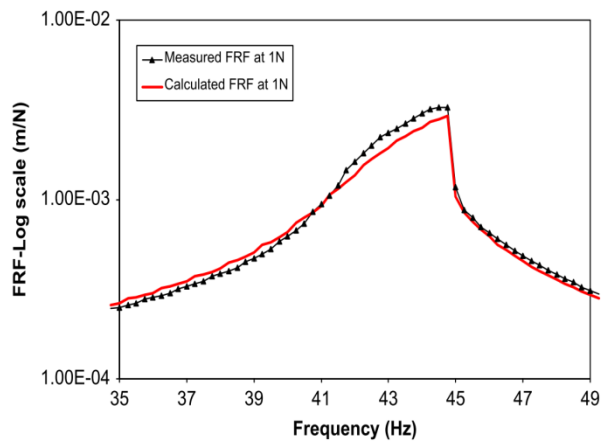


Fig. 16. Calculated and measured FRF values at 1 N.

#### 4. Conclusion

In this study two methods on the parametric identification of nonlinearities in structures are considered. The theory of the method based on modal identification [32], which has recently been proposed by two of the authors of this paper, is given in detail. The theory of the method based on describing functions is briefly summarized as it is given in detail in a recent publication [12].

Although the system used for the demonstration of the methods is modeled as a SDOF system for simplicity, both methods are applicable to MDOF systems. However, the modal identification method can be used for MDOF systems when the nonlinearity can be modeled as a single nonlinear element between any two coordinates. This method requires FRF measurements by keeping the displacement amplitude of the nonlinear element constant. Then, the nonlinear element gives additional spring and/or damping to the system, and system behaves linearly when excited harmonically at different frequencies. Modal identification of the system from the FRFs measured at each displacement level yields “displacement amplitude dependent modal parameters”. Then, the “displacement amplitude dependent modal model” can be used to calculate the FRFs of the system at any forcing level. Application of this method on a test rig which consists of a cantilever beam with cubic stiffness demonstrated that the modal model can be successfully used to predict the nonlinear behavior of the structure under any given harmonic forcing. Slight shifts observed in the predicted FRFs compared with experimental ones are believed to be due to force dropouts that were encountered during constant force tests around resonances which could not be accurately controlled. This phenomenon has also been observed in the test results given in literature [41,42].

The second method is based on classical FRF measurements. That is, exciting a nonlinear system with constant amplitude harmonic forcing in a frequency range and measuring the response. However, here the test is repeated at different force levels and these results are used to identify the type of nonlinearity. After the nonlinearity type is identified, the parametric identification of the nonlinearity in the system is achieved by using the method 2, which is based on describing function theory. The method is applied on the same test structure and the nonlinear element in the system is identified as a cubic stiffness. The cubic stiffness constant identified is then used in the dynamic model of the system to predict frequency response at several forcing levels and very good agreements are observed between experimental and predicted FRFs, even at high forcing levels where jumps occur in the frequency response.

#### References

- [1] S.F. Masri, T.K. Caughey, A nonparametric identification technique for nonlinear dynamic problems, *Transaction of ASME Journal of Applied Mechanics* 46 (1979) 433–445.
- [2] M. Mertens, H. Van der Auweraer, P. Vanherck, R. Snoeys, Detection of nonlinear dynamic behaviour of mechanical structures, in: 4th International Modal Analysis Conference, Los Angeles, CA, USA, 1986, pp. 712–719.
- [3] J. He, D.J. Ewins, A simple method of interpretation for the modal analysis of non-linear systems, in: 5th International Modal Analysis Conference, London, England, 1987, pp. 626–634.
- [4] A.F. Vakakis, D.J. Ewins, Effects of weak nonlinearities on modal analysis, in: 10th International Modal Analysis Conference, San Diego, California, USA, 1992, pp. 73–78.
- [5] S. Bohlen, L. Gaul, Vibrations of structures coupled by nonlinear transfer behaviour of joints; a combined computational and experimental approach, in: 5th International Modal Analysis Conference, London, England, 1987, pp. 86–91.
- [6] R.M. Lin, D.J. Ewins, On the location of structural nonlinearity from modal testing—a feasibility study, in: 8th International Modal Analysis Conference, Kissimmee, FL, 1990, pp. 497–515.
- [7] H.W. Song, W.L. Wang, Non-linear system identification using frequency domain measurement data, in: 16th International Modal Analysis Conference, Santa Barbara, CA, USA, 1998, pp. 746–752.
- [8] D. Goge, M. Sinapius, U. Fullekrug, M. Link, Detection and description of non-linear phenomena in experimental modal analysis via linearity plots, *International Journal of Non-Linear Mechanics* 40 (2005) 27–48.
- [9] S. Narayanan, P. Sekar, A frequency domain based numeric–analytical method for non-linear dynamical systems, *Journal of Sound and Vibration* 211 (1998) 409–424.
- [10] A.A. Muravyov, S.A. Rizzi, Determination of nonlinear stiffness with application to random vibration of geometrically nonlinear structures, *Computers and Structures* 81 (2003) 1513–1523.
- [11] H. Elizalde, M. Imregun, An explicit frequency response function formulation for multi-degree-of-freedom non-linear systems, *Mechanical Systems and Signal Processing* 20 (2006) 1867–1882.
- [12] M.B. Özer, H.N. Özgüven, T.J. Royston, Identification of structural non-linearities using describing functions and the Sherman–Morrison method, *Mechanical Systems and Signal Processing* 23 (2009) 30–44 (First presented at the 23rd International Modal Analysis Conference, Orlando, FL, 2005, pp. 199–212).
- [13] M. Thothadri, R.A. Casas, F.C. Moon, R. D'andrea, C.R. Johnson Jr., Nonlinear system identification of multi-degree-of-freedom systems, *Nonlinear Dynamics* 32 (2003) 307–322.
- [14] P. Cermelj, M. Boltezar, Modeling localized nonlinearities using the harmonic nonlinear super model, *Journal of Sound and Vibration* 298 (2006) 1099–1112.
- [15] P.W.J.M. Nuij, O.H. Bosgra, M. Steinbuch, Higher-order sinusoidal input describing functions for the analysis of non-linear systems with harmonic responses, *Mechanical Systems and Signal Processing* 20 (2006) 1883–1904.
- [16] D.E. Adams, R.J. Allemang, A. New, Derivation of the frequency response function matrix for vibrating non-linear systems, *Journal of Sound and Vibration* 227 (1999) 1083–1108.
- [17] D.E. Adams, R.J. Allemang, A frequency domain method for estimating the parameters of a non-linear structural dynamic model through feedback, *Mechanical Systems and Signal Processing* 14 (2000) 637–656.
- [18] A. Josefsson, M. Magnevall, K. Ahlin, on nonlinear parameter estimation with random noise signals, in: 25th International Modal Analysis Conference, Orlando, FL, USA, 2007, Paper no. 134.
- [19] S. Bellizzi, R. Bouc, Analysis of multi-degree of freedom strongly non-linear mechanical systems with random input Part I: non-linear modes and stochastic averaging, *Probabilistic Engineering Mechanics* 14 (1999) 229–244.
- [20] S.M. Spottswood, R.J. Allemang, Identification of nonlinear parameters for reduced order models, *Journal of Sound and Vibration* 295 (2006) 226–245.

- [21] Y.H. Chong, M. İmregün, Modal parameter extraction methods for non-linear systems, in: 16th International Modal Analysis Conference, Santa Barbara, CA, USA, 1998, pp. 728–735.
- [22] Y.H. Chong, M. İmregün, Variable modal parameter identification for nonlinear MDOF systems—Parts I & II, *Journal of Shock and Vibration* 8 (2000) 217–227.
- [23] Y.H. Chong, M. Imregun, Coupling of non-linear substructures using variable modal parameters, *Mechanical Systems and Signal Processing* 14 (2000) 731–746.
- [24] T.C. Kim, T.E. Rook, R. Singh, Super- and sub-harmonic response calculations for a torsional system with clearance nonlinearity using the harmonic balance method, *Journal of Sound and Vibration* 281 (2005) 965–993.
- [25] G. Kerschen, J.-C. Golinval, K. Worden, Theoretical and experimental identification of a non-linear beam, *Journal of Sound and Vibration* 244 (2001) 597–613.
- [26] G. Kerschen, V. Lenaerts, S. Marchesiello, A. Fasana, A frequency domain versus a time domain identification technique for nonlinear parameters applied to wire rope isolators, *Journal of Dynamic Systems, Measurements and Control* 123 (2001) 645–650.
- [27] G. Kerschen, V. Lenaerts, J.-C. Golinval, VTT benchmark: application of the restoring force surface method, *Mechanical Systems and Signal Processing* 17 (2003) 189–193.
- [28] S. Marchesiello, L. Garibaldi, A time domain approach for identifying nonlinear vibrating structures by subspace methods, *Mechanical Systems and Signal Processing* 22 (2008) 81–101.
- [29] S. Marchesiello, L. Garibaldi, Identification of clearance-type nonlinearities, *Mechanical Systems and Signal Processing* 22 (2008) 1133–1145.
- [30] K. Worden, G.R. Tomlinson, *Nonlinearity in Structural Dynamics*, Institute of Physics Publishing, 2001.
- [31] G. Kerschen, K. Worden, A.F. Vakakis, J.C. Golinval, Past, present and future of nonlinear system identification in structural dynamics, *Mechanical Systems and Signal Processing* 20 (2006) 505–592.
- [32] Ö. Arslan, H.N. Özgüven, Modal identification of non-linear structures and the use of modal model in structural dynamic analysis, in: 26th International Modal Analysis Conference IMAC, Orlando, USA, 2008, Paper no. 95.
- [33] Ö. Arslan, Modal identification of nonlinear substructures and implementation in structural coupling analysis, M.Sc. Thesis, Department of Mechanical Engineering, Middle East Technical University, Ankara, Turkey, 2008.
- [34] A. Carrella, D.J. Ewins, Identifying and quantifying structural nonlinearities in engineering applications from measured frequency response functions, doi:10.1016/j.ymsp.2010.09.011.
- [35] A.C. Gondhalekar, E.P. Petrov, M. Imregun, Parameters identification for nonlinear dynamic systems via genetic algorithm optimization, *Journal of Computational and Nonlinear Dynamics* doi:10.1115/1.3187213.
- [36] S. Setio, H.D. Setio, L. Jézéquel, Modal analysis of nonlinear multi-degree-of-freedom structures, *International Journal of Analytical and Experimental Modal Analysis* 7 (1992) 75–93.
- [37] L. Jézéquel, H. Setio, S. Setio, Nonlinear modal synthesis in frequency domain, in: 8th International Modal Analysis Conference IMAC, Orlando, USA, 1990, pp. 334–340.
- [38] A. Gelb, W.E. Vander Velde, *Multiple-Input Describing Functions and Nonlinear System Design*, McGraw-Hill, 1968.
- [39] E. Budak, H.N. Özgüven, A method for harmonic response of structures with symmetrical non-linearities, in: 15th International Seminar on Modal Analysis, Leuven, Belgium, 1990, pp. 901–915.
- [40] Ö. Tanrikulu, B. Kuran, H.N. Özgüven, M. Imregun, Forced harmonic response analysis of non-linear structures, *AIAA Journal* 31 (1993) 1313–1320.
- [41] J.V. Ferreira, Dynamic response analysis of structures with nonlinear components, Ph.D. Thesis, Department of Mechanical Engineering, Imperial College London, 1998.
- [42] H.R.E. Siller, Non-linear modal analysis methods for engineering structures, Ph.D. Thesis, Department of Mechanical Engineering, Imperial College London/University of London, 2004.
- [43] M.H. Richardson, D.L. Formenti, Parameter estimation from frequency response measurements using rational fraction polynomials, in: 1st International Modal Analysis Conference (IMAC), Orlando, USA, 1982, pp. 167–181.

# Parametric Identification of Nonlinearity from Incomplete FRF Data Using Describing Function Inversion\*

Murat Aykan<sup>1,2</sup>, H. Nevzat Özgüven<sup>1</sup>

<sup>1</sup> Department of Mechanical Engineering, Middle East Technical University, Ankara 06800, TURKEY

<sup>2</sup> Defense Systems Technologies Division, ASELSAN Inc., Ankara, 06172, TURKEY

## ABSTRACT

Most engineering structures include nonlinearity to some degree. Depending on the dynamic conditions and level of external forcing, sometimes a linear structure assumption may be justified. However, design requirements of sophisticated structures such as satellites require even the smallest nonlinear behavior to be considered for better performance. Therefore, it is very important to successfully detect, localize and parametrically identify nonlinearity in such cases. In engineering applications, the location of nonlinearity and its type may not be always known in advance. Furthermore, in most of the cases, test data will be incomplete. These handicaps make most of the methods given in the literature difficult to apply to engineering structures. The aim of this study is to improve a previously developed method considering these practical limitations. The approach proposed can be used for detection, localization, characterization and parametric identification of nonlinear elements by using incomplete FRF data. In order to reduce the effort and avoid the limitations in using footprint graphs for identification of nonlinearity, describing function inversion is used. Thus, it is made possible to identify the restoring force of more than one type of nonlinearity which may co-exist at the same location. The verification of the method is demonstrated with case studies.

## 1. Introduction

System identification in structural dynamics has been thoroughly investigated over 30 years [1]. However, most of the studies were limited to the linear identification theories. This short literature review does not cover linear identification theories which are well documented [2, 3].

In the last decade, with the increasing need to understand nonlinear characteristics of complicated structures, there were several studies published on nonlinear system identification [4-16]. Nonlinearities can be localized at joints or boundaries or else the structure itself can be nonlinear. There are various types of nonlinearities, such as hardening stiffness, clearance, coulomb friction etc. [5].

Nonlinear system identification methods can be divided into two groups, either as time and frequency domain methods [4], or as discrete and continuous time methods [6]. Most of the methods available require some foreknown data for the system. Some methods require all or part of mass, stiffness and damping values [8-10] whereas some methods [4, 11-16] require linear frequency response function (FRF) of the analyzed structure. In these methods nonlinearity type is usually determined by inspecting the describing function footprints (DFF) visually. However, although the user interpretation may be possible for a single type of nonlinearity, it may not be so easy when there is more than one type of nonlinearity present [5]. Furthermore, obtaining the linear FRF, which is usually presumed to be an easy task, may be difficult when nonlinearity is dominant at low level excitations. There are also methods using neural networks and optimization for system identification [6]. Application of optimization methods in nonlinear system identification is rather a new and promising approach. The major disadvantage of these methods is generally the computational time required.

Nonlinearity identification method presented in this study consists of four main stages. Firstly, existence of nonlinearity in the system is detected by performing step sine tests with different loads. Secondly, the location of the nonlinearity is

---

\* M. Aykan, H. N. Özgüven, Parametric Identification of Nonlinearity from Incomplete FRF Data Using Describing Function Inversion, Topics in Nonlinear Dynamics, Volume 3, Conference Proceedings of the Society for Experimental Mechanics Series, c. 28, s. 311-322, 2012. IMAC XXX Conference, Jacksonville, Florida, January 30 – February 2, 2012.

determined by using incomplete FRF data. The next step is the determination of the type of nonlinearity which is achieved by investigating the restoring force function. Finally, in the parametric identification stage the coefficients of the nonlinear elements are obtained by curve fitting techniques. The method proposed in this study is mainly an improved version of the method developed earlier by Özer *et al.* [12]. The improvement includes using incomplete FRF data which makes the method applicable to large systems, and employing describing function inversion in order to reduce the effort in identification of nonlinearity. Furthermore, using describing function inversion rather than footprint graphs makes it possible to identify the total restoring force of more than one type of nonlinearity that co-exist at the same location.

## 2. Theory

Representation of nonlinear forces in matrix multiplication form using describing functions has been employed in identification of structural nonlinearities by Özer *et al.* [12]. They developed a method starting from the formulation given in their earlier work [4] to detect, localize and parametrically identify nonlinearity in structures. As the basic theory of the method is given in detail in reference [12], here it is briefly reviewed just for the completeness.

The equation of motion for a nonlinear MDOF system under harmonic excitation can be written as

$$[M]\{\ddot{x}\} + [C]\{\dot{x}\} + [K]\{x\} + j[D]\{x\} + \{N(x, \dot{x})\} = \{f\} \quad (1)$$

where  $[M]$ ,  $[C]$ ,  $[K]$  and  $[D]$  stand for the mass, viscous damping, stiffness and structural damping matrices of the system, respectively. The response of the system and the external force applied on it are shown by vectors  $\{x\}$  and  $\{f\}$ , respectively.  $\{N\}$  represents the nonlinear internal force in the system, and it is a function of the displacement and/or velocity response of the system, depending on the type of nonlinearity present in the system. When there is a harmonic excitation on the system in the form of

$$\{f\} = \{F\} e^{j\omega t} \quad (2)$$

the nonlinear internal force can be expressed as [17]

$$\{N(x, \dot{x})\} = [\Delta(x, \dot{x})]\{x\} e^{j\omega t} \quad (3)$$

where  $[\Delta(x, \dot{x})]$  is the response dependent “nonlinearity matrix” and its elements are given in terms of describing functions  $v$  as follows:

$$\Delta_{pp} = v_{pp} + \sum_{\substack{q=1 \\ q \neq p}}^n v_{pq} \quad p = 1, 2, \dots, n \quad (4)$$

$$\Delta_{pq} = -v_{pq} \quad p \neq q \quad p = 1, 2, \dots, n \quad (5)$$

From the above equations it is possible to write the pseudo-receptance matrix for the nonlinear system,  $[H^{NL}]$ , as

$$[H^{NL}] = \left( -\omega^2 [M] + j\omega [C] + j[D] + [K] + [\Delta] \right)^{-1} \quad (6)$$

The receptance matrix of the linear counterpart of the nonlinear system can also be written as

$$[H] = \left( -\omega^2 [M] + j\omega [C] + j[D] + [K] \right)^{-1} \quad (7)$$

From equations (6) and (7), the nonlinearity matrix can be obtained as

$$[\Delta] = [H^{NL}]^{-1} - [H]^{-1} \quad (8)$$

Post multiplying both sides of equation (8) by  $[H^{NL}]$  gives

$$[\Delta][H^{NL}] = [I] - [Z][H^{NL}] \quad (9)$$

where  $[Z]$  is the dynamic stiffness matrix of the linear part:

$$[Z] = [H]^{-1} = (-\omega^2[M] + j\omega[C] + j[D] + [K]) \quad (10)$$

In order to localize nonlinearity in a system, a parameter called “nonlinearity index” is used. The nonlinearity index ( $NLI$ ) for an  $p^{th}$  coordinate is defined by taking any  $i^{th}$  column of  $[H^{NL}]$  and the  $p^{th}$  row of  $[\Delta]$  from equation (9) as follows:

$$NLI_p = \Delta_{p1} \cdot H_{1i}^{NL} + \Delta_{p2} \cdot H_{2i}^{NL} + \dots + \Delta_{pn} \cdot H_{ni}^{NL} \quad (11)$$

Here, theoretically,  $i$  can be any coordinate; however, in practical applications it should be chosen as an appropriate coordinate at which measurement can be made and also be close to suspected nonlinear element. Equation (11) shows that any nonlinear element connected to the  $p^{th}$  coordinate will yield a nonzero  $NLI_p$ . On the other hand,  $NLI_p$  can be experimentally obtained by using the right hand side of equation (9), which requires the measurement of the receptances of the system at high and low forcing levels, presuming that low level forcing will yield FRFs of the linear part:

$$NLI_p = \delta_{ip} - Z_{p1} \cdot H_{1i}^{NL} - Z_{p2} \cdot H_{2i}^{NL} - \dots - Z_{pn} \cdot H_{ni}^{NL} \quad (12)$$

## 2.1. Nonlinearity Localization from Spatially Incomplete FRF Data

The main disadvantage of the method discussed in [12] is that in order to calculate the  $NLI_p$  the whole linear FRF matrix may be required (if instead of theoretically calculated dynamic stiffness matrix, inverse of experimentally measured receptance matrix is used). When this is the case, it may not be feasible to apply the method. In this study it is proposed to use theoretically predicted values for unmeasured receptances calculated from the measured ones, and it is shown with case studies that this approach yields acceptable results.

In modal testing of complicated structures usually a shaker is attached to a specific location on the test structure and measurements are made at several locations. Usually test engineer excites the structure from 1 or 2 locations and measures the responses from many points using accelerometers. This yields 1 or 2 columns of the FRF matrix. The number of unknown elements can be reduced if reciprocity is used, which is one of the main assumptions of linearity. However, there will be still unknown terms in the FRF matrix, especially the ones related with rotational degrees of freedom may be missing. Although there are various methods to obtain FRFs at rotational degrees of freedom [18], measuring FRFs for rotational degrees of freedom is usually found very difficult and it is avoided.

Nonlinearity localization by using the right hand side of equation (9) requires either the system matrices (that can be obtained from the FE model) or the complete receptance matrix of the linear part so that it can be inverted to find  $[Z]$ . In order to obtain the missing elements of the experimentally obtained receptance matrix, the application of a well known method is proposed. Theoretically, if the modal parameters (natural frequency, damping ratio, modal constant, lower and upper residues) of a structure are obtained by linear modal identification then missing elements of the receptance matrix can be synthesized. In this study, the linear modal identification is performed by using LMS Test Lab software.

Once the modal parameters are identified, the unmeasured elements of the receptance matrix are calculated by using [19]

$$H_{pq}(\omega) = \sum_{r=1}^N \frac{1}{j2\Omega_r \sqrt{1-(\zeta_r)^2}} \phi_{pr} \phi_{qr} + \frac{(-\frac{1}{j2\Omega_r \sqrt{1-(\zeta_r)^2}} \phi_{pr} \phi_{qr})^*}{\Omega_r \zeta_r + j(\omega - \Omega_r \sqrt{1-(\zeta_r)^2})} + UA_{pq} - \frac{LA_{pq}}{\omega^2} \quad (13)$$

where,

$\Omega_r$  : Undamped natural frequency of mode r

$\zeta_r$  : Damping ratio of mode r

$\phi_{pr}, \phi_{qr}$  : Mass normalized eigenvectors for mode r

$UA_{pq}$  : Upper residual

$LA_{pq}$  : Lower residual

$N$  : Number of modes considered

## 2.2. Nonlinearity Type Determination

After determining the locations of nonlinear elements in a structural system from nonzero  $NLI$  values, equation (8) is used to evaluate the numerical values of describing functions for each nonlinear element at various response levels. The value of the describing function, when there is single nonlinearity present in the system can be obtained from experimental data at different response amplitudes by using Sherman-Morrison formulation to avoid inversion (see reference [12] for details). However, when there are multiple nonlinearities present in the system, Sherman-Morrison formulation cannot be employed. Yet, simultaneous solution of all describing function values is possible as long as the number of nonlinear elements do not exceed the total DOF of the system, which would be rather unusual in practical applications. Then, the value of each describing function can be plotted at different response amplitudes for obtaining Describing Function Footprints (DFF) which can be used for determining the type of nonlinearity, as well as for parametric identification of nonlinear element(s). Another common approach used for the same purpose is to obtain Restoring Force (RF) plots. Fig. 1 presents RF and DFF plots for some common nonlinear elements. It is clear that RF plots contain more physical information compared to DFF plots. In this study, DFF calculated as described above is inverted to obtain RF function, which is graphically investigated to evaluate the type of nonlinearity.

Nonlinearities in a structural system are usually due to nonlinear stiffness (piecewise stiffness, hardening cubic stiffness, etc.) and/or nonlinear damping (coulomb friction, quadratic damping, etc.). Describing function formulation makes it possible to handle stiffness and damping nonlinearities separately [21]. The real part of the describing function corresponds to stiffness nonlinearities whereas the imaginary part corresponds to damping nonlinearities.

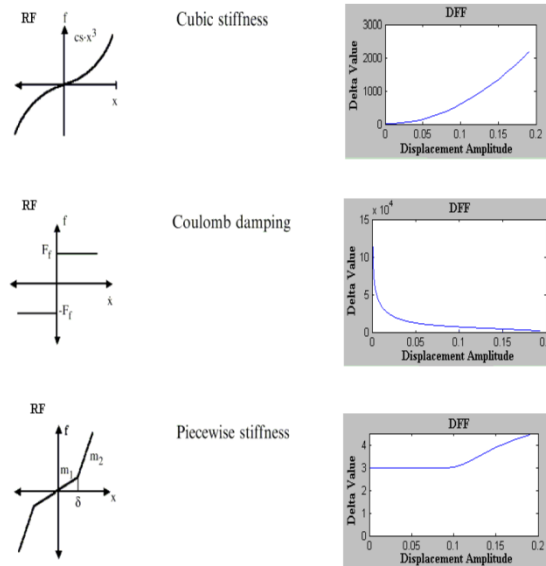


Fig. 1 RF and corresponding DFF plots

The DFF inversion has to be performed using different approaches for stiffness and damping nonlinearities when using experimental data with no knowledge on the type of the nonlinearity.

The inverse of the describing function can be obtained approximately or analytically. Gibson [20] derived inverses for real, imaginary and mean parts of a describing function. However, in this formulation the inversion of the real part and the mean of the describing function requires the information about the type of nonlinearity, but the inversion for the imaginary part works for any describing function and it does not require information about the type of nonlinearity. The only limitation for the imaginary part is that the damping nonlinearity, which yields the imaginary part of DF, should not be frequency dependent. The inverse of the imaginary part of the describing function is given as follows:

$$N(X) \approx \frac{\pi}{2} \frac{d}{dX} [X^2 v(X)] \quad (14)$$

In order to obtain the describing function inversion for the real part, the approximate inversion equations suggested by Gelb and Vander Velde [21] are used:

$$N(X) \approx 3X \sum_{i=0}^{\infty} (-2)^i v(2^{i+1} X) \quad \text{for } v(X) \text{ increasing with } X \quad (15)$$

$$N(X) \approx \frac{3X}{2} \sum_{i=0}^{\infty} \left(-\frac{1}{2}\right)^i v\left(\frac{X}{2^i}\right) \quad \text{for } v(X) \text{ decreasing with } X \quad (16)$$

where  $\{N\}$  represents the nonlinear internal force in the system.

The major drawback of these formulations is that when the describing function is inversely proportional to  $X$ , for instance due to Coulomb friction, the summation gives alternating series and a correct result cannot be obtained. However for damping the imaginary part of the describing function is to be inverted and this is achieved analytically as explained above.

Consequently, in this study it is proposed to use equation (15) or (16) for the real part of DF, which is due to stiffness type of nonlinearity, and to employ equation (14) for the imaginary part of DF, which is due to damping type of nonlinearity.

### 2.3. Parametric Identification of Nonlinearity

There are numerous ways to calculate parametric values for DFF and RF functions. Optimization and black box methods such as neural networks provide promising results if they are well guided. More direct approaches like graphical methods require the engineer to be experienced.

In this study the parametric values of the nonlinearity are obtained from RF plots by curve fitting. It is also possible to obtain the coefficients from DFF when the type of nonlinearity is known. However, for most of the nonlinearity types, DF representation is far more complicated than the corresponding RF function. It should be noted that when the RF representation of nonlinearity is already obtained, it is of little importance what the coefficients of RF function are. All the required information about nonlinear element is stored in the RF function itself which can be further employed in dynamic analysis for different inputs. Determining RF function, rather than DF may be more important when there is more than one type of nonlinearity at the same location, in which case it will be very difficult if not impossible to make parametric identification for each nonlinearity by using DFF.

## 3. Case Study

The nonlinear identification approach proposed in this study is applied to a 4 DOFs discrete system with a nonlinear elastic element represented by  $k_1^*$  (a linear stiffness of 100 N/m with a backlash of 0.005 m) between ground and coordinate 1, and a nonlinear hardening cubic spring  $k_4^*$  ( $= 10^6 * x^2$  N/m) between coordinates 3 and 4, as shown in Fig. 2.

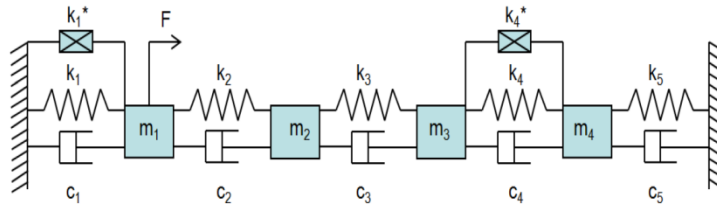


**Fig. 2 Four DOFs discrete system with two nonlinear elements**

The numerical values of the linear system elements are given as follows:

$$\begin{aligned}
 k_1 = k_2 = k_3 = k_4 = k_5 &= 500 \text{ N/m} \\
 c_1 = c_2 = c_3 = c_4 = c_5 &= 5 \text{ Ns/m} \\
 m_1 = 1 \text{ kg}, m_2 = 2 \text{ kg}, m_3 = 3 \text{ kg}, m_4 &= 5 \text{ kg}
 \end{aligned}
 \tag{17}$$

The time response of the system is first calculated with MATLAB by using the ordinary differential equation solver ODE45. The simulation was run for 32 seconds at each frequency to ensure that transients die out. The frequency range used during the simulations is between 0.0625 and 16 Hz with frequency increments of 0.0625 Hz. The linear FRFs are obtained by applying a very low forcing (0.1N) from first coordinate as presented in Fig. 2. The nonlinear FRFs are obtained by applying high forcing (10N) to the system from the first coordinate as shown in Fig. 2. Before using the calculated FRFs as simulated experimental data, they are polluted by using the “rand” function of MATLAB with zero mean, normal distribution and standard deviation of 5% of the maximum amplitude of the FRF value. A sample comparison for the nonlinear and linear FRFs ( $H_{11}$ ) is given in Fig. 3.

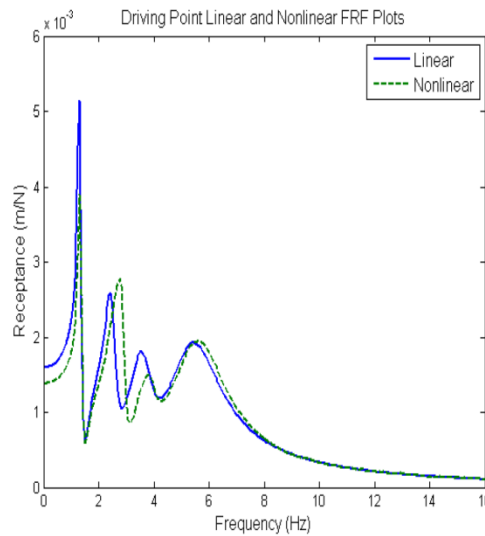


**Fig. 3 Driving point linear and nonlinear FRF plots**

It is assumed in this case study that we have only the first columns of the linear and nonlinear receptance matrices. Then, firstly the missing elements of the linear FRF matrix are calculated by using the approach discussed in section 2.1, and the  $NLI$  values are calculated for each coordinate by using equation (12). The calculated values are shown in Fig. 4a. From Fig. 4a it can easily be concluded that there are nonlinear elements between ground and coordinate 1, and between coordinates 3 and 4. Furthermore, since the nonlinearity can be stiffness and/or damping type, it is possible to make this distinction at this stage by investigating the real and imaginary parts of the describing function. The real and imaginary parts of the describing function can be summed over the frequency range and compared with each other. Fig. 4b reveals that system has stiffness type of nonlinearity since DF has much higher real part compared to imaginary part.

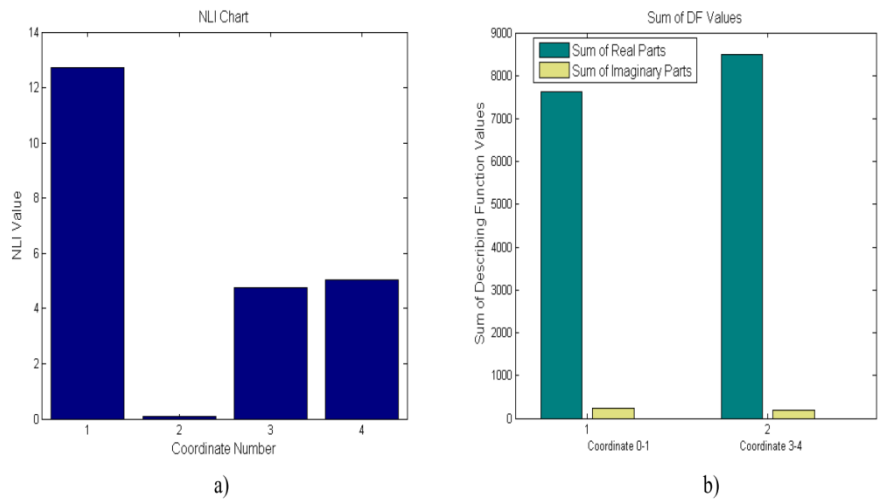


**Fig. 4 a) Nonlinearity index chart, b) Sums of real and imaginary parts of DF values at high forcing excitation**

Using the method proposed, the describing functions representing these nonlinear elements are calculated at different response amplitudes and are plotted in Fig. 5. From the general pattern of the curves it may be possible to identify the types of nonlinearity. Fitting a curve to the calculated values makes the parametric identification easier. Although identification of backlash may not be so easy from DFF, it is quite straightforward to identify the type of cubic stiffness from Fig. 5b.

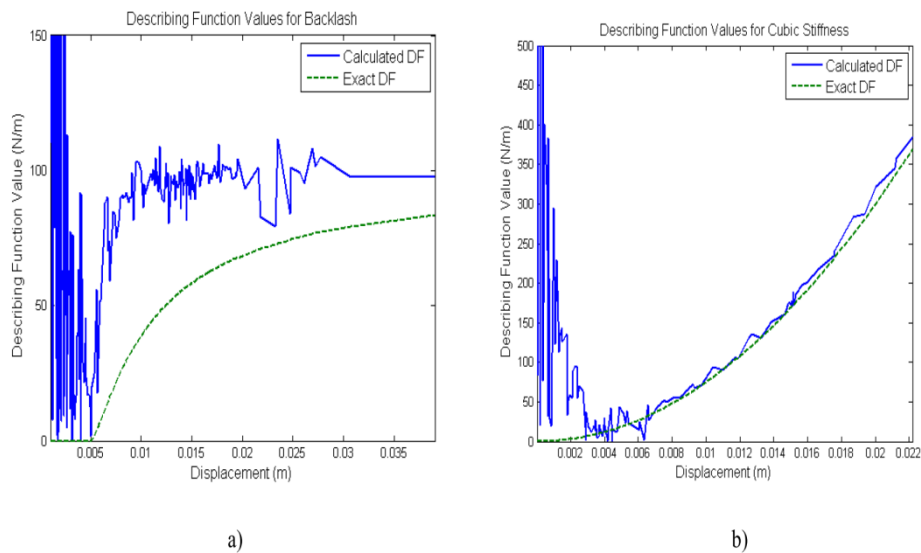


**Fig. 5 Identified and exact DFs. a) For nonlinear element between coordinate 1 and ground, b) For nonlinear element between coordinates 3 and 4**

Alternatively, the types of nonlinear elements can be identified more easily if DF inversion method proposed in this study is used. The inversion of DF is calculated for this case study by using the formulation given in section 2.2, and RF plots obtained are presented in Fig. 6. Fig. 6a gives the RF plot for the nonlinearity between the first coordinate and ground, whereas Fig. 6b shows the RF plot for the nonlinearity between coordinates 3 and 4. By first fitting curves to the calculated RF plots, parametric identification can easily be made. The parametric identification results for the nonlinear elements are tabulated in Table 1. As can be seen from the table, the identified values do not deviate from the actual values more than 12%.

Although the DF inversion formulations are based on polynomial type describing functions, it is shown in this case study that they work, at an acceptable level, for discontinuous describing functions such as backlash as well.

**Table 1 Parametric identification results for the nonlinear elements**

	Actual	Identified	Error %
Backlash (m)	0.0050	0.0044	12
Linear stiffness part of $k_1^*$ (N/m)	100	95	5
$k_2^*$ (cubic stiffness constant) N/m <sup>3</sup>	1000000	956800	4

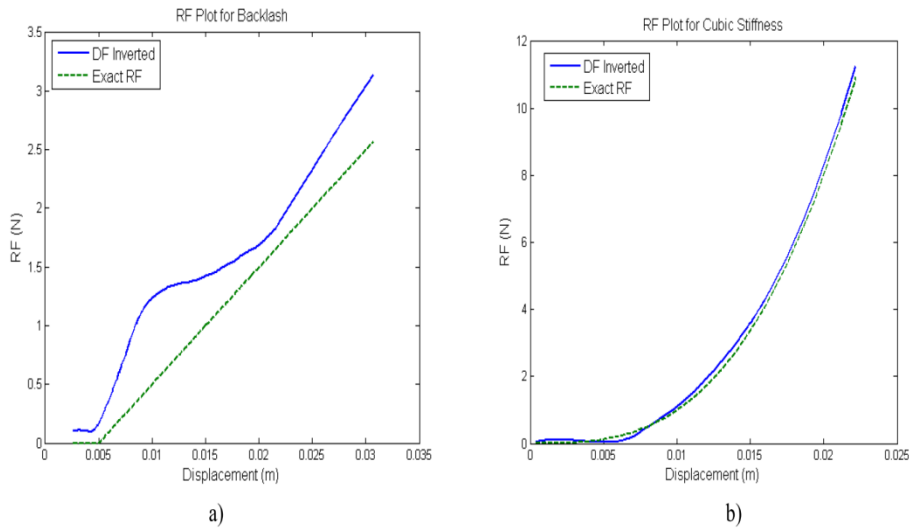


**Fig. 6 Identified and exact RF plots. a) For nonlinear element between coordinate 1 and ground, b) For nonlinear element between coordinates 3 and 4**

#### 4. Experimental Study

The proposed approach is also tested on the experimental setup used in a recent study [22]. The experimental setup and FRF plots obtained with constant amplitude harmonic forces are given in Fig. 7 and Fig. 8, respectively.

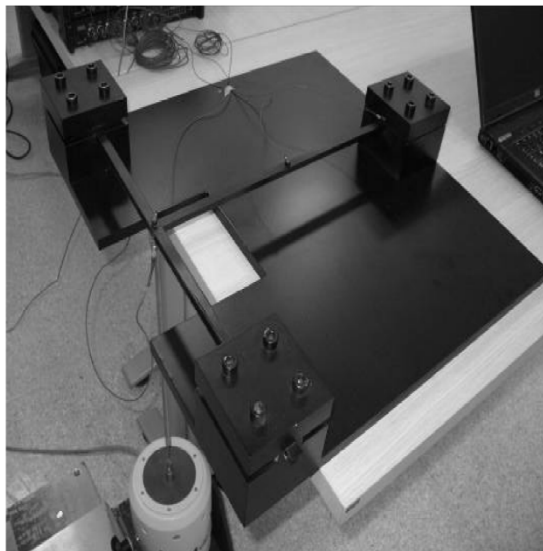


**Fig. 7 Setup used in the experimental study**

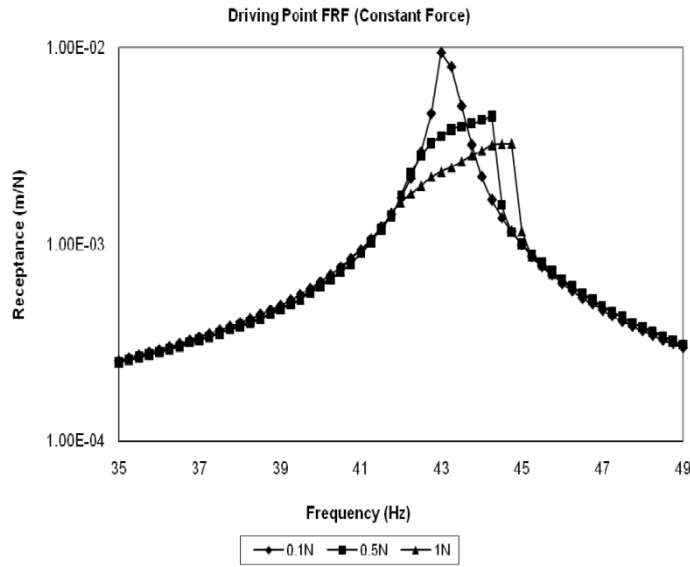


**Fig. 8 Constant force driving point FRF curves**

The test rig consists of a linear cantilever beam with its free end held between two thin identical beams which generate cubic spring effect. The cantilever beam and the thin nonlinear beams were manufactured from St37 steel. The beam can be taken as a single DOF system with a nonlinear cubic stiffness located between the ground and the equivalent mass representing the cantilever beam. This test rig is preferred for its simplicity in modeling the dynamic system since the thin beams yield only hardening stiffness nonlinearity and the structure itself can be modeled as a single degree of freedom system.

For a single degree of freedom system, the nonlinearity matrix reduces to the describing function defining the nonlinearity [4]:

$$v = \frac{H - H^{NL}}{H^{NL}H} \quad (18)$$

The describing function representation of the nonlinearity ( $v$ ) can be graphically shown as a function of response amplitude, which makes it possible to identify the type of nonlinearity and to make parametric identification by using curve fitting.

The nonlinear coefficient for the hardening cubic stiffness is first obtained by a static test. In the static test a load cell is used to measure force and a linear variable differential transformer is used to measure displacement for stepped loadings with 5 N increments. The force is applied at the point where the cantilever beam is attached to thin beams. The deflection is also measured at the same point. The results of this test are presented as a force versus deflection curve in Fig. 9.

Then, by using the DFF and DF inversion approaches for nonlinear identification, both DF and RF plots are obtained for the nonlinear element between the tip point of the cantilever beam and the ground (Fig. 10 and Fig. 11). The cubic stiffness constants identified by using DF and RF curves are  $2.667 \times 10^8 \text{ N/m}^3$  and  $2.656 \times 10^8 \text{ N/m}^3$ , respectively. The cubic stiffness constant obtained from static test, on the other hand is  $2.437 \times 10^8 \text{ N/m}^3$ . For visual comparison, force deflection curves obtained from static test and DF inversion approaches are compared with the force deflection characteristics obtained from DFF approach in Fig. 11. As can be seen, DFF and DF inversion approaches yield very close results.

Thus, it can be concluded that the accuracy in parametric identification of nonlinearity by DF inversion is comparable to that of DFF method. However, the main advantage of DF inversion is that it gives better insight into the type of the nonlinearity. Furthermore, when the RF function is obtained by DF inversion, it may be directly used in nonlinear model of the system when time domain analysis is to be used. Then, it will be possible to identify the restoring force of more than one type of nonlinearity which may co-exist at the same location.

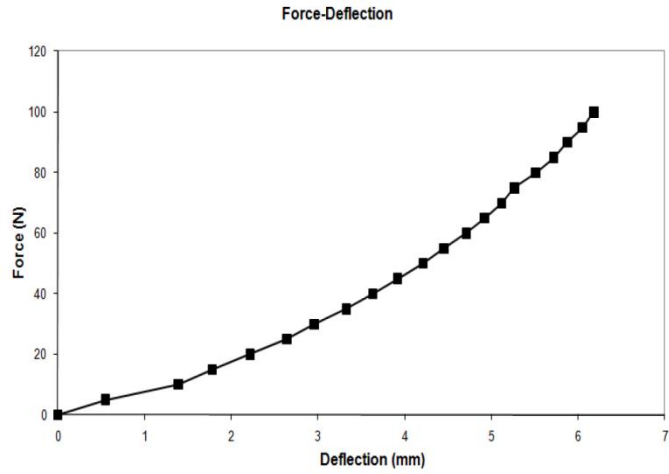


**Fig. 9** Static force-deflection curve for the cubic stiffness.

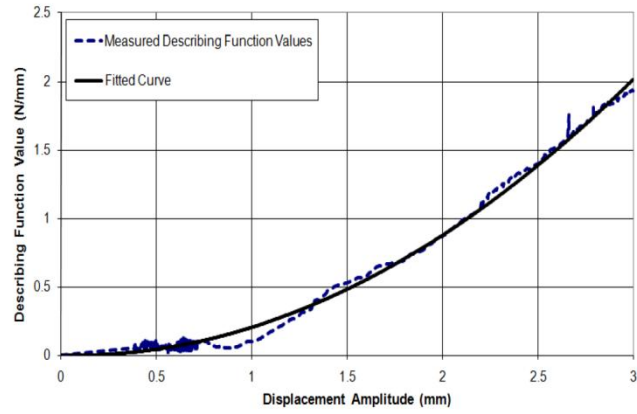


**Fig. 10** Measured describing function values and the curve fitted

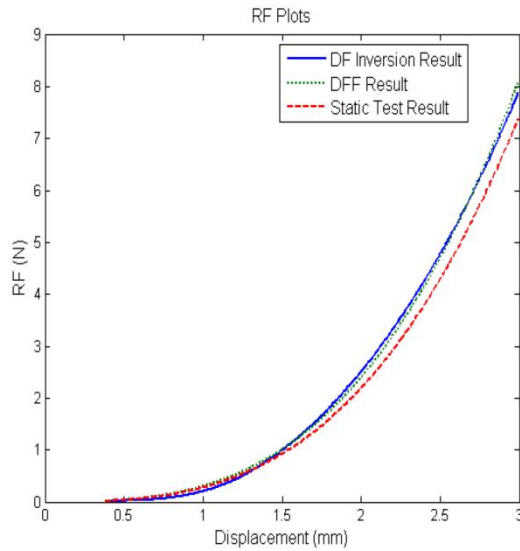


**Fig. 11** RF plots of nonlinearity for experimental study

## 5. Conclusions

It was recently shown [22] with an experimental case study that the method developed by Özer *et al.* [12] for detecting, localizing and parametrically identifying nonlinearity in MDOF systems is a promising method that can be used in industrial applications. In the study presented here some improvements are suggested to eliminate some of the practical limitations of the previously developed method. The verification of the approach proposed is demonstrated with two case studies. The main improvements are using incomplete FRF data which makes the method applicable to large systems, and employing describing function inversion which makes the identification of nonlinearity easier.

The method requires dynamic stiffness matrix of the linear part of the system which can be obtained by constructing a numerical model for the system and updating it using experimental measurements. In this study, however, it is proposed to make linear modal identification by using one column of the receptance matrix of the system experimentally measured at low forcing level, and then to calculate the missing elements of the complete FRF matrix so that the dynamic stiffness matrix required for the identification can be obtained. Note that low forcing testing will not give the linear receptances if nonlinearity is due to dry friction, since its effect will be dominant at low level vibrations. For this type of nonlinearity high forcing testing will yield the linear receptance values. The approach suggested is first applied to a lumped parameter system and it is shown that detection, localization and identification of nonlinear elements can successfully be achieved by using only one column of the linear FRF matrix.

Secondly, it is proposed in this study to use RF plots obtained from DF inversion for parametric identification, instead of DFF plots, in order to avoid the limitations in using footprint graphs. It is found easier to determine the type of nonlinearity by using RF plots, rather than DFF plots, especially for discontinuous nonlinear functions such as backlash.

The application of the approach proposed is also demonstrated on a real structural test system, and it is concluded that the accuracy in parametric determination of nonlinearity by DF inversion is comparable to that of DFF method, and since RF plots give better insight into the type of nonlinearity this approach may be preferred in several applications to identify the type of nonlinearity. Furthermore, when the RF function is obtained, it may be directly used in nonlinear model of the system if time domain analysis is to be made. Using describing function inversion rather than footprint graphs makes it possible to identify total restoring force of more than one type of nonlinearity that may co-exist at the same location. Thus, DF inversion yields an equivalent RF function that can be used in further calculations without any need to identify each nonlinearity separately. Consequently, it can be said that the approach proposed in this study is very promising to be used in practical systems, especially when there are multiple nonlinear elements at the same location.

## 6. References

- [1] Kerschen G., Worden K., Vakakis A.F., Golinval J.C., "Past, present and future of nonlinear system identification in structural dynamics", *Mechanical Systems and Signal Processing*, Volume 20, pp 505-592, 2006
- [2] Maia N. M. M., Silva J. M. M., "Theoretical and Experimental Modal Analysis", Research Studies Press LTD., 1997
- [3] Ewins D. J., "Modal Testing: Theory and Practice", Research Studies Press LTD., 1995
- [4] Özer M. B., Özgüven H. N., "A New Method for Localization and Identification of Nonlinearities in Structures", *Proceedings of ESDA2002: 6th Biennial Conference on Engineering Systems Design and Analysis, İstanbul-Turkey, 2002*
- [5] Göge D., Sinapius M., Füllekrug U., Link M., "Detection and Description of Non-Linear Phenomena In Experimental Modal Analysis Via Linearity Plots", *International Journal of Non-linear Mechanics*, Volume 40, pp 27-48, 2005
- [6] Worden K., Tomlinson G. R., "Nonlinearity in Structural Dynamics", Institute of Physics Publishing, 2001
- [7] Siller H. R. E., *Non-linear Modal Analysis Methods for Engineering Structures*, PhD Thesis in Mechanical Engineering, Imperial College London/University of London, 2004
- [8] Narayanan S., Sekar P., "A Frequency Domain Based Numeric-Analytical Method For Non-Linear Dynamical Systems", *Journal of Sound and Vibration*, Volume 211, pp 409-424, 1998
- [9] Muravyov A. A., Rizzi S. A., "Determination of Nonlinear Stiffness With Application to Random Vibration of Geometrically Nonlinear Structures", *Computers and Structures*, Volume 81, pp 1513-1523, 2003

- [10] Masri S. F., Caughey T. K., "A nonparametric identification Technique for Nonlinear Dynamic Problems, Transaction of ASME Journal of Applied Mechanics, Volume 46, pp 433-445, 1979
- [11] Elizalde H., İmregun M., "An Explicit Frequency Response Function Formulation for Multi-Degree-Of-Freedom Non-Linear Systems", Mechanical Systems and Signal Processing, Volume 20, pp 1867-1882, 2006
- [12] Özer M. B., Özgüven H. N., Royston T. J., "Identification of Structural Non-Linearities Using Describing Functions and The Sherman–Morrison Method", Mechanical Systems and Signal Processing, Volume 23, pp 30-44, 2009
- [13] Thothadri M., Casas R. A., Moon F. C., D'andrea R., Johnson Jr. C. R., "Nonlinear System Identification of Multi-Degree-of-Freedom Systems", Nonlinear Dynamics, Volume 32, pp 307-322, 2003
- [14] Cermelj P., Boltezar M., "Modeling localized nonlinearities using the harmonic nonlinear super model", Journal of Sound and Vibration, Volume 298, pp 1099-1112, 2006
- [15] Nuij P. W. J. M., Bosgra O. H., Steinbuch M., "Higher-Order Sinusoidal Input Describing Functions for the Analysis of Non-Linear Systems With Harmonic Responses", Mechanical Systems and Signal Processing, Volume 20, pp 1883-1904, 2006
- [16] Adams D. E., Allemang R. J., "A New Derivation of the Frequency Response Function Matrix for Vibrating Non-Linear Systems", Journal of Sound and Vibration, Volume 227, pp 1083-1108, 1999
- [17] Tanrıku Ö, Kuran B., Özgüven H. N., İmregun M., "Forced Harmonic Response Analysis of Non-linear Structures", AIAA Journal, Volume 31, pp 1313 - 1320, 1993
- [18] Duarte M.L.M., Experimentally-Derived Structural Models for Use in Further Dynamic Analysis, PhD Thesis in Mechanical Engineering, Imperial College London, 1996
- [19] Maia N. M. M., Silva J. M. M., "Theoretical and Experimental Modal Analysis", Research Studies Press LTD., 1997
- [20] Gibson J. E., Nonlinear Automatic Control, McGraw-Hill Book Company, Inc., 1963
- [21] A. Gelb, W. E. Vander Velde, Multiple-Input Describing Functions and Nonlinear System Design, McGraw Hill, 1968
- [22] Arslan Ö., Aykan M., Özgüven H. N., "Parametric Identification of Structural Nonlinearities from Measured Frequency Response Data", Mechanical Systems and Signal Processing, Volume 25, pp 1112-1125, 2011

# Identification of Restoring Force Surfaces in Nonlinear MDOF Systems from FRF Data Using Nonlinearity Matrix\*

Murat Aykan<sup>1,2</sup>, H. Nevzat Özgüven<sup>1</sup>

<sup>1</sup> Department of Mechanical Engineering, Middle East Technical University, Ankara 06800, TURKEY

<sup>2</sup> Defense Systems Technologies Division, ASELSAN Inc., Ankara, 06172, TURKEY

## ABSTRACT

The sensitivity of the response characteristics of a nonlinear structure to load level may prevent us to predict the linear behavior of a nonlinear system. The nonlinear identification method recently proposed by the authors is based on the measured linear and nonlinear Frequency Response Functions (FRFs). The method is easy to implement and requires standard testing methods. The data required is limited with measured linear and nonlinear FRFs. In order to obtain the linear FRFs in a nonlinear system, it is the general practice to use low level forcing, unless the nonlinearity is due to dry friction. However, depending on the level of nonlinearity it may not be possible to lower the harmonic forcing amplitude beyond a practical limit, and this may not be sufficient to obtain linear FRFs. The approach presented in this study aims to perform the nonlinear identification directly from a series of measured nonlinear FRFs. It is shown that Restoring Force Surfaces (RFS) can be identified more accurately by employing this approach. The verification of the method is demonstrated with simulated and experimental case studies.

## KEYWORDS

Nonlinear structural dynamics, nonlinear identification, parametric nonlinear identification, nonlinear structures, nonlinear vibration testing

## 1. INTRODUCTION

Traditionally, for system identification in structural dynamics, we tend to apply linear identification theories, which are well established [1,2]. However, with the increasing need to understand nonlinear characteristics of complicated structures, there were several studies published on nonlinear system identification. For instance, see [3-15]. Nonlinearities can be localized at joints or boundaries or else the structure itself can be nonlinear. There are various types of nonlinearities, such as hardening stiffness, clearance, coulomb friction etc. [4].

Nonlinear system identification methods can be divided into two groups as time and frequency domain methods [11], and time domain methods can be further divided as discrete and continuous time methods [5]. Most of the methods available require some foreknown data for the system. Some methods require all or part of mass, stiffness and damping values [7-9] whereas some methods [10-14] require linear frequency response function (FRF) of the analyzed structure. In these methods nonlinearity type is usually foreknown or determined by inspecting the describing function footprints (DFP) visually. However, although the user interpretation may be possible for a single type of nonlinearity, it may not be so easy when there is more than one type of nonlinearity present in the system [4].

The Restoring Force Surface (RFS) method, proposed by Masri *et al.* [9], constitutes one of the first attempts to identify nonlinear structures. A variant of this method was later independently developed by Crawley *et al.* [16,17] and was named as force-state mapping method. Masri *et al.* [18] extended the RFS method to MDOF systems in 1982.

The RFS method requires the time histories of the displacement and its derivatives, and the applied force to be measured or calculated. Furthermore, the mass and damping matrices can be needed. In theory, the RFS method is applicable to MDOF

---

\* presented in IMAC XXXI Conference, Orange County, California 11-14 February 2013 and will be published in Conference Proceedings of the Society for Experimental Mechanics Series

systems. However, a number of practical considerations diminish this capability, and its scope is practically bound to systems with a few degrees of freedom only [19].

The RFS method has been studied experimentally for several systems with few degrees of freedom. Kerschen *et al.* [20] demonstrated experimental identification of impacting cantilever beams with symmetrical or asymmetrical piecewise linear stiffness using the RFS method. Another experimental application of the RFS method studied by Kerschen *et al.* [21] was the VTT benchmark, which consists of wire rope isolators mounted between a load mass and a base mass. The RFS method was also used in vehicle suspension system characterization [22]. Recently, Noel *et al.* [19] demonstrated the application of the RFS method for an elastomeric connection on a real life spacecraft structure.

There are studies in the literature obtaining the nonlinear RFS [23-24] using variants of RFS method or other similar approaches like neural networks and optimization [5,25]. Application of optimization methods in nonlinear system identification is rather a new and promising approach. The major disadvantage of these methods is generally the computational time required.

Nonlinearity identification method presented in this study is an improved version of the method developed earlier by Özer *et al.* [11]. The improvement includes performing the nonlinear identification directly from a series of measured nonlinear FRFs without the need to measure the linear FRFs. Furthermore, it is shown that Restoring Force Surfaces (RFS) can be identified more accurately by employing this approach.

## 2. THEORY

Representation of nonlinear forces in matrix multiplication form using describing functions has been first given by Tanrikulu *et al.* [26], and employed in identification of structural nonlinearities by Özer *et al.* [11]. The method presented here is based on the basic theory of the identification method which is given in detail in reference [11]. Here, only the related equations are given with a brief summary.

The nonlinear internal forces in the system can be expressed in matrix form using describing functions. This approach makes it possible to represent the nonlinear stiffness and damping properties of the system in compact form as a response dependent matrix which can easily be included into the dynamic stiffness matrix of the linear system in the frequency domain. From the mathematical expressions of the FRF matrix of the nonlinear system ( $[H^{NL}]$ ) and FRF matrix of the linear part of the system ( $[H]$ ) (see reference [11] for details) the response dependent “nonlinearity matrix”  $[\Delta(x, \dot{x})]$  can be obtained as

$$[\Delta] = [H^{NL}]^{-1} - [H]^{-1} \quad (1)$$

where the elements of the nonlinearity matrix are expressed in terms of describing functions  $v$  [26].

In general applications, the linear model of the system can be obtained by using FEM, and experiments are made only on the nonlinear system. Alternatively, the FRFs of the underlying linear system can be obtained from FRF measurements in the system at very low forcing levels, where the nonlinear internal forces will be negligible. However, when there is only friction type of nonlinearity, FRFs measured at low amplitude of vibration will not represent FRFs of the underlying linear system; on the contrary, the FRFs measured at high response levels will represent FRFs of the linear counterpart. Comparison of FRFs measured at different response levels will reveal whether or not there is only friction type of nonlinearity so that the FRF measured at high response level can be taken as the FRF for the underlying linear system. Yet, if the system has multiple nonlinearities including friction type of nonlinearity, it may be difficult to measure the FRF of the underlying linear system experimentally, and using finite element model of the system seems to be the only alternative to obtain linear FRF of the linear counterpart.

In an attempt to obtain the nonlinearity matrix directly from nonlinear FRFs, the following methodology is proposed;

The nonlinearity matrix at forcing level  $F_1$  can be defined as

$$[\Delta_1] = [H_1^{NL}]^{-1} - [H]^{-1} \quad (2)$$

Changing the forcing to another level  $F_2$ , equation (2) becomes

$$[\Delta_2] = [H_2^{NL}]^{-1} - [H]^{-1} \quad (3)$$

Subtracting equation (2) from equation (3) yields

$$[\Delta_2] - [\Delta_1] = [H_2^{NL}]^{-1} - [H_1^{NL}]^{-1} \quad (4)$$

For a SDOF system, equation (4) reduces to

$$\Delta_2 - \Delta_1 = \frac{1}{H_2^{NL}} - \frac{1}{H_1^{NL}} \quad (5)$$

where the nonlinearity matrix reduces to the describing function  $v$ .

The describing function will be a function of the displacement amplitude only, when there is displacement dependent nonlinearity in the system. As the values  $\Delta_1$  and  $\Delta_2$  are obtained from the same describing function, evaluated at two different displacement amplitude levels; if a polynomial form (as shown below) is assumed for the describing function and nonlinear FRFs at two load levels ( $H_1^{NL}$  and  $H_2^{NL}$ ) are measured experimentally, the coefficients of the function that describes the nonlinearity can be calculated:

$$\Delta(X) = \sum_{i=1}^{\infty} c_i X^i \quad (6)$$

where  $X$  represents the amplitude of the harmonic response.

For a MDOF system the difference matrix ( $[\Delta_2] - [\Delta_1]$ ) is obtained from equation (4). Then, a polynomial is fitted to each element of the difference matrix separately and the coefficients of the functions that describe the nonlinearities at different coordinates can be calculated. The only difference between one nonlinear location and multiple nonlinear locations will be the number of curve fitting operations required.

## 2.1. Application of the Method

The first step is to test the nonlinear structure at two excitation levels. Equation (4) requires having the inverses of the measured nonlinear FRFs, and therefore is sensitive to noise. In order to minimize this effect, the excitation levels can be chosen high enough or averaging can be performed. However, if the forcing levels are high then friction type nonlinearities will not depict themselves in the measured values. In order to identify friction type nonlinear elements a low forcing test can also be performed. Equation (4) will give a complex result, whose real part represents the stiffness nonlinearity and the imaginary part represents the damping nonlinearity.

In order to solve equation (4) we need as many equations as the order of the polynomial that has been assumed. These equations can be generated from the nonlinear FRF values, which have distinct displacement values for each frequency. In other words, if we assume a polynomial, for instance up to the third order for the nonlinearity, we will need three equations. The following equations show the calculation procedure:

$$(c_1 X_2 + c_2 X_2^2 + c_3 X_2^3) - (c_1 X_1 + c_2 X_1^2 + c_3 X_1^3) = \frac{1}{H_2^{NL}} - \frac{1}{H_1^{NL}} \quad (7)$$

$$\begin{bmatrix} X_2 - X_1 & X_2^2 - X_1^2 & X_2^3 - X_1^3 \end{bmatrix} \begin{bmatrix} c_1 \\ c_2 \\ c_3 \end{bmatrix} = \frac{1}{H_2^{NL}} - \frac{1}{H_1^{NL}} \quad (8)$$

$$\begin{bmatrix} x_2(\omega_1) - x_1(\omega_1) & X_2^2(\omega_1) - X_1^2(\omega_1) & X_2^3(\omega_1) - X_1^3(\omega_1) \\ x_2(\omega_2) - x_1(\omega_2) & X_2^2(\omega_2) - X_1^2(\omega_2) & X_2^3(\omega_2) - X_1^3(\omega_2) \\ x_2(\omega_3) - x_1(\omega_3) & X_2^2(\omega_3) - X_1^2(\omega_3) & X_2^3(\omega_3) - X_1^3(\omega_3) \end{bmatrix} \begin{bmatrix} c_1 \\ c_2 \\ c_3 \end{bmatrix} = \begin{bmatrix} \frac{1}{H_2^{NL}(\omega_1)} - \frac{1}{H_1^{NL}(\omega_1)} \\ \frac{1}{H_2^{NL}(\omega_2)} - \frac{1}{H_1^{NL}(\omega_2)} \\ \frac{1}{H_2^{NL}(\omega_3)} - \frac{1}{H_1^{NL}(\omega_3)} \end{bmatrix} \quad (9)$$

where  $\omega$  represents the response frequency.

The FRF values at each frequency give us one equation. In general we will have more frequency values than the number of equations that is required to solve the equation for unknown coefficients. Thus, if we use “n” frequencies, equation (9) can be expanded as

$$\begin{bmatrix} x_2(\omega_1) - x_1(\omega_1) & X_2^2(\omega_1) - X_1^2(\omega_1) & X_2^3(\omega_1) - X_1^3(\omega_1) \\ x_2(\omega_2) - x_1(\omega_2) & X_2^2(\omega_2) - X_1^2(\omega_2) & X_2^3(\omega_2) - X_1^3(\omega_2) \\ x_2(\omega_3) - x_1(\omega_3) & X_2^2(\omega_3) - X_1^2(\omega_3) & X_2^3(\omega_3) - X_1^3(\omega_3) \\ \vdots & \vdots & \vdots \\ x_2(\omega_n) - x_1(\omega_n) & X_2^2(\omega_n) - X_1^2(\omega_n) & X_2^3(\omega_n) - X_1^3(\omega_n) \end{bmatrix} \begin{bmatrix} c_1 \\ c_2 \\ c_3 \end{bmatrix} = \begin{bmatrix} \frac{1}{H_2^{NL}(\omega_1)} - \frac{1}{H_1^{NL}(\omega_1)} \\ \frac{1}{H_2^{NL}(\omega_2)} - \frac{1}{H_1^{NL}(\omega_2)} \\ \frac{1}{H_2^{NL}(\omega_3)} - \frac{1}{H_1^{NL}(\omega_3)} \\ \vdots \\ \frac{1}{H_2^{NL}(\omega_n)} - \frac{1}{H_1^{NL}(\omega_n)} \end{bmatrix} \quad (10)$$

Equation (10) can be solved by pseudo inversion which will give us a least square fit solution for the polynomial coefficients. After successful identification of high forcing effective nonlinearities, the linear FRFs can be evaluated from equation (2). Thus, using equation (2) again with nonlinear FRFs obtained from low forcing level, and calculated linear FRFs, we can obtain the describing function values for low forcing nonlinearities such as friction.

The describing function inversion approach introduced recently [31] can now easily be integrated to the method proposed here. The verification and effective application of the method are shown with the case studies and experimental studies given next.

### 3. CASE STUDIES

#### 3.1. Case Study 1

The nonlinear identification approach proposed in this study is applied to a SDOF discrete system with a nonlinear elastic element represented by  $k_1^*$  (a linear stiffness of 1000 N/m with a backlash of 0.005 m) and a coulomb friction element  $c_1^*$  (= 0.001  $\text{sgn}(\dot{x})$  N), as shown in Fig. 1.

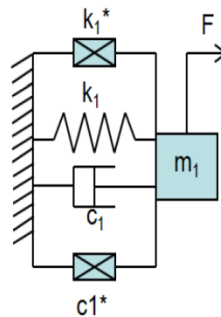


Fig. 1 SDOF discrete system with two nonlinear elements

The numerical values of the linear system elements are given as follows:

$$\begin{aligned} k_1 &= 500 \text{ N / m} \\ c_1 &= 5 \text{ Ns / m} \\ m_1 &= 1 \text{ kg} \end{aligned} \tag{11}$$

The time response of the system is first calculated with MATLAB by using the ordinary differential equation solver ODE45. The simulation was run for 32 seconds at each frequency to ensure that transients die out. The frequency range used during the simulations is between 0.0625 and 16 Hz with frequency increments of 0.0625 Hz. Three forcing levels (0.01N, 3N, 20N) are used, in turn, in the simulations. The FRF functions obtained are presented in Fig. 1. Before using the calculated FRFs as simulated experimental data, they are polluted by using the “rand” function of MATLAB with zero mean, normal distribution and standard deviation of 5% of the maximum amplitude of the FRF value. A sample comparison for the nonlinear FRFs ( $H_{11}$ ) is given in Fig. 2 for three different forcing levels.

Using the method proposed, the describing functions representing these nonlinear elements are calculated from simulated experimental results and are plotted in Fig. 3.

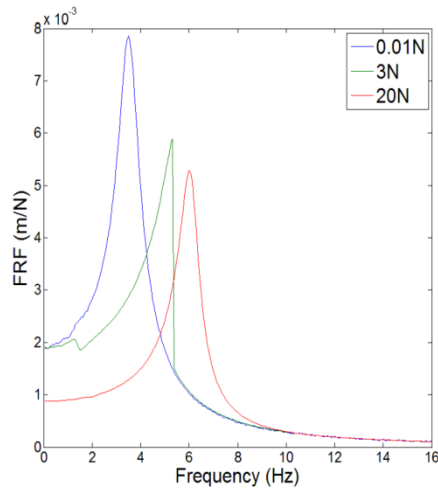


Fig. 2 Nonlinear FRF plots for different forcing levels

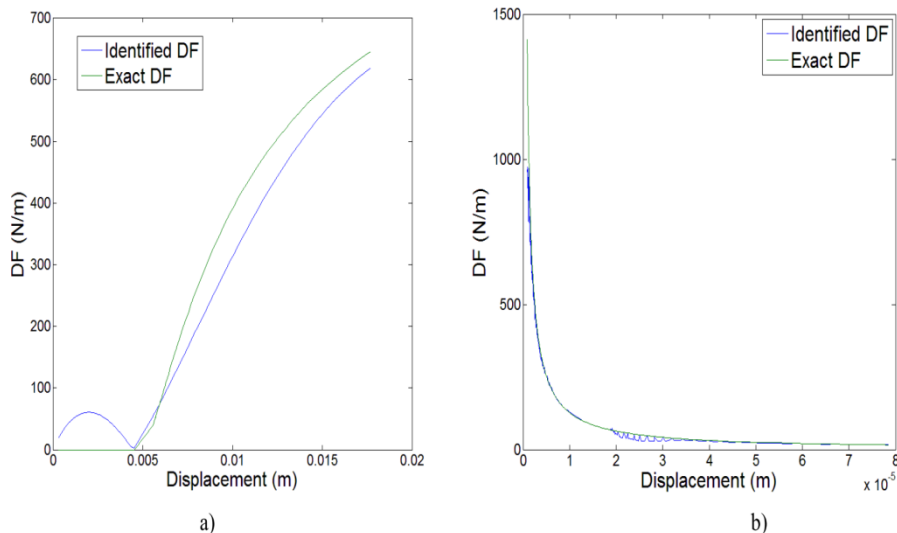
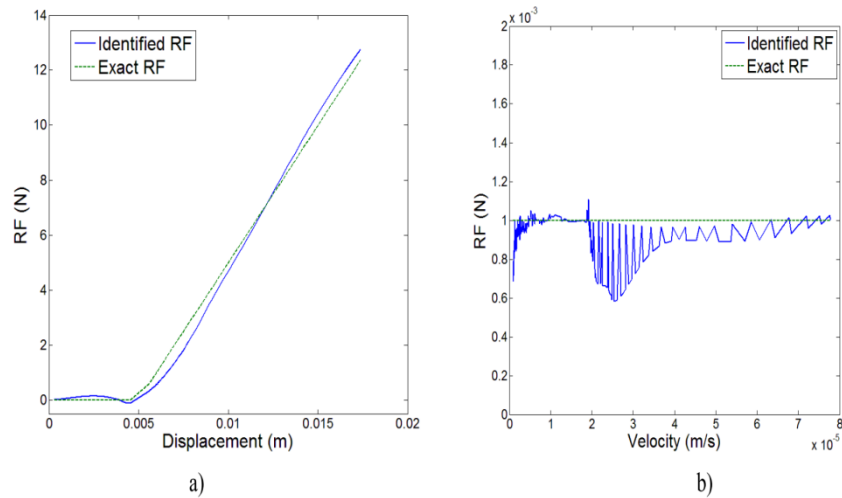


Fig. 3 Identified and exact DFs, a) stiffness type (backlash) nonlinear element, b) damping type (friction) nonlinear element

Alternatively, the types of nonlinear elements can be identified more easily if DF inversion method proposed in the previous study [31] is used. The calculated RF plots are presented in Fig. 4. By first fitting curves to the calculated RF plots, parametric identification can easily be made.



**Fig. 4 Identified and exact RF plots, a) stiffness type (backlash) nonlinear element, b) damping type (friction) nonlinear element**

Although the DF inversion formulations are based on polynomial type describing functions, it is shown in this case study that they work, with an acceptable accuracy, for even discontinuous nonlinearities such as backlash, as well as for multiple nonlinearities.

### 3.2. Case Study 2

The proposed method is again applied to the same SDOF discrete system with a nonlinear elastic element represented by  $k_1^*$  (a nonlinear hardening cubic spring =  $10^6 x^2$  N/m) and a coulomb friction element  $c_1^*$  ( $= 0.001 \text{ sgn}(\dot{x})$  N), as shown in Fig. 1. The nonlinear FRFs ( $H_{11}$ ) are given in Fig. 5 for three different forcing levels.

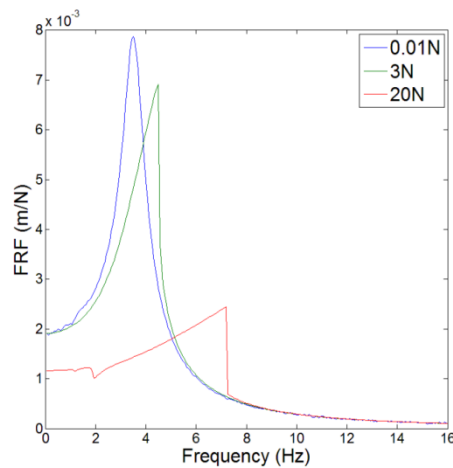


**Fig. 5 Nonlinear FRF plots for different forcing levels**

Following the same procedure we obtain the describing functions representing these nonlinear elements as given in Fig. 6.

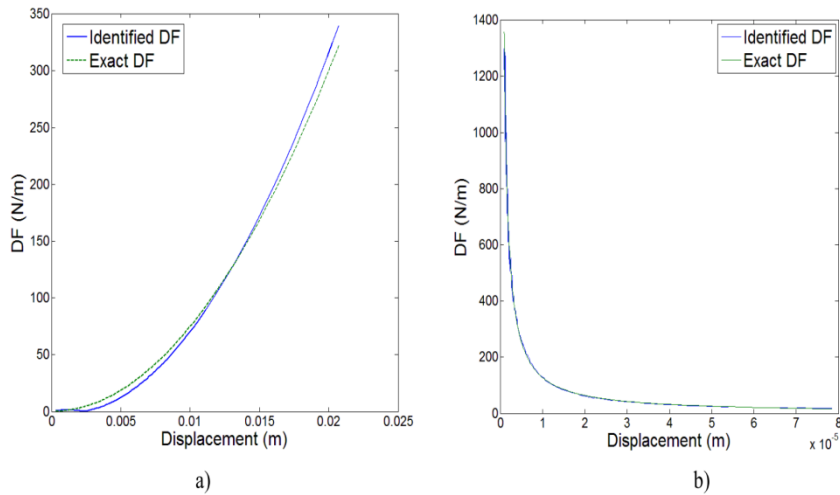


**Fig. 6 Identified and exact DFs, a) stiffness type (cubic stiffness) nonlinear element, b) damping type (friction) nonlinear element**

Similarly, the types of nonlinear elements can be identified more easily if DF inversion method is used. These plots are given in Fig. 7.

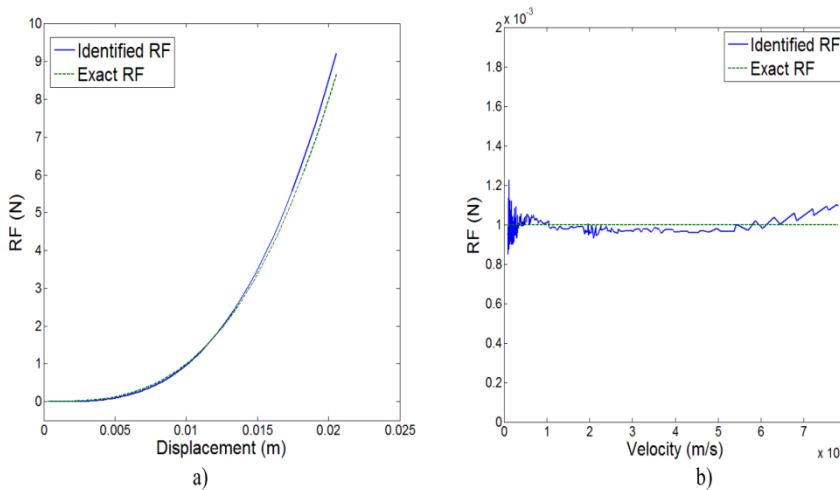


**Fig. 7 Identified and exact RF plots, a) stiffness type (cubic stiffness) nonlinear element, b) damping type (friction) nonlinear element**

### 3.3. Case Study-3

The nonlinear identification approach proposed in this study is applied to a 4 DOF discrete system with a nonlinear elastic element represented by  $k_4^*$  (a linear stiffness of 100 N/m with a backlash of 0.005 m) and a nonlinear hardening cubic spring  $k_4^{**}$  ( $= 10^6 x^2$  N/m) between coordinates 3 and 4, as shown in Fig. 8.

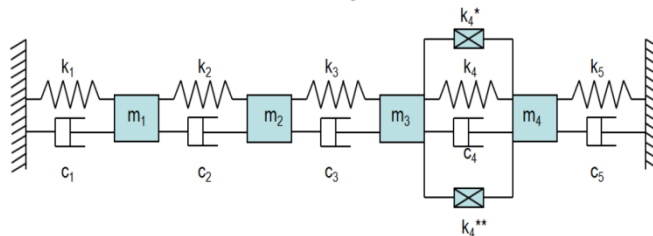


**Fig. 8 Four DOFs discrete system with two nonlinear elements**

The numerical values of the linear system elements are given as follows:

$$\begin{aligned}
 k_1 = k_2 = k_3 = k_4 = k_5 &= 500 \text{ N/m} \\
 c_1 = c_2 = c_3 = c_4 = c_5 &= 5 \text{ Ns/m} \\
 m_1 = 0.5 \text{ kg}, m_2 = 1 \text{ kg}, m_3 = 1.5 \text{ kg}, m_4 &= 3 \text{ kg}
 \end{aligned}
 \tag{12}$$

A sample comparison for the nonlinear and linear FRFs ( $H_{11}$ ) is given in Fig. 9.

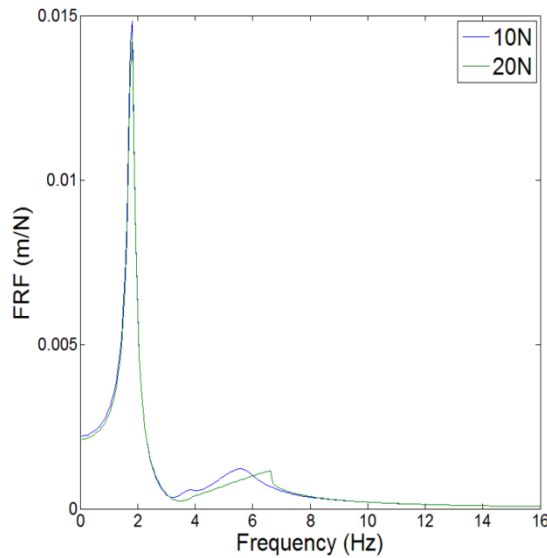


Fig. 9 Nonlinear FRF plots for different forcing levels

In this case study, the forcing is first applied from 3<sup>rd</sup> coordinate with two forcing levels, and then from 4<sup>th</sup> coordinate. Employing the method suggested and by using FRFs of the 3<sup>rd</sup> and 4<sup>th</sup> coordinates only, the describing functions representing these nonlinear elements are obtained as given in Fig. 10. As it is the case in the previous example, the total restoring force of nonlinear elements can be identified more easily when DF inversion method is used.

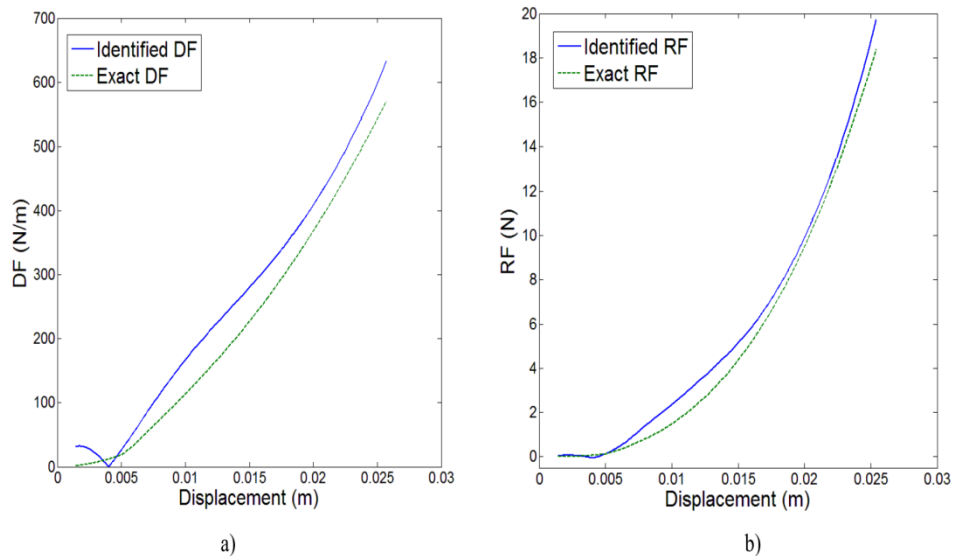
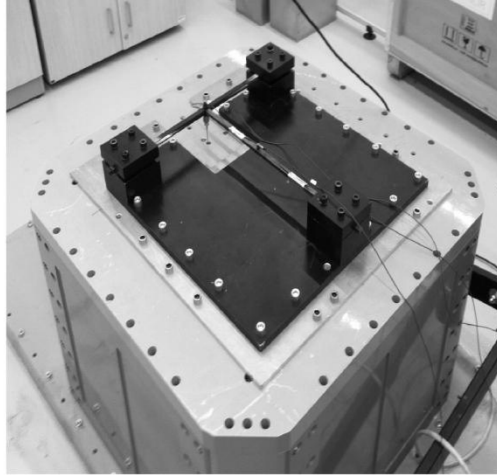


Fig. 10 Identified and exact, a) DFs, b) RFs

#### 4. EXPERIMENTAL STUDY

The proposed approach is also tested on the experimental setup used in a recent study [30]. The tests carried out in previous study [30] were repeated with better frequency resolution (0.1 Hz) and force control. The experimental setup and FRF plots obtained with constant amplitude harmonic forces are given in Fig. 11 and Fig. 12, respectively.



**Fig. 11 Setup used in the experimental study**

The test rig consists of a linear cantilever beam with its free end held between two thin identical beams which generate cubic spring effect. The cantilever beam and the thin nonlinear beams were manufactured from St37 steel. The beam can be taken as a single DOF system with a nonlinear cubic stiffness located between the ground and the equivalent mass representing the cantilever beam. This test rig is preferred for its simplicity in modeling the dynamic system since the thin beams yield only hardening stiffness nonlinearity and the structure itself can be modeled as a single degree of freedom system.

For a single degree of freedom system, the nonlinearity matrix reduces to the describing function defining the nonlinearity [11]:

$$v = \frac{H - H^{NL}}{H^{NL}H} \quad (13)$$

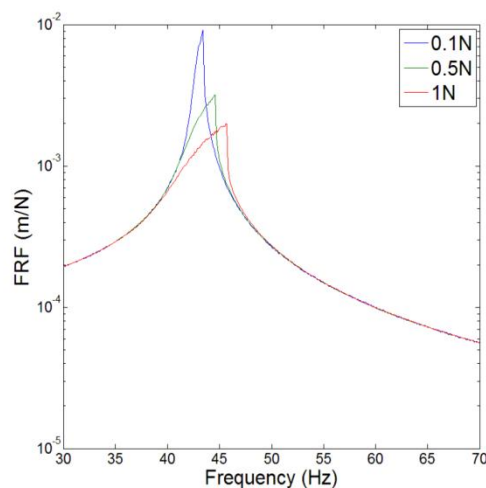


**Fig. 12 Constant force driving point FRF curves for different forcing levels**

As discussed in section 2, the method requires the linear FRFs. Thus, we may assume that the lowest force level that we can achieve gives the linear FRF. However, the method proposed in this study shows that the linear FRF may not always be obtained accurately by low forcing even though there is no friction type of nonlinearity (Fig. 13).

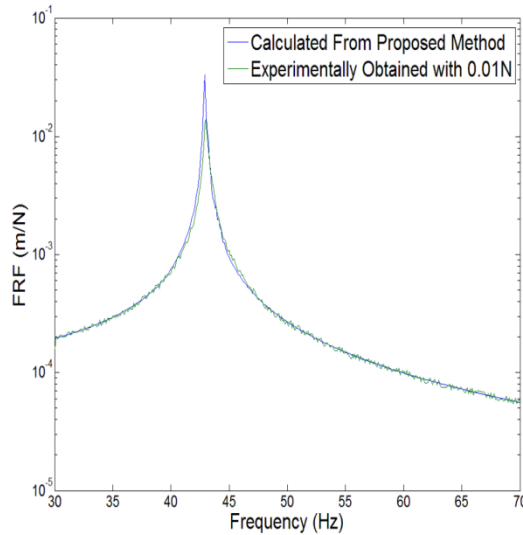


Fig. 13 Linear FRF curves

If we cannot apply sufficiently low forcing level or if there is friction type of nonlinearity in the system then the approach proposed becomes more valuable. The describing function representation of the nonlinearity ( $v$ ) can be graphically shown as a function of response amplitude, which makes it possible to identify the type of nonlinearity and to make parametric identification by using curve fitting (Fig. 14a). The restoring force plot is also given in Fig. 14b. From Fig. 14b the nonlinearity coefficient is found by curve fitting as  $6.18 \cdot 10^8 \text{ N/m}^2$ .

The nonlinear FRFs are calculated [11] using the identified nonlinearity coefficient at forcing levels of 0.5 N and 1 N and are compared with experimentally measured values in Fig. 15. As can be seen from the figure, better agreements are obtained between experimental and predicted responses with the new method.

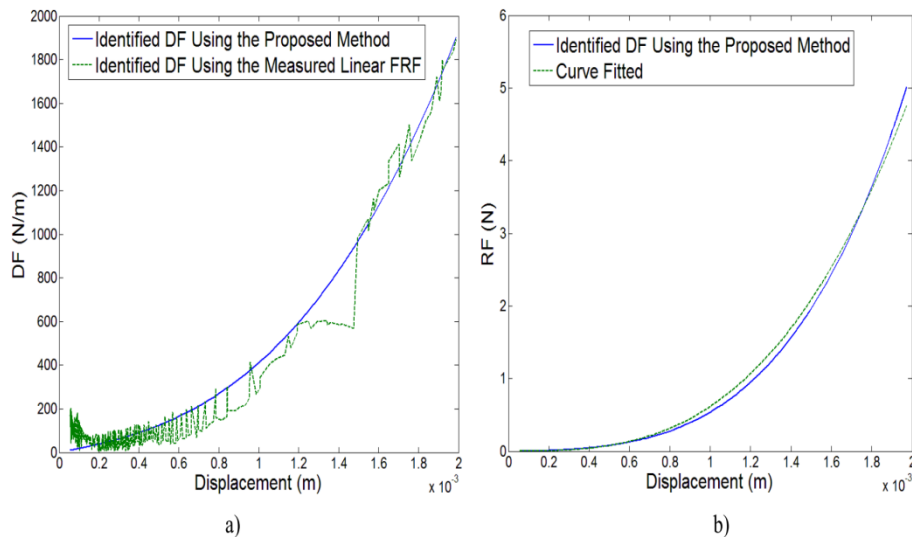


Fig. 14 a) DF curve and fitted curve, b) RF curve and fitted curve

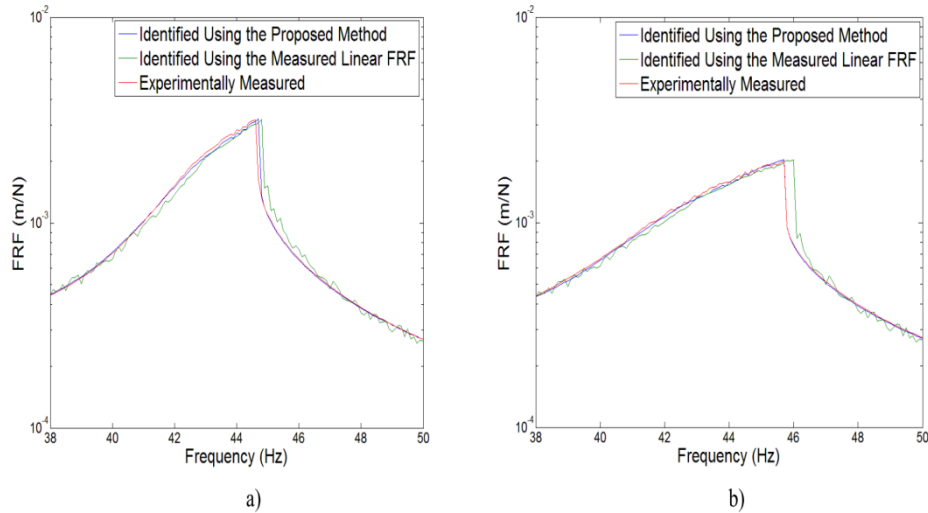


Fig. 15 Identified and measured nonlinear FRF curves at forcing level of a) 0.5N, b) 1N

#### 4. CONCLUSIONS

It was recently shown [30] with an experimental case study that the method developed by Özer *et al.* [11] for detecting, localizing and parametrically identifying nonlinearity in MDOF systems is a promising method that can be used in industrial applications. In the study presented here some improvements are suggested to eliminate some of the practical limitations of the previously developed method. The verification of the approach proposed is demonstrated with three case studies. The main improvement is obtaining the nonlinearity matrix directly from nonlinear FRFs eliminating the need for obtaining linear FRFs.

The original method requires dynamic stiffness matrix of the linear part of the system which can be obtained by constructing a numerical model for the system and updating it using experimental measurements. Alternatively, low forcing measurements can be used to obtain the linear FRFs. However, low forcing testing may not always give the linear FRFs accurately when nonlinearity is high, and furthermore, if nonlinearity is due to dry friction, low forcing level testing will not give linear FRFs at all, since its effect will be dominant at low level vibrations. For this type of nonlinearity, on the contrary, high forcing testing will yield the linear FRFs. To overcome such problems, in the approach developed in this study it is proposed to test the structure at two forcing levels and calculate the nonlinearity matrix directly from these measurements.

The approach suggested is first applied to lumped parameter systems and it is shown that identification of nonlinear elements can successfully be achieved even when there is more than one nonlinear element with different characters at the same coordinate.

The application of the approach proposed is also demonstrated on a real structural test system, and it is concluded that the accuracy in parametric determination of nonlinearity by the proposed method gives better results than the method of Özer *et al.* [11] where low forcing tests were used to obtain linear FRFs. It is concluded in this study that the approach proposed is very promising to be used in practical systems, especially when there are multiple nonlinear elements at the same location.

#### 5. REFERENCES

- [1] Maia N. M. M., Silva J. M. M., "Theoretical and Experimental Modal Analysis", Research Studies Press LTD., 1997
- [2] Ewins D. J., "Modal Testing: Theory and Practice", Research Studies Press LTD., 1995
- [3] Kerschen G., Worden K., Vakakis A.F., Golinval J.C., "Past, present and future of nonlinear system identification in structural dynamics", *Mechanical Systems and Signal Processing*, Volume 20, pp 505-592, 2006
- [4] Göge D., Sinapius M., Füllekrug U., Link M., "Detection and Description of Non-Linear Phenomena In Experimental Modal Analysis Via Linearity Plots", *International Journal of Non-linear Mechanics*, Volume 40, pp 27-48, 2005
- [5] Worden K., Tomlinson G. R., "Nonlinearity in Structural Dynamics", Institute of Physics Publishing, 2001

- [6] Siller H. R. E., Non-linear Modal Analysis Methods for Engineering Structures, PhD Thesis in Mechanical Engineering, Imperial College London/University of London, 2004
- [7] Narayanan S., Sekar P., "A Frequency Domain Based Numeric–Analytical Method For Non-Linear Dynamical Systems", *Journal of Sound and Vibration*, Volume 211, pp 409-424, 1998
- [8] Muravyov A. A., Rizzi S. A., "Determination of Nonlinear Stiffness With Application to Random Vibration of Geometrically Nonlinear Structures", *Computers and Structures*, Volume 81, pp 1513-1523, 2003
- [9] Masri S. F., Caughey T. K., "A nonparametric identification Technique for Nonlinear Dynamic Problems, Transaction of ASME Journal of Applied Mechanics, Volume 46, pp 433-445, 1979
- [10] Elizalde H., İmregun M., "An Explicit Frequency Response Function Formulation for Multi-Degree-Of-Freedom Non-Linear Systems", *Mechanical Systems and Signal Processing*, Volume 20, pp 1867-1882, 2006
- [11] Özer M. B., Özgüven H. N., Royston T. J., "Identification of Structural Non-Linearities Using Describing Functions and The Sherman–Morrison Method", *Mechanical Systems and Signal Processing*, Volume 23, pp 30-44, 2009
- [12] Thothadri M., Casas R. A., Moon F. C., D'andrea R., Johnson Jr. C. R., "Nonlinear System Identification of Multi-Degree-of-Freedom Systems", *Nonlinear Dynamics*, Volume 32, pp 307-322, 2003
- [13] Cermelj P., Boltezar M., "Modeling localized nonlinearities using the harmonic nonlinear super model", *Journal of Sound and Vibration*, Volume 298, pp 1099-1112, 2006
- [14] Nuij P. W. J. M., Bosgra O. H., Steinbuch M., "Higher-Order Sinusoidal Input Describing Functions for the Analysis of Non-Linear Systems With Harmonic Responses", *Mechanical Systems and Signal Processing*, Volume 20, pp 1883-1904, 2006
- [15] Adams D. E., Allemang R. J., "A New Derivation of the Frequency Response Function Matrix for Vibrating Non-Linear Systems", *Journal of Sound and Vibration*, Volume 227, pp 1083-1108, 1999
- [16] Crawley E.F., Aubert A.C., "Identification of nonlinear structural elements by force-state mapping", *AIAA Journal*, Volume 24, pp 155–162 (Sections 3.2, 6.1), 1986
- [17] Crawley E.F., O'Donnell K.J., "Identification of nonlinear system parameters in joints using the force-state mapping technique", *AIAA Paper*, Volume 86-1013, pp 659–667 (Sections 3.2, 6.1), 1986
- [18] Masri S.F., Sass H., Caughey T.K., "A Nonparametric Identification of Nearly Arbitrary Nonlinear Systems", *Journal of Applied Mechanics*, Volume 49, pp 619-628, 1982
- [19] Noel J.P., Kerschen G., Newerla A., "Application of the Restoring Force Surface Method to a Real-life Spacecraft Structure", *Proceedings of the SEM IMAC XXX Conference*, Volume 3, Jacksonville, FL USA, 2012
- [20] Kerschen G., Golinval J.C., "Theoretical and Experimental Identification of a Nonlinear Beam", *Journal of Sound and Vibration*, Volume 244(4), pp 597-613, 2001
- [21] Kerschen G., Lenaerts V., Golinval J.C., "VVT Benchmark: Application of the Restoring Force Surface Method", *Mechanical Systems and Signal Processing*, Volume 17(1), pp 189-193, 2003
- [22] Worden K., Hickey D., Haroon M., Adams D.E., "Nonlinear System Identification of Automotive Dampers: A Time and Frequency-domain Analysis", *Mechanical Systems and Signal Processing*, Volume 23, pp 104-126, 2009
- [23] Xueqi C., Qiuhai L., Zhichao H., Tieneng G., "A Two-step Method to Identify Parameters of Piecewise Linear Systems", *Journal of Sound and Vibration*, Volume 320, pp 808-821, 2009
- [24] Haroon M., Adams D.E., Luk Y.W., Ferri A.A., "A time and Frequency Domain Approach for Identifying Nonlinear Mechanical System Models in the absence of an Input Measurement", *Journal of Sound and Vibration*, Volume 283, pp 1137-1155, 2005
- [25] Liang Y.C., Feng D.P., Cooper J.E., "Identification of Restoring Forces in Non-linear Vibration Systems Using Fuzzy Adaptive Neural Networks", *Journal of Sound and Vibration*, Volume 242(1), pp 47-58, 2001
- [26] Tanrıku Ö, Kuran B., Özgüven H. N., İmregun M., "Forced Harmonic Response Analysis of Non-linear Structures", *AIAA Journal*, Volume 31, pp 1313 - 1320, 1993
- [27] Duarte M.L.M., Experimentally-Derived Structural Models for Use in Further Dynamic Analysis, PhD Thesis in Mechanical Engineering, Imperial College London, 1996
- [28] A. Gelb, W. E. Vander Velde, Multiple-Input Describing Functions and Nonlinear System Design, McGraw Hill, 1968
- [29] Gibson J. E., Nonlinear Automatic Control, McGraw-Hill Book Company, Inc., 1963
- [30] Arslan Ö., Aykan M., Özgüven H. N., "Parametric Identification of Structural Nonlinearities from Measured Frequency Response Data", *Mechanical Systems and Signal Processing*, Volume 25, pp 1112-1125, 2011
- [31] Aykan M., Özgüven H.N. "Parametric Identification of Nonlinearity from Incomplete FRF Data Using Describing Function Inversion", *Proceedings of the SEM IMAC XXX Conference*, Volume 3, Jacksonville, FL USA, 2012

# Detection of Structural Damage through Nonlinear Identification by Using Modal Testing\*

Murat Aykan<sup>1,2</sup>, H. Nevzat Özgüven<sup>1</sup>

<sup>1</sup> Department of Mechanical Engineering, Middle East Technical University, Ankara 06800, TURKEY

<sup>2</sup> Defense Systems Technologies Division, ASELSAN Inc., Ankara, 06172, TURKEY

## ABSTRACT

Structural damages usually introduce nonlinearity to the system. A previously developed nonlinear identification method is employed to detect crack type structural damage. The method requires the measurement of FRFs at various points in order to locate the damage. The method makes it also possible to determine the extent of damage by identifying the level of nonlinearity. The verification of the method is demonstrated with experimental case studies using beams with different levels of cracks. The approach proposed in this study is very promising to be used in practical systems, but still open to further improvements.

## KEYWORDS

Damage detection, nonlinear structural dynamics, nonlinear structures, nonlinear identification, nonlinear testing

## 1. INTRODUCTION

Structural damage is defined as a permanent change in the mechanical state of a structural material that may affect their performance [1]. Common sources of damage in materials and structural components include micro-structural defects (dislocations, voids, inclusions), corrosion (loss of material), residual stress, cracking (fatigue, matrix, ply), fastening fault (weld crack, bolt preload, broken rivet), adhesive fault (de-bonding, delamination, separation), and instability (thermo-mechanical buckling) [1].

Successful damage detection and localization in structures is essential for health monitoring and maintenance. Non-destructive testing methods which can identify damage can be used for this purpose. However, most of the non-destructive methods, such as ultrasonic methods require the suspected location of the damage and that location must be accessible. The methods which use vibration responses usually do not suffer from these limitations.

The basis of vibration response methods is that damage changes the dynamic behavior of the structure. Salawu [2] presented a review on damage detection methods which use the shift in natural frequencies. The measurement of natural frequency changes is very simple but less informative compared to the mode shapes and can lead to wrong crack locations. Thus, methods which use mode shapes and their derivatives for damage detection were developed [3]-[6]. Recently, Yan *et al.* [7] presented a review for the advances in vibration based damage detection methods. The recent vibration based methods use the basic dynamic information of structures such as Frequency Response Functions (FRF) [8] and modal parameters [9]-[13]. Some of the vibration methods use wavelet analysis [14]-[16] and some use neural network analysis [17, 18]. These methods are based on linear models.

Damage can also add nonlinearity in structural systems which have otherwise linear responses [19]. The most common type of damage which introduces nonlinearity is breathing cracks which behave as bilinear stiffness elements. Many researchers have investigated different aspects of nonlinear damage identification using different approaches. These approaches include, for example, using nonlinear output FRFs [20], NARMAX modeling [21], using nonlinear characteristics of forced response of structures [22], and bifurcation boundary analysis [23].

---

\* presented in IMAC XXXI Conference, Orange County, California 11-14 February 2013 and will be published in Conference Proceedings of the Society for Experimental Mechanics Series

Damage detection method presented in this study consists of two main stages. Firstly, existence of damage in the system is detected by performing step sine tests with different loads. Secondly, the location of the damage is determined by using incomplete FRF data. The work presented in this study is mainly an experimental application of the method suggested by Aydođan [24] which was verified only by simulated data. The approach is based on the nonlinearity identification method developed by Özer *et al.* [25, 26].

## 2. Theory

Representation of nonlinear forces in matrix multiplication form using describing functions has been first given by Tanrıkuu *et al.* [27] and employed in identification of structural nonlinearities by Özer *et al.* [25, 26]. As the basic theory of the identification method is given in detail in reference [25] and [26], here only the nonlinearity localization equations are given.

The nonlinear internal forces in the system can be expressed by using describing functions. This approach makes it possible to represent the nonlinear stiffness and damping properties of the system as a response dependent matrix which can easily be included into the dynamic stiffness matrix of the linear system in the frequency domain. From the mathematical expressions of the FRF matrix of the nonlinear system ( $[H^{NL}]$ ) and FRF matrix of the linear part of the system ( $[H]$ ) (see reference [26] for details) the response dependent “nonlinearity matrix”  $[\Delta(x, \dot{x})]$  can be obtained as

$$[\Delta] = [H^{NL}]^{-1} - [H]^{-1} \quad (1)$$

where the elements of the nonlinearity matrix are expressed in terms of describing functions  $v$  [27].

Post multiplying both sides of equation (1) by  $[H^{NL}]$  gives

$$[\Delta][H^{NL}] = [I] - [Z][H^{NL}] \quad (2)$$

where  $[Z]$  is the dynamic stiffness matrix of the linear part.

In order to localize nonlinearity in a system, a parameter called “nonlinearity index” is used. The nonlinearity index ( $NLI$ ) for an  $p^{th}$  coordinate is defined by taking any  $i^{th}$  column of  $[H^{NL}]$  and the  $p^{th}$  row of  $[\Delta]$  from equation (2) as follows:

$$NLI_p = \Delta_{p1} \cdot H_{1i}^{NL} + \Delta_{p2} \cdot H_{2i}^{NL} + \dots + \Delta_{pn} \cdot H_{ni}^{NL} \quad (3)$$

Here, theoretically,  $i$  can be any coordinate; however, in practical applications it should be chosen as an appropriate coordinate at which measurement can be made and also is close to suspected nonlinear element. Equation (3) shows that any nonlinear element connected to the  $p^{th}$  coordinate will yield a nonzero  $NLI_p$ . On the other hand,  $NLI_p$  can be experimentally obtained by using the right hand side of equation (2), which requires the measurement of the receptances of the system at high and low forcing levels, presuming that low level forcing will yield FRFs of the linear part:

$$NLI_p = \delta_{ip} - Z_{p1} \cdot H_{1i}^{NL} - Z_{p2} \cdot H_{2i}^{NL} - \dots - Z_{pn} \cdot H_{ni}^{NL} \quad (4)$$

It should be noted that when there is only friction type of nonlinearity, then low level of forcing will yield  $H^{NL}$  and high level of forcing will approximately give  $H$ .

The main drawback of the method presented in [26] is that in order to calculate  $NLI_p$  from experimental  $H$  values, the whole linear FRF matrix is required (alternatively, theoretically calculated dynamic stiffness matrix can be used). Then it may not be feasible to apply the method with experimentally measured  $H$  values. In a recent study [28] it was proposed to use theoretically predicted values for unmeasured receptances calculated from the measured ones, and it is shown with case studies that this approach yields acceptable results.

In this present study, the damage locations are determined from NLI values calculated from vibration tests. Theoretically, if a nonlinear element is between a coordinate and ground, we would expect to have high NLI value for that coordinate only, and if a nonlinear element is between two coordinates, we would expect to have high NLI values at these two coordinates. In the

simulated cantilever beam case studies given in [24], it is concluded that, in order to observe such characteristics we need to measure the rotational coordinates which are affected the most from crack type nonlinearities. If translational coordinates are measured, then this method gives us an indication of the crack location by yielding a high peak only at the coordinate right after the crack closer to the fixed boundary. When this is the case, further investigations should be carried out by NDT methods around the coordinate with high NLI to pinpoint the crack.

### 3. Experimental Studies

#### 3.1. Experimental Study 1

For the implementation and validation of the method given above, step sine tests with different load levels are performed with four hollow square beams which are all manufactured from aluminum. The beams have 2.5 mm, 5.5 mm and 7.5 mm cracks, respectively. In order to see the effect of measurement noise on NLI values calculated from experimental measurements, a fourth beam with no crack is also tested. The cracks are produced by creating an indentation of 1mm first with a saw and then bending the beam several times until the desired crack is obtained. The test rig manufactured for this study, dimensions and technical details are given in Fig. 1 and Fig. 2, respectively. This test rig is preferred for its simplicity. The test rig consists of a cantilever beam with a crack between 4th and 5th coordinates. The modal test setup configuration with its elements is shown in Fig. 3. For step sine testing, a shaker (PCB) is connected to the free end (point 1) of the cantilever beam via a push-rod with a PCB 208C01 force transducer. The vibration responses are measured using six miniature PCB 352C65 and one PCB 352A24 accelerometers. The frequency resolution is 0.1 Hz. The crack in the system causes changes in the frequency response around resonance frequencies. Ability to observe this phenomenon is closely related to the frequency resolution employed in the harmonic vibration tests. The force closed loop control is achieved by the SCADAS-III data acquisition system.

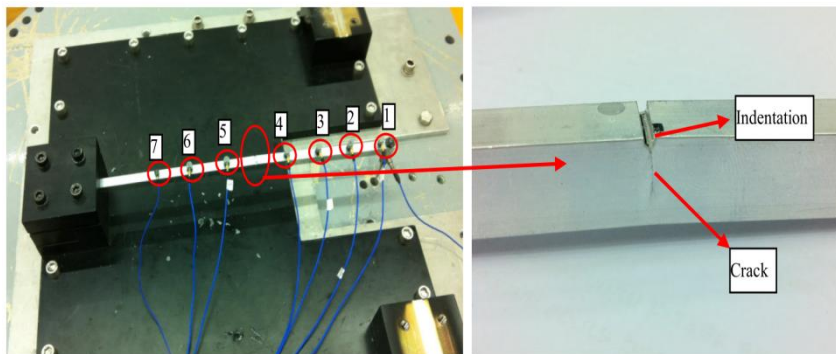


Fig. 1 Setup used in the experimental study-1

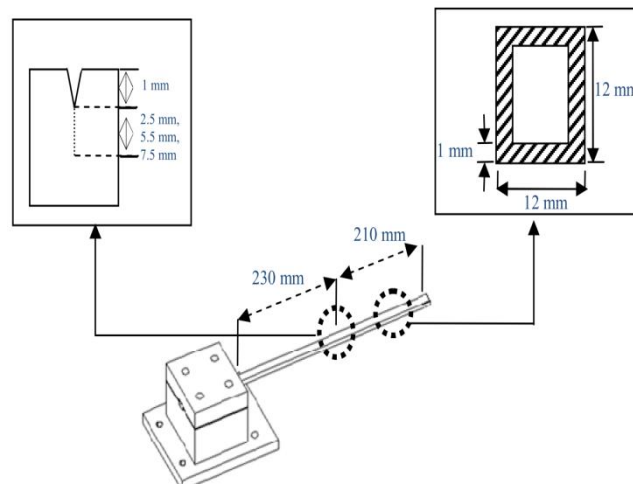


Fig. 2 Dimensions of experimental study-1

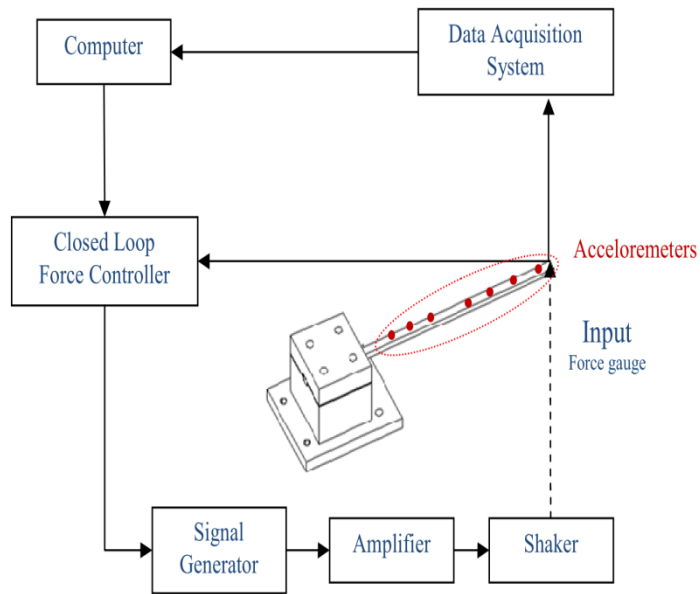


Fig. 3 Test setup of experimental study-1

The modal tests are performed using harmonic forcing with amplitudes of 0.01N and 0.05N at point 1 and measuring responses from 7 points. The FRFs obtained for the constant amplitude force tests with an undamaged beam and with three different crack lengths ( $h=2.5$  mm, 5.5 mm and 7.5 mm) are shown in Fig. 4-Fig. 7. The FRFs obtained with 0.01N amplitude harmonic forcing are taken as linear FRFs of the system.

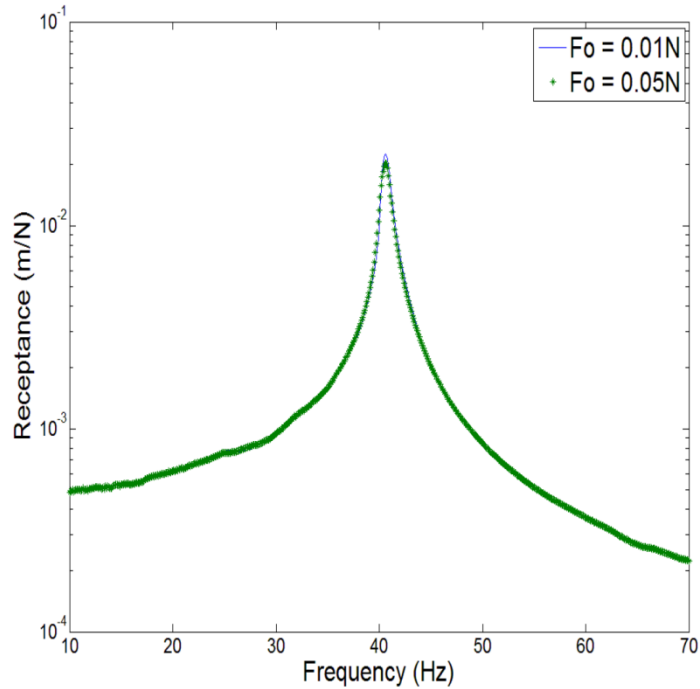


Fig. 4 Linear and nonlinear direct point FRFs at 1 (undamaged)

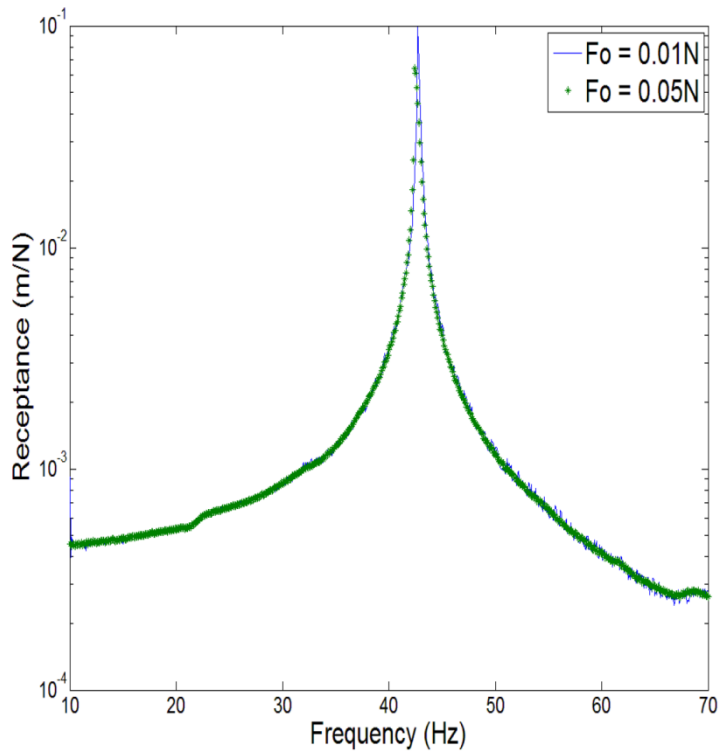


Fig. 5 Linear and nonlinear direct point FRFs at 1 ( $h = 2.5$  mm)

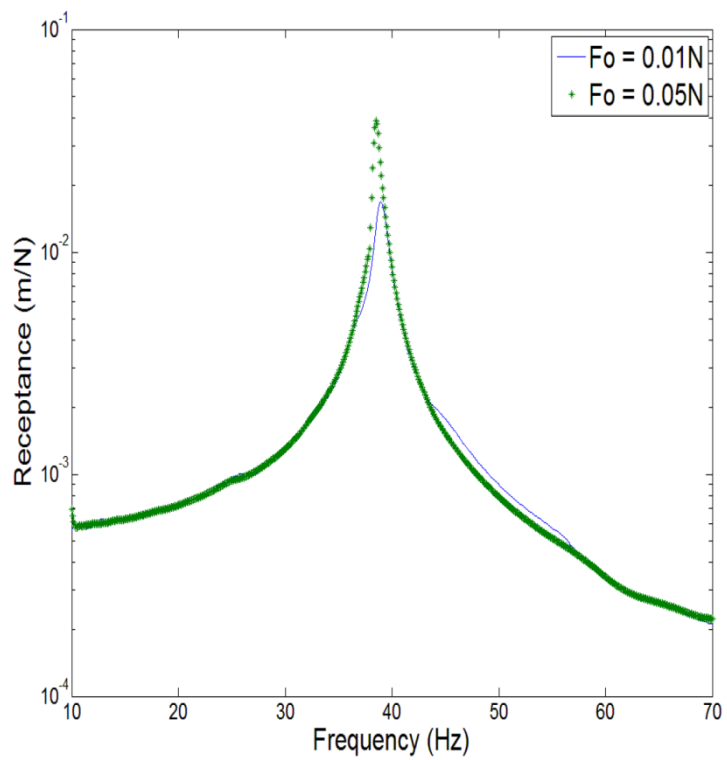


Fig. 6 Linear and nonlinear direct point FRFs at 1 ( $h = 5.5$  mm)

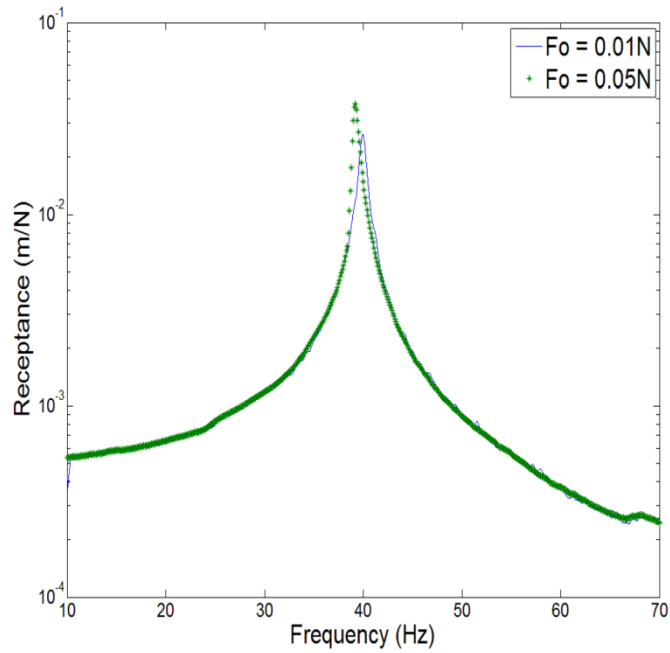


Fig. 7 Linear and nonlinear direct point FRFs at 1 (h= 7.5 mm)

In this experimental study, we measured only the first columns of the linear (0.01N forcing) and nonlinear receptance (0.05N forcing) matrices. Then, firstly the missing elements of the linear FRF matrix are calculated by using the approach mentioned in section 2, and the NLI values are calculated for each coordinate by using equation (4). Note that here only translational DOFs are used. The calculated NLI values are shown in Fig. 8-Fig. 11. The coordinates which are affected from nonlinearity can be determined from the NLI values obtained for each coordinate. The crack is located between the 4<sup>th</sup> and 5<sup>th</sup> coordinates so one expects to find two high peaks at these coordinates. In the simulated case studies given in [24], it is stated that, in order to observe such a chart we have to measure FRFs at the rotational coordinates which are affected the most from the nonlinearity. If translational coordinates are measured, then this method gives us an indication about the crack location by giving a high peak only at the coordinate right after the crack closer to the fixed boundary. The results obtained verify this expectation: We have high peaks at 5<sup>th</sup> coordinate. However, the NLI values we obtain are not much smaller than that of coordinate 5, unless the crack gets deeper (when we have deeper cracks the NLI value of 5<sup>th</sup> coordinate increases considerably, compared to other NLI values).

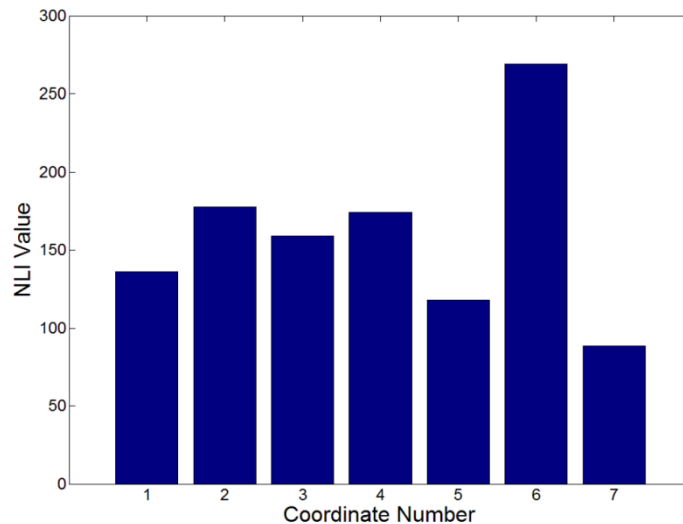
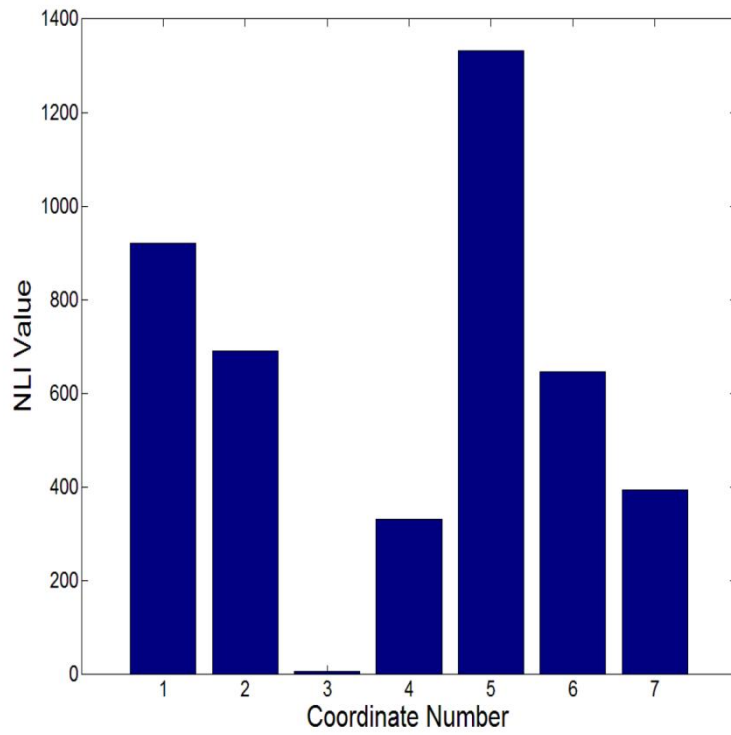
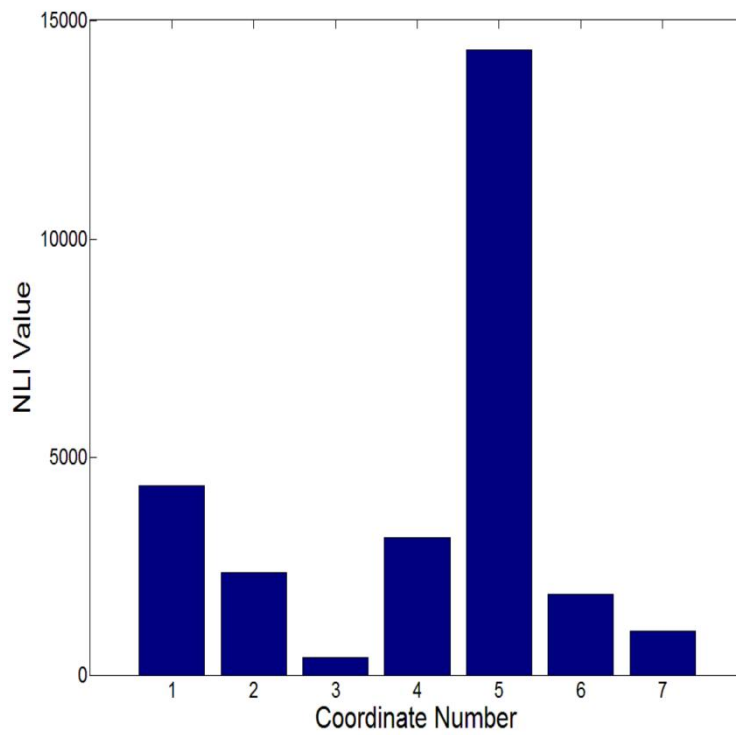


Fig. 8 Uncracked Nonlinearity Index Chart



**Fig. 9 2.5 mm Nonlinearity Index Chart**



**Fig. 10 5.5 mm Nonlinearity Index Chart**

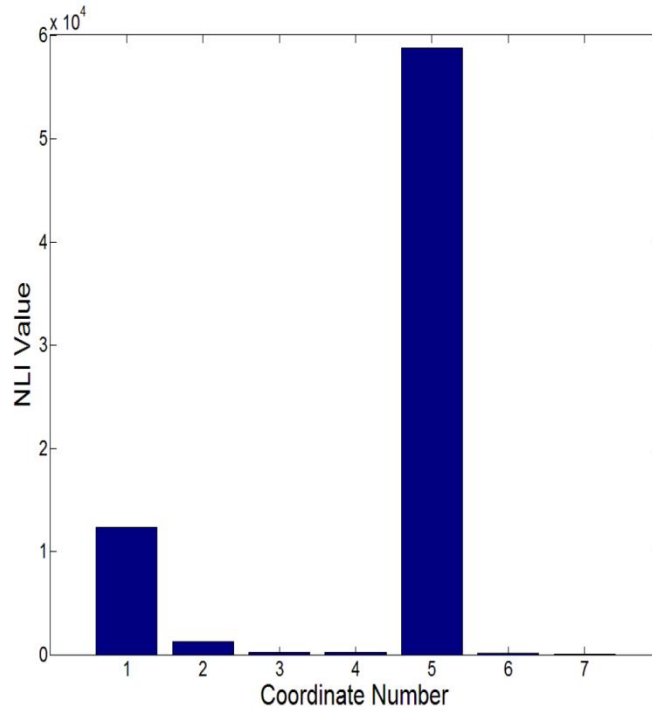


Fig. 11 7.5 mm Nonlinearity Index Chart

### 3.2. Experimental Study 2

In the first experimental study step sine testing with a shaker is preferred for the validation of the method. With this case study it is intended to demonstrate that this method can also be used with impact testing. However, it must be noted that the change in the FRFs with different impact levels will not be as much as that observed in closed loop shaker testing since it is more difficult to apply considerably higher force levels in impact testing. In this experimental study, the test specimen is changed to E-Glass reinforced plastic (E-GFRP). The damage is located between the same coordinates but this time the extent of damage is not known since the damage is created by simply bending the sheet. The test rig manufactured for this study, dimensions and technical details are given in Fig. 12 and Fig. 13, respectively. For impact testing, an impact hammer (PCB 086C01) is used and the structure is hit at the 7<sup>th</sup> coordinate. The vibration responses are measured using six miniature PCB 352C65 and one PCB 352A24 accelerometers. The frequency resolution is 0.3125 Hz. The crack in the system causes changes in the frequency response around resonance frequencies. Ability to observe this phenomenon is closely related to the frequency resolution employed in the harmonic vibration tests.

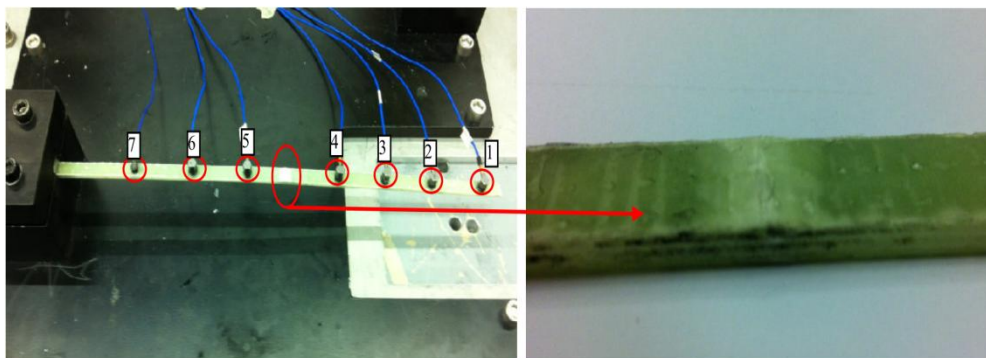
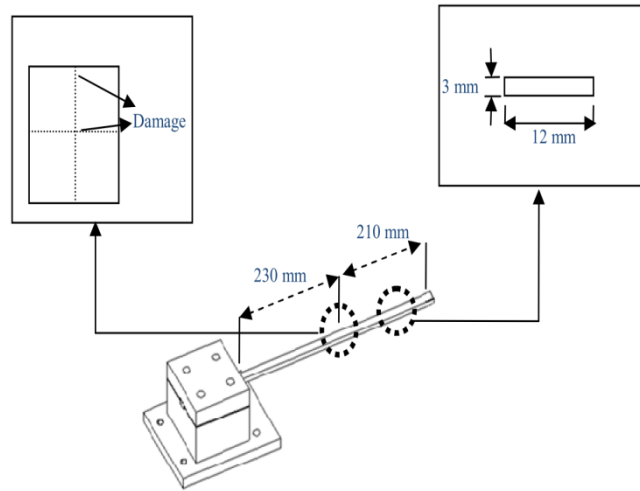
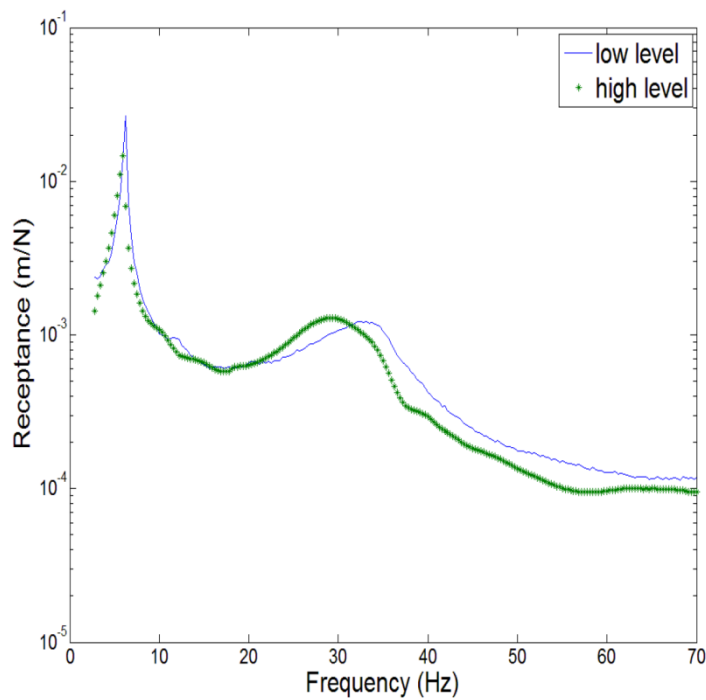


Fig. 12 Setup used in the experimental study-2



**Fig. 13 Dimensions of experimental study-2**

The modal tests are performed by hitting the structure with low and high impact forces. The FRFs obtained for two load levels are shown in Fig. 14. The FRFs obtained with low amplitude forcing are taken as linear FRFs of the system.



**Fig. 14 E-GFRP impact tests, tip point FRF curves**

In this experimental study, we measure only the first columns of the linear (low forcing) and nonlinear receptance (high forcing) matrices. Then, firstly the missing elements of the linear FRF matrix are calculated as discussed in section 2, and the NLI values are calculated for each coordinate by using equation(4). The calculated NLI values are shown in Fig. 15. The NLI chart shows the coordinates which are affected from nonlinearity. High NLI values at 4th and 5th coordinates indicate the damage between these coordinates. Relatively high value obtained for NLI at 6th coordinate may be due to the damage that might be extended to that coordinate. However, we observe from the experimental results that the method proposed may yield nonzero NLI values at some other coordinates as well, although they are not adjacent to damaged region. This is most

probably due to using only translational FRFs and not including those related with rotational DOF in the computation of NLI values. Fortunately, these nonzero NLI values are not as high as the ones obtained at damaged locations.

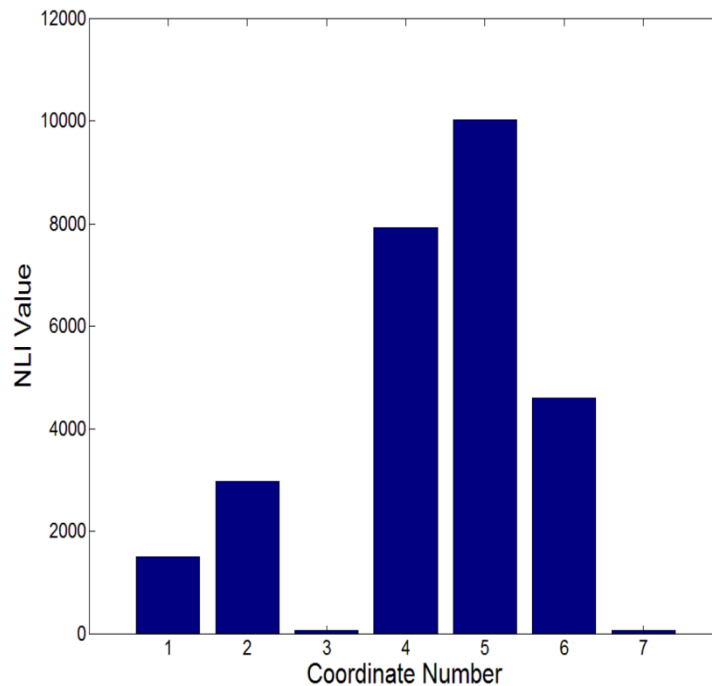


Fig. 15 E-GFRP Nonlinearity Index Chart

#### 4. Conclusions

It was recently shown [29] with an experimental case study that the method developed by Özer *et al.* [26] for detecting, localizing and parametrically identifying nonlinearity in MDOF systems is a promising method that can be used in industrial applications. In the study presented here it is shown that the same method can also be used for damage detection and localization for the type of damages which introduce nonlinearity to the structure. The verification of the approach proposed is demonstrated with two experimental studies.

The approach suggested is first applied to an aluminum beam with a breathing crack and it is shown that detection and localization of damage can be achieved by exciting the system from only one point and measuring the responses at all other coordinates (or only at the coordinates around which there might be a crack).

Secondly, it is shown in this study that the same method can also be employed to localize damage by using impact testing, which is more practical. The tests are conducted on a composite sheet and it is concluded that the accuracy in damage localization with impact testing is comparable to that of a shaker testing. Impact testing has many advantages over shaker testing as the most important one being the reduction of setup and test duration. Furthermore, the possibility of damaging the specimen during localization tests is much less in impact testing. The nonzero and relatively high NLI values obtained at coordinates not adjacent to damaged locations are believed to be due to measuring only translational FRFs and not including those related with rotational DOF. Consequently, it can be said that the approach proposed in this study is very promising to be used in practical systems, but still open to further improvements.

#### 5. References

- [1] Adams D.E., "Health Monitoring of Structural Materials and Components", John Wiley and Sons, Chichester, 2007
- [2] Salawu O.S., "Detection of structural damage through changes in frequency: a review", *Engineering Structures*, Volume 19 (9), pp 718–723, 1997
- [3] Pandey A.K., Biswas M., Samman M.M., "Damage detection from changes in curvature mode shapes", *Journal of Sound and Vibration*, Volume 145 (2), pp 321–332, 1991

- [4] Ratcliffe C.P., "Damage detection using a modified Laplacian operator on mode shape data", *Journal of Sound and Vibration*, Volume 204 (3), pp 505–517, 1997
- [5] Maia N.M.M., Silva J.M.M., Almas E.A.M., "Damage detection in structures: from mode shape to frequency response function methods", *Mechanical Systems and Signal Processing*, Volume 17 (3), pp 489–498, 2003
- [6] Whalen T.M., "The behavior of higher order mode shape derivatives in damaged beam-like structures", *Journal of Sound and Vibration*, Volume 309 (3–5), pp 426–64, 2008
- [7] Yan Y.J., Cheng L., Wu Z.Y., Yam L.H., "Development in vibration-based structural damage detection technique", *Mechanical Systems and Signal Processing*, Volume 21, pp 2198–2211, 2007
- [8] Huynh D., He J., Tran D., "Damage location vector: A non-destructive structural damage detection technique", *Computers & Structures*, Volume 83, pp 2353–2367, 2005
- [9] Rizos D.D., Fassois S.D., Marioli-Riga Z.P., Karanika A.N., "Vibration-based skin damage statistical detection and restoration assessment in a stiffened aircraft panel", *Mechanical Systems and Signal Processing*, Volume 22, pp 3151–337, 2008
- [10] Radziński M., Krawczuk M., Palacz M., "Improvement of damage detection methods based on experimental modal parameters", *Mechanical Systems and Signal Processing*, Volume 25, pp 2169–2190, 2011
- [11] Wang J., Qiao P., "On irregularity-based damage detection method for cracked beams", *Solids and Structures*, Volume 45, pp 688–704, 2008
- [12] Huang Q., Gardoni P., Hurlbaeus S., "A probabilistic damage detection approach using vibration-based nondestructive testing", *Structural Safety*, Volume 38, pp 11–21, 2012
- [13] Qiao P., Lu K., Lestari W., Wang J., "Curvature mode shape-based damage detection in composite laminated plates", *Composite Structures*, Volume 80, pp 409–428, 2007
- [14] Xiang J., Liang M., "A two-step approach to multi-damage detection for plate structures", *Engineering Fracture Mechanics*, Volume 91, pp 73–86, 2012
- [15] Wu N., Wang Q., "Experimental Studies on damage detection of beam structures with wavelet transform", *International Journal of Engineering Science*, Volume 49, pp 253–261, 2011
- [16] Fan W., Qiao P., "A 2-D continuous wavelet transform of mode shape data for damage detection of plate structures", *International Journal of Solids and Structures*, Volume 46, pp 4379–4395, 2009
- [17] Bakhary N., Hao H., Deeks A. J., "Damage detection using artificial neural network with consideration of uncertainties", *Engineering Structures*, Volume 29, pp 2806–2815, 2007
- [18] Yu L., Cheng L., Yam L.H., Yan Y.J., Jiang J.S., "Experimental validation of vibration-based damage detection for static laminated composite shells partially filled with fluid", *Composite Structures*, Volume 79, pp 288–299, 2007
- [19] Nichols J.M., Seaver M., Trickey S.T., Todd M.D., Olson C., Overbey L., "Detecting nonlinearity in structural systems using the transfer entropy", *Physical Review*, Volume E 72, 046217, 2005
- [20] Lang Z.Q., Park G., Farrar C.R., Todd M.D., Mao Z., Zhao L., Worden K., "Transmissibility of non-linear output frequency response functions with application in detection and location of damage in MDOF structural systems", *International Journal of Non-Linear Mechanics*, Volume 46, pp 841–853, 2011
- [21] Peng Z.K., Lang Z.Q., Wolters C., Billings S.A., Worden K., "Feasibility study of structural damage detection using NARMAX modeling of Nonlinear Output Frequency Response Function based analysis", *Mechanical Systems and Signal Processing*, Volume 25, pp 1045–1061, 2011
- [22] Andreus U., Baragatti P., "Experimental damage detection of cracked beams by using nonlinear characteristics of forced response", *Mechanical Systems and Signal Processing*, Volume 31, pp 382–404, 2012
- [23] Eftekhari S.A., Bakhtiari-Nejad F., Dowell E.H., "Bifurcation boundary analysis as a nonlinear damage detection feature: does it work?", *Journal of Fluids and Structures*, Volume 27, pp 297–310, 2011
- [24] Aydoğan M.Ö., *Damage Detection in structures using vibration measurements*, MSc Thesis in Mechanical Engineering, Middle East Technical University, 2003
- [25] Özer M. B., Özgüven H. N., "A New Method for Localization and Identification of Nonlinearities in Structures", *Proceedings of ESDA2002: 6th Biennial Conference on Engineering Systems Design and Analysis*, İstanbul-Turkey, 2002
- [26] Özer M. B., Özgüven H. N., Royston T. J., "Identification of Structural Non-Linearities Using Describing Functions and The Sherman–Morrison Method", *Mechanical Systems and Signal Processing*, Volume 23, pp 30–44, 2009
- [27] Tanrıku Ö, Kuran B., Özgüven H. N., İmregun M., "Forced Harmonic Response Analysis of Non-linear Structures", *AIAA Journal*, Volume 31, pp 1313 - 1320, 1993
- [28] Aykan M., Özgüven H.N. "Parametric Identification of Nonlinearity from Incomplete FRF Data Using Describing Function Inversion", *Proceedings of the SEM IMAC XXX Conference*, Volume 3, Jacksonville, FL USA, 2012
- [29] Arslan Ö., Aykan M., Özgüven H. N., "Parametric Identification of Structural Nonlinearities from Measured Frequency Response Data", *Mechanical Systems and Signal Processing*, Volume 25, pp 1112–1125, 2011

## VITA

<b>PERSONAL INFORMATION</b> Surname, Name: Aykan, Murat Nationality: Turkish (TC) Date and Place of Birth: 2 April 1979, Germany-Mainz Marital Status: Married Phone: +9 0 312 386 21 71 Cell Phone: +9 0 533 727 98 50 email: <a href="mailto:m.aykan@hotmail.com.tr">m.aykan@hotmail.com.tr</a>	
<b>EDUCATION:</b>	B.S. in Mechanical Engineering, METU, Ankara Date of Graduation: June, 2002  M.Sc. in Mechanical Engineering, METU, Ankara Date of Graduation: June, 2005
<b>CAREER RELATED EXPERIENCE:</b>	<u>ASELSAN</u> , Ankara, April 2009- Mechanical Design Department –Analysis and Test Division – Senior Expert Mechanical Analysis and Test Engineer/Division Supervisor.  <u>ASELSAN</u> , Ankara, June 2002-April 2008 Mechanical Design Department – Mechanical Analysis and Test Division – Expert Mechanical Analysis and Test Engineer.  <u>TOYOTA</u> , Sakarya, Summer Practice 2001  <u>TEI</u> , Eskişehir, Summer Practice 2000
<b>PUBLICATIONS:</b>	M. Aykan, M. Çelik, Vibration Fatigue Analysis and Multiaxial Effect in Testing of Aerospace Structures, Mechanical Systems and Signal Processing 23(3) (2009) 897-907.  Ö. Arslan, M. Aykan, H.N. Özgüven, Parametric Identification of Structural Nonlinearities from Measured Frequency Response Data, Mechanical Systems and Signal Processing 25 (2011) 1112-1125.  M. Aykan, H.N. Özgüven , Parametric Identification of Nonlinearity from Incomplete FRF Data Using Describing Function Inversion, Proceedings of the SEM IMAC XXX Conference, Jacksonville, FL USA, 2012.  M. Aykan, H.N. Özgüven , Identification of Restoring Force Surfaces in Nonlinear MDOF Systems from FRF Data Using Nonlinearity Matrix, Proceedings of the SEM IMAC XXXI Conference, Orange County, CA USA, 2013.  M. Aykan, H.N. Özgüven , Detection of Structural Damage through Nonlinear Identification by Using Modal Testing, Proceedings of the SEM IMAC XXXI Conference, Orange County, CA USA, 2013.  M. Aykan, M. Çelik, F.S. Kadioğlu, Hava Platformlarında Titreşim Frekans Alanı Yorulma Analizleri, Timak06- Tasarım İmalat ve Analiz Kongresi, 26-28 Nisan 2006, Balıkesir Üniversitesi, Balıkesir.

	<p>M. Çelik, M., Aykan, S. Özsoy, Operational Flight Tests and Numerical Analyses of an add-on Aerospace Component for Safety of Flight, 4. Ankara International Aerospace Conference-AIAC07, 10-12 September 2007, KKM-METU, Ankara.</p> <p>M. Çelik, M. Aykan, Tank Namlusunun Operasyonel Modal ve Deplasman Analizi, Makine Tasarım ve İmalat Dergisi, Cilt 5, Sayı 3, Mayıs 2004.</p>
--	--